

# **The Properties of Hydrophobically Modified Water Soluble Polymers in Water and at Surfaces**

## **Dissertation**

Zur Erlangung des akademischen Grades

*Doctor rerum naturalium* (Dr. rer. nat.)

Vorgelegt der

Naturwissenschaftliche Fakultät II-Chemie, Physik und Mathematik

der Martin-Luther-Universität Halle-Wittenberg

von

Herrn M. Sc. Zheng Li

geb. am 10. Juli 1984 in Guangdong, China

Gutachter

1. Prof. Dr. Jörg Kressler

2. Prof. Dr. Karl-Friedrich Arndt

Halle (Saale), den 8. Oktober 2012

**To my parents**

**Table of Content**

<b>Table of Content .....</b>	<b>iii</b>
<b>Abbreviations.....</b>	<b>vi</b>
<b>Symbols .....</b>	<b>ix</b>
<b>Chapter 1 General Introduction .....</b>	<b>1</b>
1.1 Hydrophobically Modified Water Soluble Polymers .....	1
1.2 Synthesis of End Capped Polymers .....	4
1.2.1 Atom transfer radical polymerization (ATRP).....	4
1.2.2 ‘Click’ chemistry.....	6
1.3 Chirality.....	9
1.3.1 General information about chirality .....	9
1.3.2 Chiral polymers .....	11
1.3.3 Chirality determination by NMR spectroscopy .....	12
1.3.4 Circular dichroism spectroscopy .....	15
1.4 Protein Resistance of Surfaces .....	18
1.5 Motivation and Objectives of This Work.....	19
1.6 References .....	21
<b>Chapter 2 The Aggregation Behavior of Poly(N-isopropylacrylamide) HMSP with a Perfluoroalkyl Segment in Water .....</b>	<b>27</b>
2.1 Introduction .....	27
2.2 Experimental Part.....	29
2.2.1 Materials.....	29
2.2.2 Measurements.....	29
2.2.3 ‘Click’ reaction.....	31
2.3 Results and Discussion.....	31

---

2.3.1	'Click' reaction for synthesis of $P_xF_9$ .....	31
2.3.2	Determination of critical micellization concentration (cmc) .....	35
2.3.3	Dynamic light scattering .....	36
2.4	Conclusion.....	47
2.5	References .....	49
<b>Chapter 3 Self-Assembly Behavior of Fluorocarbon-End Capped Poly(glycerol methacrylate) in Aqueous Solution.....</b>		<b>52</b>
3.1	Introduction .....	52
3.2	Experimental Section .....	53
3.2.1	Materials.....	53
3.2.2	Synthesis.....	54
3.2.3	Characterization .....	57
3.3	Results and Discussion.....	58
3.3.1	Polymer synthesis and characterization .....	58
3.3.2	Self-assembly of $PGMA_xF_9$ in aqueous solution .....	62
3.4	Conclusion.....	81
3.5	References .....	82
<b>Chapter 4 Influence of the Chirality of Grafted Poly(glycerol methacrylate) Chains on Protein Adsorption.....</b>		<b>86</b>
4.1	Introduction .....	86
4.2	Experimental section .....	88
4.2.1	Materials.....	88
4.2.2	Synthesis.....	89
4.2.3	SAM preparation .....	91
4.2.4	Characterization .....	92
4.3	Results and Discussion.....	94
4.3.1	Polymer synthesis and characterization .....	94
4.3.2	Physical properties of HS-PGMA in water .....	97
4.3.3	Preparation and characterization of SAMs.....	105
4.3.4	Thickness determination of SAMs by ellipsometry .....	106

4.3.5	BSA adsorption to PGMA SAMs measured by SPR.....	108
4.4	Conclusion.....	111
4.5	References .....	112
<b>Chapter 5 Detection of Chirality of Poly(glycerol methacrylate)s After Derivatization by <sup>1</sup>H NMR Spectroscopy .....</b>		<b>115</b>
5.1	Introduction .....	115
5.2	Experimental Section .....	116
5.2.1	Materials.....	116
5.2.2	NMR spectroscopy .....	116
5.3	Results and Discussion.....	117
5.4	Conclusions .....	125
5.5	References .....	126
<b>Chapter 6 Summary.....</b>		<b>128</b>
<b>Appendix.....</b>		<b>131</b>
<b>Aknowledgement.....</b>		<b>137</b>
<b>Publications.....</b>		<b>138</b>
<b>Curriculum Vitae.....</b>		<b>139</b>
<b>Declaration.....</b>		<b>140</b>

**Abbreviations**

9-AMA	9-Anthrylmethoxyacetic acid
AFM	Atom Force Microscopy
APBIB	3-Azidopropyl-2-bromoisobutyrate
ATRP	Atom Transfer Radical Polymerization
BIB	2-Bromoisobutyryl bromide
Bpy	2,2'-Bipyridine
BSA	Bovine Serum Albumin
Bu <sub>4</sub> NI	<i>N,N,N</i> -Tributyl-1-butanaminium iodide
cac	Critical Aggregation Concentration
CD	Circular Dichroism
CDA	Chiral Derivatizing Agent
CIP	Cahn-Ingold-Prelog
cmc	Critical Micellization Concentration
CRP	Controlled Radical Polymerization
CSA	Chiral Solvating Agent
CTA	Chain Transfer Agent
CuAAC	Copper(I)-Catalyzed Alkyne-Azide Cycloaddition
DCC	<i>N,N'</i> -(dicyclohexyl)carbodiimide
DEPT	Distortionless Enhancement by Polarization Transfer
DIPEA	<i>N</i> -Ethyl-diisopropylamide
DLS	Dynamic Light Scattering
DMAP	4-(Dimethylamino)pyridine
DMF	Dimethylformamide
DMSO- <i>d</i> <sub>6</sub>	Deuterated dimethylsulfoxide
DP	Degree of Polymerization
DSC	Differential Scanning Calorimetry
Et <sub>3</sub> N	Triethylamine
F <sub>9</sub>	Nonadecafluoro-1-decyl hex-5-ynoate
FDA	Food and Drug Administration
FMSP	Fluorocarbon Modified Water Soluble Polymer
FPBA	Formylphenylboronic acid
GMA	Glycerol methacrylate

FTIR	Fourier Transform Infrared
HMSP	Hydrophobically Modified Water Soluble Polymer
HSQC	Heteronuclear Single Quantum Correlation
ITC	Isothermal Titration Calorimetry
LCST	Lower Critical Solution Temperature
MBA	$\alpha$ -Methylbenzylamine
MMA	Methyl methacrylate
MPA	$\alpha$ -Methoxyphenylacetic acid
MTPA	Methoxytrifluorophenyl acetic acid
NMR	Nuclear Magnetic Resonance
NMP	Nitroxide mediated polymerization
ORD	Optical Rotatory Dispersion
PAA	Poly(acrylic acid)
PAEI	Poly( <i>N</i> -acylethylene imine)
PBuEtOx	Poly(2-butyl-4-ethyl-2-oxazoline)
PDMA	Poly(dimethylacrylamide)
PEO	Poly(ethylene oxide)
PG	Poly(glycidol)
PGMA	Poly(glycerol methacrylate)
PHEMA	Poly(2-hydroxyethyl methacrylate)
PHPMA	Poly(hydroxypropyl methacrylate)
PLA	Poly(lactic acid)
PLA- <i>co</i> -PG	Poly(lactide- <i>co</i> -glycolide)
PMMA	Poly(methyl methacrylate)
PNIPAM	Poly( <i>N</i> -isopropylacrylamide)
PPO	Poly(propylene oxide)
PSMA	Poly(solketal methacrylate)
PVA	Poly(vinyl alcohol)
P <sub>x</sub> N <sub>3</sub>	Azide terminated PNIPAM
P <sub>x</sub> F <sub>9</sub>	F <sub>9</sub> terminated PNIPAM
R	Rectus
Rac	Racemic
RAFT	Reversible Addition Fragmentation Chain Transfer
S	Sinister

SAM	Self-Assembled Monolayers
SANS	Small Angel Neutron Scattering
SAXS	Small Angel X-ray Scattering
SCMF	Single Chain Mean Field
SERS	Surface Enhanced Raman Spectroscopy
SFRP	Stable Free Radical Polymerization
SI-ATRP	Surface Initiated Atom Transfer Radical Polymerization
SLS	Static Light Scattering
SMA	Solketal methacrylate
SPR	Surface Plasmon Resonance
TBTA	Tris(benzyltriazolymethyl)amine
TFA	Trifluoroacetic acid
TFT	$\alpha,\alpha,\alpha$ -Trifluorotoluene
TGA	Thermogravimetric Analysis
THF	Tetrahydrofuran
UV	Ultraviolet
WCA	Water Contact Angle



## Symbols

$R^\bullet$	initiating radical species
$P^\bullet$	intermediate radical
$k_p$	constant of propagation
$k_d$	constant of deactivation.
$\delta$	chemical shift
$\varepsilon$	absorption coefficients
$\theta$	ellipticity
$\lambda$	wavelength
$[\theta]$	molar ellipticity
$\Delta\varepsilon$	molar circular dichroism
$\Gamma$	decay rate
$D_{app}$	apparent diffusion coefficient
$q$	scattering vector
$n_0$	refractive index
$R_h$	hydrodynamic radius
$M_n$	number average molar mass
$M_w$	weight average molar mass
$T_{cp}$	cloud point temperature
$T_{max}$	temperature of maximum heat capacity
$\Delta T_{1/2}$	width of the transition at half-height
$\Delta H$	enthalpy of transition
$\Delta C_p$	difference in the heat capacity after and before the transition
$\gamma$	surface tension
$N_{agg}$	aggregation numbers
$R_F$	fluorocarbon end capped group
$R$	gas constant
$T$	temperature in $K$
$X_{cmc}$	cmc in molar fraction
$\Delta H^0_{mic}$	standard enthalpy of micellization,
$\Delta S^0_{mic}$	standard entropy of micellization
$\Delta G^0_{mic}$	standard free energy of micellization,

$N_A$	Avogadro's number
$\Sigma$	chain density
$\Gamma$	adsorbed amount
$R_g$	gyration radius

## *Chapter 1*

### *General Introduction*

#### **1.1 Hydrophobically Modified Water Soluble Polymers**

Hydrophobically modified water soluble polymers (HMSPs) are polymers composed of a hydrophilic main chain with a small fraction of hydrophobic groups attached randomly in the chain or capped at the chain ends. Since the first study on HMSP was carried out by Strauss et al.<sup>1</sup> in the early 50s of last century, the HMSPs have invoked tremendous interest because of their unique rheological properties and potential applications.<sup>2,3</sup> The HMSPs can have different architectures such as linear, star, and hyperbranched. In this thesis, only linear HMSPs are discussed.

The self-assembly behavior of HMSPs in aqueous solution has been studied extensively and is well understood.<sup>4-11</sup> In the case of HMSPs with hydrophobic groups randomly distributed on the polymer chain, both intramolecular and intermolecular hydrophobic association can exist (Figure 1.1a and b). Basically, at low concentrations the hydrophobic groups of the same polymer chain associate via intramolecular interactions which results in a reduced coil size compared to their homopolymer counterparts.<sup>5,6</sup> With increasing concentration, the intermolecular interactions become increasing important and the polymer chains tend to form an open association with many bridges, leading to a three-dimensional network. This gives rise to a dramatic increase of the solution viscosity.<sup>8</sup> The end capped polymers are the simplest HMSPs. Above critical micellization concentration (cmc), micelles composed of a single core made up of the hydrophobic end groups and a corona consisting of the hydrophilic main chains are formed as exemplified in Figure 1.1c and d for micelles formed by one end capped (semitelechelics) and two end capped (telechelics) HSMPs.<sup>9-14</sup> In a concentrated solution, a network of micelles connected by hydrophilic main chains is formed by telechelic polymers.<sup>10-14</sup>

The fluorocarbon modified water soluble polymers (FMSPs) are known as an important class of HMSPs and they possess unique properties because of the intriguing characteristics of fluorinated moieties, which are attributed to the fact that the fluorine atom has a dense electron cloud, high ionization potential and very low polarizability.<sup>15</sup> The first FMSPs were introduced by Zhang and Hogen-Esch in 1992 by the polymerization of acrylamide and a

small amount of acrylate or methacrylate with fluorocarbon containing side chains.<sup>16</sup> Compared to their hydrocarbon counterparts, the FMSPs are more stable, surface active, and hydrophobic.<sup>15-22</sup> In terms of associative ability, one  $\text{CF}_2$  group is equivalent to 1.7  $\text{CH}_2$  groups.<sup>23</sup> Moreover, the fluorocarbon moiety is lipophobic and immiscible with hydrocarbon moieties.<sup>24-26</sup>

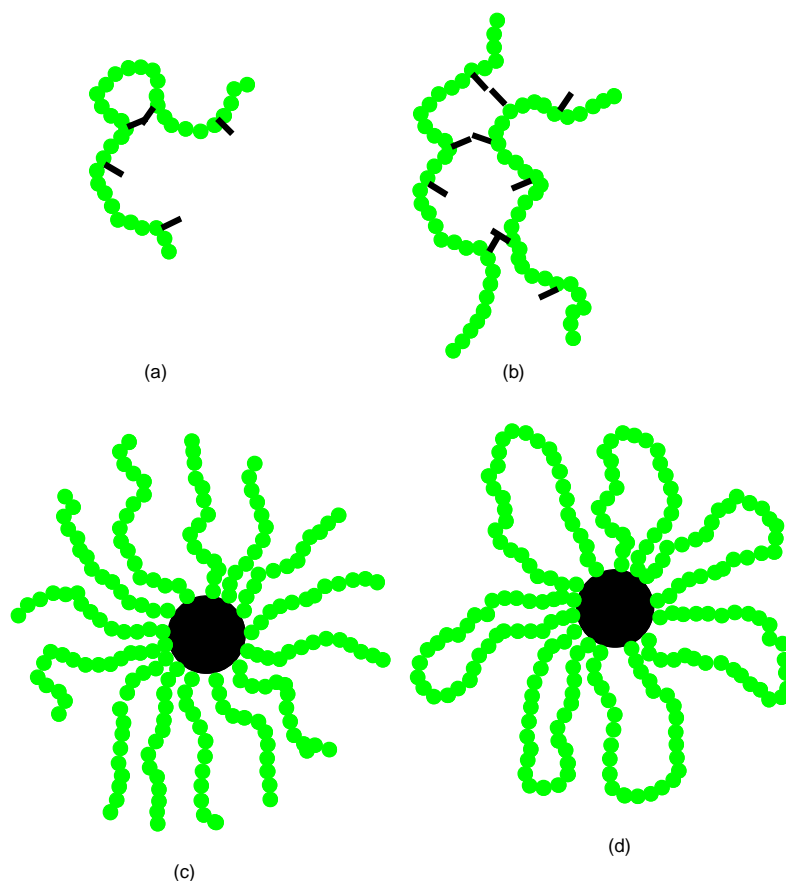


**Figure 1.1.** (a) Intramolecular and (b) intermolecular association of randomly hydrophobically modified water-soluble polymers (HMSPs) in aqueous solution. (c) Spherical core/corona micelle formed by one end capped HMSP and (d) two end capped HMSP in water.

It has been demonstrated that the end capped FMSPs can adopt a variety of unique properties such as high solubility and biological activity, which may not be achieved in randomly fluorinated polymers and fluorinated block polymers.<sup>27-28</sup> To date, a wide range of end capped FMSPs ( $R_F$ -P, where the  $R_F$  represents the fluorinated end functional group) including  $R_F$ -poly(ethylene oxide) ( $R_F$ -PEO),<sup>16, 20-22, 29-34</sup>  $R_F$ -poly(*N*-isopropyl acrylamide) ( $R_F$ -PNIPAM),<sup>19,35-37</sup>  $R_F$ -poly(acrylic acid) ( $R_F$ -PAA),<sup>38-39</sup>  $R_F$ -poly(*N*-acylethylene imine) ( $R_F$ -PAEI),<sup>40</sup>  $R_F$ -poly(dimethylacrylamide) ( $R_F$ -PDMA),<sup>41</sup>  $R_F$ -poly(lactide acid) ( $R_F$ -PLA),<sup>42-43</sup>  $R_F$ -

poly(lactide-*co*-glycolide) ( $R_F$ -(PLA-*co*-PG))<sup>44,45</sup> among others, have been prepared and their behavior in aqueous solution or at the air/water interface have been studied by a wide range of techniques, such as surface tension measurements, fluorescence spectroscopy, SLS, DLS, <sup>19</sup>F-NMR spectroscopy, SAXS, SANS, self-diffusion and ESR measurements.<sup>29-45</sup> Among them,  $R_F$ -PEO is the most widely and well studied FMSP. It has been demonstrated that  $R_F$ -PEO exhibits a stronger hydrophobic association in aqueous solution and possesses a greater viscosifying effect than its hydrocarbon analogous with comparable molar mass, which have been used as models in molecular studies on the hydrophobic association process.<sup>20</sup> Considering the noble properties of the fluorinated moiety, FMSPs have also been developed as an important class of biomedical materials. For instance, Mecozzi and coworkers<sup>15</sup> have observed that one end capped  $R_F$ -PEO generates micellar structures having a fluororous phase-based inner core in aqueous solution, and these micelles can be used as the carrier for the anesthetic Sevoflurane<sup>®</sup>. Gardella et al.<sup>45</sup> showed that the  $R_F$ -(PLA-*co*-PG) exhibit good properties in controlled cellular or tissue adhesion.

Incorporation of a fluorinated component into an amphiphilic system offers a non-ionic route to a compartmentalized core due to the strong immiscibility between the fluoro and hydrocarbon based segments. Thünemann et al.<sup>40</sup> prepared a series of  $\alpha$ -fluorocarbon- $\omega$ -hydrocarbon end-capped poly(*N*-acylethylene imine)s. The study of such telechelics showed that they formed cylindrical micelles comprised of the core containing distinct fluorocarbon and hydrocarbon domains.

## 1.2 Synthesis of End Capped Polymers

### 1.2.1 Atom transfer radical polymerization (ATRP)

ATRP together with stable free-radical polymerization (SFRP) and reversible addition-fragmentation transfer (RAFT) are classified as controlled radical polymerizations (CRP). Among them, ATRP is the most widely used CRP method for the fact that it is a simple synthetic procedure and all necessary reagents, such as initiator and catalyst, are commercially available.<sup>46-50</sup> Since the ATRP technique was reported by Sawamoto and Matyjaszewski in 1995,<sup>51,52</sup> it has been applied to design different types of polymers including, random, gradient, block and graft copolymers, with various architectures such as hyperbranched, star and brush polymers.<sup>47</sup> Moreover, the terminal halogen atom at the end of the polymer chains can be exchanged with other functional groups. This makes ATRP to be one of the most preferred choices for preparing synthetic macromolecular structures intended for post-polymerization functionalization.<sup>53</sup>

A typical ATRP employs the elements initiator, transition metal species and ligand. Essentially, all the molecules with a transferable halogen atom activated by carbonyl, phenyl, vinyl, or cyano groups can initiate an ATRP under appropriate conditions.<sup>46</sup> A suitable initiator should have a matched reactivity with the monomer.<sup>47</sup> This can be achieved by using an initiator containing a similar group as the propagating radical.<sup>47</sup> The catalyst system, which is composed of a transition metal species with any suitable ligand, plays a crucial role in ATRP since it determines the rate of exchange between the dormant and propagating species.<sup>47</sup> The most commonly used transition metal is copper. Other transition metals including Fe,<sup>54</sup> Ru,<sup>55</sup> Pd,<sup>56</sup> and Ni<sup>57</sup> have also been successfully used in ATRP. The main function of a ligand in ATRP is complexation of the transition metal salt in order to make it soluble and adjusting the redox potential of the metal center for appropriate activity.<sup>46</sup>

A generally accepted mechanism for the ATRP is shown in Figure 1.2. The generation of initiating radical species ( $R^\bullet$ ) involves a homolytic cleavage of the carbon-halogen bond of an initiator ( $R-X$ ) via a reversible redox process catalyzed by a transition metal compound ( $M_t^n/\text{Ligand}$ ). A fast and quantitative initiation is necessary for a successful ATRP since a narrow molar mass distribution is preferred if all the propagating species begin the growth at the same time. The radical either reacts with the halogen on the oxidized metal complex to regenerate  $R-X$  or adds to the monomer to form the intermediate radical ( $P^\bullet$ ). In a short time, the intermediate radical is transformed into a dormant ( $P-X$ ) state by subtraction of a halogen

atom from  $X-M_t^{n+1}/\text{Ligand}$  with a rate constant of deactivation  $k_d$ . The dormant intermediate species are subsequently activated by the  $M_t^n/\text{Ligand}$  to give the radical which undergoes further polymerization. The monomers are added to the intermediate radicals with a rate constant of propagation  $k_p$  to form polymer chains. The persistent radical or deactivator,  $X-M_t^{n+1}/\text{Ligand}$ , can reduce the stationary concentration of propagating radicals and therefore minimize the normal termination of controlled polymerization. In a successful ATRP, the concentration of the dormant species should be much higher than the concentration of propagating radicals. For instance, it can reach a factor of  $\sim 10^6$ .<sup>48</sup> The fast and quantitative initiation and rapid reversible deactivation of propagating radicals in the ATRP process ensure uniform growth of all chains and give the controlled radical character to the ATRP techniques.<sup>47</sup>

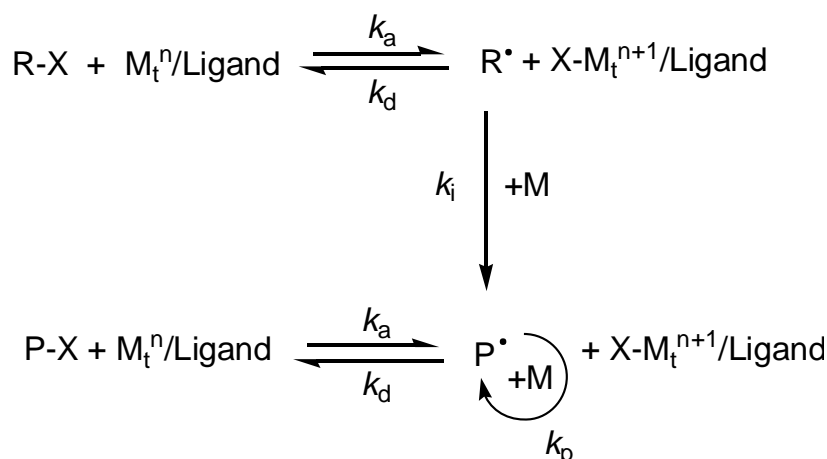


**Figure 1.2.** Mechanism of ATRP (according to ref. 47).

A variety of monomers, including styrenes,<sup>58</sup> (meth)acrylates,<sup>59</sup> (meth)acrylamides,<sup>60</sup> vinyl pyridine,<sup>61</sup> acrylonitrile,<sup>62</sup> among others have been successfully polymerized using ATRP. There are some monomers which are not suitable for ATRP for some specific reasons. Monomers with less reactivity, such as ethylene and vinyl chloride, have not been polymerized by ATRP.<sup>63</sup> Some acidic monomers such as acrylic acid can interfere with the initiator by protonation of the ligands and thus are not polymerized by ATRP.<sup>63</sup> Some nitrogen containing monomers can retard the polymerization by displacing the terminal halogen of a growing chain or by participating in transfer reactions.<sup>46</sup>

ATRP has been successfully carried out in bulk, solution, suspension, emulsion and even in the gas phase or from solid surfaces.<sup>46,47,63</sup> In solution polymerization, not only the organic solvents, but also aqueous solutions and supercritical carbon dioxide have been used as

solvent.<sup>46</sup> The growth of the polymer from the solid surface, planar surfaces or spherical particles, shows promise in the fields of lithography, lubrication and biomedicine.<sup>47</sup> In this method, the initiators are usually grafted onto the surfaces and thus the chains can be grown solely from the surfaces.<sup>64</sup>

## 1.2.2 ‘Click’ chemistry

‘Click’ chemistry is a powerful organic synthesis approach introduced by Sharpless et al. in 2001.<sup>65</sup> A reaction classified as ‘click’ chemistry should be modular, stereospecific, tolerant to functional groups, wide in scope, operational simple, give very high yields and generate only safe by-products.<sup>65</sup> Well known reactions that meet these criteria include the Diels-Alder reaction, thiol-ene reaction, and copper (I) catalyzed Huisgen 1,3-dipolar azide alkyne cycloaddition reaction (CuAAC)<sup>65</sup> as shown in Figure 1.3. Among them, the CuAAC, discovered independently by the Meldal group in ~ 2001-2002<sup>66, 67</sup> and the Sharpless group in ~ 2002<sup>68</sup>, proves superior over others for the facts that the two reactants (azide and alkyne) are of individual low reactivity and as only a catalytic quantity of the metal salt is required to accelerate the reaction.<sup>69</sup>

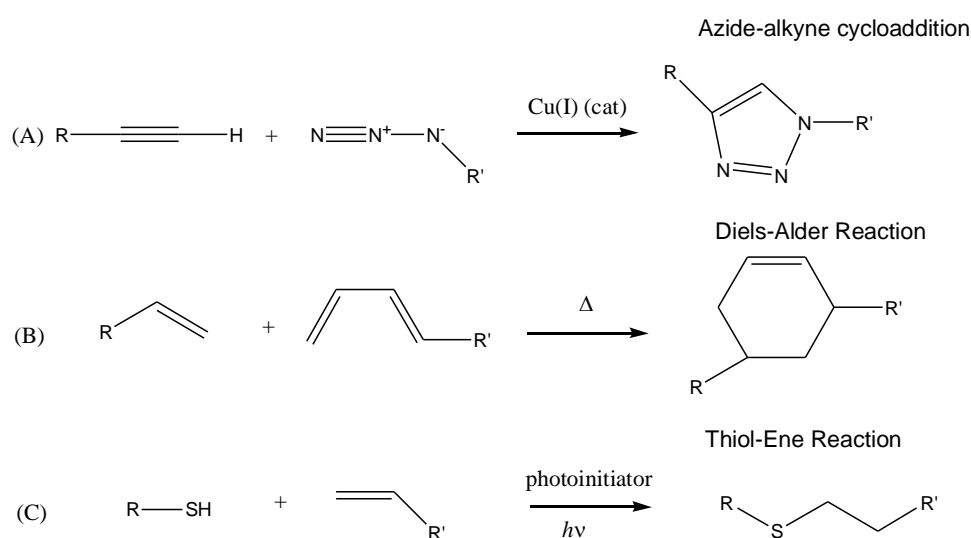


**Figure 1.3.** Examples of ‘click’ chemistry.

Compared to the pure thermal 1,3-dipolar cycloaddition reaction discovered by Huisgen, the CuAAC only gives 1,4-disubstituted 1,2,3-triazole rings and shows a much faster reaction rate.<sup>69</sup> It is considered that the unique mechanism of CuAAC is responsible for this high



regioselectivity and the rate acceleration.<sup>69</sup> The mechanism (depicted in Figure 1.4) of the CuAAC reaction has been recently explained as a stepwise process starting from the formation of a Cu(I)-acetylide  $\pi$ -complex, followed by azide complexation and cyclization.<sup>70</sup> Finally, protonation of the triazole-copper derivative and dissociation of the product regenerates the catalyst for further reaction cycles. In the reaction, the ligand is employed to protect the Cu ion from interactions and also prevent the oxidation of the Cu(I) to Cu(II).<sup>69</sup> Moreover, the ligand can function as a proton acceptor to eliminate the need for a base. Various pyridines, amines and triazoles, and phosphines have been utilized as ligands in CuAAC.<sup>71</sup> Different organic solvent, such as anisole, THF, DMF, and even water can be used as solvent.<sup>71-72</sup>

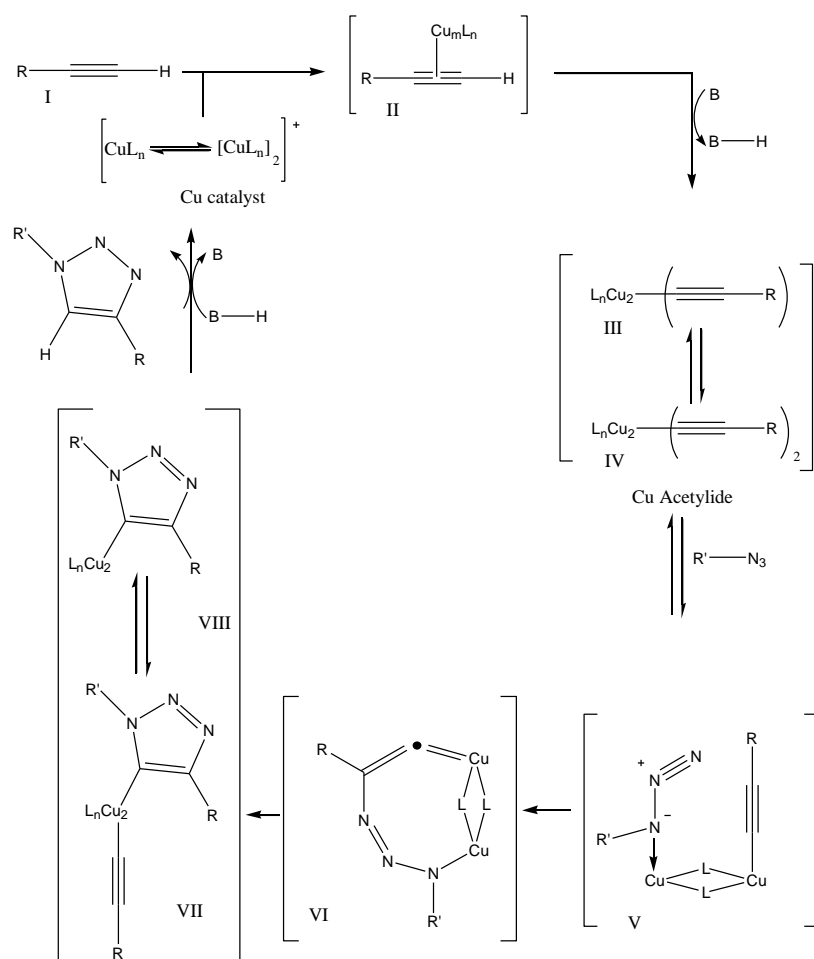


**Figure 1.4.** Proposed mechanism of CuAAC 'click' chemistry.<sup>69</sup>

Since the first applications of the CuAAC in polymer science were published in 2004,<sup>73-75</sup> it has become a very popular tool for functionalizing synthetic macromolecules to achieve various architectures and grafting the polymers onto solid surface (Figure 1.5). It is

demonstrated that CuAAC works equally well under homogeneous and heterogeneous condition.<sup>73-75</sup>

There are enormous interests in the preparation of polymers by combination of CuAAC ‘click’ chemistry with CRP, such as ATRP,<sup>71</sup> NMP,<sup>77</sup> and RAFT.<sup>78</sup> Among them, ATRP is certainly the most fitting polymerization method to be combined with the CuAAC.<sup>76</sup> Indeed, ATRP is a facile technique, which allows the preparation of well defined polymers with controlled chain length and architecture, narrow molar mass distribution, defined chain-ends, and controlled microstructure.<sup>71</sup> Basically, there are two approaches to prepare linear polymers by the combination of ATRP and CuAAC. One possibility involves the incorporation of azide/alkyne groups into the ATRP initiator structure. In this method, the polymerization process does not interfere with the presence of the azide/alkyne groups. Moreover, the one-pot sequential procedure can be used in this approach since the ATRP and CuAAC can share a similar catalyst system.<sup>71</sup> Another possibility is using conventional ATRP initiators to prepare the polymer, and then the  $\omega$ -bromine chain-ends of polymers are transformed into azides by a nucleophilic substitution reaction and subsequently reacted with alkyne functional components. This approach requires that the ATRP polymerization is not carried out to completion; usually 90% conversion is the maximum. This is because the halogen group at the polymer chain end can be lost at high conversions causing a corresponding loss of the ability to be chain end functionalized.<sup>63</sup> The final products would be a mixture of functionalized polymer and homopolymers. In this work, the first strategy with an azide functional ATRP initiator has been employed for the synthesis of linear semitelechelics since the structure–property relationship of the HMSPs is one focus of this research.

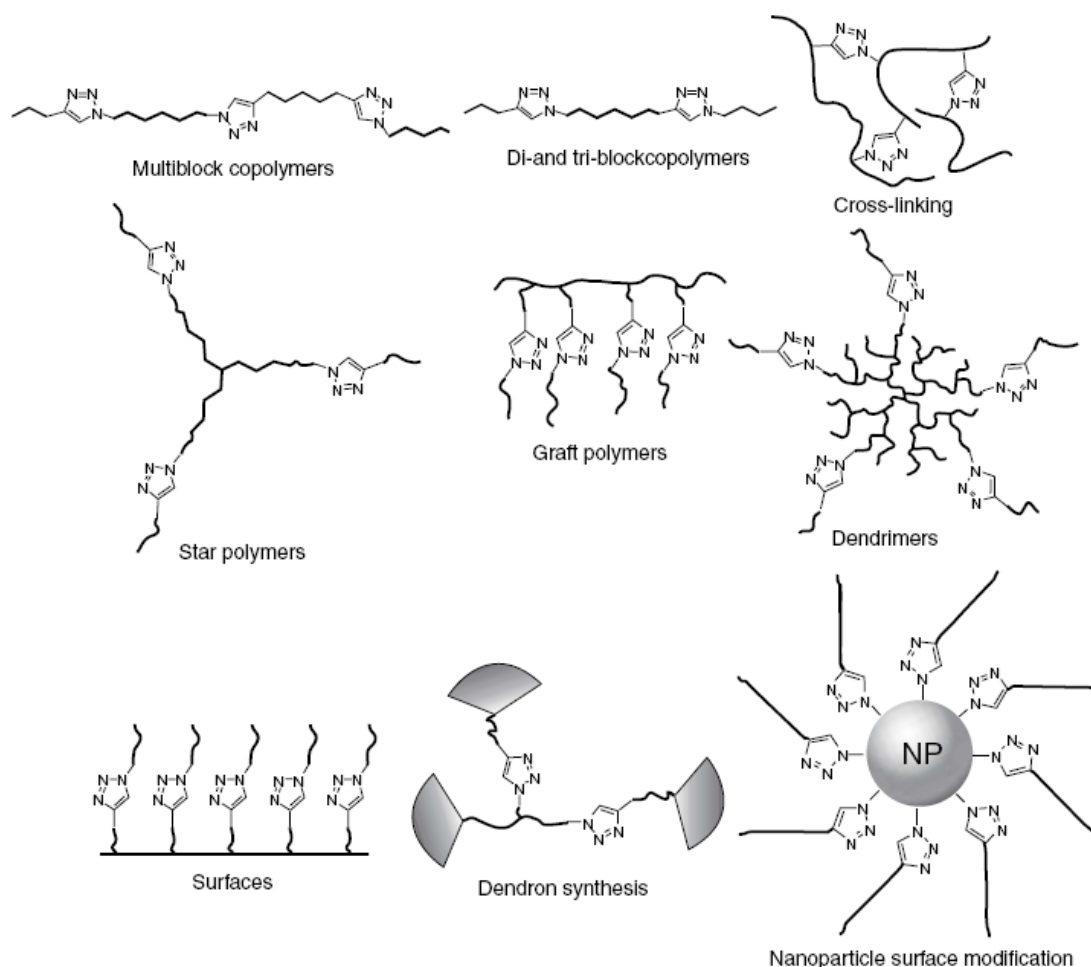


**Figure 1.5.** Polymer architectures obtained by “click” chemistry (reprint from ref. 76).

## 1.3 Chirality

### 1.3.1 General information about chirality

Chiral molecules are molecules which are not superimposable on its mirror image. Most typical examples of chiral substances are compounds that have an asymmetric carbon atom, which is a carbon atom bonded to four different groups. Some chiral molecules can lack asymmetric atoms but possess other chiral elements, such as axial, planar or helical chirality.<sup>79</sup> Figure 1.6 show molecules with different chiral elements. The two mirror images in chiral molecules are referred to as enantiomers. An unambiguous description of the absolute configuration of the enantiomers is given in the Cahn-Ingold-Prelog (CIP) rules. Detailed information about the CIP rule can be found elsewhere.<sup>80</sup> Enantiomers usually show identical chemical and physical properties in achiral environment. However, they can be distinguished from each other in an environment containing other chiral molecules via

diastereomeric interaction.<sup>79</sup> The mixture of equal amounts of left and right handed enantiomers, referred as racemate, is optically inactive and may have different properties compared to the pure enantiomers. For example, the melting point of racemic conglomerate is lower than that of the pure enantiomers.<sup>81</sup>

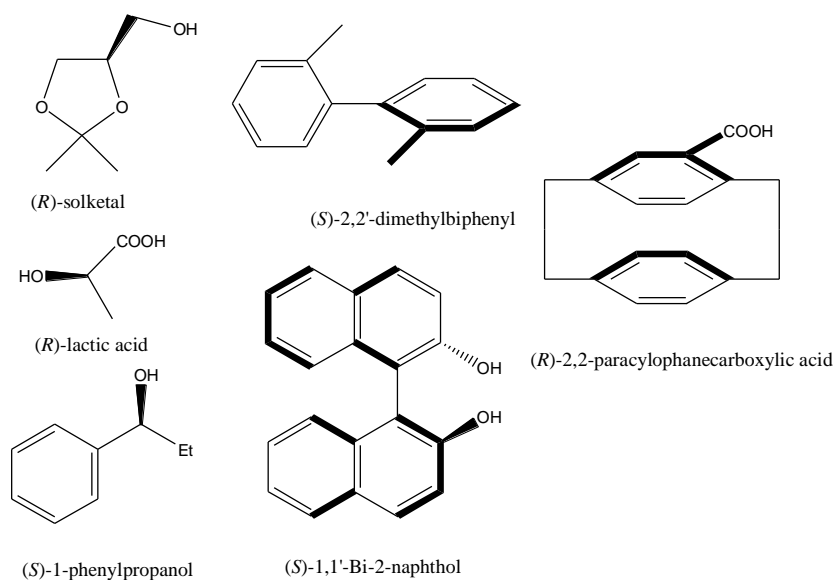


**Figure 1.6.** Chiral molecules with asymmetric carbon atom (left), chiral axis (middle) and chiral plane (right).

There is often a marked difference in the behavior of enantiomers in biological environments, which are constructed mainly by chiral molecules. Generally, in drugs, only one enantiomer is used to possess desired physiological effect while the other enantiomer is less active, inactive or results in adverse effects.<sup>81</sup> For example, in the case of propranolol, the *S*-enantiomer is responsible for the antihypertensive and antiarrhythmic property used in heart disease treatment but the *R*-enantiomer acts as a contraceptive.<sup>82</sup> The enantiomer purity is therefore especially important in drugs. Nowadays, the pharmaceutical industry has the requirement being imposed by United States Food and Drug Administration (FDA) that each enantiomer of newly produced drugs must be characterized when the product were to be marketed as a racemic mixture.<sup>84</sup>

### 1.3.2 Chiral polymers

Chiral polymers are polymers possessing a chiral structure anywhere in the polymer.<sup>85,86</sup> Most of the naturally occurring macromolecules such as polypeptides, polynucleotides, and polysaccharide are chiral polymers. They are essential for life. Recently, synthetic chiral polymers have attracted a great deal of interest for its potential applications; for example, it can be used as biological, pharmaceutical and medical materials, catalysts, and stationary phases of chromatography.<sup>87</sup>

According to the type and position of the chiral source, synthetic chiral polymers can be divided mainly into three categories, which are polymers possessing side chain chirality, polymers possessing main chain chirality (configurational backbone chirality) and helical polymers (conformational backbone chirality).<sup>85-87</sup> It has been shown in literature that chiral polymers can be prepared by various strategies, such as direct polymerization from chiral monomers (or chiral/achiral mixtures of monomers), attaching chiral ligands onto achiral polymer, polymerization of achiral monomers by using asymmetric polymerization techniques etc.<sup>88-90</sup>

For chiral polymers bearing a chiral pendant group or with configurational backbone chirality, the chirality of such polymers can be simply dependent on asymmetric centers in the chiral moieties.<sup>87</sup> Moreover, it can also arise from the main chain conformation when the polymer adopts a helical structure.<sup>88</sup> Since the first experimental evidence for the existence of helical structures in solution was reported by Pino and Lorenzi for synthetic polymer,<sup>91</sup> isotactic poly((*S*)-3-methyl-1-pentene), a synthetic helical polymer has become a main subject in the field of chiral polymers because broad applications and characteristic features are assumed.

Helical polymers can basically be divided into two groups in terms of the nature of the helical conformation. One is static helical polymers with high helix inversion barriers, while the other is dynamic helical polymer with low helix inversion barriers.<sup>90</sup> In general, the static helical polymers with a stable and rigid helical conformation are prepared by helix-sense selective polymerization using a chiral initiator or catalyst.<sup>90</sup> The helical conformation in dynamic helical polymer is easy to be changed. Therefore, it can be used to build chiral architectures that respond to interactions with small molecules, light or temperature.<sup>88</sup>

### 1.3.3 Chirality determination by NMR spectroscopy

Since the resonances of enantiotopic nuclei are isochronous while the resonances of diastereotopic nuclei are anisochronous, NMR spectroscopy does not allow distinguishing the enantiomers but allow differentiating between diastereoisomers.<sup>92</sup> The first experimental evidence of non-equivalent chemical shifts of diastereotopic nuclei in diastereoisomers was reported by Cram et al. in 1959.<sup>93</sup> By converting the enantiomers to diastereoisomers using a chiral auxiliary, the enantiomers can be distinguished according to different chemical shifts of characteristic resonance bands in their NMR spectra.<sup>92</sup> The enantiomeric purity can be further determined from the ratio of the integral of the resonance bands between the formed diastereoisomers under suitable experimental conditions, that is, no racemization and kinetic resolution. Nowadays, there are two general chiral auxiliaries used for the enantiomer determination: chiral solvating agent (CSA)<sup>94</sup> and chiral derivatizing agent (CDA).<sup>95</sup>

#### 1.3.3.1 Chiral solvating agents

In this approach, the CSA provides the chiral environment for the enantiomers in NMR spectroscopy.<sup>94</sup> The general procedure is mixing the substrate (enantiomer) with enantiopure CSA and a nonchiral standard NMR solvent (cosolvent). The enantiomers associate with the CSA through non-covalent interactions such as hydrogen bonding, dipole-dipole interaction, electrostatic interaction, steric effects or  $\pi$ -stacking between electron-rich and electron-deficient aromatic rings to form the diastereoisomeric solution complexes, which may appear at different chemical shifts in NMR spectroscopy.<sup>94</sup> The advantages of this approach is that it needs no chemical manipulations (just mixing the CSA and substrate in a NMR cosolvent),<sup>95</sup> and it has no kinetic resolution.<sup>92</sup> It is therefore suitable to be used in enantiomeric purity determination. For example, 1-(9-anthryl)-2,2,2-trifluoroethanol has been successfully used to determine the enantiomeric purity of some lactones and ethers.<sup>96</sup> However, the chemical shift difference between the two enantiomeric complexes is usually small due to the weak interaction between the CSA and substrate.<sup>94,95,97</sup> In addition, the number of the cosolvents is limited. Polar solvents such as methanol, dimethylsuloxide and acetone tend to solvate dipolar groups of the reagent and substrates, and reduce the anisochrony between diastereomeric complexes.<sup>98</sup>

### 1.3.3.2 Chiral derivatizing agents

This approach involves the derivatization of the enantiomers with the enantiopure CDA to produce diastereomeric derivatives.<sup>95</sup> In contrast to using CSAs, the association between the CDAs and substrates is covalent. The resulting diastereoisomers have therefore much greater chemical shifts difference than those obtained by using CSAs. However, racemization and kinetic resolution are possible to occur during the formation of diastereoisomers during some derivatization processes. Generally, this problem can be minimized by employing excess CDA.<sup>98</sup>

One of the most important and promising applications of CDA is to determine the absolute configuration of chiral molecules. Methoxytrifluorophenyl acetic acid (MTPA), introduced by Mosher in 1969, is one of the most commonly used CDAs.<sup>99</sup> It has been successfully used to assign the absolute configuration of a broad range of alcohols and amines. Until now, numerous CDAs including  $\alpha$ -methoxyphenylacetic acid (MPA),<sup>100-101</sup> 9-anthrylmethoxyacetic acid (9-AMA)<sup>102-103</sup>, *N*-acetylphenylglycineboronic acid,<sup>104</sup> 1,1'-bi-2-naphthol<sup>105</sup> among others, have been developed to determine the chirality of chiral alcohols and amines. Most of these CDAs contain the following two groups for specific functions. One is the functional group, such as  $-\text{COOH}$  or  $-\text{B}(\text{OH})_2$ , to provide a reaction site with the substrates.<sup>95</sup> Another is the group which can produce the space-oriented anisotropic effect that selectively affects the specific constituents on the substrate, for example, aromatic or carbonyl groups.<sup>95</sup> Figure 1.7 lists several commonly used CDAs. Until now, the most commonly used nuclei in NMR spectroscopy are  $^1\text{H}$  and  $^{19}\text{F}$ .<sup>100-105</sup>  $^{29}\text{Si}$ <sup>106</sup> and  $^{31}\text{P}$ <sup>107</sup> nuclei have also been employed for the case of using silicon and phosphorus containing CDAs, respectively.

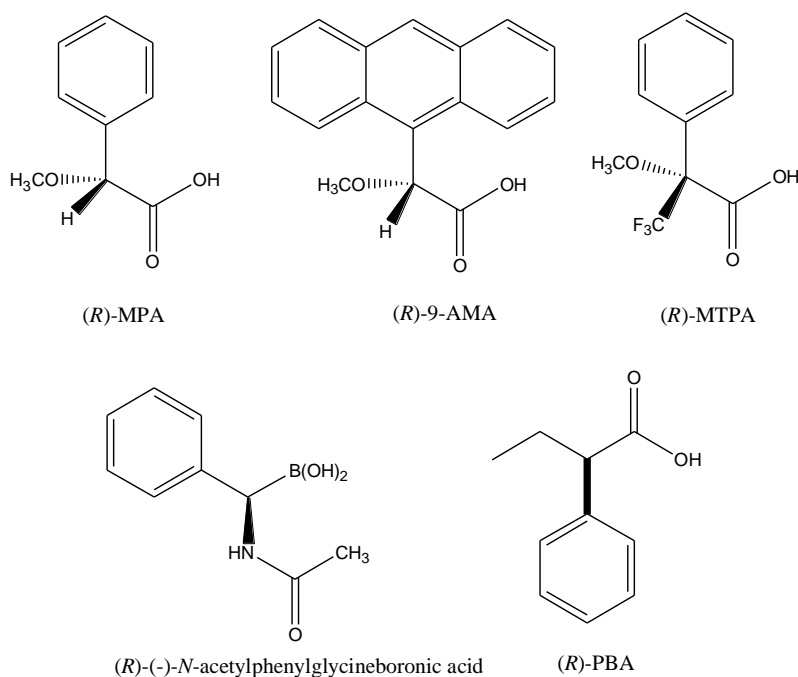


**Figure 1.7.** Examples of CDAs with *R* configuration.

Generally, NMR-based methods for the determination of the absolute configuration require the transformation of the chiral substrate to two different species that can be differentiated by NMR spectroscopy.<sup>92</sup> One popular procedure is that an enantiopure substrate is derivatized with the *R* and *S* enantiomers of the CDA to afford two diastereoisomers and the NMR spectra of the formed diastereoisomers are compared. The unknown configuration of the substrate can be correlated from known absolute configuration of the CDA according to the information obtained from NMR spectra.<sup>95</sup>

The relative positions of the substituents in the substrate with respect to the anisotropic group can be assigned with the help of the magnetic anisotropy effect,<sup>98</sup> i.e. the chemical shift changes depending on the special relationship between a proton and a nearby functional group, produced by the specific functional group (such as, but not limited to, aromatic rings, sulfoxides, and carbonyl groups) in CDAs. The anisotropy effect caused by the aromatic rings is the most dramatic example. Basically, the protons placed above the aromatic ring suffer a large shielding effect ( $-\delta$ ) while the protons at the side of the aromatic ring suffer a smaller deshielding effect ( $+\delta$ ).<sup>98</sup> Thus, most CDAs contain aromatic rings in order to mark the chemical shift difference. The signal of the chemical shift differences, expressed as ( $\Delta\delta$ ), of the specific protons/groups in the diastereoisomers derivatized by *R* and *S* CDAs provides information about the configuration of the substrate. In this approach,  $\Delta\delta^{RS}$ , calculated by using the chemical shift of one proton/group in the *R*-CDA derivative minus the



corresponding chemical shift in the *S*-CDA derivative, is preferably to be used as the expression of  $\Delta\delta^{RS}$ . In the case of a large anisotropy effect being produced by the CDAs, the chiral substrate may also be derivatized with only one enantiopure CDA (*R* or *S* form). The NMR spectrum of the derivate is directly compared with the pure substrate prior to derivatization.

### 1.3.4 Circular dichroism spectroscopy

Circular dichroism (CD) spectroscopy is a form of light absorption spectroscopy that measures the difference in absorption of right (*R*) and left (*L*) circularly polarized light by a substance. The CD spectroscopy plays an important role in biological research for the fact that it has a high sensitivity to ordered structures.<sup>108-112</sup> The most notable use of CD spectroscopy is for protein investigations such as the amount of secondary structures, the effects of environment (e.g. temperature, drug binding) on protein structure, protein-protein and protein-nucleic acid interactions, protein folding ect.<sup>108-110</sup> In the field of supramolecular chemistry, CD also has several interesting applications. In particular, the assembly of the molecules including monomers or polymers to form regular superstructures can be investigated.<sup>111,112</sup>

The superposition of the *R* and *L* circular polarized waves with equal amplitude and phase results in linearly polarized light. A very good animated tutorial about linear and circular polarized light as a function of time in three dimensions can be found on the website of <http://www.enzim.hu/~szia/cddemo/edemo0.htm>.

When planar polarized light passes through an optically active substance, the plane of the polarization of the polarized light will be rotated to an angle ( $\alpha$ ) because the *L* and *R* circular polarized light travel at different speeds, i.e. the medium has a different refractive index for the two forms of light ( $n_L \neq n_R$ ). This  $\alpha$  is dependent on the wavelength of the planar polarized light. Such an effect is called optical rotatory dispersion (ORD), which can be measured by ORD spectroscopy. The phenomenon of the absolute value of  $\alpha$  decreasing with the increase of wavelength, referred as plane curve, is usually observed in a chiral compound without a chromophore. An *S*-shaped component is superimposed on the plane curve in the regions of absorption, which is referred as anomalous curve, in the chiral compounds containing a chromophore.<sup>113</sup>

An absorbing optically active substance not only has the different refractive index for the *L* and *R* circularly polarized light, but also has a different absorption coefficients ( $\varepsilon$ ) for the *L* and *R* circular polarized light, that is  $\varepsilon_L \neq \varepsilon_R$ . The difference in  $\varepsilon_L$  and  $\varepsilon_R$  is the circular

dichroism. If planar polarized light passes through a molecule exhibiting a combination of ORD and CD in the regions of absorbance, the amplitude of the stronger absorbed component will be smaller than that of the less absorbed component and the polarization direction will be rotated. The consequence is that an elliptically polarized light emerges from the sample. Current CD spectroscopy measures the CD in terms of ellipticity  $\theta$  (usually expressed in milidegrees), which is mathematically determined by the angle  $\theta = \arctan(b/a)$  as shown in the Figure 1.8b. The  $\theta$  is related to the absorbance by

$$\theta = 33000 \times \Delta A = 33000 \times (\epsilon_L - \epsilon_R) \times c \times l \quad (1.1)$$

The literature data are usually reported in molar ellipticity  $[\theta]$

$$[\theta] = \theta / (10 \times c \times l) \quad (1.2)$$

where  $[\theta]$  is expressed in  $\text{deg} \times \text{cm}^2 \times \text{decimole}^{-1}$ ,  $c$  is concentration in  $\text{mol liter}^{-1}$  and  $l$  is optical path of the cell in cm.

Some references also report the CD data in molar circular dichroism  $\Delta\epsilon$ , which has the relations with  $[\theta]$  as

$$[\theta] = 3300 \times \Delta\epsilon \quad (1.3)$$

The plot of ellipticity vs wavelength of the incident light gives a CD spectrum. Depending on which circularly polarized light is absorbed stronger by an absorption band, a positive or negative CD signal is obtained. Both the CD and anomalous ORD effect are known as Cotton effect, and they are related by the so called Krönig-Kramers transformation.<sup>113</sup>

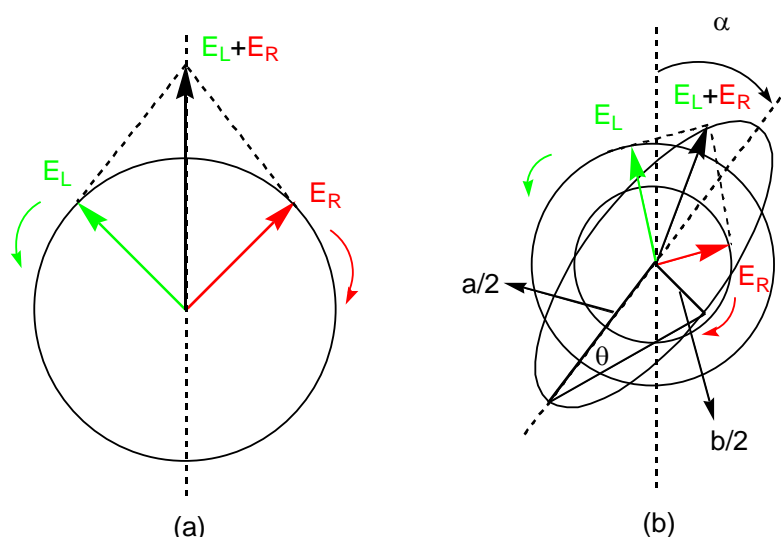


**Figure 1.8.** (a) Planar polarized light resolved into the  $L$  and  $R$  circular polarized lights with equal amplitude and phase. (b) Weaker  $L$  circular polarized light ( $E_L$ ) and stronger  $R$  circular polarized light ( $E_R$ ) absorption leads to ellipticity ( $\theta$ ), the major axis of the ellipse has been rotated through the angle  $\alpha$  due to the optical rotation.<sup>113</sup>

The Cotton effect is only possible to be observed in a substance containing a chromophore. The condition to show a Cotton effect is the possibility that the incident light can generate a helical displacement of charges. The absorption of one of the circularly polarized lights is preferred when its rotatory direction corresponds to the rotatory direction of the possible charge displacement and causes the Cotton effect.<sup>114</sup> Therefore, the nature of the asymmetric electron distribution of a molecule, which decides the left or right handedness, plays the crucial role in its CD spectrum. According to Moscovitz,<sup>115</sup> two types of chromophores can induce the Cotton effect, that is an inherently (or intrinsically) dissymmetric chromophore and a symmetrical chromophore but being dissymmetrically perturbed. The inherently asymmetric chromophore can give a strong Cotton effect since the occupied electron orbital and unoccupied orbital may be in a chiral relation. Some inherently dissymmetric chromophores are shown in Figure 1.9. Most chromophores such as carbonyl groups are locally symmetric. Their electron distribution is symmetric in an achiral environment and, therefore, they interact equally with *L* and *R* circularly polarized light. However, such kind of chromophores may have some dissymmetric perturbation of other symmetric orbitals when they are incorporated into a chiral environment, and thus give rise to a Cotton effect. For example, the observation of the Cotton effect of peptides is because of the introduction of asymmetry to the carbonyl electrons by the adjacent chiral centre.<sup>108</sup> The absorption of secondary structure of a polypeptide imposes a super-asymmetry chromophore which gives rise to characteristic Cotton effects by the coupling of oscillators with an asymmetric center or plane.<sup>110</sup>

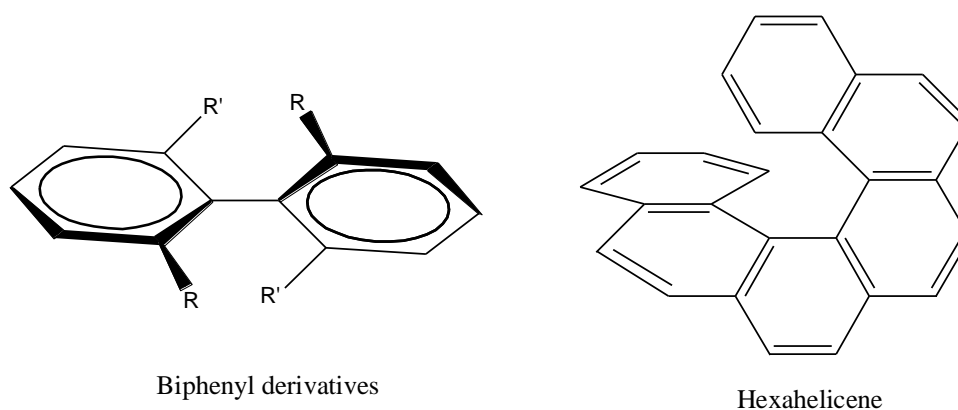


**Figure 1.9.** Examples of inherently dissymmetric chromophores.

## 1.4 Protein Resistance of Surfaces

The phenomenon of non-specific protein adsorption to surfaces has attracted much attention from many fields of sciences and industry for many years since it contributes to the degradation of the performance of surface-based diagnostic devices, biomedical implants and other medical devices.<sup>116-118</sup> It has been demonstrated that protein adsorption on surfaces is greatly influenced by molecular interactions between them. Such molecular interactions include intermolecular forces, hydrophobic interactions, hydrogen bonding, steric hindrance and electrostatic or ionic interactions.<sup>119,120</sup> Generally, coating surfaces with a thin layer for protein resistance materials, which could be small molecules or long chain polymers, is one universal method to minimize the problems arising from protein adsorption.<sup>121-126</sup> This, therefore, requires the development of materials having high efficiency for resisting protein adsorption.

To date, completely inert materials (show no adsorption for all proteins) have not been reported. After comparing a number of protein resistant small molecules, Whitesides et al. proposed properties including an overall neutral charge, hydrophilicity and the presence of hydrogen bond acceptors but not hydrogen bond donors are important for ensuring a material to resist protein adsorption.<sup>121-122</sup> However, the above mentioned structural characteristics are not adequate for some experimental data, like mannitol,<sup>123</sup> OH-terminated PEO,<sup>124-125</sup> as well as glycerol dendrol,<sup>126</sup> which contain hydrogen bond donors but exhibit high protein resistance.

Among various types of inert materials, PEO based materials are the most widely studied and best characterized systems. However, the exact mechanism for protein adsorption resistance of PEO is still unclear even many efforts have been done. Until now, several theories have been proposed, but none of them can explain the protein resistant behavior under all conditions. In the “steric repulsion” mode proposed by Andrade and de Gennes,<sup>127,128</sup> which is derived from colloidal stabilization theory and treats the protein as hard spheres and PEO chains as random coils, the water molecules bound to PEO have to be expelled when the proteins come close to the surface. This process is thermodynamically unfavourable and, thus, the PEG chains prevent the protein molecules from reaching the surface. This mode explains the system of high molar mass PEO well, but it does not fit the case of PEO always. Based on the model of Jeon et al. and using single chain mean field theory (SCMF), Szleifer proposed the loss of conformational entropy of the polymer chains during the approach of the protein molecules to be responsible for the protein repulsion.<sup>129-131</sup> The surface coverage of the polymer chains is most important. The experimental evidence was observed by Grunze et al.

that the conformation of the PEO chains plays a very important role in protein resistance. PEO on the gold surface displaying a helical conformation showed high protein resistance, whereas the densely packed “all-trans” monolayer on the silver surfaces exhibited a high fibrinogen adsorption.<sup>125</sup> Nowadays, it is generally accepted that factors including internal and terminal hydrophilicity, lateral packing density and the thickness, which can effect the structured water around the monolayer, are possibly to influence the protein resistance ability.

## 1.5 Motivation and Objectives of This Work

As remarked in the beginning of this chapter, there is a considerable and growing interest in the interpretation and understanding of the structure-properties relationships of fluorocarbon end capped water-soluble polymers for advanced applications. This motivated this research to create novel end capped hydrophobically modified water-soluble polymers.

Chapter 2 describes the investigation of the self-assembly behavior of perfluoroalkyl end-capped PNIPAM semitelechelics  $P_xF_9$  in aqueous solutions. The PNIPAM was chosen because it is a well studied thermoresponsive polymer and shows lower critical solution temperature (LCST) behavior at a specific temperature. The incorporation of a  $F_9$  segment to PNIPAM is expected to affect the LCST behavior of the polymer chains due to formation of the spherical micelles of  $P_xF_9$  in water. The  $P_xF_9$  semitelechelics are prepared by ‘clicking’ PNIPAM having an azide end group ( $P_xN_3$ ) with nonadecafluoro-1-decyl hex-5-ynoate ( $F_9$ ). The aqueous solution properties of  $P_xF_9$  semitelechelics and  $P_xN_3$  precursors at different temperatures (below, close and above the LCST) are studied and compared by dynamic light scattering (DLS) and by  $^1H$  and  $^{19}F$  NMR spectroscopy. The thermodynamics of the LCST of  $P_xF_9$  and  $P_xN_3$  in water is investigated by differential scanning calorimetry (DSC) since it can directly monitor the changes of the specific heat capacity ( $C_p$ ) of a solution as a function of temperature.

Poly(glycerol methacrylate) (PGMA) is considered as an important biocompatible polymer and it has been widely used as the hydrophilic component in amphiphilic or triphilic block copolymers showing attractive potentials as drug delivery vehicles.<sup>132-135</sup> Thus, polymers with analogous architectures as  $P_xF_9$  containing the same perfluoroalkyl end group but PGMA as the hydrophilic component are prepared via ATRP and CuAAC by using an azide functional initiator. The self-assembly behavior of perfluoroalkyl end capped PGMA ( $PGMA_xF_9$ ) in water is investigated through various techniques including surface tension measurement, DLS,  $^1H$  and  $^{19}F$  NMR spectroscopy and microscopic techniques. The strong hydrogen

bonding effect in the PGMA due to OH group on the side chains on the physical properties of PGMA<sub>x</sub>F<sub>9</sub> in water is investigated using temperature dependent <sup>1</sup>H and <sup>19</sup>F NMR spectroscopy and surface tension measurements. The thermodynamics of the micellization process of PGMA<sub>x</sub>F<sub>9</sub> in water is investigated and compared with PEO<sub>x</sub>F<sub>9</sub> via the estimation of the values of thermodynamic parameters as  $\Delta H^0_{mic}$  and  $\Delta G^0_{mic}$ , and ITC measurements. These results are give in detail in chapter 3.

PGMA is a typical chiral polymer because of the asymmetric carbon at the side chain. The enantiopure and racemic PGMA with a thiol group at one end are synthesized by ATRP. The optical activity of enantiopure PGMA is studied by using circular dichroism (CD) spectroscopy in water. The chirality of PGMA is determined via <sup>1</sup>H NMR spectroscopy employing a three-component chiral derivatizing process, involving the treatment of enantiopure polymers with 2-formylphenyl boronic acid and enantiopure  $\alpha$ -methylbenzylamine, which yields cyclic boronate diastereoisomer on the pendent groups. It is well known that biological systems are composed of many chiral biomolecules and shows a chiral preference.<sup>135</sup> To recognize the chiral effect on protein interactions, the enantiopure and racemic PGMA are grafted onto gold surfaces by immersing the gold substrates in polymer aqueous solutions to form the self-assembled monolayers (SAM) due to the strong affinity of the thiol group to gold. The protein adsorption behavior on the enantiopure and racemic polymer surfaces is measured and compared by surface plasmon resonance (SPR) using the bovine serum albumin (BSA) as a model protein. These results are discussed in chapters 4 and 5.

## 1.6 References

- (1) Strauss, U. P.; Jackson, E.G. *J Poly. Sci.* **1951**, *1*, 649-659.
- (2) Dubin, P.; Bock, J., Eds. In *Macromolecular Complexes in Chemistry and Biology*, Springer-Verlag: New York, 1994.
- (3) Glass, J. E., Eds. In *Water soluble polymers: beauty with performance, Advance in chemistry*, American Chemical Society: Washington, DC, 1986. 123.
- (4) Strauss, U. P., In *Polymers in aqueous media*, Glass, J.E. Eds., American Chemical Society: Washington DC, 1989, 223, 317-324.
- (5) Tanaka, R.; Meadows, J.; Phillips, G. O.; Williams, P. A. *Carbohydrate Polymers* **1990**, *12*, 443-459.
- (6) Aubry, T.; Moan, M. *J. Rheol* **1994**, *38*, 1681-1692.
- (7) Tam, K. C.; Farmer, M. L.; Jenkins, R. D.; Bassett, D. R. *J. Polym Sci. Part B: Polym. Phys.* **1998**, *36*, 2275-2290.
- (8) Semenov, A. N.; Joanny, J. F.; Khokhlov, A. R. *Macromolecules* **1995**, *28*, 1066-1075.
- (9) Winnik, M. A. Yekta, A. *Curr. Opin. Colloid & Interface Sci* **1997**, *2*, 424-436.
- (10) Persson, K.; Wang, G.; Olofsson, G. *J. Chem. Soc. Fara. Trans.* **1997**, *90*, 3555-3562.
- (11) Alami, E.; Almgren, M.; Brown, W., Francois, J. *Macromolecules* **1996**, *29*, 5026-5035.
- (12) Alami, E.; Almgren, M.; Brown, W. *Macromolecules* **1996**, *29*, 2229-2243.
- (13) Vorobyova, O.; Winnik, M.A. In *Associative polymers in aqueous solution*, Glass, J. R. Eds. American Chemical Society: Washington DC, 2000, 765, 143-162.
- (14) Xu, B.; Li, L.; Yekta, A.; Masoumi, Z.; Kanagalingam, S.; Winnik, M. A.; Zhang, K.; Macdonald, P. M.; Menschen, S. *Langmuir* **1997**, *13*, 2447-2456.
- (15) Hoang, K. C.; Mecozzi, S. *Langmuir* **2004**, *20*, 7347-7250.
- (16) Zhang, Y. X.; Da, A. H.; Butler, G. B.; Hogen-Esch, T. E. *J. Polym. Sci.. Part A.; Polym. Chem.* **1992**, *30*, 1383-1391.
- (17) Hwang F, S.; Hogen-Esch, T. E. *Macromolecules* **1995**, *28*, 3328-3335.
- (18) Zhou, J. C.; Zhuang; D. Q.; Yuan, X. F.; Jiang, M; Zhang Y.X. *Langmuir* **2000**; *16*, 9653-9661.
- (19) Li, M.; Jiang, M.; Zhang Y. X.; Fang Q. *Macromolecules* **1997**, *30*, 470-478.
- (20) Zhang, H. S.; Pan., J.; Hogen-Esch, T. E. *Macromolecules* **1998**, *31*, 2815-2821.
- (21) Preuschen, J.; Menschen, S.; Winnik, M. A.; Heuer, A.; Spiess, H. W. *Macromolecules* **1999**, *32*, 2690-2695.
- (22) Boschet, F.; Branger, C.; Margailan, A.; Condamine, E. *Polymer* **2002**, *43*, 5329-5334.
- (23) Racey, J. C.; Stebe, J. *Colloid Surf. A: Physiochem. Engng. Aspects* **1994**, *84*, 11.

- (24) Lodge, T. P.; Hillmyer, M. A.; Zhou, Z.; Talmon, Y. *Macromolecules* **2004**, *37*, 6680-6682.
- (25) Lodge, T. P. *Macromol. Chem. Phys.* **2003**, *204*, 265-273.
- (26) Zhou, Z.; Li, Z.; Ren, Y.; Hillmyer, M. A.; Lodge, T. P. *J. Am. Chem. Soc.* **2003**, *125*, 10182-10183.
- (27) Sawada, H. *J Fluorine Chem.* **2000**, *101*, 315-324.
- (28) Sawada, H. *J Fluorine Chem.* **2000**, *101*, 219-220.
- (29) Cathebras, N.; Collet, A.; Viguiet, M.; Berret, J. F. *Macromolecules* **1998**, *31*, 1305-1311.
- (30) Calvet, D.; Collet, A.; Viguiet, M.; Berret, J. F.; Serero, Y. *Macromolecules* **2003**, *36*, 449-457.
- (31) Berlinova, I. V.; Nedelcheva, A. N.; Samichkov, V.; Ivanov, Y. *Polymer* **2002**, *43*, 7243-7250.
- (32) Liao, D S.; Dai, S.; Tam, K. C. *Macromolecules* **2007**, *40*, 2936-2945.
- (33) Li, H.; Chen, H. Q.; Qing, S.; Zhang, Y. M. *J. Polym. Res* **2011**, *18*, 645-650.
- (34) Zhou, J. C.; Zhuang, D. Q.; Yuan, X. F.; Jiang, M.; Zhang, Y. X. *Langmuir* **2000**, *16*, 9653-9661.
- (35) Liu, R. C. W.; Cantin, S.; Perrot, F.; Winnik, F. M. *Polym: Adv: Tech:* **2006**, *17*, 798-803.
- (36) Zhang Y. X.; Fang, Q.; Fu, Y. Q.; Da, A. H.; Zhang, Y. B.; Wu, C.; Hogen-Esch, T. E. *Polym. Int.* **2000**, *49*, 763-774.
- (37) Zhang, Y. B.; Li, M.; Fang, Q.; Zhang, Y. X. Jiang, M.; Wu, C.; *Macromolecules* **1998**, *31*, 2527-2532.
- (38) Chen, J. Y.; Jiang, M.; Zhang, Y. X.; Zhou, H. *Macromolecules* **1999**, *32*, 4861-4866.
- (29) Zhuang, D. Q.; Hogen-Esch, T. E.; Zhang, Y. X. *J. Appl. Polym. Sci.* **2004**, *92*, 1279-1285.
- (40) Kubowicz, S.; Thünemann, A. F.; Weberskirch, R.; Möhwald, H. *Langmuir* **2005**, *21*, 7214-7219.
- (41) Chen, J.; Du, L. B.; Zhang, Y. X.; Hogen-Esch, T. E.; Jiang, M. *Polym. Int.* **2001**, *50*, 148-156.
- (42) Yoon, S. Y.; Lee, J. K.; Chung, I.; Park, S. S.; Lee, W. K. *Macromol. Symp.* **2007**, *150*, 431-436.
- (43) Lee, W. K.; Jeon, S.; Yoon, S. Y.; Lee, J. K.; Ha, C. S.; Gardella, J. A. *Macromolecular Research* **2006**, *14*, 487-490.



- (44) Cui, W.; Bei, J.; Wang, S.; Zhi, G.; Zhao, Y.; Zhou, X.; Zhang, H.; Xu, Y. *J. Biomed. Mater. Res. B Appl. Biomater.* **2005**, *73*, 171-178.
- (45) Lee, W. K.; Losito, I.; Gardella, J. A.; Hicks, W. *Macromolecules* **2001**, *34*, 3000-3006.
- (46) Matyjaszewski, K.; In *Controlled and Living Polymerizations*; Matyjaszewski, K.; Müller, A. H. E, Eds, WILEY-VCH Verlag GmbH&Co.KGaA: Weinheim, 2009; 103-166.
- (47) (a) Matyjaszewski, K.; Xia, J. *Chem. Rev.* **2001**, *101*, 2921-2990. (b) Matyjaszewski, K., *Macromolecules* **2012**, *45*, 4015-4039.
- (48) Tsarevsky, N. V.; Matyjaszewski, K. *Chem. Soc.* **2007**, *107*, 2270-2299.
- (49) Kamigaito, M.; Ando, T.; Sawamoto, M. *Chem. Rev.* **2001**, *101*, 3689-3745.
- (50) Patten, T. E.; Matyjaszewski, K. *Acc. Chem. Res.* **1999**, *32*, 895-903.
- (51) Kato, M.; Kamigaito, M.; Sawamoto, M.; Higashimura, T. *Macromolecules* **1995**, *28*, 1721-1723.
- (52) Wang, J. S.; Matyjaszewski, K. *J. Am. Chem. Soc.* **1995**, *117*, 5614-5615.
- (53) Cossens, V.; Nakagawa, Y.; Matyjaszewski, K. *Polym. Bull.* **1998**, *40*, 135-140.
- (54) Ando, T.; Kamigaito, M.; Sawamoto, M. *Macromolecules* **1997**, *30*, 4507-4510.
- (55) Ando, T.; Kamigaito, M.; Sawamoto, M. *Macromolecules* **1996**, *30*, 2244-2248.
- (56) Lecomte, Ph, Drapier, I.; Dubois, Ph.; Teyssie, Ph.; Jerome, R. *Macromolecules* **1997**, *30*, 7631-7633.
- (57) Granel, C.; Dubois, Ph.; Jerome, R; Teyssie, Ph. *Macromolecules* **1996**, *29*, 8576-8582.
- (58) Qiu, J.; Matyjaszewski, K. *Macromolecules* **1997**, *30*, 5643-5648.
- (59) Wang, J. L.; Grimaud, T.; Shipp, D. A.; Matyjaszewski, K. *Macromolecules* **1998**, *31*, 1527-1534.
- (60) Neugebauer, D.; Matyjaszewski, K. *Macromolecules* **2003**, *36*, 2598-2603.
- (61) Tsarevsky, N. V.; Braunecker, W.A.; Brooks, S.J.; Matyjaszewski, K. *Macromolecules* **2006**, *39*, 6817-6824.
- (62) Matyjaszewski, K.; Jo, S. M.; Paik, H. J.; Gaynor, S. G. *Macromolecules* **1997**, *30*, 2244-2248.
- (63) Ordian, G. In *Principles of polymerization*. 4<sup>th</sup> Edition, Wiley-Interscience, New Jersey, 2004.
- (64) Brantley, E. L.; Holmes, T. C.; Jennings, G. K. *J. Phys. Chem. B* **2004**, *108*, 16077-16084.
- (65) Kolb, H. C.; Finn, M. G.; Sharpless, K. B. *Angew. Chem., Int., Ed.* **2001**, *40*, 2004-2021.
- (66) Meldal, M.; Tornøe, C. W. In *proceedings of the second International and the Seventeenth American Peptide Symposium*, **2001**; 263-264.
- (67) Tornøe, C. W.; Christensen, C.; Meldal, M. *J. Org. Chem.* **2002**, *67*; 3057-3064.
- (68) Rostovtsev, V. V.; Green, L. G.; Fokin, V. V.; Sharpless, K. B. *Angew. Chem. Int. Ed.* **2002**, *41*, 2596-2599.
- (69) Binder, W. H.; Sachsenhofer, R. *Macromol. Rapid Commun.* **2007**, *28*, 15-54.
- (70) Bock, V. D.; Hiemstra, H.; Maarseveen, J.H. *Eur. J. Org. Chem.* **2006**, *1*, 51-68.

- (71) Golas, P. L.; Tsarevsky, N. V.; Sumerlin, B. S.; Matyjaszewski, K. *Macromolecules* **2006**, *39*, 6451-6457.
- (72) Chan, T. R.; Hilgraf, R.; Sharpless, K. B.; Fokin, V. V. *Org. Lett.* **2004**, *6*, 2853-2856.
- (73) Scheel, A. J.; Komber, H.; Voit, B. I. *Macromol. Rapid Commun.* **2004**, *25*, 1175-1180.
- (74) Helms, B.; Mynar, J. L.; Hawker, C. J.; Frechet, J.M. J. *J. Am. Chem. Soc.* **2004**; *126*, 15020-15021.
- (75) Binder, W. H.; Kluger, C. *Macromolecules* **2004**; *37*;9321-9330.
- (76) Binder, W. H.; Zirbs, R. In *Encyclopedia of Polymer Science and Technology*. John Wiley & Son Inc. 2009; 1-45
- (77) Binder, W. H.; Gloger, D.; Weinstabl, Allmaier, G.; Pittenauer, E. *Macromolecules* **2007**, *40*, 3097-3107.
- (78) Barner, L.; Davis, T. P.; Stenzel, M. H.; Barner-Kowollik, C. *Macromol. Rapid, Commun.* **2007**, *28*, 539-559.
- (79) Wolf, C. In *Dynamic Stereochemistry of chiral compounds: Principles and applications*. RSC Publishing, Cambridge. 2008.
- (80) Prelog, V.; Helmchen, G. *Angew. Chem. Int. Ed. Engl.* **1982**, *21*, 567-583.
- (81) Allinger, N. L.; Eliel, E. L., Eds, In *Topics in Stereochemistry*. John Wiley & Son, Inc. 1967.
- (82) Hulst, R.; Kellogg, R. M.; Feringa, B. L. *Recueil des Travaux chimiques des Pays-Bas*, **1995**; *114*, 115-138.
- (84) Eichelbaum, M.; Testa, B.; Somogyi, A. In *Atereochemical aspect of drug action and disposition*, Springer 2003, Berlin.
- (85) Okamoto, Y., Nakano, T. *Chem. Rev.* **1994**, *94*, 349-372.
- (86) Wulff, G. *Angew. Chem. Int. Ed.* **1989**, *28*, 21-37.
- (87) Kakuchi, T.; Sakai, R. In *Enciclopedia of polymer science and technology*, John Wiley & Sons, Inc. 2009.
- (88) Cornelissen, J. J. L. M.; Rowan, A. E.; Nolte, R. J. M.; Sommerdijk, N. A. J. M. *Chem. Rev.* **2001**, *102*, 4039-4070.
- (89) Hill, D. J.; Mio, M. J.; Prince, R. B.; Hughes, T. S.; Moore, J. S. *Chem. Rev.* **2001**, *101*, 3893-4012.
- (90) Nakano, T.; Okamoto, Y. *Chem. Rev.* **2001**, *101*, 4013-4038.
- (91) Pino, P.; Lorenzi, G. P. *J. Am. Chem. Soc.* **1960**, *82*, 4745-4747.
- (92) Parker, D. *Chem. Rev.* **1991**, *91*, 1441-1457.
- (93) Cram, D. J.; Mateos, J. L. *J. Am. Chem. Soc.* **1959**, *81*, 5150-5160.
- (94) Weisman, G. R. In *Nuclear Magnetic Resonance Analysis using Chiral Solvating Agents. In Asymmetric Synthesis*. Morrison, J. D. Ed.; Academic Press; New York, 1983, 153.
- (95) Seco, J. M.; Quinoa, E.; Riguera, R. *Chem. Rev.* **2004**, *104*, 17-117.

- (96) (a) Pirkle, W. H. *J. Am. Chem. Soc.* **1966**, *88*, 1837-1838. (b) Pirkle, W. H.; Adams, P. E. *J. Org. Chem.* **1980**, *45*, 4117-4121. (c) Pirkle, W. H.; Boeder, C. W. *J. Org. Chem.* **1977**, *42*, 3697-3700.
- (97) Pirkle, W. H.; Hoover, D. J. *Top Stereochem.* **1982**, *13*, 263-331.
- (98) Schreier, P.; Bernreuther, A.; Huffer, M. In *Analysis of chiral organic molecules: methodology and application.*; Walter de Gruyter & Co., Berlin, 1995.
- (99) Dale, J. A.; Dull, D. L.; Mosher, H. S. *J. Org. Chem.* **1969**, *34*, 2543-2549.
- (100) Trost, B. M.; Curran, D. P. *Tetrahedron Lett.* **1981**, *22*, 1287-1290.
- (101) Trost, B. M.; O'Krongly, D. O.; Belletire, J. L. *J. Am. Chem. Soc.* **1980**, *102*, 7595-7596.
- (102) Ferreira, M. J.; Latypov, Sh. K.; Quinta, E.; Riguera, R. *Tetrahedron: Asymmetry* **1996**, *7*, 2195-2198.
- (103) Latypov, Sh. K.; Quinta, E.; Riguera, R. *J. Am. Chem. Soc.* **1998**, *120*, 4771-4783.
- (104) Caselli, E.; Danieli, C.; Moranti, S.; Bonfiglio, B.; Forni, A.; Prati, F. *Org. Lett.* **2003**, *5*, 4863-4866.
- (105) Freire, F.; Quinta, E.; Riguera, R. *Chem Comm.* **2008**, *44*, 4147-4149.
- (106) Chan, T. H.; J-Peng, Q.; Wang, D.; Guo, J. A. *J. Chem. Soc., Chem. Commun.* **1987**, 325-330.
- (107) Anderson, R. C.; Shapiro, M. J. *J. Org. Chem.* **1984**, *49*, 1304-1305.
- (108) Bulheller, B. M.; Rodger, A.; Hirst, J. *Phys. Chem. Chem. Phys.* **2007**, *9*, 2020-2035.
- (109) Bayley, P. M. *Prog. Biophys. Mol. Biol.* **1973**, *27*, 1-76.
- (110) Oakley, M. T.; Bulheller, B. M.; Hirst, J. D. *Chirality*, **2006**, *18*, 340-347.
- (111) Amabilino, D. B. *Top Curr. Chem.* **2006**, *265*, 253-301.
- (112) Gottarelli, G.; Lena, S.; Masiero, S.; Pieraccini, S.; Spada, G. P. *Chirality* **2008**, *20*, 471-485.
- (113) Nakanishi, K.; Berova, N.; Woody, R. W.; Eds *Circular Dichroism Principles and applications*, VCH, 1994.
- (114) Snatzke, G. *Angew. Chem. Int. Ed.* **1968**, *7*, 14-25.
- (115) Moscovitz, A. *Tetrahedron* **1961**, *13*, 48-56.
- (116) Nuzzo, R. G.; Dubois, L. H.; Allara, D. L. *J. Am. Chem. Soc.* **1990**, *112*, 558-569.
- (117) Seigel, R. R.; Harder, P.; Dahint, R.; Grunze, M.; Josse, F.; Meksich, M.; Whiteside, G. M.; *Anal. Chem.* **1997**, *69*, 3321-3328.
- (118) Ulman, A.; In *An introduction to ultrathin organic films: from Langmuir-Blodgett to self assembly*. Academic Press: Boston, 1991.
- (119) Laibinis, P. E.; Whitesides, G. M.; Allara, D. L.; Tao, Y. T.; Parikh, A. N.; Nuzzo, R. G. *J. Am. Chem. Soc.* **1991**, *113*, 7152-7167.
- (120) Prime, K. L.; Whitesides, G. M. *Science* **1991**, *252*, 1164-1167.
- (121) Holmlin, R. E.; Chen, X.; Chapman, R. G.; Takayama, S.; Whitesides, G. M. *Langmuir* **2001**, *17*, 2841-2850.
- (122) Chapman, R. G.; Ostuni, E.; Takayama, S.; Holmlin, R. E.; Yan, L.; Whitesides, G. M. *J. Am. Chem. Soc.* **2000**, *122*, 8303-8304.

- (123) Luk, Y. Y.; Kato, M.; Mrksich, M. *Langmuir* **2000**, *16*, 9604-9608.
- (124) Prime, K. L.; Whitesides, G. M. *J. Am. Chem. Soc.* **1993**, *115*, 10714-10721.
- (125) Herrwerth, S.; Eck, W.; Reinhardt, S.; Grunze, M. *J. Am. Chem. Soc.* **2003**, *125*, 9359-9366.
- (126) Wyszogrodzka, M.; Haag, R. *Biomacromolecules* **2009**, *10*, 1043-1054.
- (127) Andrade, J. D.; Hladz, V. *Adv. Poly. Sci.* **1986**, *79*, 1-63.
- (128) Jeon, S. I.; Lee, J. H.; Andrade, J. D.; De Gennes, P. G. *J. Colloid Interface Sci.* **1991**, *142*, 149-158.
- (129) Szleifer, I. *Curr. Opin. Solid State Mater. Sci.* **1997**, *2*, 337-344.
- (130) Szleifer, I. *Curr. Opin. Colloid Interface Sci.* **1996**, *1*, 416-423.
- (131) Fang, F.; Szleifer, I. *Biophys. J.* **2001**, *80*, 2568-2589.
- (132) Pilon, L. N.; Armes, S. P.; Findlay, P.; Rannard, S. P. *Langmuir* **2005**, *21*, 3808-3813.
- (133) Kyeremateng, S. O.; Henze, T.; Busse, K.; Kressler, J. *Macromolecules* **2010**, *43*, 2502.
- (134) Thompson, K. L.; Armes, S. P.; York, D. W.; Burdis, J. A. *Macromolecules* **2010**, *43*, 2169-2177.
- (135) Zhang, M. X.; Qing, G. Y.; Sun, T. L. *Chem. Soc. Rev.* **2012**, *41*, 1972-1984.

## Chapter 2

### *The Aggregation Behavior of Poly(*N*-isopropylacrylamide) HMSP with a Perfluoroalkyl Segment in Water*

#### 2.1 Introduction

Poly(*N*-isopropylacrylamide) (PNIPAM), a typical thermo-responsive polymer, has been investigated widely due to its interesting behavior in aqueous medium showing a lower critical solution temperature (LCST) at around 32-34 °C,<sup>1-6</sup> changing with polymer concentration.<sup>7-10</sup> However, the effect of polymer molar mass of PNIPAM on the LCST has been a controversial topic. Some studies find a molar mass dependence of the LCST<sup>7-11</sup> whereas other reports claim a independence of the LCST.<sup>3,12-13</sup> Naturally, it can be assumed that there is a strong molar mass effect when using oligomers of PNIPAM in water that levels off when high molar masses of PNIPAM are used. The thermo-responsive property of PNIPAM and its related copolymers has attracted broad interest due to its potential applications in bioengineering.<sup>14,15</sup> Since the discovery that PNIPAM changes its solubility in water as a function of temperature in 1963,<sup>16</sup> numerous reports deal with the origin of the change from solubility to insolubility at elevated temperatures.<sup>17-19</sup> Based on the study of diluted aqueous PNIPAM solutions by static and dynamic light scattering, a coil-to-globule transition caused by dehydration of polymer chains during heating was postulated.<sup>3,17-19</sup> For concentrated aqueous PNIPAM solutions, phase separation at LCST occurs as a macroscopic manifestation of the coil-to-globule transition followed by aggregation.<sup>20</sup>

Compared to PNIPAM homopolymers, hydrophobically modified PNIPAMs (HM-PNIPAM) can exhibit unusual properties. As early as in the 1990s, a series of amphiphilic PNIPAMs was synthesized by free radical copolymerization using functionalized azo-initiators carrying a small number of long *n*-alkyl chains of C<sub>14</sub> or C<sub>18</sub> by Winnik et al.<sup>21,22</sup> For the random HM-PNIPAMs copolymers, micelles having a hydrophobic core and a PNIPAM corona are formed even in very diluted aqueous solutions at temperatures below the LCST. Above LCST the polymer micelles were disrupted and the hydrocarbon segments were distributed randomly among collapsed and aggregated PNIPAM chains.<sup>21</sup> More recently, PNIPAM with octadecyl terminus was prepared by free radical polymerization and studied by fluorescence spectroscopy.<sup>23</sup> At temperatures below LCST, also the formation of micelles in water was observed but at LCST the PNIPAM chains just collapsed onto the hydrophobic core but did not disrupted it. Winnik et al. have reported that HM-PNIPAM copolymers do not show a

strong change of the LCST compared to the unmodified PNIPAM caused by the fact that hydrophobic groups in the micelle core are not exposed to water but surrounded by PNIPAM chains.<sup>24</sup> In contrast, an extended conformation without any micelles or aggregates for HM-PNIPAMs was adopted in a good solvent as DMF at low concentrations.<sup>25</sup>

Among various types of hydrophobic groups, perfluorinated carbon chains are the most hydrophobic and their tendency to separate from water or hydrophilic groups is the largest.<sup>26</sup> It was reported that for non-ionic surfactants one CF<sub>2</sub> group is equivalent to 1.7 CH<sub>2</sub> groups.<sup>27</sup> Fluorocarbon-modified water soluble polymers are expected to exhibit unique properties in aqueous solution due to their high hydrophobicity. The fluorocarbon modified copolymers have a more pronounced tendency to form aggregates in water compared to their hydrocarbon analogues.<sup>28</sup>

This chapter focuses mainly on the temperature dependent phase transition behavior of perfluoroalkyl modified PNIPAM HMSP polymers (P<sub>x</sub>F<sub>9</sub>,  $x$  being the degree of polymerization of PNIPAM) in aqueous solution. The perfluorinated endgroup was obtained by attaching an alkyne functionalized perfluoroalkyl segment (F<sub>9</sub>) to the azide end group of PNIPAM (P<sub>x</sub>N<sub>3</sub>) through copper catalyzed 1,3-dipolar cycloaddition ('click') reaction.<sup>29</sup> The azide terminated P<sub>x</sub>N<sub>3</sub> was obtained by polymerization of NIPAM using functionalized azide-initiators.<sup>30</sup> The aqueous solution properties of P<sub>x</sub>N<sub>3</sub> precursors and the respective P<sub>x</sub>F<sub>9</sub> semitelechelics were investigated by NMR spectroscopy, dynamic light scattering (DLS) and differential scanning calorimetry (DSC). The results from various techniques suggest that the core-shell type micelles are formed for P<sub>x</sub>F<sub>9</sub> even at very dilute aqueous solutions (0.02 mg mL<sup>-1</sup>) at temperatures below LCST. The formation of micelles has an influence on the thermodynamics and kinetics of the LCST behavior of the P<sub>x</sub>F<sub>9</sub> HMSP.

## 2.2 Experimental Part

### 2.2.1 Materials

All chemicals were purchased from Sigma-Aldrich unless otherwise stated. Azide end-functionalized poly(*N*-isopropylacrylamide)s (P<sub>x</sub>N<sub>3</sub>) with different molar masses were synthesized as described elsewhere.<sup>30</sup> Nonadecafluoro-1-decyl hex-5-ynoate was synthesized according to the procedure described in literature.<sup>31</sup> *N*-Ethyl-diisopropylamine (DIPEA) (98%), tris(benzyltriazolymethyl)amine (TBTA) (97%), *n*-hexane (97%) and copper bromide (CuBr) (99.99%) were used without further purification. Tetrahydrofuran (THF) (99.5%) was distilled from potassium hydroxide and stored over molecular sieve.

### 2.2.2 Measurements

#### 2.2.2.1 NMR spectroscopy

The NMR measurements were performed on a “Gemini 2000” spectrometer (Varian) operating at 400 MHz for <sup>1</sup>H and 200 MHz for <sup>19</sup>F. <sup>1</sup>H and <sup>19</sup>F NMR data were obtained in CDCl<sub>3</sub> and D<sub>2</sub>O using a concentration of 20 mg mL<sup>-1</sup> for P<sub>x</sub>N<sub>3</sub> and P<sub>x</sub>F<sub>9</sub> at 27 °C and 25-55 °C, respectively. For a better accuracy the <sup>19</sup>F NMR spectra of P<sub>137</sub>F<sub>9</sub> in D<sub>2</sub>O were taken with a concentration of 40 mg mL<sup>-1</sup>.

#### 2.2.2.2 Size exclusion chromatography (SEC)

The molar masses and polydispersities ( $M_w/M_n$ ) were obtained using a Viskotek VE 2001 column equipped with RI detector Viscotek 3580 in *N,N*-dimethylformamide (DMF) using a flow rate of 1 mL min<sup>-1</sup> at room temperature. Monodisperse polystyrene was used as calibration standard.

#### 2.2.2.3 FTIR spectroscopy

FTIR spectra of the polymers were obtained using polymer powder pressed in KBr tablets by a Bruker Tensor 37 MIR Spectrometer. The sample was measured in transmission mode using a resolution of 2 cm<sup>-1</sup>.

#### 2.2.2.4 Surface tension measurements

All surface tension measurements were carried out on a DCAT11 tensiometer (DataPhysics Instruments GmbH, Filderstadt, Germany) by the Wilhelmy plate method. The temperature was kept at 23 °C with a circulating water bath system. The concentration of solutions was varied by the addition of aliquots of stock solution.

#### 2.2.2.5 Dynamic light scattering (DLS)

All DLS measurements were carried out on a commercial apparatus of ALV-Laser Vertriebsgesellschaft GmbH, Langen, Germany. The light source was a vertically polarized green neodymium: YAG DPSS-200 laser ( $\lambda = 532$  nm) from Coherent, Auburn, CA, USA, with a power output of 200 mW. The correlation functions from DLS were analyzed by the CONTIN method giving information on the distribution of decay rate ( $\Gamma$ ). Apparent diffusion coefficients were obtained from  $D_{\text{app}} = \Gamma/q^2$ , where  $\Gamma$  is the reciprocal of the characteristic decay time,  $q = (4\pi n_0/\lambda) \sin(\theta/2)$  being the scattering vector,  $n_0$  is the refractive index of the medium,  $\lambda$  is the wavelength of the light,  $\theta$  is the scattering angle. The samples were dissolved in Milli-Q water at several concentrations and then filtered through PTFE filters with 0.45  $\mu\text{m}$  pore size in order to remove the dust. The hydrodynamic radii ( $R_h$ ) were recorded for scattering angles from 30 to 130° in the temperature range of 5 to 55 °C. For the determination of the cloud point ( $T_{\text{cp}}$  identical with LCST), the scattering light intensity was measured at 90° from 5 to 55 °C after equilibrating the sample at a given temperature for 30 min. The average of two runs (60 s each) was recorded. The relative peak intensity is scaled with respect to the peak of the highest intensity which is put to an intensity of 1.

#### 2.2.2.6 Differential scanning calorimetry (DSC)

The thermal analyses were performed on a VP-DSC microcalorimeter (MicroCal Inc.) with a cell volume of 0.517 mL. The sample concentration was 2 mg mL<sup>-1</sup>. The heating and cooling rate was 1 °C min<sup>-1</sup>. The data were analyzed using MicroCal Origin 5.1 software supplied by the manufacturer.



### 2.2.3 ‘Click’ reaction

Generally, in a Schlenk flask equipped with a magnetic stirrer containing 0.03 mmol P<sub>x</sub>N<sub>3</sub> and 0.07 mmol nonadecafluoro-1-decyl hex-5-ynoate (F<sub>9</sub>), 5 mL THF was added and stirred for complete dissolution under nitrogen. Catalytic amounts of 0.12 mmol DIPEA, 0.007 mmol TBTA and 0.03 mmol CuBr were added to the solution. Further purging with nitrogen was carried out for another 10 min and the flask was placed in an oil bath at 50 °C for 48 h. The product was purified by passing through the silica column with THF as eluent, followed by precipitation into excess *n*-hexane. The product was dialyzed using a multi-purpose dialysis tubing (Spectra/Por 7 Membrane: MWCO: 2000 or 3500 Da) in water, and finally freeze-dried to give the purified P<sub>x</sub>F<sub>9</sub>. Yield: 62.9% for P<sub>28</sub>F<sub>9</sub> (containing 28 NIPAM units) and 48.1% for P<sub>137</sub>F<sub>9</sub> (containing 137 NIPAM units).

For P<sub>x</sub>N<sub>3</sub>

<sup>1</sup>H NMR (CDCl<sub>3</sub>, 400 MHz):  $\delta$  = 3.99 [s, -CH(CH<sub>3</sub>)<sub>2</sub>], 3.42 [s, -CH<sub>2</sub>CH<sub>2</sub>N<sub>3</sub>], 2.16 [s, -CH<sub>2</sub>CO], 1.63 [s, -CH<sub>2</sub>CH<sub>2</sub>CO], 1.12 [s, -CH(CH<sub>3</sub>)<sub>2</sub>].

For P<sub>x</sub>F<sub>9</sub>

<sup>1</sup>H NMR (CDCl<sub>3</sub>, 400 MHz):  $\delta$  = 4.61-4.54 [m, -CH<sub>2</sub>CF<sub>2</sub>-], 4.35-4.30 [m, -NHCH<sub>2</sub>CH<sub>2</sub>-], 3.99 [s, -CH(CH<sub>3</sub>)<sub>2</sub>], 2.77 [s, -CH<sub>2</sub>CH<sub>2</sub>CO-], 2.50-2.45 [m, -CH<sub>2</sub>(CH<sub>2</sub>)<sub>2</sub>CO-], 2.16 [s, -CH<sub>2</sub>CO], 1.63 [s, -CH<sub>2</sub>CH<sub>2</sub>CO], 1.17 [s, -CH(CH<sub>3</sub>)<sub>2</sub>].

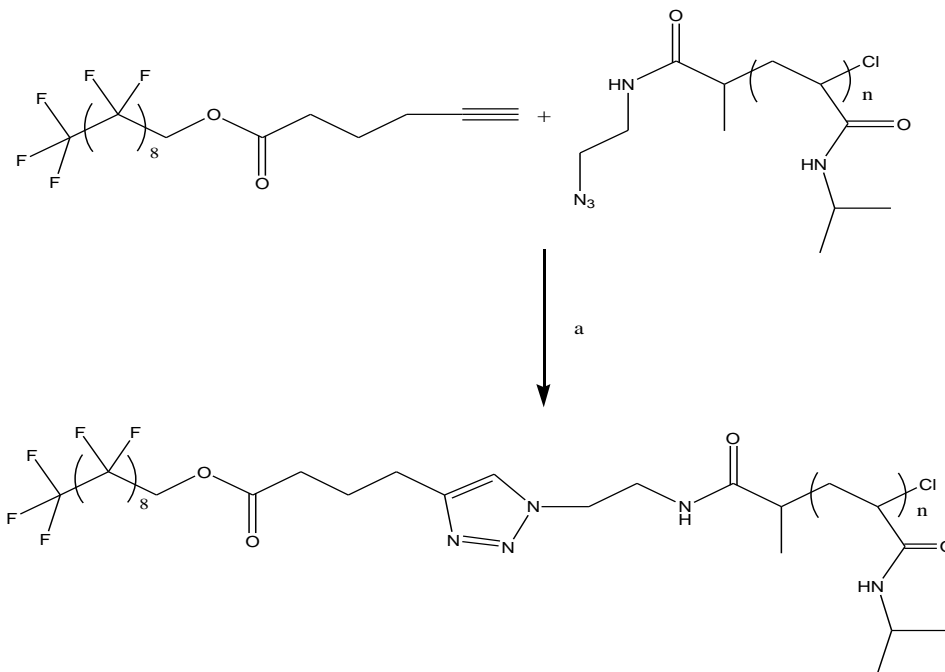
<sup>19</sup>F NMR (CDCl<sub>3</sub>, 200 MHz):  $\delta$  = -81.18 [s, -CF<sub>2</sub>CF<sub>3</sub>], -119.96 [s, -CH<sub>2</sub>CF<sub>2</sub>CF<sub>2</sub>-], -122.19- (-123.85) [m, -CF<sub>2</sub>(CF<sub>2</sub>)<sub>6</sub>CF<sub>2</sub>-], -126.56 [s, -(CF<sub>2</sub>)<sub>6</sub>CF<sub>2</sub>CF<sub>3</sub>].

## 2.3 Results and Discussion

### 2.3.1 ‘Click’ reaction for synthesis of P<sub>x</sub>F<sub>9</sub>

P<sub>28</sub>F<sub>9</sub> and P<sub>137</sub>F<sub>9</sub> are obtained by ‘click’ reaction of the alkyne functionalized F<sub>9</sub> with P<sub>x</sub>N<sub>3</sub> using the CuBr, DIPEA and TBTA catalyst system. The synthesis procedure is presented in scheme 2.1. For the reactions, a molar ratio of 2:1 for alkyne functionalized F<sub>9</sub>/P<sub>x</sub>N<sub>3</sub> is used due to the easy removal of non-reacted functionalized F<sub>9</sub> during the precipitation in *n*-hexane. The addition of small quantities of TBTA, one kind of polytriazole ligand, can stabilize Cu(I) and increases the reaction rate.<sup>32</sup> Figure 2.1 shows the SEC traces of two different P<sub>x</sub>N<sub>3</sub> samples and the corresponding ‘clicked’ samples containing the F<sub>9</sub> segment in the non-

selective solvent DMF. The traces of P<sub>28</sub>F<sub>9</sub> and P<sub>137</sub>F<sub>9</sub> shift to lower elution volume after 'click' reaction, and the polydispersities remain narrow. The characteristic data are given in the Table 2.1.



**Scheme 2.1.** 'Click' reaction of azide end-functionalized poly(*N*-isopropylacrylamide) (P<sub>x</sub>N<sub>3</sub>) and nonadecafluoro-1-decyl hex-5-ynoate (F<sub>9</sub>) using (a) CuBr, DIPEA, TBTA in THF at 50 °C.

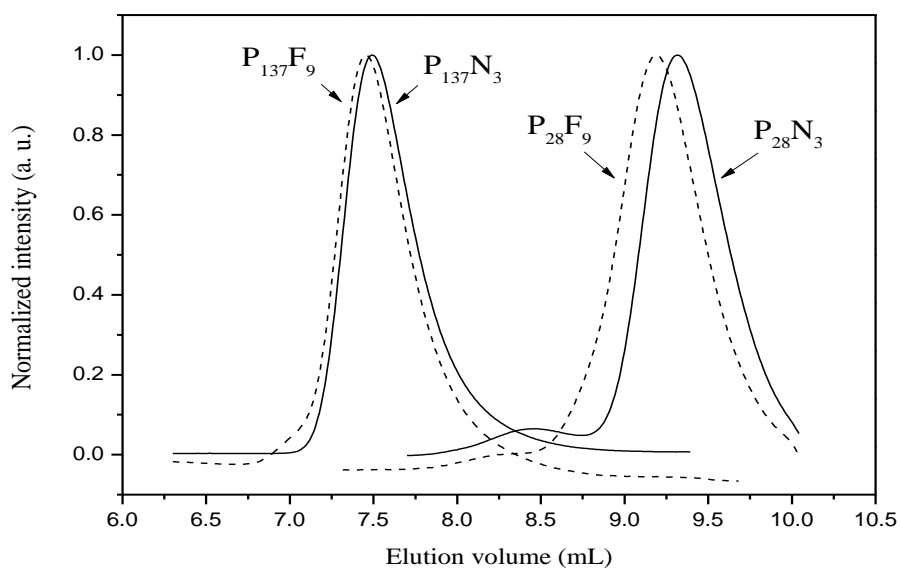


**Figure 2.1.** SEC traces of P<sub>28</sub>N<sub>3</sub>, P<sub>28</sub>F<sub>9</sub>, P<sub>137</sub>N<sub>3</sub>, and P<sub>137</sub>F<sub>9</sub> obtained at room temperature with DMF as eluent.

**Table 2.1.** Characteristic data of polymers.  $M_n$ , number average molar mass;  $M_w$ , weight average molar mass;  $T_{cp}$ , cloud point temperature;  $T_{max}$ , the temperature of maximum heat capacity;  $\Delta T_{1/2}$ , the width of the transition at half-height;  $\Delta H$ , the heat of transition per NIPAM unit;  $\Delta C_p$ , the difference in the heat capacity after and before the transition.

Polymer	$M_n$ <sup>a)</sup> (g mol <sup>-1</sup> )	$M_w/M_n$ <sup>b)</sup>	$T_{cp}$ <sup>c)</sup> (°C)	$T_{max}$ <sup>d)</sup> (°C)	$\Delta T_{1/2}$ <sup>d)</sup> (°C)	$\Delta H$ <sup>d)</sup> (kcal mol <sup>-1</sup> ·NIPAM <sup>-1</sup> )	$\Delta C_p$ <sup>d)</sup> (cal mol <sup>-1</sup> ·°C <sup>-1</sup> )
P <sub>28</sub> N <sub>3</sub>	3300	1.35	48.5	52.1	- <sup>e)</sup>	- <sup>e)</sup>	- <sup>e)</sup>
P <sub>28</sub> F <sub>9</sub>	3900	1.24	30.8	32.8	1.00	0.72	-550
P <sub>137</sub> N <sub>3</sub>	15700	1.21	35.8	36.5	- <sup>e)</sup>	- <sup>e)</sup>	- <sup>e)</sup>
P <sub>137</sub> F <sub>9</sub>	16300	1.22	32.2	33.5	0.47	1.40	-3950

<sup>a)</sup> obtained by <sup>1</sup>H NMR measurement in CDCl<sub>3</sub> at 27 °C; <sup>b)</sup> SEC measurement with DMF as eluent and PS standard; <sup>c)</sup> DLS measurement for 2 mg mL<sup>-1</sup> aqueous solution samples; <sup>d)</sup> DSC measurement for 2 mg mL<sup>-1</sup> aqueous solution samples using a heating rate of 1 °C min<sup>-1</sup>; <sup>e)</sup> data cannot be determined due to aggregation (see Figure 2.10a).

Figure 2.2 shows the <sup>1</sup>H NMR spectra of P<sub>28</sub>N<sub>3</sub> and P<sub>28</sub>F<sub>9</sub> obtained in CDCl<sub>3</sub> which is a good solvent for PNIPAM and also for the perfluorinated segment. The degree of polymerization ( $DP$ ) of the PNIPAM segment (Figure 2.2a) was calculated from the <sup>1</sup>H NMR spectra using the equation

$$DP = \frac{4 \times \text{Integral}(c)}{\text{Integral}(e, f)} \quad (2.1)$$

Both, the characteristic proton signals of PNIPAM and of the F<sub>9</sub> segment (the signals of  $g, i, j$  can be seen, the signal of  $h$  cannot be defined probably due to overlap) appear in the spectrum of P<sub>28</sub>F<sub>9</sub> (shown in Figure 2.2b) and the shift of protons  $e$  and  $f$  from 3.46 to 4.4 ppm (see inset of Figure 2.2b) indicated the successful ‘click’ reaction.<sup>30</sup> The successful reaction of P<sub>x</sub>N<sub>3</sub> and alkyne functional F<sub>9</sub> is further confirmed by FTIR measurements as shown in Figure 2.3. The characteristic absorption peak at around 2100 cm<sup>-1</sup> corresponding to the asymmetric stretching vibration of the azide group in P<sub>28</sub>N<sub>3</sub> completely disappears in the FTIR spectrum of the P<sub>28</sub>F<sub>9</sub>.

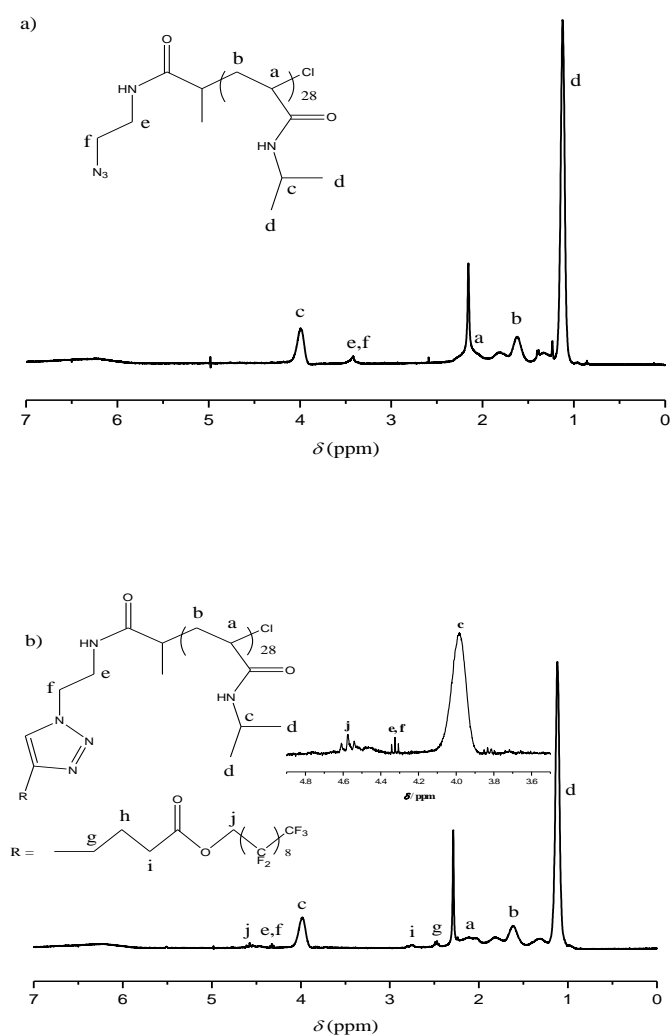


**Figure 2.2.**  $^1\text{H}$  NMR spectra obtained in  $\text{CDCl}_3$  at  $27^\circ\text{C}$ . (a)  $\text{P}_{28}\text{N}_3$ , and (b)  $\text{P}_{28}\text{F}_9$ .

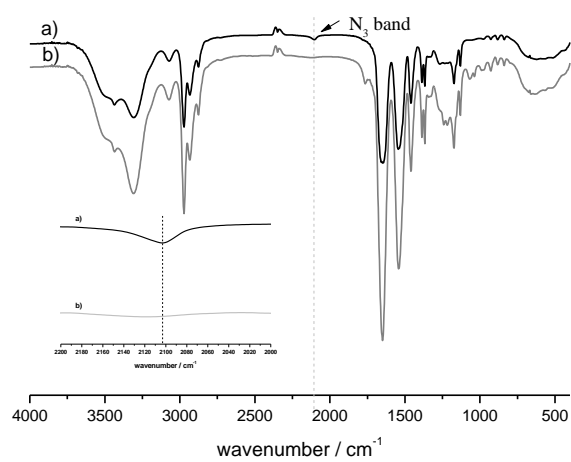


**Figure 2.3.** FTIR spectra of (a)  $\text{P}_{28}\text{N}_3$ , and (b)  $\text{P}_{28}\text{F}_9$ .

### 2.3.2 Determination of critical micellization concentration (cmc)

It is well known that the increase of surfactant concentration leads to a decrease in surface tension ( $\gamma$ ). The decrease vanishes with increasing surfactant concentration at cmc. In order to measure the cmc values of the semitelechelics P<sub>x</sub>F<sub>9</sub>, various amounts of aqueous polymer solutions were added to bidistilled water and the change of  $\gamma$  was monitored. P<sub>28</sub>F<sub>9</sub> has a cmc value of  $\sim 2.9 \times 10^{-3}$  mg mL<sup>-1</sup> (see Figure 2.4a) and P<sub>137</sub>F<sub>9</sub> shows a cmc value of  $\sim 1.5 \times 10^{-2}$  mg mL<sup>-1</sup> (see Figure 2.4b). The surface tensions of various aqueous solutions of P<sub>28</sub>N<sub>3</sub> were also measured without showing a cmc (see Figure 2.5).

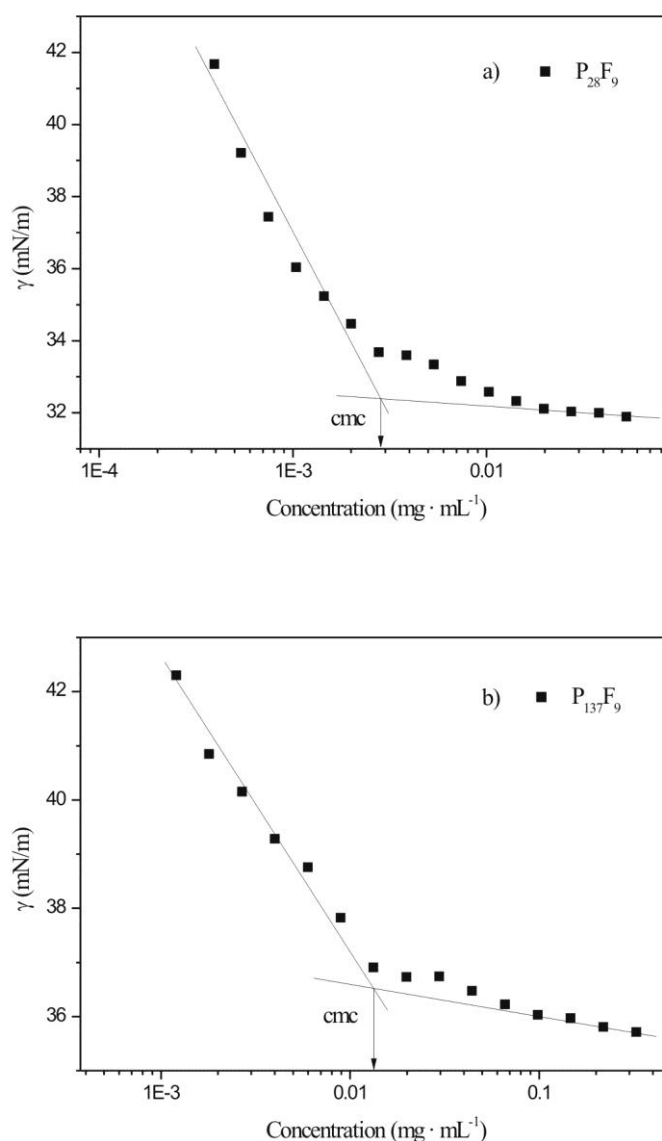


**Figure 2.4.** Determination of cmc using the surface tension ( $\gamma$ ) data for a) P<sub>28</sub>F<sub>9</sub> and b) P<sub>137</sub>F<sub>9</sub>.

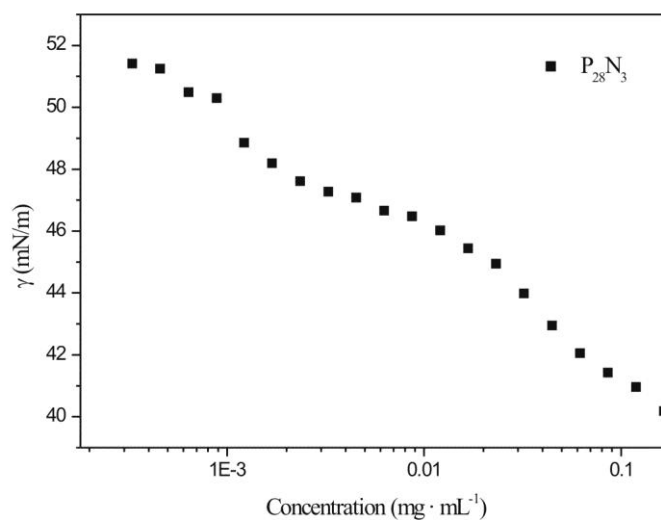


**Figure 2.5.** Surface tension ( $\gamma$ ) data at various concentrations of P<sub>28</sub>N<sub>3</sub>.

### 2.3.3 Dynamic light scattering

#### 2.3.3.1 Cloud point measurements

In light scattering measurements, the intensity of scattered light is affected by the size and the contrast of the particles. For P<sub>x</sub>N<sub>3</sub> and P<sub>x</sub>F<sub>9</sub> in water with a concentration of 2 mg mL<sup>-1</sup>, macroscopic phase separation above LCST leads to large particles and a cloudy solution. The determination of the cloud point temperatures ( $T_{cp}$ ) is shown in Figure 2.6. Below  $T_{cp}$  the scattering intensity remains nearly constant with increasing temperature. At  $T_{cp}$ , the intensity increases sharply within very narrow temperature ranges. It is clearly to see that fast transitions<sup>33</sup> are observed for the semitelechelics P<sub>x</sub>F<sub>9</sub>, while the precursors P<sub>x</sub>N<sub>3</sub> show broad transitions, which is more significant for the P<sub>28</sub>N<sub>3</sub>, showing a relatively small increase of the scattering intensity over ~ 10 °C. Such broad transition is most likely caused by the slow rate of aggregation.<sup>10</sup> This leads to the assumption that the F<sub>9</sub> segment attached to PNIPAM leads to a faster aggregation rate compared to P<sub>x</sub>N<sub>3</sub> and will be discussed below for the DSC measurements. The cloud point temperatures of all samples are listed in Table 1.  $T_{cp}$  values of 48.5 °C and 35.8 °C are obtained for P<sub>28</sub>N<sub>3</sub> and P<sub>137</sub>N<sub>3</sub>, respectively, from light scattering measurements using 2 mg mL<sup>-1</sup> solutions. These values are much higher than the  $T_{cp}$  values of PNIPAM homopolymers of similar molar mass and concentration in water reported in the literature (~ 38 °C for 2800 g mol<sup>-1</sup> and ~34 °C for 15700 g mol<sup>-1</sup>).<sup>11</sup> It suggests that azide end

groups act as a hydrophilic groups leading to an increase of  $T_{cp}$ .<sup>30</sup> The fact that the LCST of poly(*N*-alkylacrylamides), such as PNIPAM, can be raised or lowered via introduction of hydrophilic or hydrophobic comonomers was pointed out by Taylor and Cerankowski 30 years ago.<sup>34</sup> In our study, the  $T_{cp}$  of P<sub>28</sub>N<sub>3</sub> is ~ 10 °C higher compared to PNIPAM homopolymers but  $T_{cp}$  increases only by 3 °C in the case of P<sub>137</sub>N<sub>3</sub>. So the effect is more pronounced for polymers with low molar mass which is reasonable since the hydrophilic endgroup effects in polymers decrease generally with increasing molar mass. This phenomenon has also been described for the shift of the LCST to higher temperatures of poly(*N*-ethylacrylamide) in water after adding hydrophilic endgroups<sup>35</sup> After ‘clicking’ the F<sub>9</sub>-segments, the semitelechelics P<sub>28</sub>F<sub>9</sub> and P<sub>137</sub>F<sub>9</sub> showed  $T_{cp}$  values of 30.8 and 32.2 °C, respectively. The fact that only a ~ 0.8 °C difference of the cloud point temperature is observed between P<sub>137</sub>F<sub>9</sub> and PNIPAM homopolymers (see ref 11) with similar molar mass (15700 g mol<sup>-1</sup>) at a concentration of 2 mg mL<sup>-1</sup> indicates that polymer micelles with F<sub>9</sub>-segment core and PNIPAM corona have been formed which is in agreement with cmc measurements. The hydrophobic blocks forming the core of the micelles can avoid contact with water molecules which leads to the weak effect on the transition temperature.<sup>36</sup> However, there is an approximately 7 °C difference for P<sub>28</sub>F<sub>9</sub> and the PNIPAM homopolymer with similar molar mass at 2 mg mL<sup>-1</sup>. A possible explanation could be the short length of the PNIPAM segment in P<sub>28</sub>F<sub>9</sub>. It can be assumed that the micellar aggregation numbers ( $N_{agg}$ ) for P<sub>28</sub>F<sub>9</sub> is larger compared to P<sub>137</sub>F<sub>9</sub>. This has already been reported for PNIPAM telechelics with identical hydrophobic segments but different PNIPAM chain lengths.<sup>37</sup> The large  $N_{agg}$  and the short PNIPAM length of P<sub>28</sub>F<sub>9</sub> lead to a high chain density in the micelle corona. This limits the formation of water/polymer hydrogen bonds with the result of a lower LCST of P<sub>28</sub>F<sub>9</sub> compared to the PNIPAM homopolymer with similar molar mass.

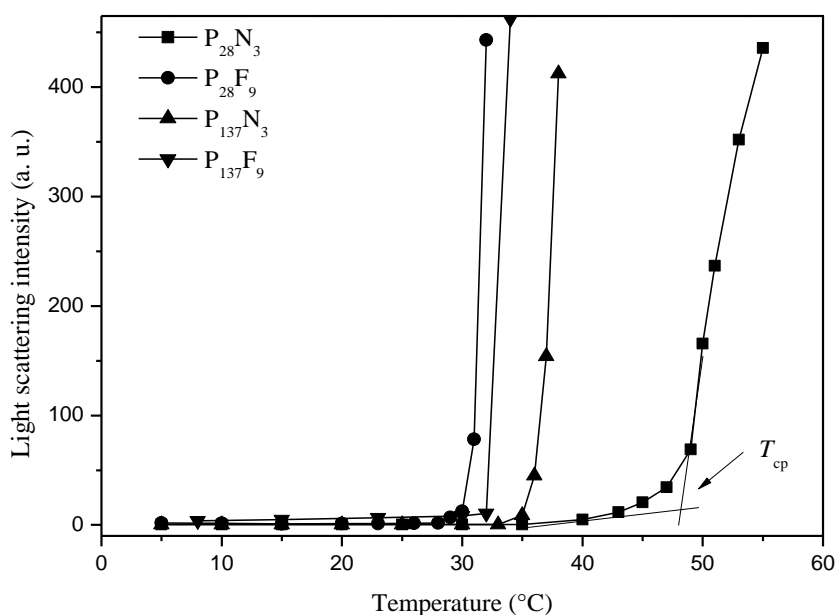


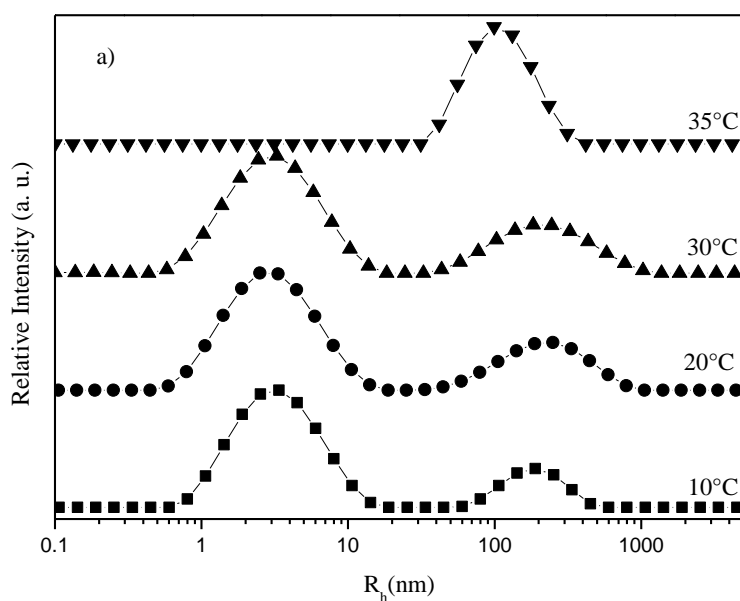
**Figure 2.6.** Cloud point temperatures ( $T_{cp}$ ) determined by measuring the light scattering intensity at  $90^\circ$  as a function of temperature for  $P_xN_3$  and  $P_xF_9$  by DLS at a concentration of  $2 \text{ mg mL}^{-1}$  in water.

### 2.3.3.2 $P_xN_3$ precursor polymers in aqueous solution

Depending on the PNIPAM concentration in water, the polymer chains can undergo macroscopic phase separation at temperatures above LCST.<sup>4</sup> Extremely diluted aqueous PNIPAM solutions do not show LCST behavior.<sup>18</sup> Figure 2.7 shows DLS measurements of a  $2 \text{ mg mL}^{-1}$   $P_{137}N_3$  aqueous solution for different temperatures below the LCST of this system ( $35.8 \text{ }^\circ\text{C}$ ). Above LCST, the solutions become turbid and DLS measurements are stopped. The temperature dependence of the hydrodynamic radius distribution calculated by Stokes-Einstein equation is depicted in Figure 2.7a. Two peaks appear in the temperature range between 10 and  $30 \text{ }^\circ\text{C}$ . The peak with higher intensity at  $\sim 3 \text{ nm}$  is observed at all angles (from  $30$  to  $130^\circ$ ) and the hydrodynamic radii are in good agreement with each other (deviation  $< 3\%$ ). This peak can be assigned to  $P_{137}N_3$  unimers. However, the peak with the weaker intensity shows a large scattering when measured at different angles at fixed temperature. The hydrodynamic radii vary in the range from 150 to 250 nm. We assume these species to be clusters of few polymer chains diffusing in a slow mode. They form loose aggregates in a dynamic exchange with unimers. Similar observations have also been reported for water soluble polymers with the tendency of self-association via hydrogen bonding, such



as poly(ethylene oxide) (PEO),<sup>38</sup> poly(vinyl alcohol) (PVA),<sup>39</sup> and poly(glycerol monomethacrylate) (PGMA).<sup>40,41</sup> By studying the temperature and salt effect on dilute aqueous PNIPAM solutions, Wu et al.<sup>42</sup> demonstrated that the slow mode is related to long range interactions between segments or ‘blobs’ of different polymer chains. Just below the LCST at 35 °C, the measurement is already influenced by the onset of the aggregation process of unimers of P<sub>x</sub>N<sub>3</sub>. A DLS signal appears exclusively for the slow mode, i.e. all unimers disappeared. This leads also to a linear plot of  $I$  over  $\sin^2(\theta/2)$ . The time dependence of hydrodynamic radii of P<sub>137</sub>N<sub>3</sub> at 35 °C is measured in order to study the kinetics of the aggregation process at 35 °C (see Figure 2.7b). The experiment at 35 °C is chosen for the time dependent measurements since the solution remained transparent at least for 2 days and became turbid within half minute when the temperature is raised by 1 °C. It can be seen that after an isothermal annealing at 35 °C for ~ 5 h ( $t_i$ ) the clusters are stable.



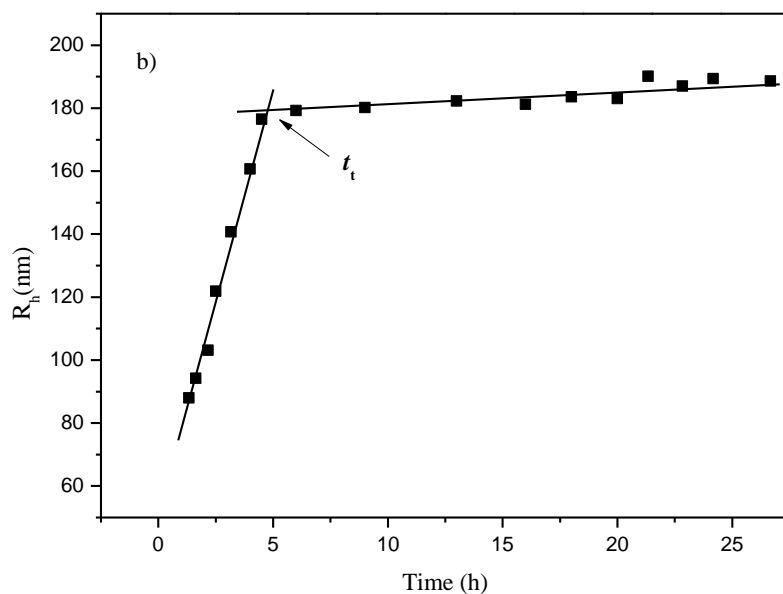


**Figure 2.7.** DLS measurements on P<sub>137</sub>N<sub>3</sub> solution samples at 2 mg mL<sup>-1</sup>,  $\theta = 90^\circ$ . (a) Temperature dependence of hydrodynamic radius distribution in water. (b) Time dependence of hydrodynamic radius at 35 °C.

### 2.3.3.3 P<sub>x</sub>F<sub>9</sub> in aqueous solution

A diluted aqueous P<sub>137</sub>F<sub>9</sub> solution is investigated by DLS at the concentration of 0.02 mg mL<sup>-1</sup> and different temperatures. Figure 2.8 shows the plots of the hydrodynamic radius  $R_h$  of P<sub>137</sub>F<sub>9</sub> as a function of temperature. The  $R_h$  value is nearly constant at ~12 nm for temperatures below the  $T_{cp}$  of 35 °C (which is slightly higher than the  $T_{cp}$  value of 32.2 °C of the same polymer at a concentration of 2 mg mL<sup>-1</sup>). This concentration dependence of the LCST is in agreement with measurements on PNIPAM homopolymers samples.<sup>7,10-11</sup> In this measurement, the solution remains transparent at 34 °C, and turns to turbid at 35 °C. As discussed above, an  $R_h$  value of ~ 3 nm was obtained for P<sub>137</sub>N<sub>3</sub> single polymer chains in water. So the species having a hydrodynamic radius of ~ 12 nm are polymeric micelles with F<sub>9</sub> segments in the core and PNIPAM as the corona. At temperatures larger than 30 °C but well below the LCST a sharp increase of  $R_h$  to ~ 110 nm is observed. The PNIPAM segments started to collapse on the micelle core, and several micelles associated together to form clusters driven by hydrophobic interactions of the collapsed dehydrated PNIPAM chains.<sup>25</sup>

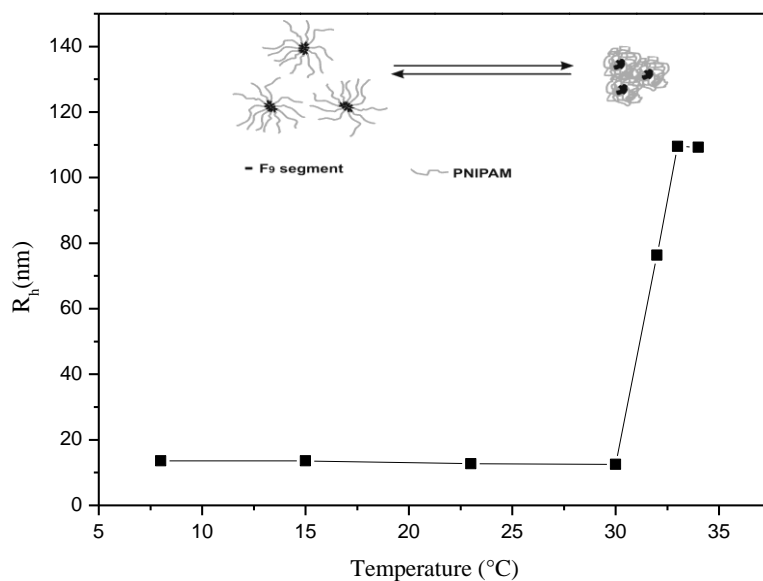


**Figure 2.8.** The hydrodynamic radius as a function of temperature for P<sub>137</sub>F<sub>9</sub> at 0.02 mg mL<sup>-1</sup>,  $\theta = 90^\circ$ . The scheme shows the temperature induced changes of the polymer aggregation behavior.

The same sample of P<sub>137</sub>F<sub>9</sub> is measured by DLS using three concentrations of 0.02, 0.2, and 2 mg mL<sup>-1</sup> in order to study the influence of concentration on the aggregation behavior. The hydrodynamic radius  $R_h$  distributions for all three concentrations measured at 23 °C are shown in Figure 2.9. A single polymer micelle peak at  $R_h$  of ~12 nm exists at the sample concentration of 0.02 mg mL<sup>-1</sup>. However, at higher concentrations of 0.2 and 2 mg mL<sup>-1</sup>, two species are coexisting with dimensions of ~12 and ~100 nm, respectively. This indicates the formation of aggregates at high polymer concentrations well below the LCST.<sup>43,44</sup>

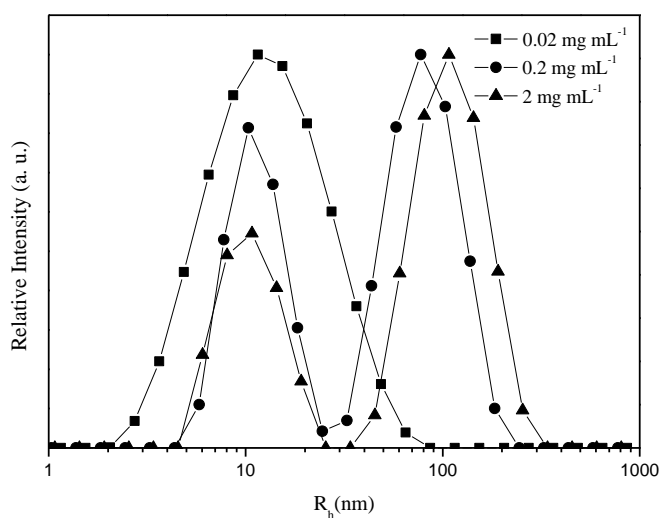


**Figure 2.9.** Concentration dependence of hydrodynamic radius distribution for P<sub>137</sub>F<sub>9</sub> aqueous solution samples at 0.02, 0.2, and 2 mg mL<sup>-1</sup> at 23 °C,  $\theta = 90^\circ$ .

### 2.3.3.4 Differential scanning calorimetry

Several studies have indicated that bound water around the amide group and the water cage around the isopropyl group lead to the water solubility of PNIPAM chains.<sup>45-48</sup> At temperatures above the LCST, these two ‘kinds’ of water would be released from the polymer chains into the bulk water.<sup>46,47</sup> DSC, which can monitor the changes of the specific heat capacity ( $C_p$ ) of a solution as a function of temperature, is a suitable tool to investigate the thermodynamics of the LCST of PNIPAM in water. Aqueous P<sub>x</sub>N<sub>3</sub> and P<sub>x</sub>F<sub>9</sub> solution samples at 2 mg mL<sup>-1</sup> were monitored by DSC using a heating rate of 1 °C min<sup>-1</sup> from 5 or 10 to 80 °C. Figure 2.10 displays the temperature dependence of  $C_p$  for P<sub>28</sub>N<sub>3</sub> and P<sub>28</sub>F<sub>9</sub> solutions. The runs for P<sub>137</sub>N<sub>3</sub> and P<sub>137</sub>F<sub>9</sub> solutions are not shown since they are very similar. DSC measurements can be influenced strongly by aggregation effects.<sup>49</sup> When large particles have formed and attached to the wall of the sample cell, they can affect the heat conductivity of the cell resulting in a strong scattering of the data. In the DSC traces of P<sub>28</sub>N<sub>3</sub> (see Figure 2.10a), a small increase in the baseline is observed until a strong endothermic peak starts to grow at 50 °C. This is the onset of the phase separation at LCST. The peak is endothermic due to the dehydration process of the macromolecules. The trace is taken up to 80 °C then the temperature is decreased to 5 °C again and a second heating run is started. A broad exothermic peak can be observed below 50 °C. This is obviously related to the dissolution process of larger aggregates that did not dissolve completely during cooling and annealing the

sample at 5 °C for 30 min. At 50 °C again the onset of the LCST is observed in the second heating trace. For the P<sub>28</sub>F<sub>9</sub> semitelechelic, narrow and completely reversible DSC heating traces are observed (see Figure 2.10b). This suggests that the collapse of P<sub>28</sub>F<sub>9</sub> at the LCST is much more cooperative than that of P<sub>28</sub>N<sub>3</sub>. Since DSC is a dynamic measurement, it can be concluded that P<sub>28</sub>F<sub>9</sub> has a fast phase transition compared to P<sub>28</sub>N<sub>3</sub>. This is in agreement with DLS data discussed above. The  $T_{\max}$  of P<sub>28</sub>F<sub>9</sub> is shifted by ~19 °C compared to P<sub>28</sub>N<sub>3</sub>. This is in agreement with cloud point measurements and the reasons for this shift have been discussed above. The characteristic data obtained from the DSC measurements for P<sub>x</sub>F<sub>9</sub> are listed in Table 2.1. The change of  $C_p$  can only be evaluated quantitatively for P<sub>x</sub>F<sub>9</sub>. The change of the heat capacity is negative when subtracting the  $C_p$  value below the LCST from the  $C_p$  value above the LCST. Similar to the phenomenon of the heat induced refolding of proteins following cold denaturation, the decreasing number of the polymer/water contact causes the decrease of the heat capacity.<sup>50</sup> A  $\Delta H$  value of the macroscopic phase separation at LCST of 1.4 kcal mol<sup>-1</sup> per NIPAM monomer unit is obtained for P<sub>137</sub>F<sub>9</sub>, which is in good agreement with the literature value of  $1.4 \pm 0.2$  kcal mol<sup>-1</sup> per NIPAM monomer unit for pure PNIPAM.<sup>51</sup> The smaller  $\Delta H$  and  $\Delta C_p$  values for P<sub>28</sub>F<sub>9</sub> compared to P<sub>137</sub>F<sub>9</sub> as seen in Table 2.1 indicate a smaller number of contacts between NIPAM monomer units and water. This results from the fact that to both precursor polymers an identical F<sub>9</sub> segment is added. Thus, P<sub>28</sub>F<sub>9</sub> is much more hydrophobic below the LCST compared to P<sub>137</sub>F<sub>9</sub>. For both semitelechelics, micelles are formed at temperatures below LCST. The PNIPAM chains close to the core of a micelle have entropic restrictions. Thus, they have difficulties to form contacts with water.<sup>52</sup> Therefore, they are less hydrophilic than the NIPAM monomer units far from the core. This leads to a higher percentage of unhydrated monomer segments in P<sub>28</sub>F<sub>9</sub> compared to P<sub>137</sub>F<sub>9</sub>.

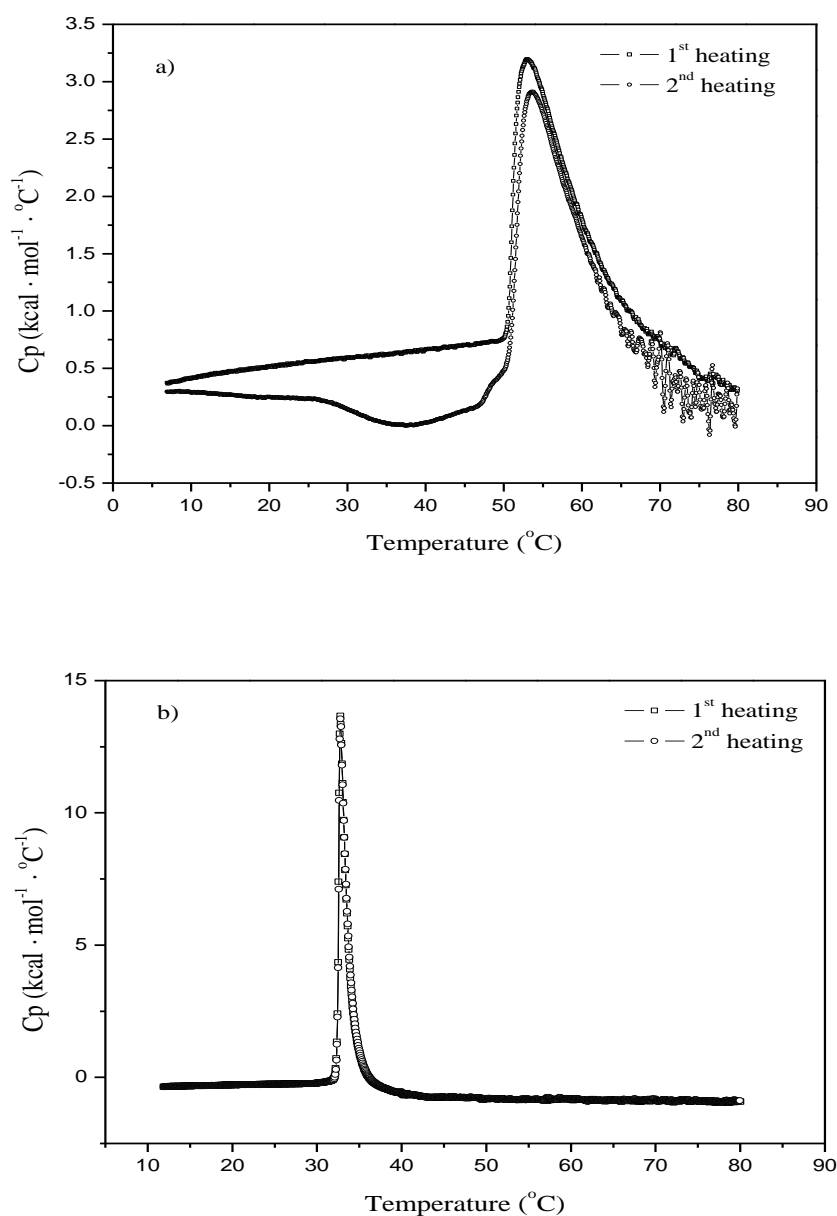


**Figure 2.10.** DSC traces for aqueous polymer solutions at 2 mg mL<sup>-1</sup> and a heating rate of 1 °C min<sup>-1</sup>. (a) P<sub>28</sub>N<sub>3</sub>, and (b) P<sub>28</sub>F<sub>9</sub>.

### 2.3.3.5 <sup>1</sup>H and <sup>19</sup>F NMR spectroscopy studies of the thermo-responsive behavior

Since NMR is able to detect the aggregation behavior of PNIPAM on a molecular level, it is an ideal technique for the determination of the thermo-responsive behavior of each component of the P<sub>x</sub>N<sub>3</sub> precursors and the P<sub>x</sub>F<sub>9</sub> semitelechelics.<sup>53</sup> <sup>1</sup>H and <sup>19</sup>F NMR spectra were recorded at various temperatures below and above LCST. Caused by the fact that solids do not contribute to the NMR signals when measured in the solution mode, the intensity of

proton signals can be used to monitor the aggregation and phase separation behavior of polymers in solvents. The <sup>1</sup>H NMR spectra of P<sub>28</sub>N<sub>3</sub> and P<sub>28</sub>F<sub>9</sub> at various temperatures are shown in Figure 2.11. The assignment of the protons is provided in detail elsewhere.<sup>53,54</sup> Both polymers P<sub>28</sub>N<sub>3</sub> and P<sub>28</sub>F<sub>9</sub> have an LCST at the temperature where the intensity of all protons decreases sharply. This decrease appears for P<sub>28</sub>N<sub>3</sub> between 51 to 52 °C as can be seen Figure 2.11a. In this temperature range the polymer chains start to aggregate and simultaneously they dehydrate. A similar behavior is observed for P<sub>28</sub>F<sub>9</sub> (see Figure 2.11b) but at lower temperatures between 35 and 36 °C in agreement with cloud point measurements. Figure 2.8c shows the <sup>1</sup>H NMR spectra of for P<sub>28</sub>N<sub>3</sub> (solid line) and P<sub>28</sub>F<sub>9</sub> (dashed line) at 25 °C using a concentration of 20 mg mL<sup>-1</sup>. It is clearly to see that the proton signal intensity of P<sub>28</sub>N<sub>3</sub> is much stronger than that of P<sub>28</sub>F<sub>9</sub>. Also the characteristic signals of methylene protons of the F<sub>9</sub>-segment cannot be seen in D<sub>2</sub>O. They are observed in CDCl<sub>3</sub> as discussed in Figure 2.2. A reasonable explanation for this behavior is that micelles with a core formed by F<sub>9</sub>-segments and a PNIPAM corona are formed. This explains also the decreased intensity of the proton signals of PNIPAM because the packing of the NIPAM chains in the corona causes reduced chain mobility. Reduction of polymer chain mobility leads to a decrease and broadening of signal intensity in <sup>1</sup>H-NMR spectra.<sup>55</sup> In addition, the PNIPAM segments close to the micelle core are less hydrated and might finally not contribute to the proton signal intensity. This effect is more obvious for P<sub>28</sub>F<sub>9</sub> compared to P<sub>137</sub>F<sub>9</sub> due to the fact that, although, the F<sub>9</sub> segment is identical in both species, the degree of polymerization of the PNIPAM chain is higher in the case of P<sub>137</sub>F<sub>9</sub>.

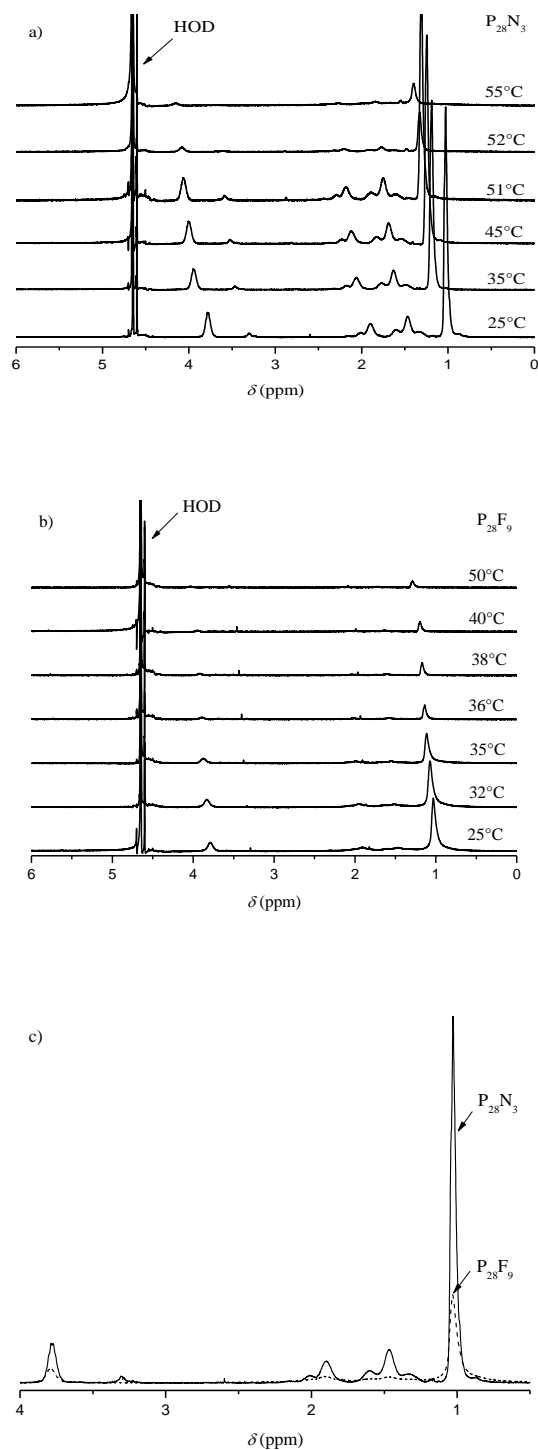


**Figure 2.11.** <sup>1</sup>H NMR spectra for P<sub>x</sub>N<sub>3</sub> and P<sub>x</sub>F<sub>9</sub> using a concentration of 20 mg mL<sup>-1</sup> at different temperatures in D<sub>2</sub>O. (a) P<sub>28</sub>N<sub>3</sub>, and (b) P<sub>28</sub>F<sub>9</sub>. (c) Comparison of proton intensity of P<sub>28</sub>N<sub>3</sub> (solid line) and P<sub>28</sub>F<sub>9</sub> (dashed line) in D<sub>2</sub>O at 25 °C.

The <sup>19</sup>F NMR spectra are recorded for P<sub>28</sub>F<sub>9</sub> in D<sub>2</sub>O at various temperatures and in CDCl<sub>3</sub> at 27 °C using a concentration of 20 mg mL<sup>-1</sup> (see Figure 2.12). The <sup>19</sup>F NMR spectrum of P<sub>28</sub>F<sub>9</sub>



in CDCl<sub>3</sub> shows peaks that can be assigned to the F<sub>9</sub> segment. Thus chloroform is a good solvent for PNIPAM and the F<sub>9</sub> segment. Water is definitively only a solvent for PNIPAM below the LCST and not a solvent for the F<sub>9</sub> segments at all temperatures below LCST. This results in a very weak <sup>19</sup>F signal which completely disappears above LCST. Identical results are obtained for P<sub>137</sub>F<sub>9</sub>. Thus the <sup>19</sup>F NMR measurements confirm the formation of micelles for P<sub>x</sub>F<sub>9</sub> in D<sub>2</sub>O below LCST.

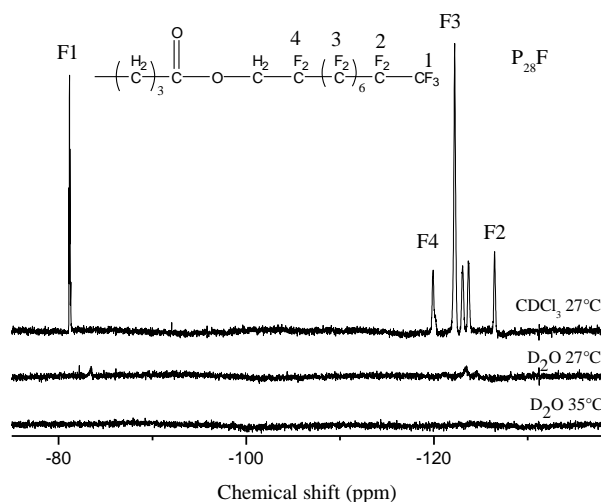


**Figure 2.12.** <sup>19</sup>F NMR spectra for P<sub>28</sub>F<sub>9</sub> using a concentration of 20 mg mL<sup>-1</sup> at 27 °C in CDCl<sub>3</sub> and at different temperatures in D<sub>2</sub>O.

## 2.4 Conclusion

The P<sub>28</sub>F<sub>9</sub> and P<sub>137</sub>F<sub>9</sub> semitelechelics were successfully synthesized by ‘clicking’ the alkyne functionalized F<sub>9</sub>-segment with the azide end group of P<sub>x</sub>N<sub>3</sub>. The aqueous solution properties of P<sub>x</sub>N<sub>3</sub> precursor polymers and P<sub>x</sub>F<sub>9</sub> semitelechelics were studied by NMR spectroscopy, DLS and DSC. The results obtained by the different methods are in excellent agreement. The LCST of P<sub>x</sub>F<sub>9</sub> semitelechelics shifted to lower temperature in comparison to their P<sub>x</sub>N<sub>3</sub> precursors. For P<sub>x</sub>F<sub>9</sub> at temperatures below LCST, single micelles with F<sub>9</sub>-segments core and PNIPAM corona were formed in diluted aqueous solutions, and clusters appeared and coexisted with micelles in concentrated solutions. Just below the LCST, first PNIPAM coronae collapsed onto the hydrophobic core, and several micelles aggregated to larger particles in the range of ~110 nm. This micelle formation is also responsible for the fact that the cloud point temperatures of P<sub>28</sub>F<sub>9</sub> and P<sub>137</sub>F<sub>9</sub> are very similar (~ 31 and ~ 32 °C at 2 mg

mL<sup>-1</sup>) in contrast to the precursors. P<sub>x</sub>N<sub>3</sub> exists in water as single chains below LCST which results in a strong molar mass dependence of the LCST as expected from the classical Flory-Huggins approach for the combinatorial entropy.<sup>56</sup> DSC measurements show that the collapse of P<sub>28</sub>F<sub>9</sub> at the LCST is much more cooperative than that of P<sub>28</sub>N<sub>3</sub>. The heat of phase separation  $\Delta H$  and the related change in specific heat capacity  $\Delta C_p$  is smaller for P<sub>28</sub>F<sub>9</sub> compared to P<sub>137</sub>F<sub>9</sub>. This indicates that P<sub>28</sub>F<sub>9</sub> is much more hydrophobic (partially dehydrated NIPAM segments) compared to P<sub>137</sub>F<sub>9</sub> below the LCST since the endothermal enthalpy change at LCST is mainly the result of dehydration of PNIPAM.

## 2.5 References

- (1) Scarpa, J. S.; Mueller, D.; Klotz, I. M. *J. Am. Chem. Soc.* **1967**, *89*, 6024-6030.
- (2) Heskins, M.; Guillet, J. E. *J. Macromol. Sci. Chem.* **1968**, *A2*, 1441-1445.
- (3) Fujishige, S.; Kubota, K.; Ando, I. *J. Phys. Chem.* **1989**, *93*, 3311-3313.
- (4) Schild, H. G. *Prog. Polym. Sci.* **1992**, *17*, 163-249.
- (5) Kawasaki, H.; Sasaki, S.; Maeda, H.; Nishinari, K. *Langmuir* **2000**, *16*, 3195-3199.
- (6) Okada, Y.; Tanaka, F. *Macromolecules* **2005**, *38*, 4465-4471.
- (7) Pamies, R.; Zhu, K. Z.; Kjøniksen, A. L.; Nyström, B. *Polym. Bull.* **2009**, *62*, 487-502.
- (8) Tong, Z.; Zeng, F.; Zheng, X.; Sato, T. *Macromolecules* **1999**, *32*, 4488-4490.
- (9) Zheng, X.; Tong, Z.; Xie, X.; Zeng, F. *Polym. J.* **1998**, *30*, 284-288.
- (10) Xia, Y.; Burke, N. A. D.; Stöver, H. D. H. *Macromolecules* **2006**, *39*, 2275-2283.
- (11) Xia, Y.; Yin, X. C.; Burke, N. A. D.; Stöver, H. D. H. *Macromolecules* **2005**, *38*, 5937-5943.
- (12) Otake, K.; Inomata, H.; Konno, M.; Saito, S. *Macromolecules* **1990**, *23*, 283-300.
- (13) Tiktopulo, E. I.; Uversky, V. N.; Lushchik, V. B.; Klenin, S. I.; Bychkova, V. E.; Ptitsyn, O. B. *Macromolecules* **1995**, *28*, 7519-7524.
- (14) Stayton, P. S.; Shimoboji, T.; Long, C.; Chilkoti, A.; Chen, G.; Harris, J. M.; Hoffman, A. S. *Nature (London)* **1995**, *378*, 472-474.
- (15) Hoffman, A. S.; Stayton, P. S. *Macromol. Symp.* **2004**, *207*, 139-151.
- (16) American Cyanamid Company 1963, *N-Isopropylacrylamide*, Brochure IC3-1354-500-4/63.
- (17) Kubota, K.; Fujishige, S.; Ando, I. *J. Phys. Chem.* **1990**, *94*, 5154-5158.
- (18) Wu, C.; Zhou, S. Q. *Macromolecules* **1995**, *28*, 8381-8387.
- (19) Wang, X.; Wu, C. *Macromolecules* **1999**, *32*, 4299-4301.
- (20) Chan, K.; Pelton, R.; Zhang, J. *Langmuir* **1999**, *15*, 4018-4020.
- (21) Ringsdorf, H.; Venzmer, J.; Winnik, F. M. *Macromolecules* **1991**, *24*, 1678-1686.
- (22) Winnik, F. M.; Davidson, A. R.; Hamer, G. K.; Kitano, H. *Macromolecules* **1992**, *25*, 1876-1880.
- (23) Yamazaki, A.; Song, J. M.; Winnik, F. M.; Brash, J. L. *Macromolecules* **1998**, *31*, 109-115.
- (24) Kujawa, P.; Goh, C. C. E.; Calvet, D.; Winnik, F. M. *Macromolecules* **2001**, *34*, 6387-6395.
- (25) Kujawa, P.; Watanabe, H.; Tanaka, F.; Winnik, F. M. *Eur. Phys. J. E.* **2005**, *17*, 129-137.

- (26) Sharma, S. C.; Acharya, D. P.; Garcia-Roman, M.; Itami, Y.; Kunieda, H. *Colloid Surf.* **2006**, *280*, 140-145.
- (27) Ravey, J. C.; Gherbi, A.; Stebe, M. J. *Prog. Colloid. Polym. Sci.* **1988**, *76*, 234-241.
- (28) "Water-Soluble Polymers: Synthesis, Solution Properties, and Applications", Shalaby, S. W.; McCormick, C. L.; Butler, G. B. Eds., ACS Symposium Series No. 467, American Chemical Society, Washington, DC, 1991.
- (29) Huisgen, R. "1, 3-Dipolar Cycloadditional Chemistry", Padwa, A. Ed., Wiley, New York, 1984, Vol. 1, p. 1.
- (30) Narumi, A.; Fuchise, K.; Kakuchi, R.; Toda, A.; Satoh, T.; Kawaguchi, S.; Sugiyama, K.; Hirao, A.; Kakuchi, T. *Macromol. Rapid Commun.* **2008**, *29*, 1126-1133.
- (31) Kyeremateng, S. O.; Amado, E.; Blume, A.; Kressler, J. *Macromol. Rapid Commun.* **2008**, *29*, 1140-1146.
- (32) Chan, T. R.; Hilgraf, R.; Sharpless, K. B.; Fokin, V. V. *Org. Lett.* **2004**, *6*, 2853-2855.
- (33) Zeng, K.; Wang, L.; Zheng, S. X. *J. Phys. Chem. B* **2009**, *113*, 11831-11840.
- (34) Taylor, L. D.; Cerankowsky, L. D. *J. Polym. Sci., Polym. Chem. Ed.* **1975**, *13*, 2551-2570.
- (35) Xue, W.; Huglin, M. B.; Jones, T. G. *J. Macromol. Chem. Phys.* **2003**, *204*, 1956-1965.
- (36) (a) Chung, J. E.; Yokoyama, M.; Aoyagi, T.; Sakurai, Y.; Okano, T. *J. Controlled Release* **1998**, *53*, 119-130; (b) Chung, J. E.; Yokoyama, M.; Suzuki, K.; Aoyagi, T.; Sakurai, Y.; Okano, T. *Colloids Surf. B* **1997**, *9*, 37-48.
- (37) Kujawa, P.; Tanaka, F.; Winnik, F. M. *Macromolecules* **2006**, *39*, 3048-3055.
- (38) Ho, D. L.; Hammouda, B.; Kline, S. R. *J. Polym. Sci., Part B: Polym. Phys.* **2003**, *41*, 135-138.
- (39) Liu, M. Z.; Cheng, R. S.; Wu, C. *J. Eur. Polym.* **1999**, *35*, 1907-1910.
- (40) Amado, E.; Augsten, C.; Mäder, K.; Blume, A.; Kressler, J. *Macromolecules* **2006**, *39*, 9486-9496.
- (41) Kyeremateng, S. O.; Amado, E.; Kressler, J. *J. Eur. Polym.* **2007**, *43*, 3380-3388.
- (42) Yuan, G. C.; Wang, C X. H.; Han, C.; Wu, C. *Macromolecules* **2006**, *39*, 6207-6209.
- (43) Kjøniksen, A. L.; Zhu, K. Z.; Pamies, R.; Nyström, B. *J. Phys. Chem. B* **2008**, *112*, 3294-3299.
- (44) Yamazaki, A.; Song, J. M.; Winnik, F. M.; Brash, J. L. *Macromolecules* **1998**, *31*, 109-115.
- (45) Ono, Y.; Shikata, T. *J. Am. Chem. Soc.* **2006**, *128*, 10030-10031.
- (46) Aseyev, V. O.; Tenhu, H.; Winnik, F. M. *Adv. Polym. Sci.* **2006**, *196*, 1-85.

- (47) Shibayama, M.; Mizutani, S.; Nomura, S. *Macromolecules* **1996**, *29*, 2019-2024.
- (48) Ebara, M.; Yamato, M.; Motohiro, H.; Aoyagi, T.; Kikuchi, A.; Sakai, K.; Okano, T. *Biomacromolecules* **2003**, *4*, 344-349.
- (49) Ding, Y. W.; Ye, X. D.; Zhang, G. *Z. Macromolecules* **2005**, *38*, 904-908.
- (50) Privalov, P.L.; Griko, Y.V.; Venyaminov, S.Y.; Kutyshenko, V.P. *J. Mol. Biol.* **1986**, *190*, 487-498.
- (51) Kujawa, P.; Winnik, F. M. *Macromolecules* **2001**, *34*, 4130-4135.
- (52) Kujawa, P.; Segui, F.; Shaban, S.; Diab, C.; Okada, Y.; Tanaka, F.; Winnik, F. M. *Macromolecules* **2006**, *39*, 341-343.
- (53) Deshmukh, M. V.; Vaidya, A. A.; Kulkarni, M. G.; Rajamohanan, P. R.; Ganapathy, S. *Polymer* **2000**, *41*, 7951-7960.
- (54) Zeng, F.; Tong, Z.; Feng, H. Q. *Polymer* **1997**, *38*, 5539-5544.
- (55) Riess, G. *Prog. Polym. Sci.* **2003**, *28*, 1107-1170.
- (56) Beaucage, G.; Stein, R. S.; Koningsveld, R. *Macromolecules* **1993**, *26*, 1603-1608.

### Chapter 3

## *Self-Assembly Behavior of Fluorocarbon-End Capped Poly(glycerol methacrylate) in Aqueous Solution*

### 3.1 Introduction

Hydrophobically modified water soluble polymers (HMSPs), which are composed of a hydrophilic main chain containing a few hydrophobic units being randomly in or at the end of the chain, have been extensively studied over the past several decades. Since the first study on a HMSP was carried out by Strauss et al.<sup>1</sup> in the early 50s of the last century, the HMSPs have invoked tremendous interest because of their unique rheological properties and potential applications, for example, they are widely used in the fields of detergent, mineral separation, pharmaceuticals, rheological control, enhanced oil recovery, paints and coating, etc.<sup>2,3</sup>

The fluorocarbon modified water soluble polymers (FMSPs) are known as one important class of HMSP and possess unique properties because of the intriguing characteristics of fluorinated moieties. Compared to the hydrocarbon group, the fluorocarbons are more stable, surface active and hydrophobic.<sup>4-11</sup> A rule of thumb for the hydrophobicity of fluorinated block is that one CF<sub>2</sub> group is equivalent to 1.7 CH<sub>2</sub> groups.<sup>12</sup> These unique properties are caused by the fact that the fluorine atom has a larger van der Waals radius, dense electron cloud, high ionization potential and very low polarizability.<sup>4</sup> Such characteristics make the FMSPs to have advantages in some aspects compared to their corresponding hydrocarbon analogous. For instance, FM-poly(ethylene oxide) (FM-PEO) presents a higher viscosifying effect than the hydrocarbon modified PEO due to the stronger hydrophobic association.<sup>9</sup>

It has been demonstrated that the end-capped FMSPs ( $R_F$ -P) can adopt a variety of unique properties such as high solubility and biological activities, which may not be achieved in randomly fluorinated polymers and fluorinated block polymers.<sup>14-15</sup> To date, a wide range of  $R_F$ -P including  $R_F$ -PEO,<sup>4,9-11,15</sup>  $R_F$ -poly(*N*-isopropylacrylamide) ( $R_F$ -PNIPAM),<sup>16-18</sup>  $R_F$ -poly(acrylic acid) ( $R_F$ -PAA),<sup>19-20</sup>  $R_F$ -poly(*N*-acylethylene imine) ( $R_F$ -PAI),<sup>21</sup>  $R_F$ -poly(dimethylacrylamide)s<sup>22</sup>,  $R_F$ -poly(lactic acid) ( $R_F$ -PLA)<sup>23,24</sup>,  $R_F$ -(poly(*L*-lactide)-co-poly(glycolide))  $R_F$ -(PLLA-*co*-PG)<sup>25,26</sup> among others, have been prepared and their behavior in aqueous solution or at the air/water interface has been studied by a wide range of

techniques, such as surface tension, fluorescence, SLS, DLS, <sup>19</sup>F NMR, SAXS, and SANS, ect.<sup>14-28</sup>

Poly(glycerol methacrylate) (PGMA) is a hydrophilic polymer which is applied for soft contact lenses, hydrogels, drug delivery and other biomedical applications.<sup>29-31</sup> In past decades, various PGMA based amphiphilic or triphiphilic polymers have been prepared and their aqueous solution properties have been investigated.<sup>32-35</sup> To the best of our knowledge, however, no attempt has been made to investigate the self-assembling behavior of the end capped PGMA (*R<sub>F</sub>*-PGMA). Whereas *R<sub>F</sub>*-PEOs and *R<sub>F</sub>*-PNIPAMs may show lower critical solution temperature (LCST) behavior, FM-PGMAs have the advantage of being water soluble at all temperatures and as such they are suitable candidates for applications where high temperatures maybe a prerequisite.

With this in mind, we synthesized *R<sub>F</sub>*-PGMAs with the architecture composed of the PGMA main chain and a perfluoroalkyl group capped at one end, which could be considered as the analogous to the well studied *R<sub>F</sub>*-PEO semitelechelics. The *R<sub>F</sub>*-PGMAs semitelechelics are obtained by employing atom transfer radical polymerization (ATRP) and copper(I)-catalyzed alkyne-azide cycloaddition reaction (CuAAC), also referred to as “click” chemistry, in which the degree of polymerization (DP) of PGMA varies from 14 to 113 whereas the perfluoroalkyl end group is always the same. The self-assembly behavior of FM-PGMAs in aqueous solution is investigated by various techniques including surface tension, ITC, NMR, DLS, and microscopic techniques including AFM, SEM and TEM. The thermodynamics of micellization processing of PGMAF<sub>9</sub> and PEOF<sub>9</sub> are compared.

## 3.2 Experimental Section

### 3.2.1 Materials

All reagents are purchased from Sigma-Aldrich unless otherwise stated. 3-Bromo-1-propanol (97%), *N,N,N*-tributyl-1-butanaminium iodide (Bu<sub>4</sub>NI), solketal (98%), ammonium chloride (NH<sub>4</sub>Cl), (99.5%) dicyclohexano-18-crown-6 (97%), methacryloyl chloride (Alfa-Aesar, 97%), sodium azide (NaN<sub>3</sub>), (99.5%),  $\alpha$ -bromoisobutyryl bromide (98%), hex-5-ynoic acid (97%), nonadecafluoro-1-decanol (97%), 4-(dimethylamino)pyridine (DMAP) (99%), 2,2'-bipyridine (bpy), copper bromide (CuBr, 99.999%), 1,4-dioxane (99%), tetrahydrofuran (THF) (99.5%), *n*-hexane (97%), benzene (Roth, 99%), acetone (98%), and ethanol (98%) were used as received. Anisole (Alfa-Aesar, 99%),  $\alpha,\alpha,\alpha$ -trifluorotoluene (98%) (TFT), 2-

butanone (99%) and triethylamine (Et<sub>3</sub>N) (99.8%) were dried overnight with CaH<sub>2</sub>, distilled and stored over molecular sieve.

### 3.2.2 Synthesis

#### 3.2.2.1 Preparation of 3-azidopropyl-2-bromoisobutyrate (APBIB)

The azide functional ATRP initiator, APBIB, was synthesized according to a procedure described elsewhere with some modification.<sup>36</sup> In a round-bottom flask equipped with a reflux column, 3-bromo-1-propanol (5 g, 36 mmol), NaN<sub>3</sub> (4 g, 61.5 mmol), Bu<sub>4</sub>NI (2 g, 5.5 mmol), and dicyclohexano-18-crown-6 (10 mg, 0.025 mmol) were dissolved in 30 mL 2-butanone and stirred under reflux at 80 °C for 24 h. The liquid phase was separated by filtration and then the 2-butanone was removed by evaporation. Pure 3-azide-1-propanol was obtained by distillation.

In a 250 mL round bottom flask with a magnetic stirrer,  $\alpha$ -bromoisobutyryl bromide (7.2 g, 31.3 mmol) dissolved in 50 mL THF was added dropwise to 50 mL THF solution containing 3-azido-1-propanol (3 g, 30 mmol), and Et<sub>3</sub>N (4.6 g, 45 mmol) under nitrogen. The reaction was carried out at room temperature overnight. The excess acid bromide was quenched by ethanol. After filtration, the solvent was evaporated. The crude product was dissolved in CH<sub>2</sub>Cl<sub>2</sub> and washed with saturated NH<sub>4</sub>Cl solution and water, dried over sodium sulphate. The solvent was filtered and concentrated to obtain pale yellow oil, and the vacuum was kept for overnight. <sup>1</sup>H NMR (400MHz, DMSO-*d*<sub>6</sub>):  $\delta$  (ppm) = 1.86-1.98 (-(CH<sub>3</sub>)<sub>2</sub>Br, CH<sub>2</sub>-CH<sub>2</sub>-CH<sub>2</sub>-), 3.42 (N<sub>3</sub>-CH<sub>2</sub>-), 4.25 (-CH<sub>2</sub>-CH<sub>2</sub>-O-). <sup>13</sup>C NMR (400 MHz, DMSO-*d*<sub>6</sub>):  $\delta$  (ppm) = 27.9 (N<sub>3</sub>-CH<sub>2</sub>-CH<sub>2</sub>-), 30.7 (-C(CH<sub>3</sub>)<sub>2</sub>-Br), 48.0 (N<sub>3</sub>-CH<sub>2</sub>-CH<sub>2</sub>-), 55.6 (-C(CH<sub>3</sub>)Br) 62.7 (-CH<sub>2</sub>-CH<sub>2</sub>-CH<sub>2</sub>-O-), 171.7 (OCO-C(CH<sub>3</sub>)<sub>2</sub>Br).

#### 3.2.2.2 Synthesis of nonadecafluoro-1-decyl hex-5-ynoate (F<sub>9</sub>)

The synthesis of nonadecafluoro-1-decyl hex-5-ynoate (F<sub>9</sub>) was synthesized according to the literature reported elsewhere.<sup>37</sup> Generally, it was accomplished in two steps. First, the solution of hex-5-ynoic acid (3 g, 26.8 mmol) in 20 mL anhydrous dichloromethane (CH<sub>2</sub>Cl<sub>2</sub>) was added to the solution of 1,3-(dicyclohexyl)carbodiimide (DCC) (2.76 g, 11.34 mmol) in 10 mL anhydrous CH<sub>2</sub>Cl<sub>2</sub> and reacted for 40 h. The crude product was precipitated in *n*-hexane to afford the hexynoic acid anhydride. In the second step, hexynoic acid anhydride (4.2 g, 20



mmol) was esterified with nonadecafluoro-1-decanol (5 g, 10 mmol) in the presence of DMAP (1.2 g, 10mmol) and pyridine (1.6 g, 20 mmol) using THF as solvent at room temperature. After 40 h, the THF was removed and the crude product was dissolved in CH<sub>2</sub>Cl<sub>2</sub>, then the solution was washed twice with Na<sub>2</sub>CO<sub>3</sub> (10%) and NaHSO<sub>4</sub> (10%) aqueous solution. The final product was obtained by passing through the silica column using a mixture of hexane:ethanol (10:1) as eluent and then the solvent was removed by rotary evaporator. <sup>1</sup>H NMR (400 MHz, CDCl<sub>3</sub>):  $\delta$  (ppm) = 1.83-1.90 (-CH<sub>2</sub>-CH<sub>2</sub>-CH<sub>2</sub>-), 1.96 (HC≡C-), 2.27 (≡C-CH<sub>2</sub>-CH<sub>2</sub>), 2.56 (CH<sub>2</sub>-CH<sub>2</sub>-C(O)-), 4.58 (O-CH<sub>2</sub>-CF<sub>2</sub>-). <sup>19</sup>F NMR (200MHz, DMSO-*d*<sub>6</sub>):  $\delta$  (ppm) = -126.13 (-(CF<sub>2</sub>)<sub>6</sub>-CF<sub>2</sub>-CF<sub>3</sub>), -122.06 (-(CF<sub>2</sub>)<sub>6</sub>-CF<sub>2</sub>-CF<sub>3</sub>), -118.93 (-CH<sub>2</sub>-CF<sub>2</sub>-(CF<sub>2</sub>)<sub>6</sub>-), -80.63 (-(CF<sub>2</sub>)<sub>6</sub>-CF<sub>2</sub>-CF<sub>3</sub>).

### 3.2.2.3 Synthesis of azide terminated poly(solketal methacrylate) (PSMA-N<sub>3</sub>) via ATRP

The synthesis of solketal methacrylate (SMA), used for the polymerizations was reported elsewhere.<sup>38</sup> In a typical ATRP experiment, APBIB (22.5 mg, 0.09 mmol), CuBr (13 mg, 0.09 mmol) and bpy (42 mg, 0.27 mmol) were placed in a Schlenk flask equipped with a magnetic stirrer. The flask was evacuated and purged with nitrogen three times before leaving it under nitrogen. 2 mL degassed anisole was added and bubbled with nitrogen for 20 min under stirring to form a homogenous mixture and the catalyst-ligand complex. A specific amount of SMA dissolved in anisole was added into the flask via a nitrogen-purged syringe. Further purging with nitrogen was carried out for another 20 min and the flask was placed in an oil bath at 50 °C overnight. The product was purified by passing through the silica column with THF as eluent, and precipitated into excess cold *n*-hexane and dried under vacuum at room temperature. <sup>1</sup>H NMR (400 MHz, DMSO-*d*<sub>6</sub>):  $\delta$  (ppm) = 0.60-0.99 (-C-CH<sub>3</sub>), 1.17-1.39 (-C-(CH<sub>3</sub>)<sub>2</sub>), 1.52-2.09 (-CH<sub>2</sub>-C-CH<sub>3</sub>), 3.76-4.11 (-CH<sub>2</sub>-CH(O)-CH<sub>2</sub>-), 4.14-4.32 (-CH<sub>2</sub>-CH(O)-CH<sub>2</sub>-).

### 3.2.2.4 Synthesis of PSMAF<sub>9</sub> via “click” chemistry

In a Schlenk flask equipped with a magnetic stirrer, CuBr (13 mg, 0.09mmol), bpy (42 mg, 0.27 mmol), PSMA-N<sub>3</sub> (0.09 mmol) and F<sub>9</sub> (107 mg, 0.18 mmol) were mixed and then it was evacuated and purged with nitrogen three times. 6 mL degassed anisole/trifluorotoluene (2/1, v/v) were added and stirred for complete dissolution under nitrogen. The reaction was carried

out in an oil bath at 50 °C for 48 h. The product was purified by passing through the silica column with THF as eluent, followed by precipitation into excess *n*-hexane. <sup>1</sup>H NMR (400 MHz, DMSO-*d*<sub>6</sub>):  $\delta$  (ppm) = 0.60-0.99 (-C-CH<sub>3</sub>), 1.17-1.39 (-C-(CH<sub>3</sub>)<sub>2</sub>), 1.52-2.09 (-CH<sub>2</sub>-C-CH<sub>3</sub>), 3.76-4.11 (-CH<sub>2</sub>-CH(O)-CH<sub>2</sub>-), 4.14-4.32 (-CH<sub>2</sub>-CH(O)-CH<sub>2</sub>-), 4.55 (-CH<sub>2</sub>-CF<sub>2</sub>-), 7.59 (N-CH=C). <sup>19</sup>F NMR (200 MHz, DMSO-*d*<sub>6</sub>):  $\delta$  (ppm) = -126.13 (-(CF<sub>2</sub>)<sub>6</sub>-CF<sub>2</sub>-CF<sub>3</sub>), -122.06 (-(CF<sub>2</sub>)<sub>6</sub>-CF<sub>2</sub>-CF<sub>3</sub>), -118.93 (-CH<sub>2</sub>-CF<sub>2</sub>-(CF<sub>2</sub>)<sub>6</sub>-), -80.63 (-(CF<sub>2</sub>)<sub>6</sub>-CF<sub>2</sub>-CF<sub>3</sub>).

### 3.2.2.5 Preparation of PGMAF<sub>9</sub>

The PGMAF<sub>9</sub> was obtained by hydrolysis of PSMAF<sub>9</sub> with 1 N HCl in 1,4-dioxane. Pure products were obtained by dialysis of the polymer aqueous solution against water using a multi-purpose dialysis tubing (Spectra/Por 7 Membrane: molar mass cut off =1 000 Da) and freeze-drying. <sup>1</sup>H NMR (400 MHz, DMSO-*d*<sub>6</sub>):  $\delta$  (ppm) = 0.60-0.99 (-C-CH<sub>3</sub>), 1.52-2.09 (-CH<sub>2</sub>-C-CH<sub>3</sub>), 3.76-4.11 (-CH<sub>2</sub>-CH(O)-CH<sub>2</sub>-), 4.14-4.32 (-CH<sub>2</sub>-CH(O)-CH<sub>2</sub>-), 4.55 (-CH<sub>2</sub>-CF<sub>2</sub>-), 4.69 (-CH(OH)-CH<sub>2</sub>(OH)), 4.95 (-CH(OH)-CH<sub>2</sub>(OH)), 7.59 (N-CH=C). <sup>19</sup>F NMR (200MHz, DMSO-*d*<sub>6</sub>):  $\delta$  (ppm) = -126.13 (-(CF<sub>2</sub>)<sub>6</sub>-CF<sub>2</sub>-CF<sub>3</sub>), -122.06 (-(CF<sub>2</sub>)<sub>6</sub>-CF<sub>2</sub>-CF<sub>3</sub>), -118.93 (-CH<sub>2</sub>-CF<sub>2</sub>-(CF<sub>2</sub>)<sub>6</sub>-), -80.63 (-(CF<sub>2</sub>)<sub>6</sub>-CF<sub>2</sub>-CF<sub>3</sub>).

### 3.2.2.6 Synthesis of PEO<sub>44</sub>F<sub>9</sub>.

The PEO<sub>44</sub>F<sub>9</sub> semitelechelic was prepared by attaching an alkyne functionalized perfluoroalkyl segment (F<sub>9</sub>) to the azide end group of PEO through 1,3-dipolar cycloaddition ('click') reaction.

### 3.2.2.7 The determination of the degree of polymerization (DP) of PGMA block

The DPs of the PGMA blocks of PGMAF<sub>9</sub> were estimated from <sup>19</sup>F and <sup>1</sup>H spectra of PSMAF<sub>9</sub> recorded in DMSO-*d*<sub>6</sub> which contained 0.2 vol% TFT as an internal reference standard, using the formula as following:

$$DP = A \times \frac{5I_p}{3I_{TFT}} \quad (3.1)$$

where  $A$  is the integral ratio of the CF<sub>3</sub> peak of TFT to that of PSMAF<sub>9</sub> in the <sup>19</sup>F spectrum.  $I_p$  and  $I_{TFT}$  represent the integral values of the back bone methyl protons of the polymer and the phenyl protons of TFT, respectively, in the <sup>1</sup>H NMR spectrum.

### 3.2.3 Characterization

#### 3.2.3.1 NMR spectroscopy.

The NMR measurements were performed on a Gemini 2000 spectrometer (Varian) operating at 400 MHz for <sup>1</sup>H and <sup>19</sup>F. The samples were prepared either in DMSO-*d*<sub>6</sub> or in D<sub>2</sub>O. The CF<sub>3</sub>COOD was added as an internal standard for the <sup>19</sup>F NMR spectroscopy. The experimental conditions including concentration, temperature and number of the scans for each spectrum are indicated in the following discussion.

#### 3.2.3.2 Size exclusion chromatography (SEC)

The polydispersities ( $M_w/M_n$ ) were obtained using a Viskotek VE 2001 column equipped with an RI detector Viscotek 3580 in THF using a flow rate of 1 mL min<sup>-1</sup> at room temperature. Poly(methyl methacrylate) (PMMA) was used as calibration standard.

#### 3.2.3.3 Surface tension measurement

All surface tensions of the aqueous solutions of the polymer samples at different concentrations were measured with a DCAT11 tensiometer (DataPhysics Instruments GmbH, Filderstadt, Germany) by the Wilhelmy plate method. The temperature was controlled by a circulating water bath system accurated to  $\pm 0.1$  °C. The polymer concentration in the thermostated glass vessel was varied by the injection of aliquots of stock solution. Following each injection, the surface tension is then measured after 10 min of stirring and 1.5 h waiting period.

### 3.2.3.4 Dynamic light scattering (DLS)

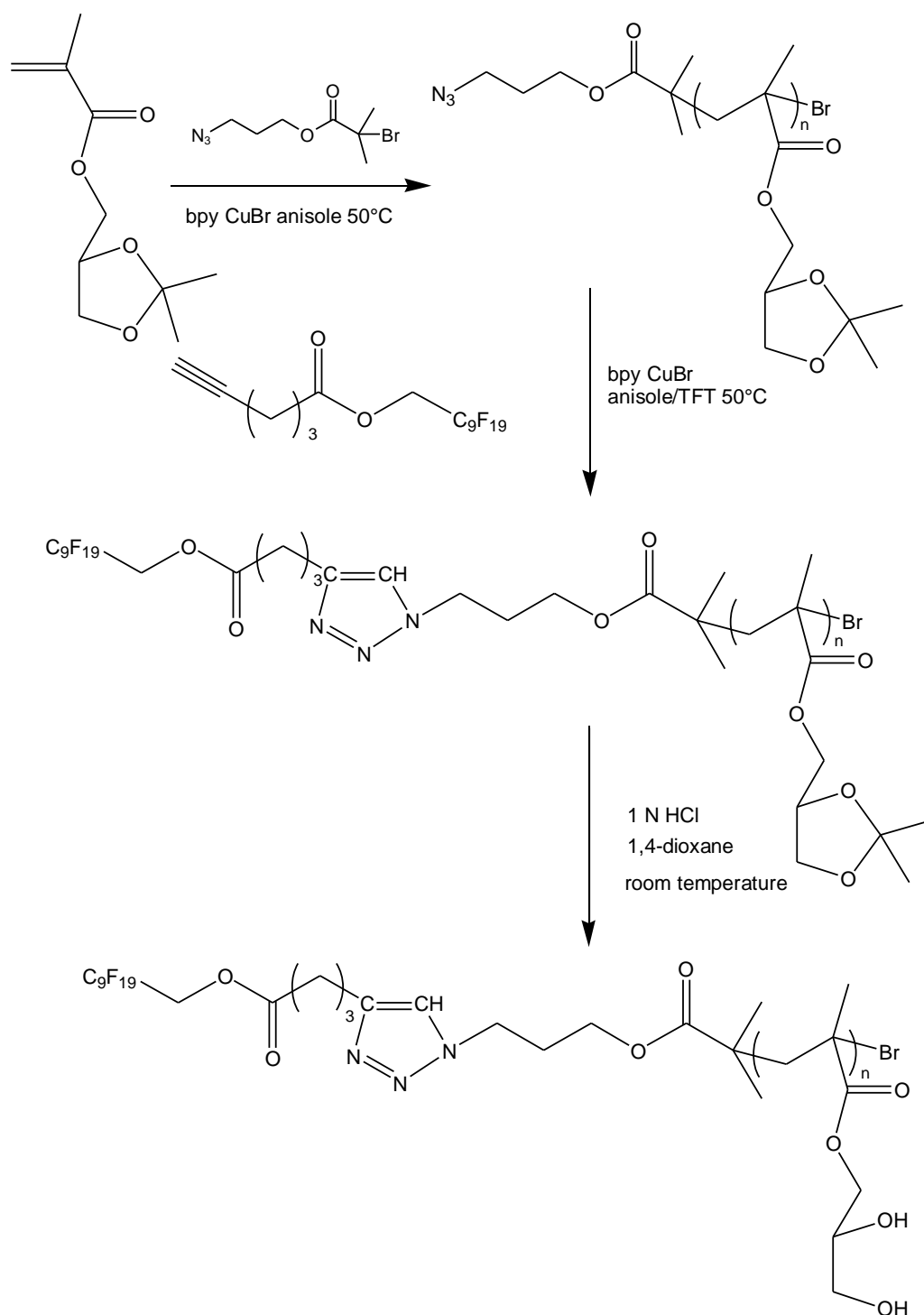
All DLS measurements were carried out on a commercial apparatus of ALV-Laser Vertriebsgesellschaft GmbH, Langen, Germany. The light source was a vertically polarized green neodymium: YAG DPSS-200 laser ( $\lambda = 532$  nm) from Coherent, Auburn, CA, USA, with a power output of 200 mW. The correlation functions from DLS were analyzed by the CONTIN method giving information on the distribution of decay rate ( $\Gamma$ ). Apparent diffusion coefficients were obtained from  $D_{\text{app}} = \Gamma/q^2$ , where  $\Gamma$  is the reciprocal of the characteristic decay time,  $q = (4\pi n_0/\lambda) \sin(\theta/2)$  being the scattering vector,  $n_0$  is the refractive index of the medium,  $\lambda$  is the wavelength of the light,  $\theta$  is the scattering angle. The corresponding apparent hydrodynamic radius,  $R_h$ , are obtained via the Stokes-Einstein equation  $R_h = kT/(6\pi\eta D_{\text{app}})$ , where  $k$  is the Boltzmann constant and  $\eta$  is the viscosity of the solvent, water in this case, corrected at the temperature  $T$ . The samples were dissolved in Milli-Q water and then filtered through PTFE filters with 0.45  $\mu\text{m}$  pore size in order to remove the dust. The  $R_h$  values were recorded for scattering angles from 50 to 130° after equilibrating the sample at a given temperature for 30 min. The average of two runs (60 s each) was recorded. The relative peak intensity is scaled with respect to the peak of the highest intensity which is put to an intensity of 1.

## 3.3 Results and Discussion

### 3.3.1 Polymer synthesis and characterization

The synthesis of perfluoroalkyl functional PGMA semitelechelics, abbreviated as PGMA<sub>x</sub>F<sub>9</sub> ( $x$  is the  $DP$  of PGMA main chains, 9 represents the number of CF<sub>2</sub>/CF<sub>3</sub> groups in perfluoroalkyl segment), is depicted in scheme 3.1, involving the polymerization of the PSMA<sub>x</sub>N<sub>3</sub> by ATRP using an azide functionalized initiator, coupling the alkyne functional perfluoroalkyl segment with the PSMA<sub>x</sub>N<sub>3</sub> via CuAAC and cleaving the ketal groups on the side chains of PSMA to afford the PGMA<sub>x</sub>F<sub>9</sub>. The different  $DP$ s of the PGMA blocks are achieved by varying the molar ratio of SMA to initiator. Compared to the transformation of terminal halides at the polymer chain end with sodium azide to yield the azide group, PSMA<sub>s</sub> with 100% azide functionality can be achieved easily by using the azide functional ATRP initiator. It is generally believed that the azide group of the initiator will not be influenced during the polymerization process.<sup>40</sup> This avoids the problem that the halogen end group at

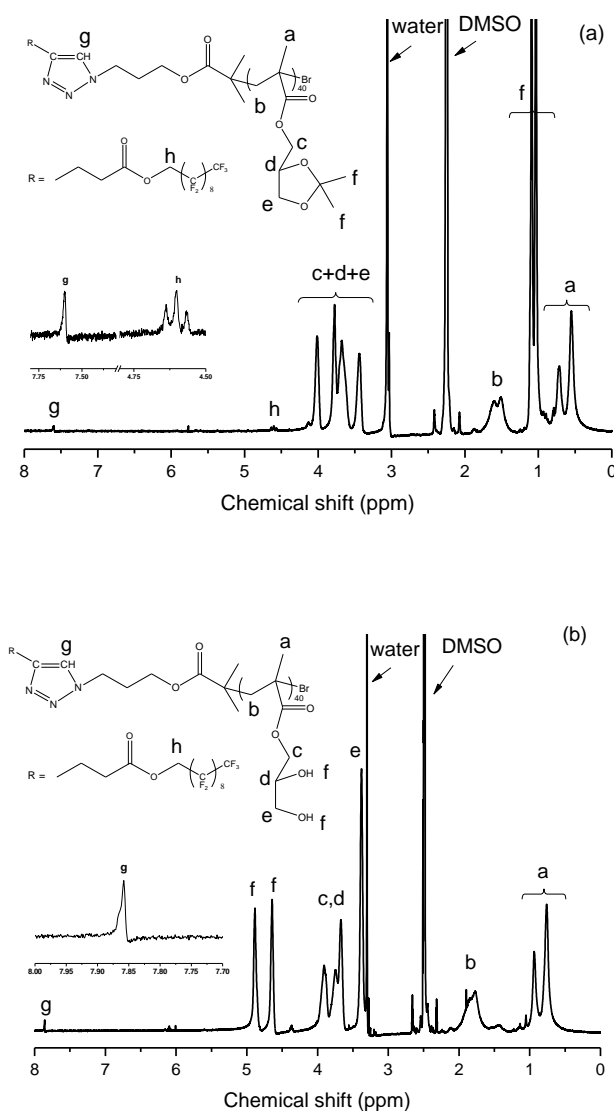
the polymer end can be lost at high conversions and causes a corresponding loss of the ability to be functionalized.<sup>40</sup>



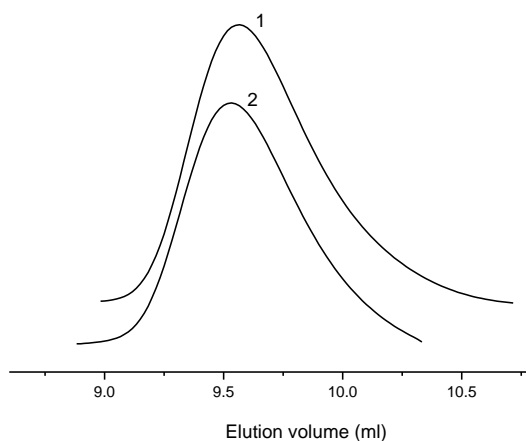
**Scheme 3.1.** The synthetic route for the preparation of PGMA<sub>x</sub>F<sub>9</sub> semitelechelics.

Figure 3.1 shows the <sup>1</sup>H NMR spectra of PSMA<sub>40</sub>F<sub>9</sub> (a) and PGMA<sub>40</sub>F<sub>9</sub> (b) in DMSO-*d*<sub>6</sub> with the proton assignment. It is clearly evident the resonance peaks attributed to the proton signed

as *g* on the triazole ring at  $\sim 7.7$  ppm and methylene group on the F<sub>9</sub> segment signed as *h* at  $\sim 4.5$  ppm appear in the spectrum, indicating the addition of F<sub>9</sub> segments to the PSMA chain. The *DP* of PSMA<sub>14</sub>F<sub>9</sub> and PSMA<sub>40</sub>F<sub>9</sub> can be calculated using 2 times the integral of resonance peak *a* to 3 times the integral of peak *h*. The values are in good agreement with *DP*s calculated by eq (3.1). However, the resonance signals from F<sub>9</sub> segments cannot be resolved well in PSMA<sub>85</sub>F<sub>9</sub> and PSMA<sub>113</sub>F<sub>9</sub> due to the small amount of the F<sub>9</sub> segments compared to the polymer main chain. All samples (PSMA<sub>*x*</sub>F<sub>9</sub>) are analyzed by SEC in THF and they have monomodal molar mass distributions and polydispersities (*PD*) between 1.10-1.35. The typical SEC traces of the PSMA<sub>40</sub>N<sub>3</sub> and PSMA<sub>40</sub>F<sub>9</sub> with THF as eluent are shown in Figure 3.2. The trace of PSMA<sub>40</sub>F<sub>9</sub> shifts to lower elution volumes compared to PSMA<sub>40</sub>N<sub>3</sub>, reflecting the increase of *M<sub>n</sub>* due to the addition of the F<sub>9</sub> segment. The number average molar mass (*M<sub>n</sub>*) and *PD* values are summarized in Table 3.1.



**Figure 3.1.** <sup>1</sup>H NMR spectra of (a) PSMA<sub>40</sub>F<sub>9</sub> and (b) PGMA<sub>40</sub>F<sub>9</sub> in DMSO-*d*<sub>6</sub> at 25 °C.



**Figure 3.2.** SEC traces of (1) PSMA<sub>40</sub>N<sub>3</sub> and (2) PSMA<sub>40</sub>F<sub>9</sub> with THF as eluent at room temperature. For molar mass calculations PMMA standard are used.

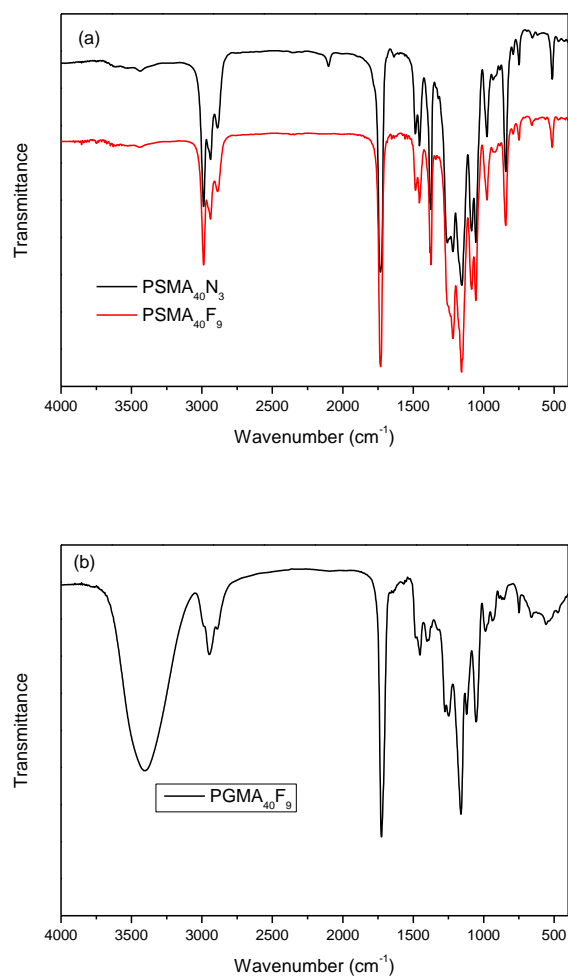


**Figure 3.3.** FTIR spectra of (a) PSMA<sub>40</sub>N<sub>3</sub> (black), PSMA<sub>40</sub>F<sub>9</sub> (red) and (b) PGMA<sub>40</sub>F<sub>9</sub> recorded in KBr.

The complete conversion during CuAAC is confirmed by the disappearance of the azide absorption band at a wavenumber of  $\sim 2100 \text{ cm}^{-1}$  in the FTIR spectrum of PSMAF<sub>9</sub> as shown in Figure 3.3. The PGMA<sub>x</sub>F<sub>9</sub> polymers are obtained by hydrolysis of the acetonide rings of PSMA to give the hydroxyl groups. Ideally, the *DPs* of PGMA<sub>x</sub>F<sub>9</sub> should be the same as the *DPs* of their precursors PSMA<sub>x</sub>F<sub>9</sub>. As shown in Figure 3.1, the disappearance of the resonance signals of pendent methyl groups at 1.28 and 1.34 ppm and the appearance of the resonance peaks of the hydroxyl groups at 4.64 and 4.88 ppm give clear evidence that the SMA units are completely converted to GMA units. The successful cleavage is also confirmed by the decrease of in the intensities of the CH<sub>3</sub> symmetric and asymmetric stretching vibration bands at 2887 and 2988  $\text{cm}^{-1}$ , and the appearance of a broad and strong OH stretching band at wavenumber of 3750-3000  $\text{cm}^{-1}$  in the FTIR spectra (Figure 3.3).

**Table 3.1.** Characteristic data of the synthesis PGMA<sub>x</sub>F<sub>9</sub> semitelechelics.

Polymers	$M_w/M_n^a$	$M_n \text{ (g mol}^{-1}\text{)}^b$	cmc ( $10^{-5} \text{ mol L}^{-1}\text{)}^c$
PGMA <sub>14</sub> F <sub>9</sub>	1.18	3000	0.67
PGMA <sub>40</sub> F <sub>9</sub>	1.21	7200	1.35
PGMA <sub>85</sub> F <sub>9</sub>	1.25	14300	3.5
PGMA <sub>113</sub> F <sub>9</sub>	1.23	18800	--

<sup>a</sup>Obtained from SEC measurements on PSMA<sub>x</sub>F<sub>9</sub> with THF as eluent and PMMA as standard.

<sup>b</sup>Calculated from <sup>1</sup>H and <sup>19</sup>F NMR spectroscopy. <sup>c</sup>Obtained from surface tension measurement at 25 °C.

### 3.3.2 Self-assembly of PGMA<sub>x</sub>F<sub>9</sub> in aqueous solution

It is well established that amphiphilic diblock copolymers which consist of a larger hydrophilic block and a relatively small hydrophobic block associate into spherical micelles with a small dense core and a large solvated corona above the critical micellization concentration (cmc).<sup>41</sup> The cmc, defined as the copolymer concentration above which the formation of micelles becomes a dominant effect, is a fundamental parameter in characterizing the association properties of a given copolymer-solvent system.<sup>42</sup> Measuring the surface tensions over a wide range of concentrations is one of the commonly used methods to determine the cmc. In a polymer-solvent system, the surface tension gradually decreases with increasing concentration due to the fact that hydrophobic polymer chains are adsorbed at the air/water interface. When the polymer concentration reaches the cmc, the



surface tension is obviously no longer changed. The cmc is indicated by the intersection of the extrapolation of the two linear regimes where the curves show an abrupt change in the slope. The surface tension measurements were carried out at 25 °C using aqueous solutions of PGMA<sub>x</sub>F<sub>9</sub> and the corresponding cmc data are summarized in Table 3.1. It is clearly evident that the cmc values show a significant increase with increasing PGMA content, since the longer soluble blocks usually carry higher “free energy cost” for being transferred from the unimer state to the micellar corona.<sup>43</sup> The measurements carried out at 25 °C using an aqueous solution of PGMA<sub>113</sub>F<sub>9</sub> showed a continuous decrease of  $\gamma$  with increasing concentration, indicating that no micelles have been formed in the measured concentration range. This suggests the existence of a critical PGMA length in PGMA<sub>x</sub>F<sub>9</sub> above which the micellization is suddenly hindered.

The surface tension measurements of PGMA<sub>40</sub>F<sub>9</sub> in aqueous solutions were also carried out at 15, 25, 35 and 45 °C to investigate the temperature effect on the aggregation behavior. The cmc values obtained from the measurements are summarized in Table 3.2. Figure 3.4a represents the surface tensions obtained for PGMA<sub>40</sub>F<sub>9</sub> in water as a function of polymer concentration at 15 and 45 °C. As can be seen from Figure 3.4c, the cmc values exhibit a gradual increase with increasing temperature. At 45 °C, the cmc value of PGMA<sub>40</sub>F<sub>9</sub> is about 2 times larger compared to the value at 15 °C. A similar behavior was also observed for PGMA<sub>14</sub>F<sub>9</sub>. Such increase of the cmc with temperature is similar to the micellization of some block copolymers in organic solvent, such as poly(styrene)-*b*-poly(tert-butylstyrene) in *N,N*-dimethylacetamide,<sup>44</sup> since the increasing temperature can usually improve the solvent quality to both blocks of block copolymers in organic solvent.<sup>45</sup> The amphiphilic polymers in aqueous solution usually show the opposite result, that is, the cmc becomes smaller with increasing temperature. This is because the hydrocarbon becomes more hydrophobic at higher temperatures.<sup>45</sup> For comparison, the PEO<sub>44</sub>F<sub>9</sub> with the same hydrophobic group was prepared, and the cmc were measured at the same temperatures as PGMA<sub>40</sub>F<sub>9</sub>. The PEO is chosen as hydrophilic block for two reasons. The first is that the hydrophobically end-capped PEO has been widely studied and thus a large amount of data about the self-assembly behavior is available.<sup>46-48</sup> The second reason is that PEO has a significantly different chemical structure compared to PGMA. Figure 3.4b shows the surface tension measurements of PEO<sub>44</sub>F<sub>9</sub> over a range of concentrations at 15 and 45 °C. The determined cmc values are summarized in Table 3.2. As expected, the cmc values show a gradual decrease with increasing temperature as shown in Figure 3.4c. This is in good agreement with the hydrophobically modified PEOs reported in literature.<sup>46-48</sup>

Generally, the variation of the cmc values for amphiphilic substances in aqueous solutions is found to depend on the alteration of the interaction between the hydrophilic or/and hydrophobic blocks with water.<sup>45</sup> It should be noted that PGMA is a polymer with abundant hydroxyl (-OH) and carbonyl groups. When PGMA is dissolved in water, the polymer is able to form inter/intra molecular hydrogen bonds with polymer chains and intermolecular hydrogen bonds with water. The increase of temperature, which weakens the hydrogen bonding effect, has two opposite effects on the PGMA chain. On one hand, the increase of temperature may decrease hydrogen bonding between the OH groups of PGMA and water molecules, which results in the dehydration of the PGMA block and favours the micellization. On the other hand, the increase of temperature can reduce the hydrogen bonding between the PGMA polymer chains and make the PGMA chains more hydrated, which hinders the micellization. In terms of magnitude, the endothermic enthalpy associated with breaking of alkyl-OH---OH-alkyl interactions is smaller than the exothermic enthalpy associated with formation of alkyl-OH---HOH (hydration).<sup>49</sup> Therefore, the PGMA chains are become more hydrophilic at higher temperatures since more inter and intra molecular hydrogen bonds are broken and OH group of the polymer chains become available for hydration. When the temperature is raised, water becomes progressively a worse solvent for the hydrophobic block.<sup>45</sup> In other words, the hydrophobicity of the F<sub>9</sub> is enhanced, which is favorable for micellization. From the data of the cmc values, it seems that the PGMA effect dominates the cmc values at increasing temperatures and results in more hydrophilic PGMA<sub>x</sub>F<sub>9</sub> semitelechelics at higher temperatures. For PEO<sub>44</sub>F<sub>9</sub>, increasing temperature decreases the solvent quality for both the PEO and F<sub>9</sub> blocks and thus leads to a cmc decrease with increasing temperature. The increase of the hydrophilicity of the hydrophilic block in amphiphilic copolymers was also been observed by Halacheva et al. They found that the cmc of poly(glycidol)-poly(propylene oxide)-poly(glycidol) (PG-PPO-PG) block copolymers is less temperature sensitive than their PEO-PPO-PEO analogues due to the weakening of the hydrogen bonding between the OH groups at the PG side chains.<sup>50</sup>

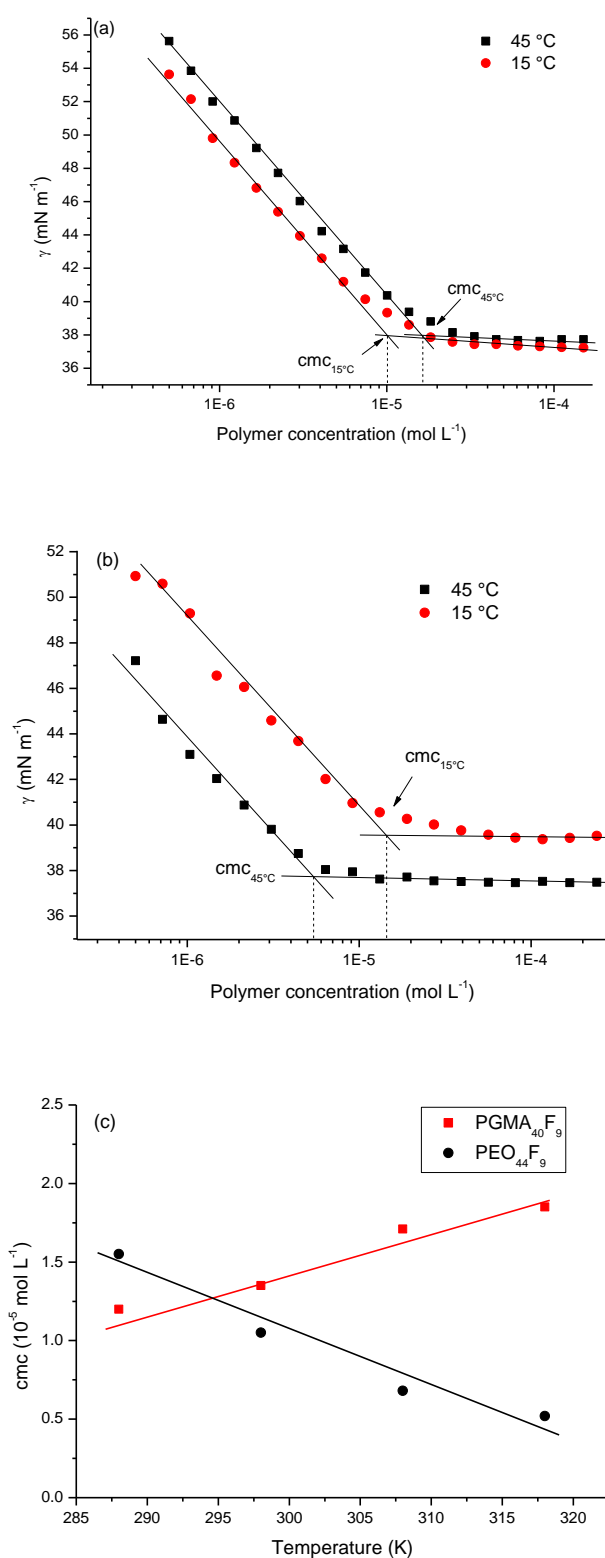


**Figure 3.4.** Critical micellization concentration (cmc) determination from surface tension measurements as a function of the concentration of (a) PGMA<sub>40</sub>F<sub>9</sub> and (b) PEO<sub>44</sub>F<sub>9</sub> at 15 °C and 45 °C. (c) The cmc values of PGMA<sub>40</sub>F<sub>9</sub> and PEO<sub>44</sub>F<sub>9</sub> at various temperatures.

**Table 3.2.** cmc and Gibbs free energy of micellization ( $\Delta G_{\text{mic}}^0$ ) of PGMA<sub>40</sub>F<sub>9</sub> and PEO<sub>44</sub>F<sub>9</sub> in aqueous solution at various temperatures.

Temperature (K)	PGMA <sub>40</sub> F <sub>9</sub>		PEO <sub>44</sub> F <sub>9</sub>	
	cmc (10 <sup>-5</sup> M)	$\Delta G_{\text{mic}}^0$ (kJ mol <sup>-1</sup> )	cmc (10 <sup>-5</sup> M)	$\Delta G_{\text{mic}}^0$ (kJ mol <sup>-1</sup> )
288	1.20	-36.7	1.55	-36.1
298	1.35	-37.7	1.05	-38.4
308	1.71	-38.4	0.68	-40.7
318	1.85	-39.4	0.52	-42.8

The driving force for the micellization of the PGMA<sub>40</sub>F<sub>9</sub> and PEO<sub>44</sub>F<sub>9</sub> could be identified from the thermodynamic parameters extracted from the cmc values at various temperatures. For a micellization process with significant association number the use of the relations below to calculate the standard free energy of micellization,  $\Delta G_{\text{mic}}^0$ , based on the cmc values is tolerable within experimental error.<sup>51</sup>

$$\Delta G_{\text{mic}}^0 = \Delta H_{\text{mic}}^0 - T\Delta S_{\text{mic}}^0 = RT \ln(X_{\text{cmc}}) \quad (3.2)$$

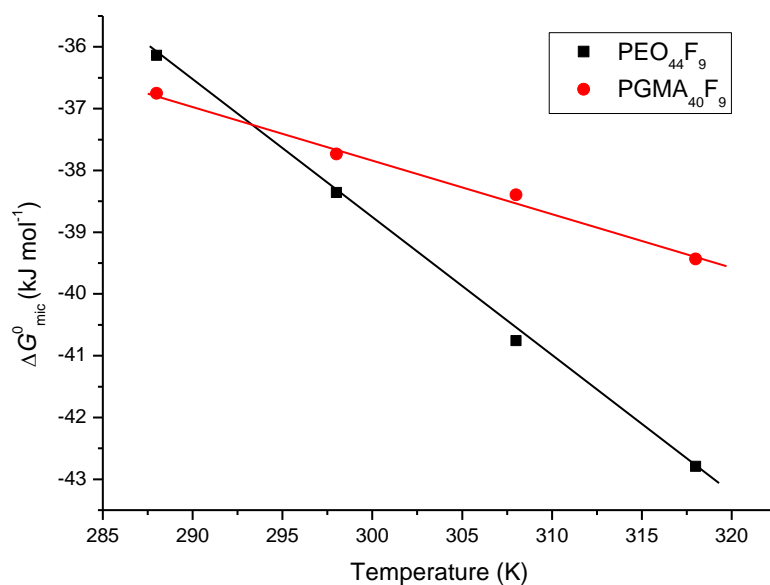
Where  $R$  is the gas constant,  $T$  is the temperature in  $K$  and  $X_{\text{cmc}}$  is the cmc in molar fraction at temperature  $T$ . The obtained  $\Delta G_{\text{mic}}^0$  values are plotted as a function of temperature for PGMA<sub>40</sub>F<sub>9</sub> and PEO<sub>44</sub>F<sub>9</sub> in Figure 3.5. The intercepts and the slopes of the linear fits of the plots give the standard enthalpy of micellization,  $\Delta H_{\text{mic}}^0$ , and standard entropy of micellization  $\Delta S_{\text{mic}}^0$  according to eq. 3.2. The values estimated for PGMA<sub>40</sub>F<sub>9</sub> and PEO<sub>44</sub>F<sub>9</sub> by this method are summarized in Table 3.3.

**Table 3.3.** Standard enthalpy ( $\Delta H_{\text{mic}}^0$ ) and standard entropy ( $\Delta S_{\text{mic}}^0$ ) of micellization estimated from the standard free energy of micellization ( $\Delta G_{\text{mic}}^0$ ) versus thermodynamic temperature ( $T$ ) plot.

Polymers	$\Delta H_{\text{mic}}^0$ (kJ mol <sup>-1</sup> )	$\Delta S_{\text{mic}}^0$ (kJ mol <sup>-1</sup> K <sup>-1</sup> )
PGMA <sub>40</sub> F <sub>9</sub>	-11.7 ± 1.5	0.087 ± 0.007
PEO <sub>44</sub> F <sub>9</sub>	28.2 ± 1.4	0.223 ± 0.005

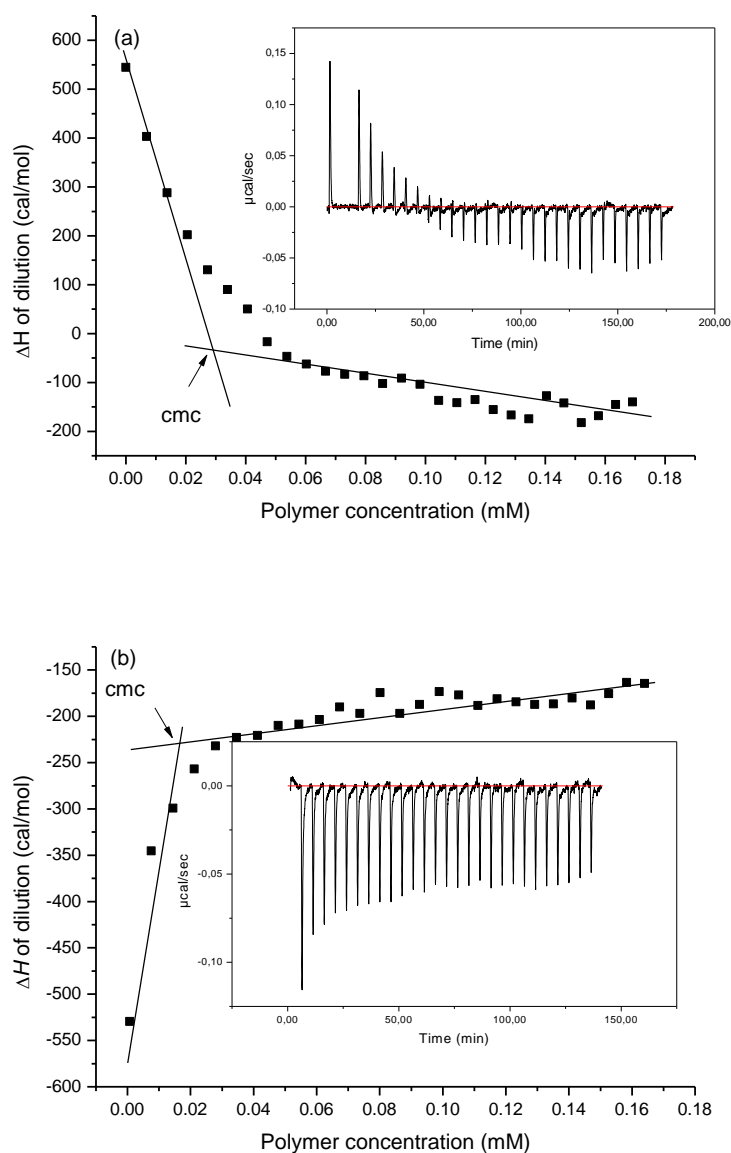
Table 3.3 shows that both PGMA<sub>40</sub>F<sub>9</sub> and PEO<sub>44</sub>F<sub>9</sub> have a positive  $\Delta S_{\text{mic}}^0$  value, indicating that the micellization processes of them are entropically driven. It is generally accepted that the gain in entropy during the micellization process arises from the release of water molecules in the hydration shells surrounding the hydrophobic groups.<sup>52</sup> Moreover, the mobility of the hydrophobic segments increases when they are removed from the aqueous solution to the core.<sup>54</sup> The positive  $\Delta H_{\text{mic}}^0$  for PEO<sub>44</sub>F<sub>9</sub> suggests that the micellization process is enthalpically not favored. This behavior is widely observed in the micellization of the amphiphilic polymers in aqueous solution. It is interesting to note that PGMA<sub>40</sub>F<sub>9</sub> shows a negative  $\Delta H_{\text{mic}}^0$ , suggesting that this micellization processes in aqueous solution is enthalpically favored. Thus, the micellization process of PGMA<sub>40</sub>F<sub>9</sub> in aqueous solution is driven by both the increase of entropy and the loss of enthalpy.

It has been demonstrated that there are basically two contributions to the  $\Delta H_{\text{mic}}^0$  in the micellization process of surfactants in aqueous solution. The first contribution arises from the transfer of the hydrophobic segments from the aqueous phase to the micelle core. This process is accompanied by a release of the water molecules surrounding the hydrophobic segments to the aqueous solution, which are structured differently from the water molecules in bulk. This effect results in an exothermic enthalpy.<sup>52,53</sup> The second contribution is associated with the hydrophilic block. The hydrophilic repulsion due to the hydration and excluded volume forces of the hydrophilic chain give an endothermic contribution to  $\Delta H_{\text{mic}}^0$ .<sup>54-56</sup> It is obvious that this large difference of  $\Delta H_{\text{mic}}^0$  between PEO<sub>44</sub>F<sub>9</sub> and PGMA<sub>40</sub>F<sub>9</sub> comes from the hydrophilic blocks since they share the same F<sub>9</sub> segments. It should be noted that the intra/intermolecular hydrogen bonding plays an important role for the PGMA blocks. The formation of hydrogen bonds between the hydroxyl groups in micelles can weaken the hydration and excluded volume forces of the PGMA chains. In conclusion, the reduction of the endothermic contribution from the hydrophilic blocks during solvation leads to decrease of  $\Delta H_{\text{mic}}^0$  (it becomes more exothermic).



**Figure 3.6.** Free energy of micellization,  $\Delta G_{mic}^0$  as a function of temperature for PEO<sub>44</sub>F<sub>9</sub> and PGMA<sub>40</sub>F<sub>9</sub>.

ITC directly measures the heat effects accompanying association or disassociation between the molecular entities.<sup>57</sup> For the association behavior of a surfactant in solution, ITC has the advantage that the cmc and  $\Delta H_{mic}^0$  can be determined directly. To obtain further information on the micellization of PGMA<sub>40</sub>F<sub>9</sub> and PEO<sub>44</sub>F<sub>9</sub> in aqueous solution, ITC experiments are carried out at 20 °C. In a typical measurement, small aliquots of stock polymer solution are injected into water kept in the titration cell of the calorimeter at constant temperature. The heat evolved after each injection is registered as a peak, and the area under each peak is plotted against polymer concentration in the titration cell.



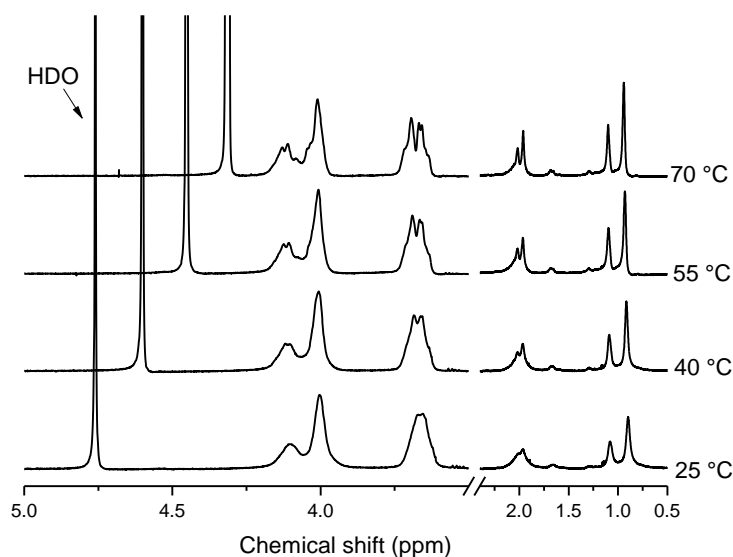
**Figure 3.7.** The integrated heat per injection (normalized with respect to the injected number of moles of polymer) as a function of the total concentration of polymer in the sample cell. Titration curve (inset) observed after injections (a) PGMA<sub>40</sub>F<sub>9</sub> and (b) PEO<sub>44</sub>F<sub>9</sub> of 1 mM aqueous solution at 20 °C (baseline corrected).

Figure 3.7 shows the dilution enthalpograms with the heat per injection as a function polymer concentration and the titration curves (inset) of the addition of 1 mM PGMA<sub>40</sub>F<sub>9</sub> (a) and 1 mM PEO<sub>44</sub>F<sub>9</sub> aqueous solution (b) to water. The enthalpograms of both semitelechelics do not show a sigmoidal shape but instead exhibit a gradual change of enthalpy with polymer concentration caused by the fact that they assemble via a noncooperative process. Such a phenomenon is common in the self-assembly of polymers. The dilution enthalpograms can

be subdivided into two concentration regions and reflect different processes.<sup>57b,57c</sup> In the low concentration region, a large enthalpic effect is observed attributed to the dilution of micelles, demicellization of micelles and dissolution of the individual polymer chains. The semitelechelics concentration in the sample cell is below the cmc, and the micelles of the injected aliquots disaggregate. At the polymer concentration in the calorimeter cell above the cmc, the reaction enthalpies keep constant and the measured heat comes only from the dilution of the micelles. The intercept of the linear fits to the demicellization range and the micellar solution dilution range is taken as cmc. The cmc values determined by this method are ~ 0.028 mM and 0.018 mM for PGMA<sub>40</sub>F<sub>9</sub> and PEO<sub>44</sub>F<sub>9</sub>, respectively. Nevertheless, Figure 3.7 clearly reflects that the PGMA<sub>40</sub>F<sub>9</sub> exhibits an exothermic micellization process, whereas an endothermic micellization process is observed for PEO<sub>44</sub>F<sub>9</sub>. This is in good agreement with the temperature dependent surface tension measurements.

Figure 3.8 compares the systematic changes in the <sup>1</sup>H NMR spectra of PGMA<sub>40</sub>F<sub>9</sub> recorded at 25, 40, 55 and 70 °C in D<sub>2</sub>O. The temperature-dependent residual HDO resonance signal is corrected for each temperature according to the studies by Gottlieb et al.<sup>58</sup> The resonance bands of OH groups on the side chains of PGMA do not appear in the spectra because of the D/H exchange (the assignment is shown in the experimental part). Examination of Figure 3.8 shows that the resolution of the resonance signals is gradually improved with increasing temperature. For instance, the band at ~3.3 ppm, which is attributed to the methylene group adjacent to the OH on the PGMA side chains, shows a distinct hyperfine structure at 70 °C. This hyperfine structure progressively broadens with decreasing temperature, and completely disappears at 25 °C. This observation indicates that the mobility of the PGMA chains increase with temperature. Such behavior can be attributed to the weakening of the hydrogen bonding between the partially self-associated OH groups on the GMA units with increasing temperature, resulting in increasing solubility and mobility of the PGMA chains in aqueous solution.





**Figure 3.8.** Effect of temperature on the  $^1\text{H}$  NMR spectra of 1.5 mM PGMA<sub>40</sub>F in D<sub>2</sub>O at 400 MHz.

$^{19}\text{F}$  NMR spectroscopy is a powerful tool to investigate the self-assembly behavior of fluorocarbon containing polymers since the chemical shift of fluorine nuclei is very sensitive to changes of the environment.<sup>59-61</sup> Figure 3.9 shows the  $^{19}\text{F}$  NMR spectra of PGMA<sub>40</sub>F<sub>9</sub> recorded in (a) DMSO-*d*<sub>6</sub> and (b) D<sub>2</sub>O with a polymer concentration of ~ 1.5 mM at 25 °C. Six sharp and well resolved resonance signals are observed and assigned in the  $^{19}\text{F}$  NMR spectrum recorded in DMSO-*d*<sub>6</sub> since it is a non-selective solvent for the semitelechelic and the F<sub>9</sub> segments exposed directly to the solvent. However, only four weak, broader and attenuated resonance signals are observed in the spectrum recorded in D<sub>2</sub>O. The peaks attributed to the CF<sub>2</sub> units numbered as “3”, which appear as three well separated peaks in DMSO-*d*<sub>6</sub>, show only two attenuated peaks in D<sub>2</sub>O. The peak of the CF<sub>2</sub> unit numbered as “4” closest to the PGMA block completely disappeared. Furthermore, the comparison of Figure 3.9a and b shows that all the peaks shift to lower chemical shift in D<sub>2</sub>O than DMSO-*d*<sub>6</sub>. For instance, the peak of the trifluoromethyl group (CF<sub>3</sub>) at the end of the F<sub>9</sub> segments appears at ~ -80.0 ppm in DMSO-*d*<sub>6</sub>, whereas at ~ -83.3 ppm in D<sub>2</sub>O. Generally, the upfield shift of the peaks suggests the more shielded nuclei.<sup>6</sup> It is reasonable considering that the fluorine nuclei are transferred into a fluorocarbon rich environment rather than in D<sub>2</sub>O. This evidence clearly demonstrates that polymeric micelles with F<sub>9</sub> segments as the core are formed. The resonance signal of the terminal CF<sub>3</sub> group in the fluorocarbon chain is most sensitive to the micellization.<sup>62</sup> It is confirmed from the literature that the resonance peak at ~ -83.0 ppm

shown in D<sub>2</sub>O is the characteristic signal of trifluoromethyl groups (CF<sub>3</sub>) in the aggregated state.<sup>6,63</sup>

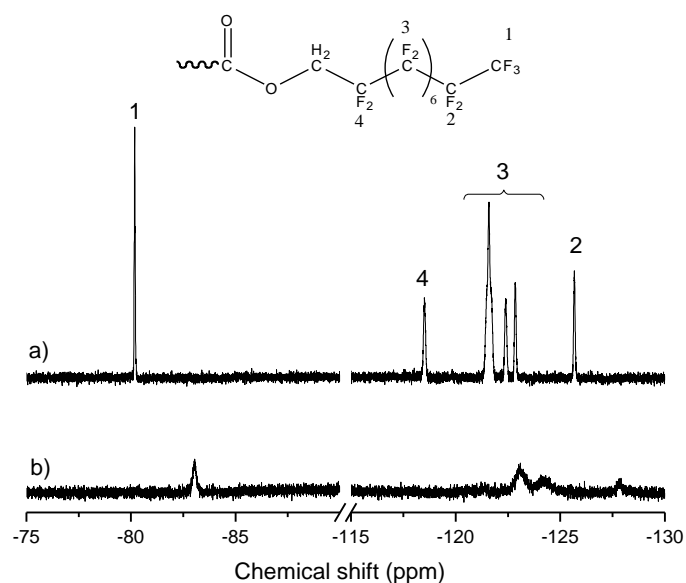


**Figure 3.9.** <sup>19</sup>F NMR spectra of 1.5 mM PGMA<sub>40</sub>F<sub>9</sub> at 25 °C and 400 MHz, in (a) DMSO-*d*<sub>6</sub> (32 scans) (b) D<sub>2</sub>O (260 scans).

To probe the effect of temperature on the aggregation behavior of the F<sub>9</sub> segment, the <sup>19</sup>F NMR spectra of PGMA<sub>40</sub>F<sub>9</sub> are recorded at 25, 35, 45 and 55 °C. These spectra are depicted in Figure 3.10. Similar as the temperature dependent <sup>1</sup>H NMR spectra discussed above, the resolution of the spectrum is gradually improved with increasing temperature. At 25 °C, there are only four broad and attenuated resonance peaks shown in the spectrum. Upon increasing the temperature to 55 °C, six resonance signals are considerably resolved similar to the spectrum in DMSO-*d*<sub>6</sub>. Specifically, the signal from the CF<sub>2</sub> unit closest to the PGMA block (labelled as number “4” in Figure 3.9a) which is not seen at 25 °C appears at 35, 45 and 55 °C. In the literature, such increase in signal resolution has been attributed to increasing mobility of the fluorocarbon moieties.<sup>10</sup>

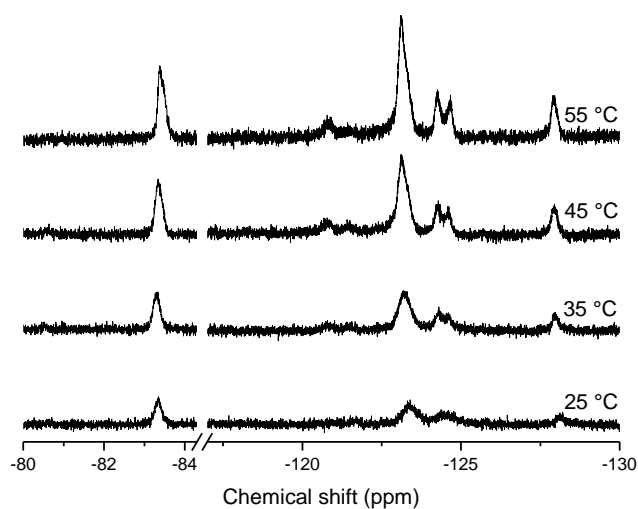


**Figure 3.10.** Effect of temperature on the  $^{19}\text{F}$  NMR spectra of 1.5 mM PGMA<sub>40</sub>F<sub>9</sub> in D<sub>2</sub>O at 400 MHz (260 scans).

The  $^{19}\text{F}$  NMR resonances of the  $\text{CF}_3$  groups of PGMA<sub>40</sub>F<sub>9</sub>, PGMA<sub>85</sub>F<sub>9</sub> and PGMA<sub>113</sub>F<sub>9</sub> at 0.5 mM recorded at 55 °C are displayed in Figure 3.11. It is interesting to note that two well resolved peaks are visible in the spectrum of PGMA<sub>85</sub>F<sub>9</sub>, indicating that two types of F<sub>9</sub> segments are existing in the solution. The upfield peak represents the associated polymer, while the downfield resonance may represent the single chains. A similar phenomenon has been reported widely for fluorocarbon PEO telechelics.<sup>6,63</sup> The well separated downfield and upfield resonance signals at -80.0 and -83.3 ppm indicate that the exchange rate of the polymer chains between the dissociated and associated form is slow with respect to the  $^{19}\text{F}$  NMR characteristic time scale.<sup>63</sup> Generally, only the associated polymer resonance peak can be observed when the concentration is above a certain value, which is related to the cmc of the polymer. The lack of the downfield peak in the spectra of 1.5 mM PGMA<sub>40</sub>F<sub>9</sub> in Figure 3.9 and 3.10 can be caused by the fact that the concentration is much higher than the cmc value. The fractions of dissociated polymer and associated polymer can usually be estimated directly from the ratio of the integrals of their corresponding peaks.<sup>64</sup> It is clearly evident from Figure 3.11 that the ratio of the upfield peak to the downfield peak decrease with the increasing PGMA chain length, indicating that the fraction of the dissociated polymer chains increase with PGMA chain length. This is presumably a result of the greater excluded volume interaction for the longer water soluble polymer chains.<sup>9</sup> The extremely weak associated peak for the associated polymer chains in PGMA<sub>113</sub>F<sub>9</sub> supports the assumption that the polymer

chains are not associated to form the regular micelles in water due to the large excluded volume force arising from the long PGMA chains.

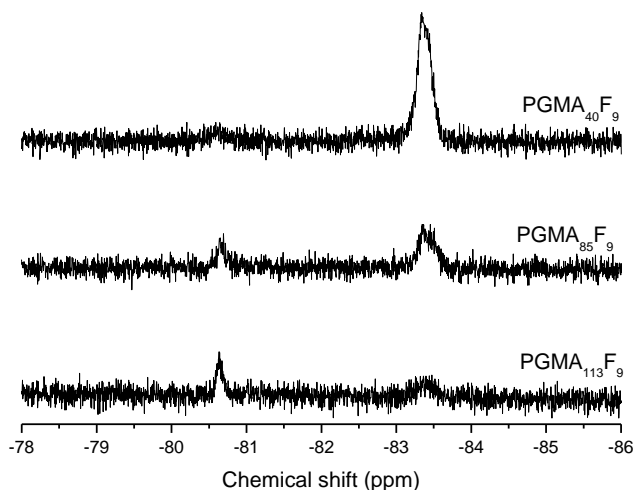


**Figure 3.11.** <sup>19</sup>F NMR spectra of 0.5 mM PGMA<sub>40</sub>F<sub>9</sub> (500 scans), PGMA<sub>85</sub>F<sub>9</sub> (1500 scans) and PGMA<sub>113</sub>F<sub>9</sub> (2000 scans) in D<sub>2</sub>O at 55 °C and 400 MHz.

Figure 3.12a shows the size distributions of 288 μM aqueous solutions of PGMA<sub>40</sub>N<sub>3</sub> and PGMA<sub>40</sub>F<sub>9</sub> semitelechelics at 25 °C obtained from DLS measurements. There are two relaxation modes in PGMA<sub>40</sub>N<sub>3</sub> and PGMA<sub>40</sub>F<sub>9</sub>. The decay rates ( $I$ ) of these two modes show a linear dependence on the square of the scattering vectors,  $q^2$  ( $q = (4n\pi/\lambda_0)\sin(\theta/2)$ ), and the extrapolations at  $q \rightarrow 0$  pass through the origin which confirm the diffusive character of these two modes. The fast modes ( $R_h$  of ~ 2.5 nm in PGMA<sub>40</sub> and ~ 6 nm in PGMA<sub>40</sub>F<sub>9</sub>) are considered to belong to the unimers and polymeric micelles, respectively, in terms of the particle size. It has reported that interpolymer complexes can be formed by secondary binding forces including van der Waals forces, hydrophobic interactions, electrostatic interactions and hydrogen bonding.<sup>65,66</sup> Polymer hydrogen bonding complexes have been observed in many donor/acceptors containing polymers, such as the hydroxyl group bearing polymers.<sup>67,68</sup> Recently, PGMA homopolymer and block copolymer chains were reported to show high affinity to each other to form clusters via intermolecular hydrogen bonding between the hydroxyl groups.<sup>34-35</sup> It is, therefore, reasonable to conclude that the formation of polymer clusters with the  $R_h$  of ~ 105 nm in PGMA<sub>40</sub>N<sub>3</sub> aqueous solution is mainly driven by intermolecular hydrogen bonding. The slow mode with  $R_h$  of ~ 80 nm in PGMA<sub>40</sub>F<sub>9</sub> aqueous solution is attributed to the clusters of micelles. Such micellar clusters are also observed in PEO based diblock copolymers aqueous solution.<sup>69</sup> The presence of this cluster can be

attributed to intermolecular hydrogen bonding between PGMA chains on different micelle surfaces. There is an overlapping region where polymer chains can interpenetrate and squeeze out some solvent molecules when two micelles come into contact.<sup>69-70</sup> This interpenetration of PGMA chains provides a possibility to form intermolecular hydrogen bonding between polymer chains.

The hydrogen bonding effect was further confirmed by the additional of trifluoroacetic acid (TFA), commonly used for hydrogen bond breaking. Figure 3.12b shows the size distributions of 288  $\mu\text{M}$  PGMA<sub>40</sub>F<sub>9</sub> and PGMA<sub>40</sub>N<sub>3</sub> aqueous solution with 0.2 M TFA. After adding TFA, the slow mode was significantly suppressed in both homopolymer and semitelechelic. For PGMA<sub>40</sub>N<sub>3</sub> with TFA, the amplitude ratio of the scattering intensity of the fast mode to the slow mode exhibits a strong increase compared to the solutions without TFA, suggesting that the number of the polymer clusters is largely reduced. In PGMA<sub>40</sub>F<sub>9</sub>, the slow mode disappeared completely after the addition of TFA. Moreover, the  $R_h$  of the PGMA<sub>40</sub>F<sub>9</sub> micelles increases from  $\sim 6$  nm to  $\sim 8$  nm. This can be attributed to the fact that polymer micelles become less compact due to the weakening of inter and intra- molecular hydrogen bonding.

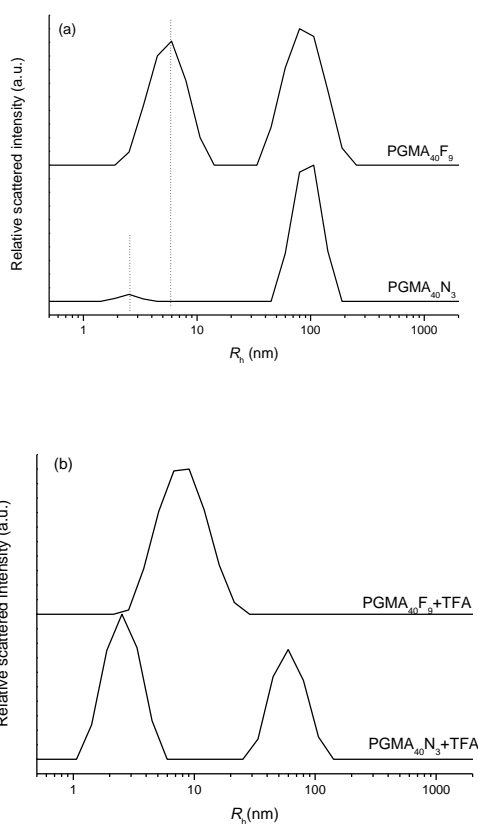


**Figure 3.12.** DLS results of (a) PGMA<sub>40</sub>F<sub>9</sub> and PGMA<sub>40</sub>N<sub>3</sub> in water at 288  $\mu\text{M}$  at 25  $^{\circ}\text{C}$ ,  $\theta = 90^{\circ}$  and (b) with the addition of 0.2 M TFA.

The annealing step is conducted on PGMA<sub>40</sub>F<sub>9</sub> aqueous solution with a concentration of 70  $\mu\text{M}$ . Figure 3.13 shows the  $R_h$  distributions of three PGMA<sub>40</sub>F<sub>9</sub> aqueous solutions with concentration of 70  $\mu\text{M}$  but obtained from the different preparation procedures. Sample “1” is prepared directly by dissolving the polymers at room temperature and stirring overnight. The sample “2” and “3” were obtained by stirring the polymer solutions, which are prepared as sample “1”, at 80 °C for 3 h and then cooled to room temperature with the slow rate of  $\sim 0.5$  °C  $\text{min}^{-1}$  and with the fast rate (quenching in a water bath at 22 °C), respectively. We now return to Figure 3.13 and analyse the  $R_h$  variation. The two modes in the sample “1” correspond to polymer micelles and clusters as discussed earlier. The micelles and clusters are observed also in the sample “2” with the identical particle sizes as sample “1”. Moreover, particles with large  $R_h$  of  $\sim 1200$  nm appeared. In DLS, the scattered intensity is roughly proportional to the sixth power of the size, thus, the number of these large particles is much smaller than that of the micelles and clusters. The large particles with the values of  $\sim 1000$  to  $1500$  nm were also reported by Rangelov et al. for aqueous solutions of PG-PPO-PG.<sup>71</sup> They attributed these particles to aggregates of polymers with compact PPO domains dispersed in a less compact PG medium due to the equal hydrophobic and hydrogen bonding interactions in the system. We assume that the large aggregates in sample “2” may have a similar structure due to the strong hydrogen bonding effect in the PGMA chains. Moreover, these large particles can also be simply attributed to the aggregates of micelles. In contrast to the fast mode observable for the sample “1” and “2”, the fast mode in the sample “3” with  $R_h$  of  $\sim 2.5$  nm reflects the Brownian motion of unimers rather than the micelles. Furthermore, a peak having the  $R_h$  of  $\sim 250$  nm with a shoulder at  $R_h$  of  $\sim 30$  nm is observed in sample “3”.

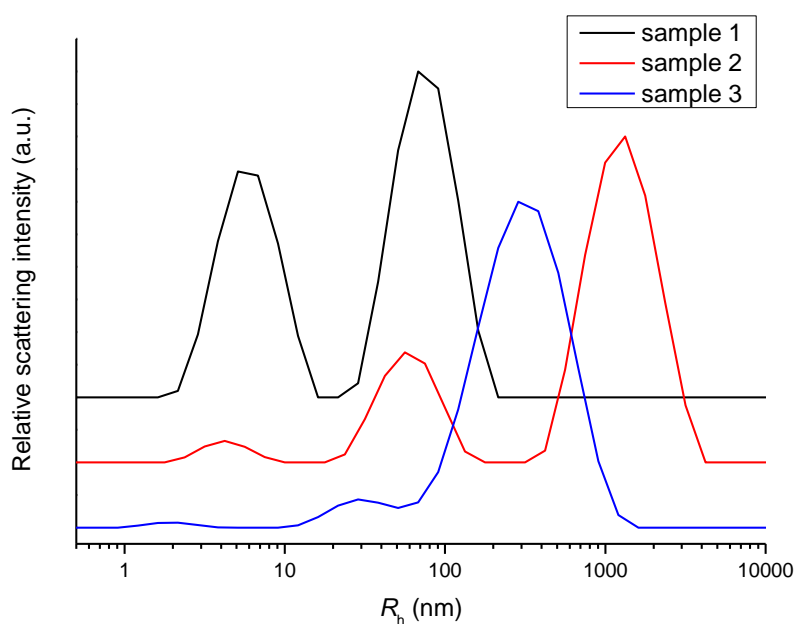


**Figure 3.13.** DLS data of 70  $\mu\text{M}$  PGMA<sub>40</sub>F<sub>9</sub> aqueous solution prepared by directly dissolving at room temperature and stirring for overnight (sample “1”), stirring at 80 °C for 3 h and cooling with a rate of  $\sim 0.5$  °C  $\text{min}^{-1}$  to room temperature (sample “2”) and stirring at 80 °C for 3 h and cooling to room temperature by water bath at 22 °C (sample “3”).

Additional information about the self-assembled structures of PGMA<sub>40</sub>F<sub>9</sub> in sample “2” and “3” were obtained from AFM measurements at room temperature. The samples for AFM measurements are prepared by coating the silicon substrates with polymer solutions with a concentration of 30  $\mu\text{M}$  and drying at the room temperature, followed by washing with Milli-Q water and drying under ambient conditions. Figure 3.14 shows the phase images of aggregated structures formed by the PGMA<sub>40</sub>F<sub>9</sub> in sample “2” (left) and “3” (right). The particles with the diameters of  $\sim 5$ -10,  $\sim 100$  and  $\sim 1000$ -1500 nm are well distributed in the image of sample “2”. In the image of sample “3”, the spherical structures with the size ranging from 20 -500 nm are observed.

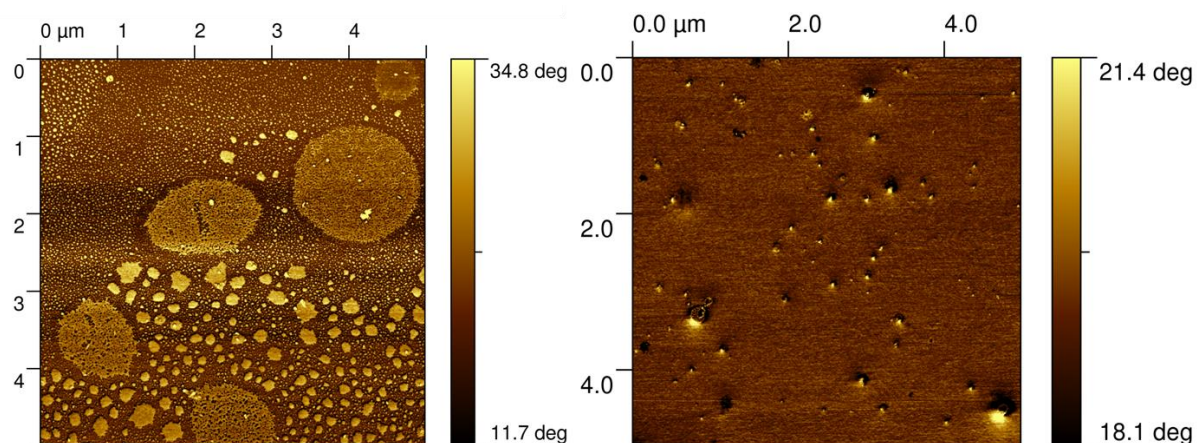


**Figure 3.14.** AFM phase images obtained after coating a silicon substrate with 30  $\mu\text{M}$  aqueous PGMA<sub>40</sub>F<sub>9</sub> solution of sample “2” (left) and “3” (right).

Additional SEM measurements were conducted to directly observe the morphology and size of the aggregates in samples “2” and “3”. It shows abundant single polymeric micelles with the diameter of  $\sim 8$  to 10 nm and big aggregates with diameters of  $\sim 100$  nm and  $\sim 800$ -1000 nm for the sample 2 as shown in Figure 3.15 (a) -(c). In the case of sample “3”, the spherical particles with various diameters from  $\sim 50$  to 100 nm are well distributed together with some big aggregates with diameters of  $\sim 300$  nm (Figure 3.15 (d)). It is noteworthy that the polymeric micelle sizes in AFM and SEM images are smaller than that obtained by DLS measurements. Such a difference is reasonable since DLS determines the  $R_h$  or the “equivalent sphere radius” in solution, whereas the AFM and SEM images were obtained in the absence of the solvent.



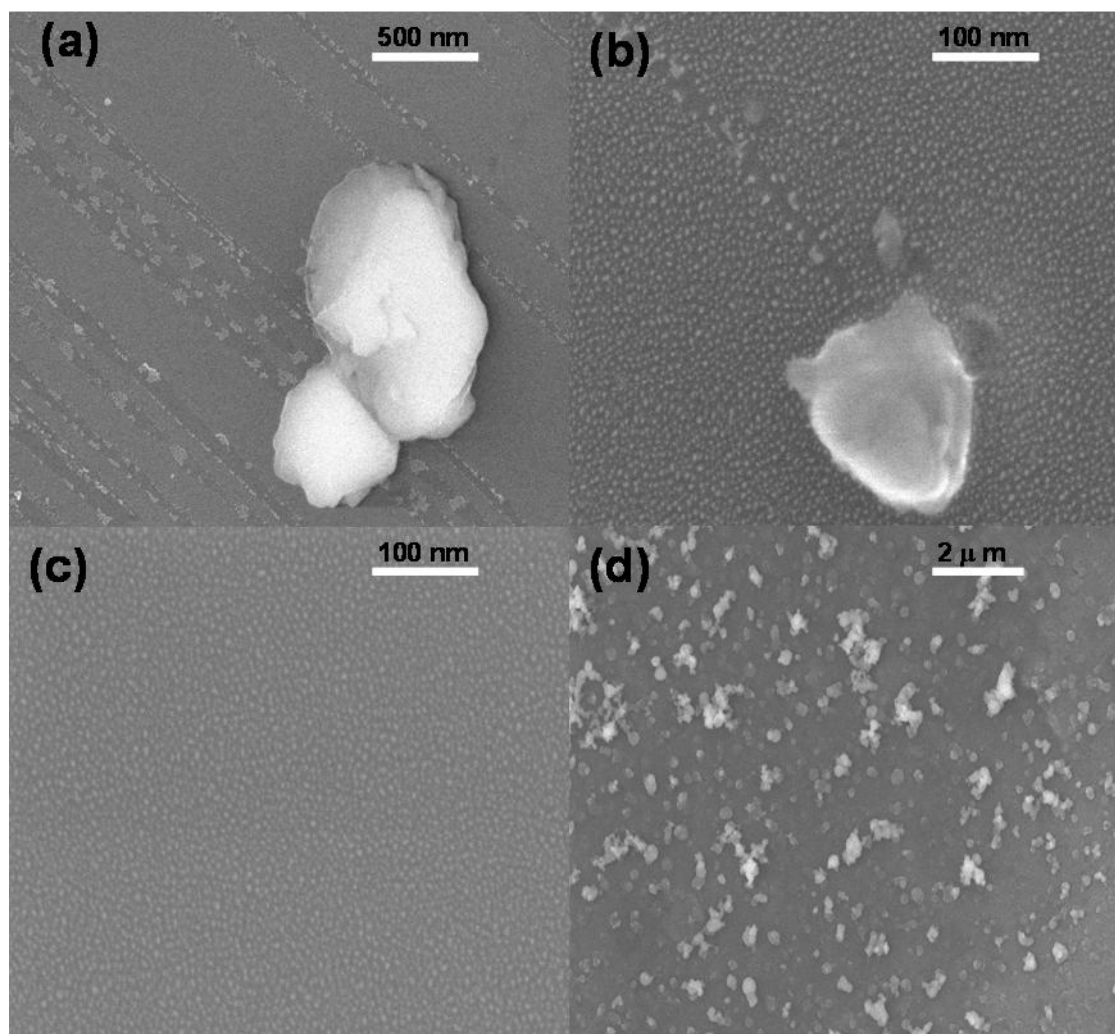


**Figure 3.16.** SEM images obtained after coating the silicon substrates with 0.25 mg mL<sup>-1</sup> sample “2” [images (a)-(c)] and sample “3” [image (d)] and evaporation of water at room temperature, followed by washing with Milli-Q water and drying at ambient condition. The four images have a different scale bar.

TEM measurements were applied to explore the structure of the large aggregates formed in sample “3”. Figure 3.17 shows the TEM image of a large particle formed in sample “3” obtained by coating a 30 μM aqueous solution of sample “3” on a carbon-coated copper grid and evaporation of water at room temperature without staining since the aggregated fluorocarbons domains are known to create a dark contrast in TEM images because of their high electron density.<sup>72</sup> The image shows a large aggregate with clustering of spherical aggregates of micelle cores with a diameter size of ~ 400 nm. The dark domains with diameters of ~ 8 to 10 nm are attributed to the aggregated F<sub>9</sub> segments forming an inner core, and the surrounding outer shell is obviously caused by the PGMA. This suggests that the

aggregate, indeed, consists of individual micelles which are composed of distinct F<sub>9</sub> inner core and PGMA coroneae.

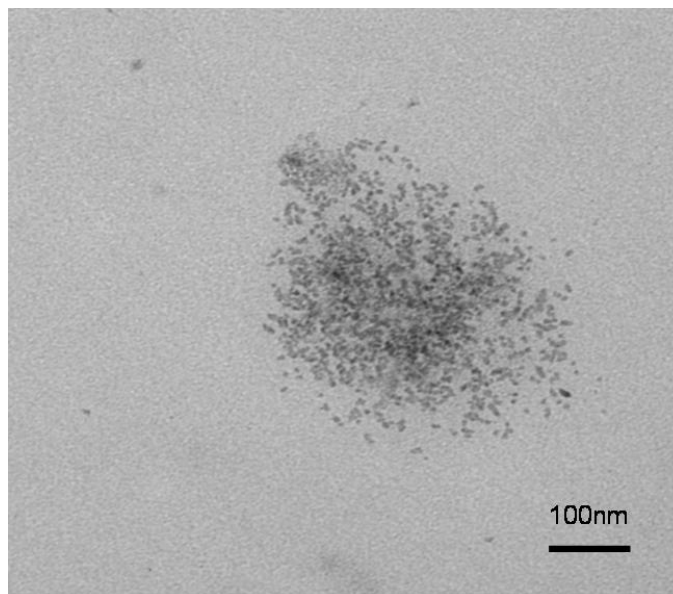


**Figure 3.17.** TEM image of sample “3” obtained after coating a carbon coated copper grid with 30  $\mu\text{M}$  solution.

From the experiments discussed above we know that the association of PGMA<sub>x</sub>F<sub>9</sub> in aqueous solution consists two attractive processes. These are the hydrophobic interactions in the F<sub>9</sub> segments and the intra- and intermolecular hydrogen bonding of the PGMA chains. Depending on the procedure of the polymer solution preparation, these two processes may take place simultaneously or with either of them preceding the other which leads to a different aggregation behavior.<sup>71</sup> This is also the reason to cause the different particles in the samples “2” and “3”, which are caused by a different thermal history.

### 3.4 Conclusion

In this chapter, perfluoroalkyl end capped PGMA<sub>s</sub> with different chain length were prepared applying a three-step procedure. At first an azide functional initiator was used to polymerize SMA by ATRP followed by the attachment of the F<sub>9</sub> segment to the polymers by CuAAC to yield the PSMAF<sub>9</sub>, the precursor of the PGMAF<sub>9</sub>. Finally, the protective group on each SMA repeat unit was cleaved to get the PGMAF<sub>9</sub>. Both the polymerization and modification reactions were found to proceed in a controllable and predictable way.

PGMA<sub>40</sub>F<sub>9</sub> shows a different association behavior in aqueous solution compared to the corresponding PEO<sub>44</sub>F<sub>9</sub> as follows: (i) the cmc values of PGMA<sub>40</sub>F<sub>9</sub> show a gradual increase with increasing temperature, as determined from surface tension measurements. This is in contrast to usual amphiphilic semitelechelics in water. (ii) PGMA<sub>40</sub>F<sub>9</sub> chains show an increasing mobility and solubility with increase temperature as evidenced from temperature dependent <sup>1</sup>H and <sup>19</sup>F NMR spectroscopy measurements. (iii) The thermodynamic data,  $\Delta H^0_{mic}$  and  $\Delta S^0_{mic}$ , calculated from the cmc at different temperatures show that the micellization process of PGMA<sub>40</sub>F<sub>9</sub> in aqueous solution is driven by both a decrease of enthalpy and an increase of entropy of micellization, whereas the micellization of PEO<sub>44</sub>F<sub>9</sub> is an entropy driven process which is not favored by the enthalpy of micelleization. Such a trend was also observed in ITC measurements. These significant differences arise from the partial self-association through hydrogen bonding which occurs among the PGMA chains. Two attractive processes occur in the micellization of PGMAF<sub>9</sub> in aqueous solution; hydrophobic interactions between the end groups and hydrogen bonding between PGMA. Consequently, the competition of these two processes results in a different aggregation behavior of the polymeric solution with different thermal history.

### 3.5 References

- (1) Strauss, U. P.; Jackson, E.G. *J Poly. Sci.* **1951**, *1*, 649-659
- (2) Dubin, P.; Bock, J., Eds. In *Macromolecular Complexes in Chemistry and Biology*, Springer-Verlag: New York, 1994.
- (3) Glass, J. E., Eds. In *Water soluble polymers: beauty with performance, Advances in chemistry*, American Chemical Society: Washington, DC, 1986. 123.
- (4) Hoang, K. C.; Mecozzi, S. *Langmuir* **2004**, *20*, 7347-7250.
- (5) Zhang, Y. X.; Da, A. H.; Butler, G. B.; Hogen-Esch, T. E. *J. Polym. Sci. Part A.; Polym. Chem.* **1992**, *30*, 1383-1391.
- (6) Hwang F, S.; Hogen-Esch, T. E. *Macromolecules* **1995**, *28*, 3328-3335.
- (7) Zhou, J. C.; Zhuang; D. Q.; Yuan, X. F.; Jiang, M; Zhang Y.X. *Langmuir* **2000**; *16*, 9653.
- (8) Li, M.; Jiang, M.; Zhang Y. X.; Fang Q. *Macromolecules* **1997**, *30*, 470-478.
- (9) Zhang, H. S.; Pan., J.; Hogen-Esch, T. E. *Macromolecules* **1998**, *31*, 2815-2821.
- (10) Preuschen, J.; Menschen, S.; Winnik, M. A.; Heuer, A.; Spiess, H. W. *Macromolecules* **1999**, *32*, 2690-2695.
- (11) Boschet, F.; Branger, C.; Margaillan, A.; Condamine, E. *Polymer* **2002**, *43*, 5329-5334.
- (12) Racey, J. C.; Stebe, J. *Colloid Surf. A: Physiochem. Eng. Aspects* **1994**, *84*, 11-31.
- (13) Sawada, H. *J. Fluorine Chem.* **2000**, *101*, 315-324.
- (14) Sawada, H. *J. Fluorine Chem.* **2000**, *101*, 219-220.
- (15) Cathebras, N.; Collet, A.; Viguier, M.; Berret, J. F. *Macromolecules* **1998**, *31*, 1305-1311.
- (16) Liu, R. C. W.; Cantin, S.; Perrot, F.; Winnik, F. M. *Polymers for advanced technologies* **2006**, *17*, 798-803.
- (17) Zhang Y. X.; Fang, Q.; Fu, Y. Q.; Da, A. H.; Zhang ,Y. B.; Wu, C.; Hogen-Esch. T, E. *Polym. Int.* **2000**, *49*, 763-774.
- (18) Zhang, Y. B.; Li, M.; Fang, Q., Zhang, Y. X. Jiang, M.; Wu, C.; *Macromolecules* **1998**, *31*, 2527-2532.
- (19) Chen, J. Y.; Jiang, M.; Zhang, Y. X.; Zhou, H. *Macromolecules* **1999**, *32*, 4861-4866.
- (20) Zhuang, D. Q.; Hogen-Esch, T. E.; Zhang, Y. X. *J. Applied Polym. Sci.* **2004**, 1279-1285.
- (21) Kubowicz, S.; Thünemann, A. F.; Weberskirch, R.; Möhwald, H. *Langmuir* **2005**, *21*, 7214-7219.
- (22) Chen, J.; Du, L. B.; Zhang, Y. X.; Hogen-Esch, T. E.; Jiang, M. *Polym. Int.* **2001**, *50*, 148-156.

- (23) Yoon, S. Y.; Lee, J. K.; Chung, I.; Park, S. S.; Lee, W. K. *Macromol. Symp.* **2007**, *150*, 431-436.
- (24) Lee, W. K.; Jeon, S.; Yoon, S. Y.; Lee, J. K.; Ha, C. S.; Gardella, J. A. *Macromolecular Research* **2006**, *14*, 487-490.
- (25) Cui, W.; Bei, J.; Wang, S.; Zhi, G.; Zhao, Y.; Zhou, X.; Zhang, H.; Xu, Y. *J. Biomed. Mater. Res. B Appl. Biomater.* **2005**, *73*, 171-178.
- (26) Lee, W. K.; Losito, I.; Gardella, J. A.; Hicks, W. *Macromolecules* **2001**, *34*, 3000-3006.
- (27) Abrahmsen-Alami, S.; Stilbs, P., *J. Phys. Chem.* **1994**, *98*, 6359-6367.
- (28) Persson, K.; Bales, B. L., *J. Chem. Soc., Fara. Trans.* **1995**, *91*, 2863-2870.
- (29) Gates, G.; Harmon, J. P.; Ors, J.; Benz, P., *Polymer* **2003**, *44*, 207-214.
- (30) Gates, G.; Harmon, J. P.; Ors, J.; Benz, P.; *Polymer* **2003**, *44*, 215-222.
- (31) Leung, B. K.; Robinson, G. B.; *J. Appl. Polym. Sci.* **1993**, *47*, 1207-1214.
- (32) Amado, E.; Kressler, J.; *Soft Matter* **2011**, *7*, 7144-7149.
- (33) Amado, E.; Augsten, C.; Mäder, K.; Blume, A.; Kressler, J. *Macromolecules* **2006**, *39*, 9486-9496.
- (34) Kyeremateng, S. O.; Henze, T.; Busse, K.; Kressler, *Macromolecules*, **2010**, *43*, 2502-2511.
- (35) Kyeremateng, S. O.; Busse, K.; Kohlbrecher, Kressler, J., *Macromolecules* **2011**, *44*, 583-593.
- (36) Urien, M.; Erothu, H.; Cloutet, E.; Hiorns, R. C.; Vignau, L.; Cramail, H. *Macromolecules* **2008**, *41*, 7033-7040.
- (37) Li, Z.; Kyeremateng, S. O.; Fuchise, K.; Kakuchi, R.; Sakai, R.; Kakuchi, T.; Kressler, J. *Macromol. Chem. Phys.* **2009**, *210*, 2138-2147.
- (38) Kyeremateng, S. O.; Amado, E.; Kressler, J. *Eur. Polym. J.* **2007**, *43*, 3380-3391.
- (39) Golas, P. L.; Tsarevsky, N.V.; Sumerlin, B. S.; Matyjaszewski, K. *Macromolecules* **2006**, *39*, 6451-6457.
- (40) Ordian, G. In *Principles of polymerization*. 4<sup>th</sup> Edition, Wiley-Interscience, New Jersey, 2004.
- (41) Hamley, I. W. In *the Physicals of Block Copolymers*; Hamley, I. W.; Ed.; Oxford University Press: Oxford, 1998. 131-220.
- (42) Chu, B.; Zhou, Z. K.; In *Nonionic Surfactants polyoxyalkylene block copolymers*; Nace, V. M.; Ed.; Marcel Dekker Inc.: New York, 1996. 67-144.
- (43) LaRue, I.; Adam, M.; Zhulina, E.; Rubinstein, M.; Pitsikalis, M.; Hadjichristidis, N.; Ivanov, D.; Gearba, R. I.; Anokhin, D. V.; Sheiko, S. S., *Macromolecules* **2008**, *41*, 6555-6563.

- (44) Zhou, Z. K.; Chu, B.; Peiffer, D. G., *Macromolecules* **1993**, *26*, 1876-1883
- (45) Alexandridis, P.; Lindman, B. eds, *Amphiphilic block copolymers, self-assembly and application*, Elsevier, 2000., Amsterdam
- (46) Dai, S.; Tam, K. C., *Colloids and Surfaces A: Physicochem. Eng. Aspects* **2003**, *229*, 157-168.
- (47) Olofsson, G., *J. Phys. Chem.* **1985**, *89*, 1473-1477.
- (48) Mai, S. M.; Booth, C.; Kellarakis, A.; Havredaki, V.; Ryan, A. J. *Langmuir* **2000**, *16*, 1681-1688.
- (49) Graziano, G. *Phys. Chem. Chem. Phys.* **1999**, *1*, 3567-3576.
- (50) Halacheva, S.; Rangelov, S.; Tsvetanov, C., *Macromolecules* **2006**, *39*, 6845-6852.
- (51) Hunter, R. J. *Foundations of Colloid Science*; Oxford University Press: New York, 1987; Vol 1.
- (52) Tanford, C., *The Hydrophobic Effect* 1973, Wiley, New York.
- (53) Grosmaire, L.; Chorro, M.; Chorro, C.; Partyka, S.; Zana, R., *J. Colloid and Interface Science* **2002**, *246*, 175-181.
- (54) Pestman, J. M.; Kevelam, J.; Blandamer, M. J.; von Doren, H. A.; Kellogg, R. M., Engberts, J. B. F. N., *Langmuir* **1999**, *15*, 2009-2014.
- (55) Moroi, Y.; Nishikido, N.; Uehara, H.; Matura, R., *J. Colloid. Interface Sci.* **1975**, *50*, 254-263.
- (56) Corkill, J. M.; Goodman, J. F.; Tate, J. R., *Hydrogen-Bonded Solvent Ayst. Proc. Symp.* **1968**, 181.
- (57) (a) Okhrimenko, O.; Jelesarov, L., *J. Mol. Recongnit.* **2008**, *21*, 1-19. (b) Raju, B. B.; Winnik, F. M.; Morishima, Y., *Langmuir* **2001**, *17*, 4416-4421. (c) Kujawa, P.; Goh, C. C E.; Calvet, D.; Winnik, F. M., *Macromolecules* **2001**, *34*, 6387-6395.
- (58) Gottlieb, H. E.; Kotlyar, V.; Nudelman, A. *J. Org. Chem.* **1997**, *62*, 7512-7515
- (59) Bossev, D. P.; Matsumoto, M.; Makahara, M. *J. Phys. Chem.B*, **2000**, *104*, 155-158.
- (60) Endres, F.; Bukowski, M.; Hempelmann, R.; Natter, H. *Angew. Chem. Int. Ed.* **2003**, *42*, 3428-3430.
- (61) Bühler, G.; Feldmann, C. *Angew. Chem., Int. Ed.* 2006, *45*, 4864-4867.
- (62) Ohta, A.; Murakam, R.; Urata, A., Asakawa, T.; Miyagishi, S.; Aratono, M., *J. Phys. Chem. B* **2003**, *107*, 11502-11507.
- (63) Hoang, K. C.; Mecozzi, S., *Langmuir* **2004**, *20*, 7347-7350.
- (64) Petit, F.; Iliopoulos, I.; Audebert, R., *polymer*, **1998**, *39*, 751-753.
- (65) Ilmain, F.; Tanaka, T.; Kokufuta, E., *Nature* **1991**, *349*, 400-401.

- (66) Deng, L.; Wang, C. H.; Li, Z. C.; Liang, D. H., *Macromolecules* **2010**, *43*, 3004-3010.
- (67) Madsen, J.; Arms, S. P. *Biomacromolecules* **2009**, *10*, 1875-1887.
- (68) Fang, L. Brown, W. *Macromolecules* **1990**, *23*, 3284-3290.
- (69) Lombardo, D.; Micali, N.; Villari, V.; Kiselev, M. A. *Phys. Rev. E* **2004**, *70*, 21402-21408.
- (70) Lobry, L.; Micali, N.; Mallamace, F.; Liao, C.; Chen, S. H., *Phys. Rev. E* **1999**, *60*, 7076-7087.
- (71) Rangelov, S.; Almgren, M.; Halacheva, S.; Tsvetanov, C., *J. Phys. Chem. C* **2007**, *111*, 13185-13191.
- (72) Busse, K.; Kressler, J.; Eck, D.; Höring, S., *Macromolecules* **2002**, *35*, 178-184.

## Chapter 4

### *Influence of the Chirality of Grafted Poly(glycerol methacrylate) Chains on Protein Adsorption*

#### 4.1 Introduction

The ability to resist non-specific protein adsorption is essential for many *in vivo* or *in vitro* biomedical applications.<sup>1</sup> For example, the non-specific protein adsorption can reduce the functionality of implants,<sup>2</sup> catheters,<sup>3</sup> or hip joint replacements<sup>4,5</sup> by producing undesirable features. Coating the surface with a thin layer of protein repelling material is one universal approach for minimizing the problems arising from protein adsorption. Recently, synthetic polymers are of great interest because of their controllable structures, compositions and properties.<sup>6</sup> To date, several polymers were demonstrated to reduce non-specific protein adsorption, including poly(ethylene oxide) (PEO),<sup>7-9</sup> polyglycerol,<sup>10,11</sup> poly(hydroxypropyl methacrylate) (PHPMA),<sup>12</sup> poly(2-hydroxyethyl methacrylate) (HEMA),<sup>13</sup> poly(*N*-isopropylacrylamide) (PNIPAM),<sup>14</sup> zwitterionic polymers,<sup>15-17</sup> etc. Among them, PEO is the most commonly studied material. Although the underlying physical mechanisms and thermodynamic origins of the protein resistance of PEO are not fully understood, studies over the past few decades suggest that the terminal group, chain length and the grafting density play an important role in the protein repelling ability.<sup>18-23</sup>

Biological systems are often chiral many biomolecules in organism show a high chiral preference.<sup>24,25</sup> Recognizing the chiral effect is very important in the design of biomaterials for the treatment of surfaces or interfaces since it may further influence biological processes such as protein adsorption and cell adhesion.<sup>26-28</sup> In the 90th of the last century, Addadi and coworkers found that epithelial cells exhibit different adhesion to (*S,S*)-tartrate tetrahydrate crystals compared to (*R,R*)-crystals.<sup>26</sup> Recently, Sun et al. observed that plasmid DNA exhibits a more relaxed conformation on the *L*-cysteine surface<sup>27</sup> and proteins show a preference towards to the poly(*N*-acryloyl-*L*-valine) surface compared to the *D*-surfaces.<sup>28</sup> This phenomenon is considered to be a result of the stereospecific hydrogen bonding or hydrophobic interactions between the surfaces and DNA/protein. Furthermore, they also found that COS-7 and bEnd.3 cells show a similar preference as proteins to chiral surfaces.<sup>28</sup>



To date, the influence of stereochemistry on the protein repelling ability of surfaces is still unclear. For example, different results were obtained for the protein repelling properties of surfaces covered by sorbitol and mannitol groups, which differ only in the chirality of one asymmetric carbon, by experimental methods and molecular simulations.<sup>29</sup> In the work by Ostuni et al.,<sup>29a</sup> sorbitol covered surfaces were shown to have higher protein adsorption than mannitol surfaces. However, Jiang et al.<sup>29b</sup> found that these two surfaces create the same repulsive force on approached proteins by using molecular simulations. The surface resonance plasmon (SPR) results of permethoxylated polyesters having different stereochemical repeating units demonstrated that the polymer stereochemistry does not have much effect on the protein-resistant properties.<sup>30</sup> In a separate study of Luk et al., they observed self-assembled monolayers (SAMs) with *D*-, *L*- and racemic mixtures of mannonamide groups support ~ 21%, ~ 7% and ~ 1% BSA adsorption, respectively, compared to pentadecanethiol surfaces, but further explanation was not given.<sup>31</sup>

“Grafting from” and “grafting to” are two common methods to achieve a permanent covalent grafting of polymers on solid surfaces.<sup>32-34</sup> The “grafting from” method involves the polymer growing from initiator groups on substrate surface, such as surface initiated atom transfer radical polymerization (SI-ATRP).<sup>32,34</sup> By using this method, the polymers can be grafted on surfaces densely to form highly stretched polymer brushes.<sup>34</sup> The “grafting to” method involves a chemical reaction between polymer molecules with the substrate surface, resulting in the formation of tethered chains. Compared to the “grafting from” method, well defined polymer brushes can be easier obtained by the “grafting to” method since the synthesis of polymers can be better controlled in solution than on solid surfaces, and the polymers can be characterized thoroughly via various methods in solution.<sup>33</sup>

Poly(glycerol methacrylate) (PGMA) is a hydrophilic polymer with two hydroxyl (OH) groups, which can be easily derivatized, on each repeat unit and has a wide use in biomedical and pharmaceutical applications such as hydrogels, soft contact lenses and drug delivery.<sup>35,36</sup> Moreover, PGMA is also a typical chiral polymer due to the asymmetric carbon atom on each repeat unit. However, most of the studies of PGMA ignore this important fact, even it plays an important role in the biological mechanism. Herein, the enantiopure and racemic HS-PGMAs (see Chart 4.1), HS-PGMA(*S*)<sub>28</sub>, HS-PGMA(*R*)<sub>24</sub>, and HS-PGMA(*rac*)<sub>27</sub>, were specifically prepared to examine the influence of surface stereochemistry on the protein adhesion. The subscripts 28, 24 and 27 are the degree polymerizations (*DPs*) of PGMA. These three polymers are synthesized with similar *DPs* under the same experimental conditions by ATRP. PGMA SAMs, which provide a chemically and structurally well-defined platform for

studying the protein adsorption, are prepared by the “grafting to” method via immersing gold surfaces into the HS-PGMAs aqueous solutions. The polymers are attached onto the gold surfaces since the thiol group has a strong affinity to gold by forming chemical bonds. SPR spectroscopy is used to detect the adsorption of bovine serum albumin (BSA) on PGMA surfaces.

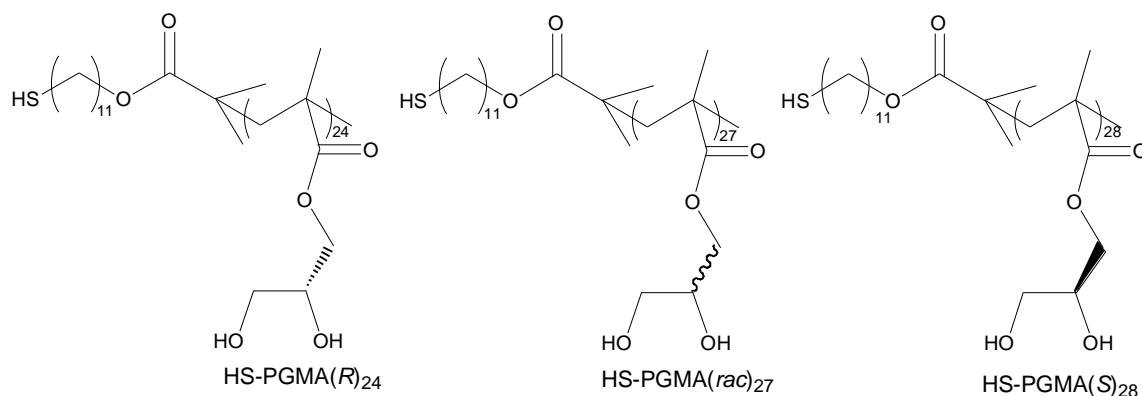


**Chart 4.1.** The synthesized enantiopure and racemic thiol functional PGMA polymers.

## 4.2 Experimental section

### 4.2.1 Materials

All chemicals were purchased from Sigma-Aldrich unless otherwise stated. Solketal (98%), (*S*)-(+)-solketal (98%), (*R*)-(-)-solketal (98%), triethylamine (Et<sub>3</sub>N) (≥99%), methacryloyl chloride (97%), benzene (Alfa Aesar, 99%), sodium sulphate (Roth, ≥99.0%), 11-mercapto-1-undecanol (97%), 1-fluoro-2,4-dinitrobenzen, chloroform (≥99%), hydrochloric acid (HCl),  $\alpha$ -bromoisobutyryl bromide (BIB) (98%), methanol, anisole (99%), copper(I)bromide (≥98%), 2,2'-bipyridine (bpy) (≥98.0%), tetrahydrofuran (THF) (Roth, 99.9%), *n*-hexane, dimethylformamide (DMF) (99.8%), 1-propanethiol (≥99%) and 1,4-dioxane (Alfa Aesar, ≥98%) were used as received. Chloroform and anisole were dried over calciumhydride overnight, distilled and stored over molecular sieve. Copper(I)bromide was purified by stirring in glacial acetic acid, washing with methanol, and then dried under vacuum at 80 °C.

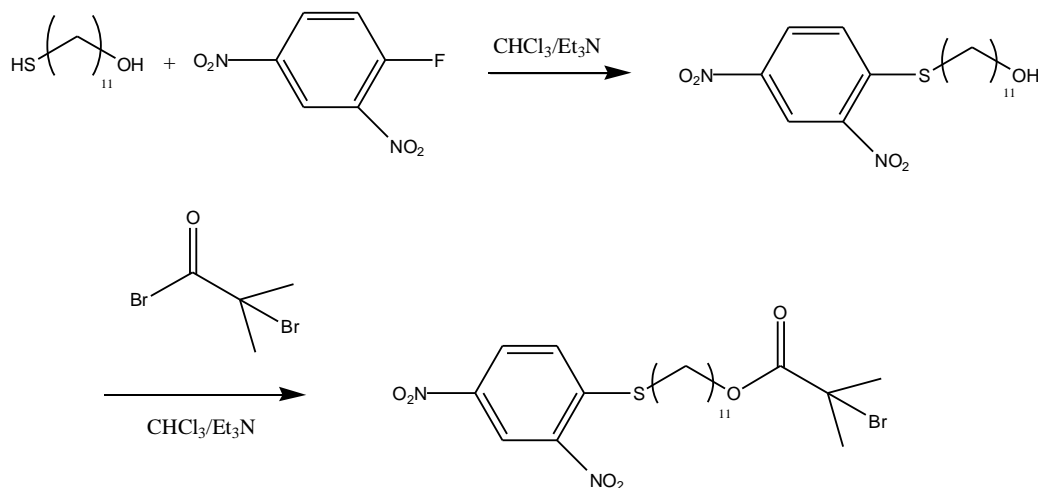
## 4.2.2 Synthesis

### 4.2.2.1 Synthesis of 11-(2,4-dinitrophenylthio)undecyl-2-bromo-methylpropionate

The synthesis of the initiator, 11-(2,4-dinitrophenylthio)undecyl-2-bromo-methylpropionate, was carried out according to a procedure described elsewhere<sup>37,38</sup> with some modifications (Scheme 4.1). In a 100 mL two necked round bottom flask, a mixture of 2.04 g (0.01 mol) 11-mercapto-1-undecanol and 3.04 g (0.03 mol) Et<sub>3</sub>N in 20 mL chloroform were added to a solution of 1.86 g (0.01 mol) 1-fluoro-2,4-dinitrobenzen in 20 mL of chloroform dropwise under nitrogen atmosphere at room temperature. The mixture was stirred for 20 h at room temperature. A yellow precipitate was separated from the liquid phase by filtration, washed with 1M HCl and distilled water, and then dried in a vacuum oven at room temperature for overnight. For further purification, chloroform was used to extract the product. The extracted solution was kept at room temperature for overnight to get yellow crystals. Pure 11-(2,4-dinitrophenylthio)-1-undecanol was obtained by filtration and drying in a vacuum oven for overnight (yield: 85 %).

In a 500 mL two-necked round bottom flask fitted with a magnetic stirrer, 3.22 g (0.014 mol) BIB dissolved in 50 mL chloroform was added dropwise into the solution of 2.59 g (0.007 mol) 11-(2,4-dinitrophenylthio)-1-undecanol and 2.13 g (0.021 mol) Et<sub>3</sub>N in 100 mL chloroform. The solution was stirred for 20 h at room temperature and then condensed to remove most of the solvent. A yellow precipitate was formed after the addition of methanol and then washed by 1M HCl and distilled water. The crystals were filtered and dried at room temperature in a vacuum oven for overnight. The pure product was obtained by recrystallization from methanol (yield: 83 %).

The <sup>1</sup>H-NMR spectrum (400 MHz, CDCl<sub>3</sub>) showed: 9.05 ppm (1H, -Ar), 8.33 ppm (1H, -Ar), 7.53 ppm (1H, -Ar), 4.15 ppm (2H, -COOCH<sub>2</sub>-), 3.01 ppm (2H, -SCH<sub>2</sub>-), 1.90 ppm (-6H, -C(CH<sub>3</sub>)<sub>2</sub>), 1.76 ppm (2H, -SCH<sub>2</sub>CH<sub>2</sub>-), 1.66 ppm (2H, -COOCH<sub>2</sub>CH<sub>2</sub>-), 1.60-1.20 ppm (14H, -CH<sub>2</sub>CH<sub>2</sub>(CH<sub>2</sub>)<sub>7</sub>CH<sub>2</sub>CH<sub>2</sub>-). The <sup>13</sup>C-NMR spectra (100 MHz, CDCl<sub>3</sub>) showed: 171.66 ppm (-COOCH<sub>2</sub>-), 147.45 ppm (-Ar), 144.73 ppm (-Ar), 143.56 ppm (-Ar), 126.90 ppm (-Ar), 126.75 ppm (-Ar), 121.69 ppm (-Ar), 66.01 ppm (-COOCH<sub>2</sub>-), 55.93 ppm (-C(CH<sub>3</sub>)<sub>2</sub>-), 32.59 ppm (-SCH<sub>2</sub>-), 30.74-27.43 ppm (-CH<sub>2</sub>(CH<sub>2</sub>)<sub>9</sub>CH<sub>2</sub>-), 25.68 ppm (-C(CH<sub>3</sub>)<sub>2</sub>-).



**Scheme 4.1.** Synthetic route for the synthesis of 11-(2,4-dinitrophenylthio)undecyl-2-bromo-methylpropionate.

#### 4.2.2.2 Synthesis of 2,4-dinitrophenyl protected poly(solketal methacrylate) (PSMA)

The synthesis of SMA<sup>39</sup> is reported elsewhere. In this study, the *R*-, *S*- and *rac*- SMA monomers were synthesized from the reactions of methacryloyl chloride and *S*-, *R*-, and *rac*-solketal, respectively. The 2,4-dinitrophenyl protected PSMA(*rac*)<sub>27</sub>, PSMA(*R*)<sub>24</sub> and PSMA(*S*)<sub>28</sub> were prepared from the 2,4-dinitrophenyl functional initiator by ATRP of *rac*-, *R*-, and *S*- SMAs, respectively, using CuBr as catalyst, bpy as ligand and anisole as solvent with a [catalyst]<sub>0</sub>: [ligand]<sub>0</sub> ratio of 1: 3 and [SMA]<sub>0</sub>/[initiator]<sub>0</sub> ratio of 30. In a typical ATRP procedure, 0.172 g (0.33 μmol) initiator, 0.05 g (0.33 μmol) CuBr and 0.158 g (1 μmol) bpy were added to a 50 mL Schlenk tube with a magnetic stirrer. Then the Schlenk tube was capped with a rubber septum, and cycled five times in vacuum and nitrogen to remove oxygen. 10 mL distilled anisole was added into the Schlenk tube and bubbled with nitrogen for 20 min under vigorous stirring. 2 g (10 μmol) SMA in 8 mL degassed anisole was added into the tube and bubbled with nitrogen for another 15 min. The polymerization was carried out at 60 °C in an oil bath for 20 h. The product was purified by passing through the silica column with THF as eluent, followed by precipitation into an excess of cold *n*-hexane.

<sup>1</sup>H NMR spectrum (400 MHz, DMSO-*d*<sub>6</sub>) showed: 8.85 ppm (1H, -Ar), 8.41 ppm (1H, -Ar), 7.85 ppm (1H, -Ar), 4.33-3.59 ppm (5H, -OCH<sub>2</sub>CH(O-)CH<sub>2</sub>-), 1.97-1.59 ppm (2H, -CH<sub>2</sub>(CH<sub>3</sub>)C(COO-)), 1.46-1.10 ppm (6H, -OC(CH<sub>3</sub>)CO-); 18H, -CH<sub>2</sub>(CH<sub>2</sub>)<sub>9</sub>CH<sub>2</sub>-; 6H, -C(CH<sub>3</sub>)<sub>2</sub>-), 1.07-0.63 ppm (3H, -CH<sub>2</sub>C(CH<sub>3</sub>COO-)-).

#### 4.2.2.3 Deprotection of 2,4-dinitrophenyl protected PSMA to afford thiol functional PSMA (HS-PSMA)

5 equivalent (equiv) Et<sub>3</sub>N and 15  $\mu$ L Milli-Q water were added to 2 mL DMF solution containing 1 equiv 2,4-dinitrophenyl protected PSMA and 10 equiv 1-propanthiol. The mixture was stirred at room temperature for 20 h, and then the solvent was evaporated to give an orange gel liquid. The pure HS-PSMA was obtained by dissolving the crude product in 3-5 mL THF and precipitating into cold *n*-hexane.

<sup>1</sup>H NMR spectrum (400 MHz, DMSO-*d*<sub>6</sub>) showed: 4.35-3.55 ppm (5H, -OCH<sub>2</sub>CH(O-)CH<sub>2</sub>-), 2.03-1.63 ppm (2H, CH<sub>2</sub>(CH<sub>3</sub>)C(COO-) ), 1.47-1.10 ppm (6H, -OC(CH<sub>3</sub>)CO-; 18H, -CH<sub>2</sub>(CH<sub>2</sub>)<sub>9</sub>CH<sub>2</sub>-; 6H, -C(CH<sub>3</sub>)<sub>2</sub>-), 1.09-0.62 ppm (3H, -CH<sub>2</sub>C(CH<sub>3</sub>COO-)-).

#### 4.2.2.4 Preparation of high purified HS-PGMA

The HS-PGMA was obtained by hydrolysis of HS-PSMA with 1 N HCl in 1,4-dioxane at room temperature for 48 h. The product was dissolved in water and dialyzed against water using a multi-purpose dialysis tubing (Spectra/Por 7 Membrane: MWCO: 1000), and finally freeze-dried to give the purified HS-PGMA.

<sup>1</sup>H NMR spectrum (400MHz, DMSO-*d*<sub>6</sub>) showed: 4.98-4.54 ppm (2H, CH<sub>2</sub>(OH)CH(OH)-), 4.07-3.33 ppm (5H, CH<sub>2</sub>(OH)CH(OH)CH<sub>2</sub>-), 1.99-1.46 ppm (2H, -CH<sub>2</sub>C(CH<sub>3</sub>COO-)-), 1.37-1.14 ppm (18H, -CH<sub>2</sub>(CH<sub>2</sub>)<sub>9</sub>CH<sub>2</sub>-; 6H, -C(CH<sub>3</sub>)<sub>2</sub>-), 1.11-0.61 ppm (3H, -CH<sub>2</sub>C(CH<sub>3</sub>COO-)-).

#### 4.2.3 SAM preparation

The gold substrates for ellipsometry, and surface enhanced Raman spectroscopy (SERS) measurements were prepared by vapour deposition of 100 nm gold onto silicon wafers in high-vacuum. A layer of titanium (~ 10 nm thick) was applied for adhesion of the gold film. Prior to chemisorption, the substrates were immersed in Piranha solution (H<sub>2</sub>SO<sub>4</sub>/H<sub>2</sub>O<sub>2</sub>=3/1, v/v) for 5 min and then ultrasonicated in ethanol for 30 min and in Milli-Q water for 5 min. The cleaned substrates were dried under a stream of nitrogen. The gold sensors for SPR, and water contact angle measurement, are purchased from IBIS Technologies BV (Enschede, Netherlands) and washed by ethanol and water before use. SAMs were formed by dipping the

gold coated substrates in 4 mg mL<sup>-1</sup> polymer aqueous solutions at room temperature under dark condition. After 24 h, the substrates were rinsed in water to remove the unbound polymer, and dried under nitrogen stream.

#### 4.2.4 Characterization

##### 4.2.4.1 Dynamic light scattering (DLS)

All DLS measurements were carried out using a commercial apparatus of ALV-Laser Vertiebsgesellschaft GmbH (Langen, Germany). The light source was a vertically polarized green neodymium: YAG DPSS-200 laser (wavelength 532 nm) from Coherent, Auburn, CA, USA, with a power output of 200 mW. The correlation functions from DLS were analyzed by the CONTIN method, giving information on the distribution of decay rate ( $\Gamma$ ). Apparent diffusion coefficients were obtained from  $D_{\text{app}} = \Gamma/q^2$ , where  $\Gamma$  is the reciprocal of the characteristic decay time,  $q = (4\pi n_0/\lambda) \sin(\theta/2)$  being the scattering vector,  $n_0$  is the refractive index of the medium,  $\lambda$  is the wavelength of the light,  $\theta$  is the scattering angle. The corresponding apparent hydrodynamic radii,  $R_h$ , were obtained via the Stokes-Einstein equation  $R_h = kT/(6\pi\eta D_{\text{app}})$ , where  $k$  is the Boltzmann constant and  $\eta$  is the viscosity of the solvent, water in this case, corrected at the absolute temperature  $T$ . The samples were prepared by dissolving the polymers in Milli-Q water with a concentration of 4 mg mL<sup>-1</sup> and then filtered through PTFE filters with 0.45  $\mu\text{m}$  pore size in order to remove the dust. The  $R_h$  distributions were recorded for scattering angles from 50 to 140 ° at 25 °C after at least 30 min equilibration.

##### 4.2.4.2 Circular dichroism spectroscopy (CD)

Circular dichroism (CD) spectra were recorded on a Jasco J-810 CD spectrometer equipped with a PTC-423S temperature controller. Measurements were performed in a 1 mm quartz cell with 4 mg mL<sup>-1</sup> polymer aqueous solutions at 25 °C. A typical measurement was performed with a scanning rate of 50 nm min<sup>-1</sup> and 30 accumulations.

#### 4.2.4.3 Ultraviolet (UV) spectroscopy

UV absorption spectra were measured on a HP 8453 spectrophotometer with a HP 89090A temperature controller. The measurements were performed at 25 °C and on the quartz cell containing 2 mg mL<sup>-1</sup> polymer aqueous solution.

#### 4.2.4.4 Surface enhanced Raman spectroscopy (SERS)

The SERS spectra were recorded on a Bruker FRA 106 Raman spectrometer (HeNe laser at 633 nm) with a MCT detector cooled by liquid nitrogen. All the measurements were recorded on the SAM surfaces at room temperature with the band resolution of 4 cm<sup>-1</sup>.

#### 4.2.4.5 Water contact angle measurement

The water contact angles (WCAs) of polymer surfaces were measured by a sessile drop method on an OCA 15 Plus device from Dataphysics (Filderstadt, Germany) using Milli-Q water in ambient condition. Five droplets of 3 µL were applied to five different locations on each sample and the obtained values were used to calculate mean values and standard deviations. The standard deviation of each sample is within 15 %.

#### 4.2.4.6 Ellipsometry

The thicknesses of dehydrated PGMA layers on the gold surfaces were determined by means of ellipsometry (M-2000V, J.A. Woollam Co. Inc., Lincoln, NE, USA). The measurements were performed at incident angles of 65° and 70° under ambient conditions at room temperature. Initially, the bare gold substrates were tested and taken as references for the analysis of the adsorbed polymer layers. The PGMA layer thicknesses were evaluated using an Au/PGMA two layer model. A refractive index of PGMA equal to 1.525 is assumed to be that of bulk poly(glycidyl methacrylate).<sup>40</sup> The experimental data were analyzed with the WVase32 software. Five measurements at different locations were carried out for each sample. Each polymer was repeated at least on three separately prepared gold substrates. All samples showed reproducible result and an error smaller than 15%.

From the obtained thickness of the dehydrated PGMA layer, the adsorbed amount  $\Gamma$  ( $\text{mg m}^{-2}$ ) of each polymer on the surface was calculated by<sup>41,42</sup>

$$\Gamma = h\rho \quad (4.1)$$

Where  $h$  is the thickness of the dehydrated PGMA layer.  $\rho$  is the density of PGMA, which is assumed to be the same as poly(propyl methacrylate) with a value of  $1.08 \text{ g cm}^{-3}$ .<sup>40</sup>

The chain density,  $\Sigma$  ( $\text{chains nm}^{-2}$ ), i.e., the inverse of the average area per adsorbed chains was determined by<sup>41,42</sup>

$$\Sigma = \Gamma N_A (10^{-21}) / M_n = 602.3 \Gamma / M_n \quad (4.2)$$

Where  $N_A$  is the Avogadro's number and  $M_n$  ( $\text{g mol}^{-1}$ ) is the number average molar mass of the polymers.

The hydrated thickness of the SAMs in water was measured by ellipsometry equipped with a liquid cell at  $70^\circ$  at room temperature. The bare gold in the water was measured initially as reference. The final thickness of hydrated polymer was obtained by fitting the experimental data to a three layer model:  $\text{H}_2\text{O}/\text{PGMA}/\text{Au}$ .

#### 4.2.4.7 Surface plasmon resonance (SPR)

All SPR measurements were performed on an *i*SPR-device (IBIS Technologies BV, Enschede, Netherlands).  $1 \text{ mg mL}^{-1}$  BSA in phosphate buffered saline (PBS) and PBS (pH = 7.4) solutions were freshly prepared before the measurements. A typical SPR measurement was performed at  $25^\circ \text{C}$  involving the following procedures. The PBS solution was flowed onto the sensor surface until a stable baseline was achieved. Then the BSA solution was injected onto the surface and allowed to adsorb for 36 min. Finally the PBS solution was allowed to flow over the surface to remove unbound BSA. The flow rate in the experiments was  $3 \mu\text{L sec}^{-1}$ . Each polymer surface was measured on two independently prepared sensors, including two measurements on two different locations for each sensor.

### 4.3 Results and Discussion

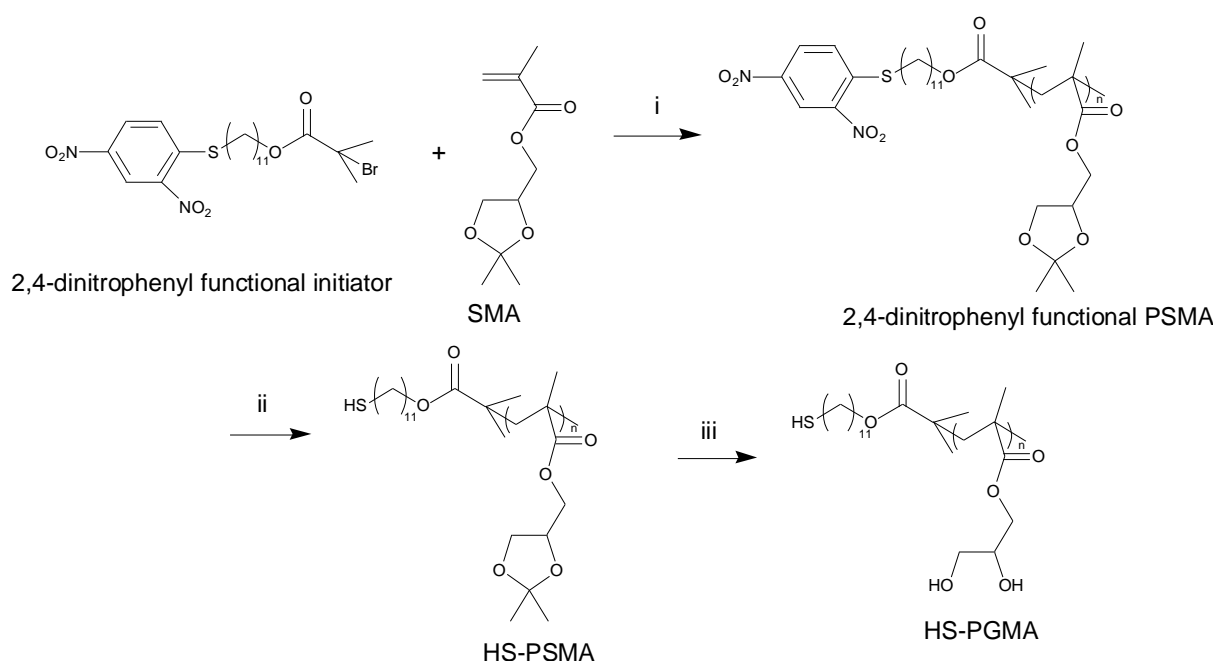
#### 4.3.1 Polymer synthesis and characterization

Generally, PGMA can be polymerized by ATRP from the glycerol methacrylate (GMA)<sup>43</sup> directly or from the protected monomer, e.g. SMA<sup>36,39,44</sup>. However, the high polarity of GMA



and PGMA makes it necessary to use very polar solvents, such as DMF, dimethyl sulfoxide (DMSO) or water to dissolve them, which can dramatically affect the structure and function of the catalytic species involved in ATRP<sup>45</sup>. Furthermore, the enantiopure GMA monomers with high purity are not easy to prepare. SMA is used as the monomer in this study for the following reasons. i) the ATRP procedure is similar as for methyl methacrylate (MMA), which has been well studied and documented,<sup>46</sup> ii) the reagents, methacryloyl chloride and enantiopure solketal, used for synthesis of enantiopure SMAs are commercially available.

The preparation of HS-PGMA is summarized in scheme 4.2, involving the polymerization of SMA monomers to obtain the 2,4-dinitrophenyl functional PSMA by ATRP, conversion of the 2,4-dinitrophenyl group to the thiol group through an aromatic nucleophilic displacement reaction and hydrolysis of the PSMA to cleave the ketal groups to give PGMA. Since thiol groups are well known to undergo readily oxidation to form disulfides, the 2,4-dinitrophenyl functional initiator was employed in the polymerization process. This group was found to be suitable as a protecting group due to the fact that it does not interact with the polymerization process and it can easily be removed using mild experimental condition.<sup>37</sup> Furthermore, the characteristic resonance peaks of the protons on the aromatic ring provide an excellent reference for the determination of the *DP* of the polymers by <sup>1</sup>H NMR spectroscopy.



**Scheme 4.2.** Synthesis of PGMA with a thiol end group. (i) ATRP, CuBr/bpy/anisole, 60 °C, 20 h; (ii) deprotection, 1-propanethiol/Et<sub>3</sub>N/water, room temperature, 20 h; (iii) hydrolysis, 1N HCl/1,4-dioxane, room temperature, 48 h.

Figure 4.1 shows the  $^1\text{H}$  NMR spectra of (a) 2,4-dinitrophenyl functionalized PSMA(*rac*)<sub>27</sub>, (b) HS-PSMA(*rac*)<sub>27</sub> and (c) HS-PGMA(*rac*)<sub>27</sub> in DMSO-*d*<sub>6</sub>. The successful synthesis of HS-PGMA(*rac*)<sub>27</sub> is confirmed by the disappearance of the resonance peaks at 8.85, 8.41 and 7.85 ppm with equivalent integrated areas attributed to the protons on the aromatic ring of the 2,4-dinitrophenyl group (see the inset of Figure 4.1) and the resonance peaks at 1.33 and 1.26 ppm attributed to the methyl peaks of the ketal groups at the SMA repeat units. The bands at 4.87 and 4.62 ppm in the spectrum of HS-PGMA(*rac*)<sub>27</sub> are attributed to the OH groups of PGMA. The *DP* of the polymer is calculated by using the integral of the resonance peak of the methyl group attached to the backbone (assigned with number “2”) divided by 3 times of the integral of resonance peak of the proton at the 6<sup>th</sup> position of the aromatic ring of the 2,4-dinitrophenyl group (assigned as number “1”) from the  $^1\text{H}$  NMR spectrum of 2,4-dinitrophenyl functionalized PSMA(*rac*)<sub>27</sub>. The chemical structure of HS-PGMA(*S*)<sub>28</sub>, HS-PGMA(*R*)<sub>24</sub> and HS-PGMA(*rac*)<sub>27</sub> were further confirmed by FTIR spectra of the polymer in KBr (shown in Figure A5). All samples have monomodal molar mass distributions and polydispersities ( $M_w/M_n$ ) of  $\sim 1.2$  by measuring the SEC of 2,4-dinitrophenyl functional PSMA in THF. The glass transition temperatures ( $T_g$ ) and decomposition temperatures ( $T_d$ ) are measured by DSC and TGA, respectively. The characteristic data for these three polymers are listed in Table 4.1.

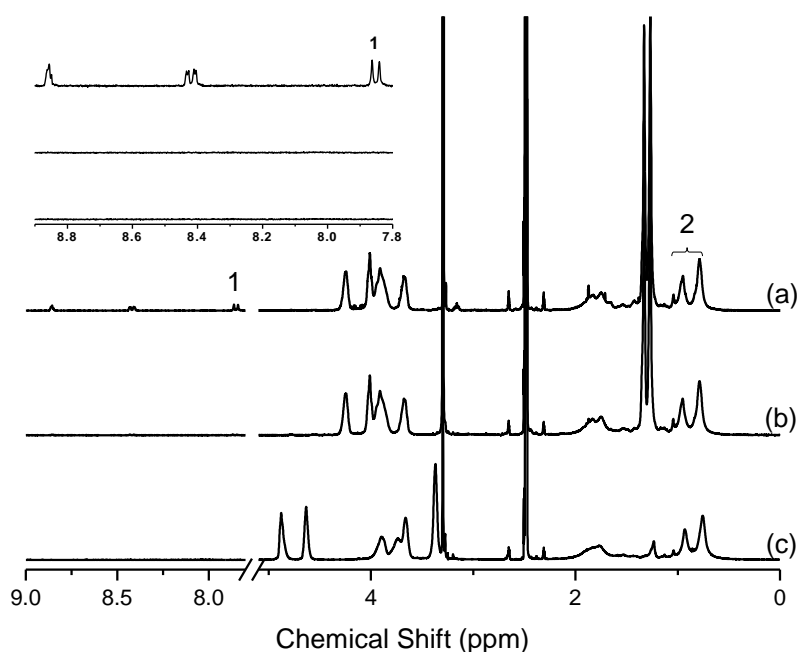


**Figure 4.1.**  $^1\text{H}$  NMR spectra of (a) 2,4-dinitrophenyl functionalized PSMA(*rac*)<sub>27</sub>, (b) HS-PSMA(*rac*)<sub>27</sub> and (c) HS-PGMA(*rac*)<sub>27</sub> in DMSO-*d*<sub>6</sub>, 400 MHz.

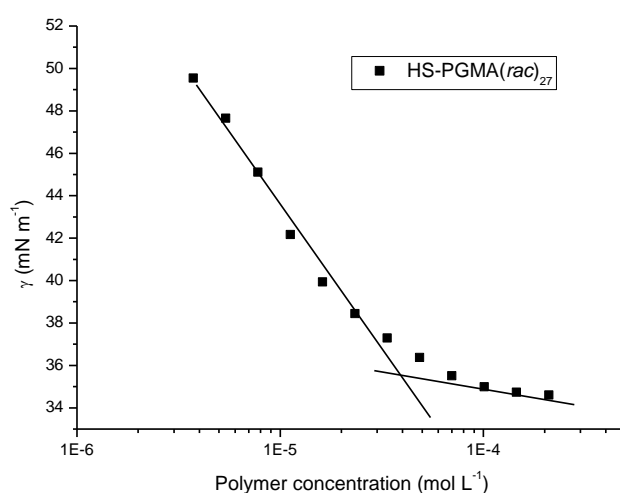
**Table 4.1.** Characteristic data of HS-PGMAs.

Polymers	$M_n^a$ (g mol <sup>-1</sup> )	$M_w/M_n^b$	$cac^c$ ( $\times 10^{-5}$ mol L <sup>-1</sup> )	$T_g^d$ (°C)	$T_d^e$ (°C)
HS-PGMA( <i>rac</i> ) <sub>27</sub>	4800	1.23	4.0	55	312
HS-PGMA( <i>R</i> ) <sub>24</sub>	4300	1.21	4.6	90	317
HS-PGMA( <i>S</i> ) <sub>28</sub>	4900	1.17	4.3	82	315

<sup>a</sup>calculated from <sup>1</sup>H NMR spectroscopy <sup>b</sup>obtained from SEC with THF as eluent and PMMA as standard <sup>c</sup>obtained from surface tension measurement at 25°C <sup>d</sup>obtained from DSC measurements <sup>e</sup>obtained from TGA analysis.

### 4.3.2 Physical properties of HS-PGMA in water

The HS-PGMAs may self-assemble to form polymeric micelles in water due to the existence of 11 CH<sub>2</sub> repeat units between the thiol group and the PGMA segment. Figure 4.2 shows the plots of the surface tensions of HS-PGMA(*rac*)<sub>27</sub>, HS-PGMA(*R*)<sub>24</sub> and HS-PGMA(*S*)<sub>28</sub> aqueous solutions vs polymer concentrations at 25 °C. Analysis of these plots reveals that the curves show slight change in slope at certain polymer concentrations (the values are summarized in Table 4.1), which are defined as critical aggregation concentration (*cac*).



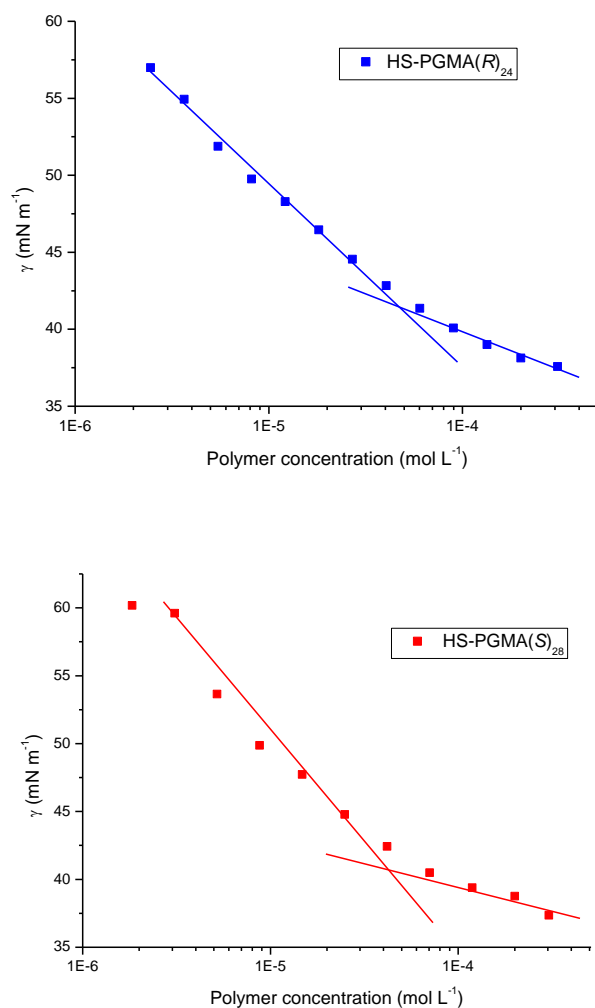


**Figure 4.2.** Critical aggregation concentration (cac) determination of HS-PGMA(*rac*)<sub>27</sub>, HS-PGMA(*R*)<sub>24</sub> and HS-PGMA(*S*)<sub>28</sub> from surface tension measurements of aqueous solution as a function of polymer concentration at 25 °C.

Figure 4.3 shows the  $^1\text{H}$  NMR spectra of HS-PGMA(*rac*)<sub>27</sub> in (a) DMSO-*d*<sub>6</sub> and (b) D<sub>2</sub>O measured at the polymer concentration of 8  $\text{mg mL}^{-1}$ . The vanish of the OH resonance bands in the  $^1\text{H}$  NMR spectrum of HS-PGMA(*rac*)<sub>27</sub> in D<sub>2</sub>O is attributed to the H/D exchange (for assignment see experiment part). It is evident that the resonance peak at  $\sim 1.23$  ppm appeared in DMSO-*d*<sub>6</sub> (assigned with asterisk) corresponding to the CH<sub>2</sub> groups between the PGMA and the thiol group diminishes in the spectrum recorded in D<sub>2</sub>O, indicating that the aggregates with the alkyl terminal groups surrounded by PGMA chains are formed in water. The HS-PGMA(*R*)<sub>24</sub> and HS-PGMA(*S*)<sub>28</sub> have identical  $^1\text{H}$  NMR spectra as HS-PGMA(*rac*)<sub>27</sub> in both DMSO-*d*<sub>6</sub> (the spectra are shown in Figure 5.1) and D<sub>2</sub>O (Figure 4.4).

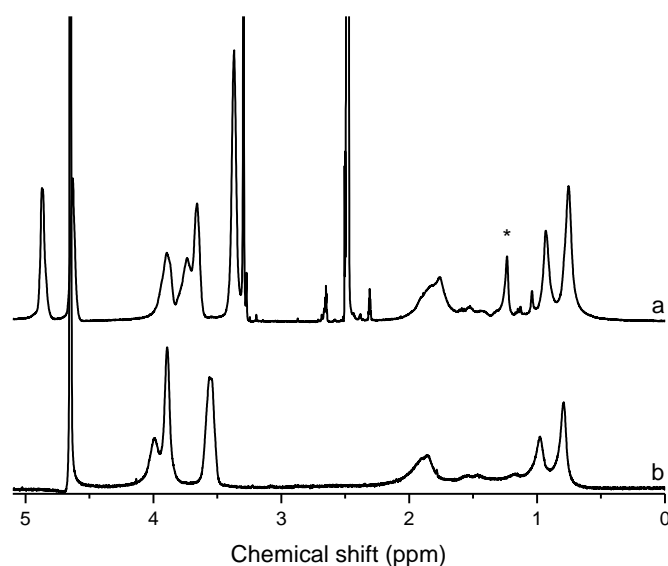


**Figure 4.3.**  $^1\text{H}$ -NMR spectra of HS-PGMA(*rac*)<sub>27</sub> in (a) DMSO-*d*<sub>6</sub> and (b) D<sub>2</sub>O at 27 °C, 400 MHz at the polymer concentration of 8 mg mL<sup>-1</sup>.

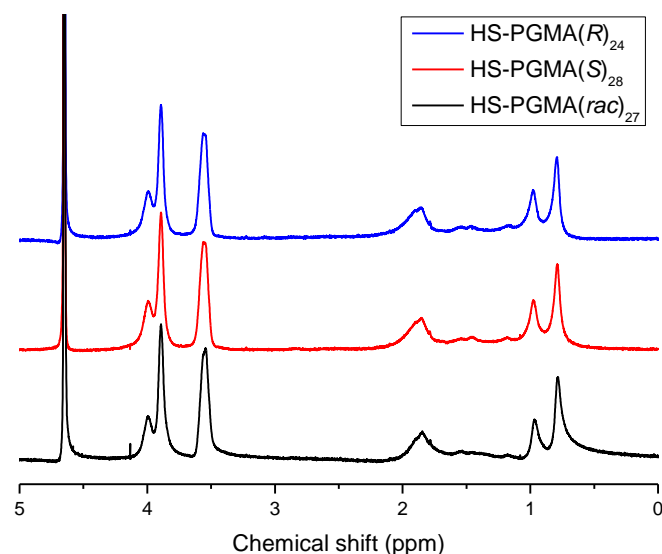


**Figure 4.4.**  $^1\text{H}$  NMR spectra of HS-PGMA(*rac*)<sub>27</sub> (black), HS-PGMA(*R*)<sub>24</sub> (blue) and HS-PGMA(*S*)<sub>28</sub> (red) in D<sub>2</sub>O.

Figure 4.5 depicts the hydrodynamic radius ( $R_h$ ) distributions of HS-PGMA(*rac*)<sub>27</sub>, HS-PGMA(*R*)<sub>24</sub> and HS-PGMA(*S*)<sub>28</sub> at a concentration of 4 mg mL<sup>-1</sup> in aqueous solution. Two relaxation modes are observed in the aqueous solutions of these three polymers. The decay rates ( $\Gamma$ ) of these two modes show a linear dependence on the square of the scattering vector,  $q^2$ , and the extrapolations at  $q \rightarrow 0$  pass through the origin (shown in the inset of Figure 4.4

and Figure A6 in appendix). This confirms the diffusive characters of these two species. The  $R_h$  values summarized in Table 4.2 are calculated from the apparent diffusion coefficient constants ( $D_{app}$ ) according to the Stokes-Einstein equation. Since the scattered intensity in DLS is roughly proportional to the sixth power of the size, the number of particles with the slow modes in the system is much less than the fast modes. The slow modes in the polymer solutions are considered to belong to the clusters stabilized by intermolecular hydrogen bonds of PGMA, which was discussed in the chapter 3 and earlier studies.<sup>44</sup>

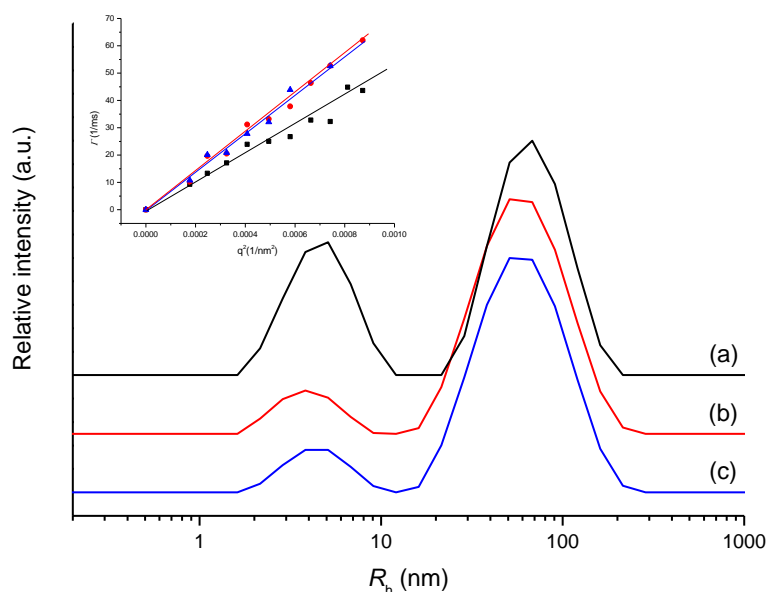


**Figure 4.5.** DLS measurements of 4 mg mL<sup>-1</sup> (a) HS-PGMA(*rac*)<sub>27</sub>, (b) HS-PGMA(*S*)<sub>28</sub>, and (c) HS-PGMA(*R*)<sub>24</sub> aqueous solutions at 25 °C and 90°. The inset shows the relaxation rate ( $\Gamma$ ) as a function of the square of the scattering vector ( $q^2$ ) at 25 °C for the fast modes of HS-PGMA(*rac*)<sub>27</sub>, HS-PGMA(*R*)<sub>24</sub> and HS-PGMA(*S*)<sub>28</sub>.

To obtain information about the size of the PGMA unimers in water, the gyration radius ( $R_g$ ) and  $R_h$  of HS-PGMA in water are estimated by the following equations assuming water is a good solvent for the polymer:<sup>47</sup>

$$R_g = a(N/6)^{0.5} \quad (4.3)$$

$$R_g/R_h = 1.5045 \quad (4.4)$$

Where  $N$  is the degree of polymerization and  $a$  is the statistical segment length. The  $a$  for PGMA is assumed to be the same as for poly(methyl methacrylate) with a value of  $\sim 0.6$  nm.<sup>48</sup>

The estimated  $R_g$  and  $R_h$  of HS-PGMA(*rac*)<sub>27</sub>, HS-PGMA(*R*)<sub>24</sub> and HS-PGMA(*S*)<sub>28</sub> are ~ 1.30, 1.20, 1.27 nm and 0.87, 0.80, 0.84 nm, respectively. Therefore, the fast modes related to  $R_h$  values of ~ 3-5 nm for HS-PGMAs cannot be caused by unimers. Together with conclusion from the previous surface tension and <sup>1</sup>H NMR measurements, they are considered to be caused by small aggregates. The aggregation number of these small aggregates can be estimated from equations 4.3 and 4.4 by using the  $R_h$  values obtained from the DLS listed in Table 4.2. The calculated aggregation numbers are 30, 22 and 23 for the small aggregates in HS-PGMA(*rac*)<sub>27</sub>, HS-PGMA(*R*)<sub>24</sub> and HS-PGMA(*S*)<sub>28</sub> aqueous solutions, respectively.

**Table 4.2.** The  $R_h$  values obtained from the the slow modes and fast modes of HS-PGMAs in water measured by DLS, the  $R_h$  are given in nm.

	HS-PGMA( <i>rac</i> ) <sub>27</sub>	HS-PGMA( <i>R</i> ) <sub>24</sub>	HS-PGMA( <i>S</i> ) <sub>28</sub>
slow mode	62 ± 4	50 ± 2	52 ± 3
fast mode	4.8 ± 0.42	3.8 ± 0.27	4.0 ± 0.25

The results in from Table 4.2 indicate that the enantiopure polymers HS-PGMA(*R*)<sub>24</sub> and HS-PGMA(*S*)<sub>28</sub> have similar particle sizes obtained from both fast and slow modes. However, the  $R_h$  values obtained from both two modes in HS-PGMA(*rac*)<sub>27</sub> aqueous solution are clearly larger compared to the values of enantiopure polymers. Two possibilities to cause this particle size difference. One is the aggregates in HS-PGMA(*rac*)<sub>27</sub> have a larger aggregation number ( $N_{agg}$ ) than the enantiopure counterparts. Another possibility is that the polymer chains in the aggregates are more compacted in the case of HS-PGMA(*R*)<sub>24</sub> and HS-PGMA(*S*)<sub>28</sub> than HS-PGMA(*rac*)<sub>27</sub>. The exact reason leading to this difference is still unclear. It can be assumed that the stereochemistry of the pendent group of the polymer is responsible for this difference. The stereochemistry effect on the self-assembly of chiral polymers in liquids has been observed before. For instance, micelles formed by self-assembly of amphiphilic block copolymers based on racemic poly(2-butyl-4-ethyl-2-oxazoline) (PBUeTOx) show a different morphology compared to polymers based on enantiopure PBUeTOx.<sup>49</sup>

Furthermore, it is evident from Figure 4.5 that the fast mode in HS-PGMA(*rac*)<sub>27</sub> aqueous solution shows a much higher relative intensity than the fast modes in HS-PGMA(*R*)<sub>24</sub> and HS-PGMA(*S*)<sub>28</sub> aqueous solutions. The ratio of number concentrations of fast mode to slow mode ( $n_{fast\ mode}/n_{slow\ mode}$ ) is given by the relative amplitudes of scattering intensity ( $I_{fast\ mode}/I_{slow\ mode}$ ) divided by the 9<sup>th</sup> power of relative hydrodynamic radius, ( $R_{h, fast\ mode}/R_{h, slow\ mode}$ )

mode), assuming that both the fast and slow modes are hard sphere with uniform density. Using the  $R_h$  and  $I$  values from Figure 4.5, the  $n_{\text{fast mode}}/n_{\text{slow mode}}$  values of HS-PGMA(*rac*)<sub>27</sub>, HS-PGMA(*R*)<sub>24</sub> and HS-PGMA(*S*)<sub>28</sub> aqueous solutions are  $\sim 5.7 \times 10^9$ ,  $3.2 \times 10^9$  and  $2.3 \times 10^9$ , respectively. More smaller aggregates are existed in HS-PGMA(*rac*)<sub>27</sub> than HS-PGMA(*R*)<sub>24</sub> and HS-PGMA(*S*)<sub>24</sub>.

Figure 4.6 shows the UV-*vis* spectra of HS-PGMA(*S*)<sub>28</sub>, HS-PGMA(*R*)<sub>24</sub> and HS-PGMA(*rac*)<sub>27</sub> in aqueous solution with a concentration of  $2 \text{ mg mL}^{-1}$ . The carbonyl group of the ester bond system of the side chains contribute to the main absorption with a maximum at a wavelength of  $\sim 210 \text{ nm}$ . Mercaptans (R-SH) are weak acids and give rise to equilibrium in aqueous solution to form the thiolate ions, which show an absorption in the UV region.<sup>50</sup> The shoulder with a maximum absorption at  $\sim 250 \text{ nm}$  can be attributed to the thiolate form of the thiol end group. The yellow colour of the polymer in solution with a broad absorption maximum at  $\sim 370 \text{ nm}$  is related to this fact.

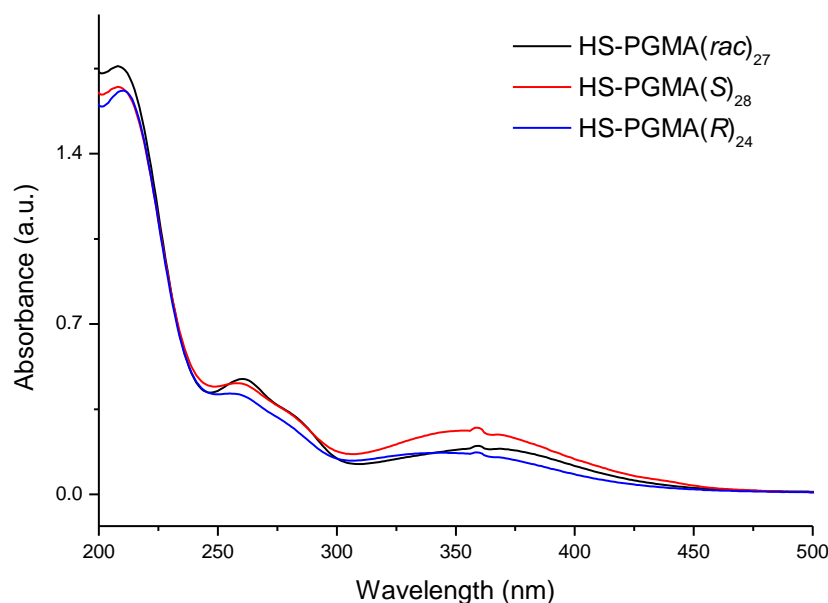


**Figure 4.6.** UV-*vis* spectra of HS-PGMA(*S*)<sub>28</sub>, HS-PGMA(*R*)<sub>24</sub> and HS-PGMA(*rac*)<sub>27</sub> at a concentration of  $2 \text{ mg mL}^{-1}$  polymer in water.

The polymer conformation of HS-PGMA(*S*)<sub>28</sub>, HS-PGMA(*R*)<sub>24</sub> and HS-PGMA(*rac*)<sub>27</sub> in aqueous solution was investigated by CD spectroscopy, which has a high sensitivity to ordered structures. Figure 4.7 depicts the CD spectra of HS-PGMA(*rac*)<sub>27</sub>, HS-PGMA(*S*)<sub>28</sub>, and HS-PGMA(*R*)<sub>24</sub> measured in aqueous solution at  $25 \text{ }^\circ\text{C}$ . The HS-PGMA(*S*)<sub>28</sub> and HS-



PGMA(*R*)<sub>24</sub> exhibit a strong Cotton effect at 216 nm arising from the  $n\text{-}\pi^*$  transition of the ester chromophore in the side chain of polymers. The mirror image CD spectra of HS-PGMA(*S*)<sub>28</sub> and HS-PGMA(*R*)<sub>24</sub> indicate that they adopt the same conformation but with opposite handedness. In contrast, HS-PGMA(*rac*)<sub>27</sub> exhibits no Cotton effect in the measured wavelength range. It has been seen both in computational modelling<sup>51</sup> and experiments<sup>52</sup> that an ordered structure can be induced by chiral side chains in polymers. It is reasonable to assume that the enantiopure HS-PGMAs chains adopt certain ordered conformations to provide an asymmetric environment for the ester chromophores on the side chains of polymers, while the racemic HS-PGMA does not. This polymer conformation difference between the enantiopure and racemic polymers was e.g. observed in poly(2-oxazoline)s.<sup>53</sup>

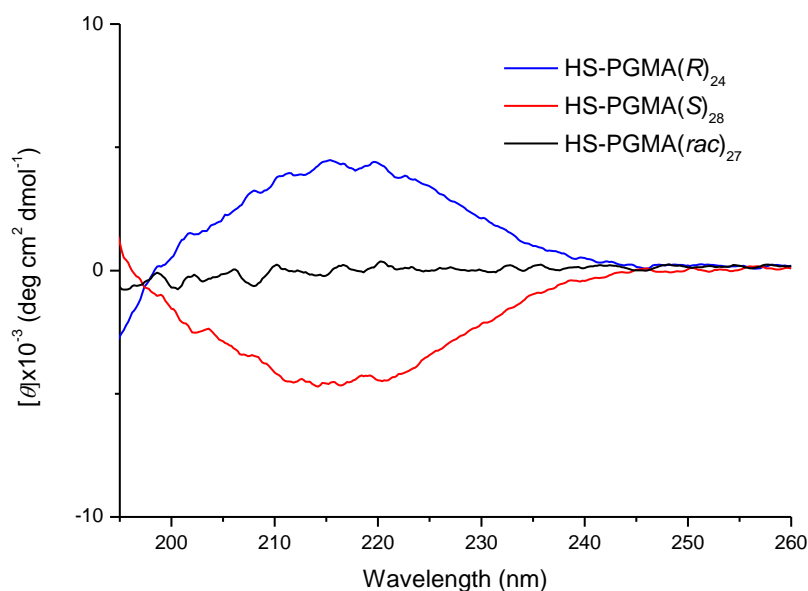


**Figure 4.7.** CD data of HS-PGMA(*S*)<sub>28</sub>, HS-PGMA(*R*)<sub>24</sub> and HS-PGMA(*rac*)<sub>27</sub> in water measured at 25 °C.

From the thermodynamic point of view, chains of flexible polymers prefer to adopt random coils rather than ordered conformations since the process of forming ordered structures is entropically unfavored. Intramolecular hydrogen bonds are considered as one of the most important interactions in the stabilization of ordered structures in many natural<sup>54</sup> and synthetic polymers<sup>55</sup>, such as the helical structure of DNA<sup>54</sup> and poly(*N*-alkynylamides).<sup>55</sup> The CD spectra of HS-PSMAs, the precursors of HS-PGMAs, and HS-PGMAs were measured in an ethanol/water mixture (v/v=9/1) and the results are shown in Figure 4.8. The use of this mixture as solvent is selected for the following reasons: (i) it can dissolve both PGMA and PSMA, and (ii) it is transparent in the measured range of wavelengths. The HS-PGMA(*R*)<sub>24</sub>

and HS-PGMA(*S*)<sub>28</sub> in an ethanol/water mixture showed identical CD spectra as in water, implying that a similar conformation is adopted for the polymer chains. It is clear that the Cotton effects are completely disappeared in HS-PSMA(*R*)<sub>24</sub> and HS-PSMA(*S*)<sub>28</sub> solutions. It should be noted here that the only difference between PGMA and PSMA is that the OH groups in PGMA are replaced by ketal groups in PSMA as shown in scheme 4.2. Thus, it is reasonable to envisage that the ordered conformation in the enantiopure PGMA which give rise to the Cotton effect is stabilized by intramolecular hydrogen bonds between the OH groups and the carbonyl groups in the side chains of polymers. This hydrogen bonding is further confirmed by the carbonyl groups in PGMA which are shift onto lower wavenumbers compared to PSMA in the FTIR spectra. Figure 4.9 shows the carbonyl asymmetric stretching absorption bands of solid HS-PSMA(*S*)<sub>28</sub> and HS-PGMA(*S*)<sub>28</sub> in KBr measured by FTIR. The carbonyl absorption band in PSMA appears the wavenumber at  $\sim 1732\text{ cm}^{-1}$ , while it shifts to  $\sim 1722\text{ cm}^{-1}$  in PGMA. This significant wavenumber decrease gives clear evidence that hydrogen bonds are formed in PGMA. However, we cannot distinguish inter- and intramolecular hydrogen bonds since both can contribute to this wavenumber shift. A similar behavior is also observed in PGMA(*R*)<sub>24</sub>.

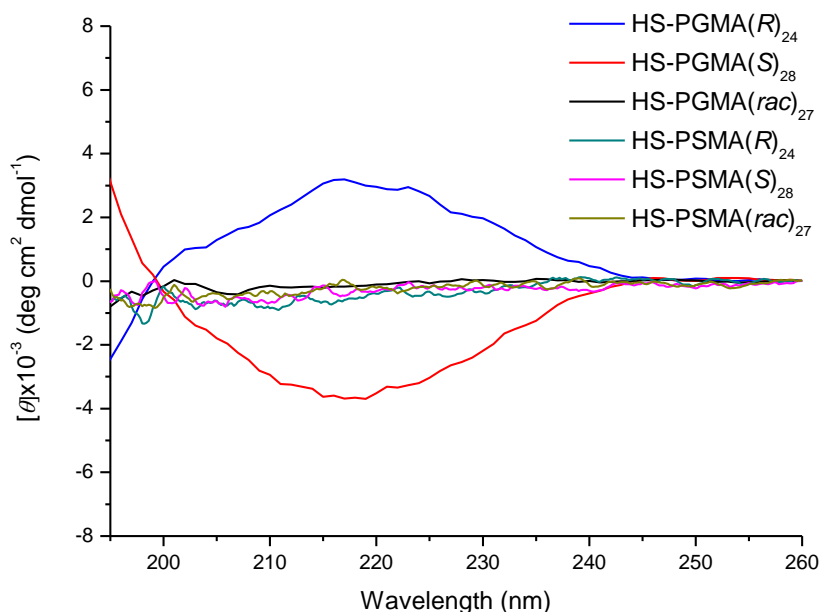


**Figure 4.8.** CD spectra of  $4\text{ mg mL}^{-1}$  HS-PGMA(*S*)<sub>28</sub>, HS-PGMA(*R*)<sub>24</sub>, HS-PGMA(*rac*)<sub>27</sub> and their precursors HS-PSMA(*S*)<sub>28</sub>, HS-PSMA(*R*)<sub>24</sub> and HS-PSMA(*rac*)<sub>27</sub> in ethanol/water ( $v/v = 9/1$ ).

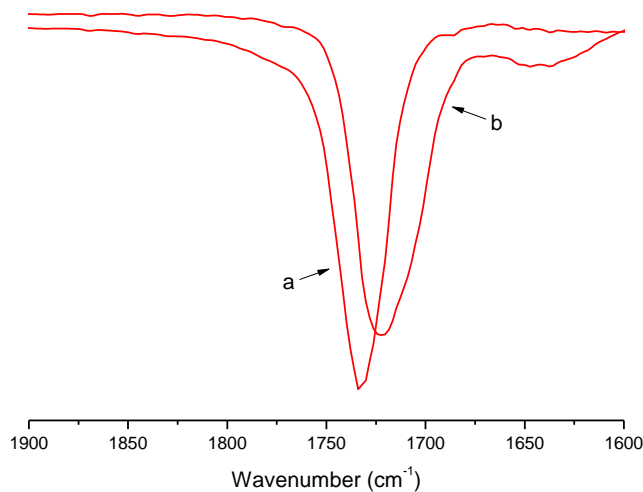


**Figure 4.9.** FTIR spectra of HS-PSMA(S)<sub>28</sub> (a), HS-PGMA(S)<sub>28</sub> (b) in the solid state in KBr at the wavenumber range from 1600 to 1900 cm<sup>-1</sup>.

### 4.3.3 Preparation and characterization of SAMs

The adsorption of polymers onto solid surfaces from polymeric micellar solutions has been extensively investigated both theoretically<sup>56</sup> and experimentally.<sup>57</sup> It is believed that the monolayer composed of a dense inner layer and an extended out layer can be formed when a surface repels the soluble block but adsorbs the nonsoluble block. With this in mind, we conclude that the polymer monolayers with PGMA segments extending into water are formed on gold surfaces since the thiol groups, which have a high affinity to the gold surface, are connected to the hydrophobic terminals. The polymeric aggregates in the HS-PGMA aqueous solution cannot adsorb on the surface directly but serve as reservoirs.

The HS-PGMA(S)<sub>28</sub>, HS-PGMA(R)<sub>24</sub> and HS-PGMA(*rac*)<sub>27</sub> SAMs were prepared under identical experimental conditions. Water contact angles (WCAs) were measured before and after the immobilization of PGMA polymers onto the gold surfaces. The PGMA SAM surfaces have a significant lower WCA (25 ~ 28 °) compared with bare gold surfaces (~ 70 °), reflecting the hydrophilic nature imparted on the grafted PGMA surfaces. The WCA values of the polymer grafted surfaces are summarized in Table 4.3. It is evident that the chirality does not influence the WCA value of the polymer surfaces.

SERS has been well documented in literature to characterize SAMs on gold or silver surfaces.<sup>58</sup> Figure 4.10 shows the SERS spectra of PGMA(S)<sub>28</sub>, PGMA(R)<sub>24</sub> and PGMA(*rac*)<sub>27</sub> surfaces. The characteristic peaks, including the C-S bond stretching vibration

peak at  $\sim 610\text{ cm}^{-1}$ , C=O stretching peak at  $\sim 1730\text{ cm}^{-1}$ , CH stretching peak between  $\sim 2800\text{ cm}^{-1}$  to  $3100\text{ cm}^{-1}$ ,  $\text{CH}_3$  rocking vibrations at  $\sim 1450\text{ cm}^{-1}$ , of the spectra indicate that the polymers are successfully grafted on the gold surfaces. It is clearly evident that the PGMA(*rac*)<sub>27</sub> SAM has a significantly stronger intensity than PGMA(*R*)<sub>28</sub> and PGMA(*S*)<sub>24</sub> SAMs, implying that the PGMA(*rac*)<sub>27</sub> surface has a higher grafting density compared to enantiopure polymer surfaces.<sup>59</sup>

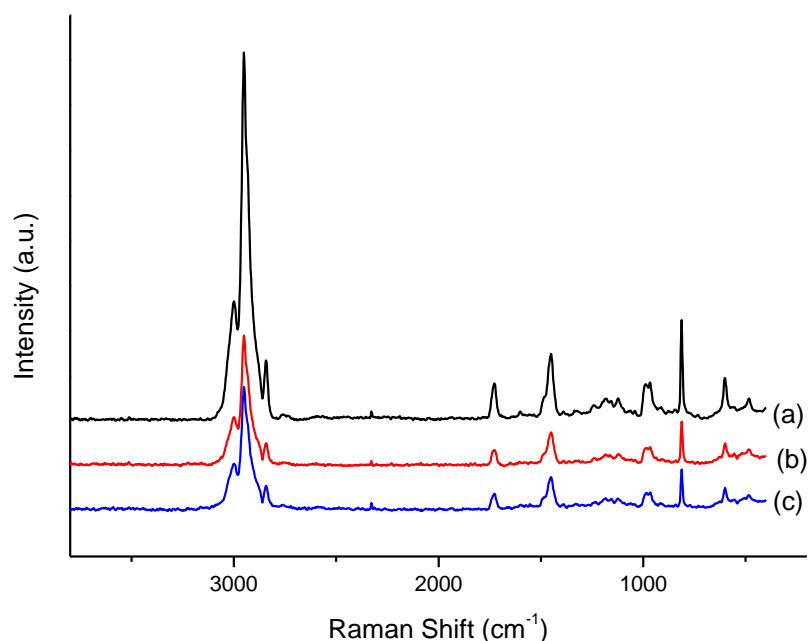


**Figure 4.10.** Surface enhanced Raman spectra of (a) PGMA(*rac*)<sub>27</sub>, (b) PGMA(*S*)<sub>28</sub>, and (c) PGMA(*R*)<sub>24</sub> SAMs on gold surface.

#### 4.3.4 Thickness determination of SAMs by ellipsometry

The dehydrated thicknesses of the PGMA SAMs on gold surfaces were evaluated from ellipsometry measurements and the values are listed in Table 4.3. The PGMA(*S*)<sub>28</sub> and PGMA(*R*)<sub>24</sub> surfaces give a similar dehydrated thickness with a value of  $\sim 2.2\text{ nm}$ . Whereas, the PGMA(*rac*)<sub>27</sub> surface has a significantly larger dehydrated thickness with a value of  $\sim 3.4\text{ nm}$ . With an estimation of the polymer density  $\rho = 1.08\text{ g cm}^{-3}$ , the value of poly(propyl methacrylate), the grafting densities of polymer chains on the gold surfaces can be calculated from the dehydrated SAM thickness according to eqs. 4.1 and 4.2. The following results for the grafting densities of the SAMs are obtained, PGMA(*rac*)<sub>27</sub> surface has a much higher

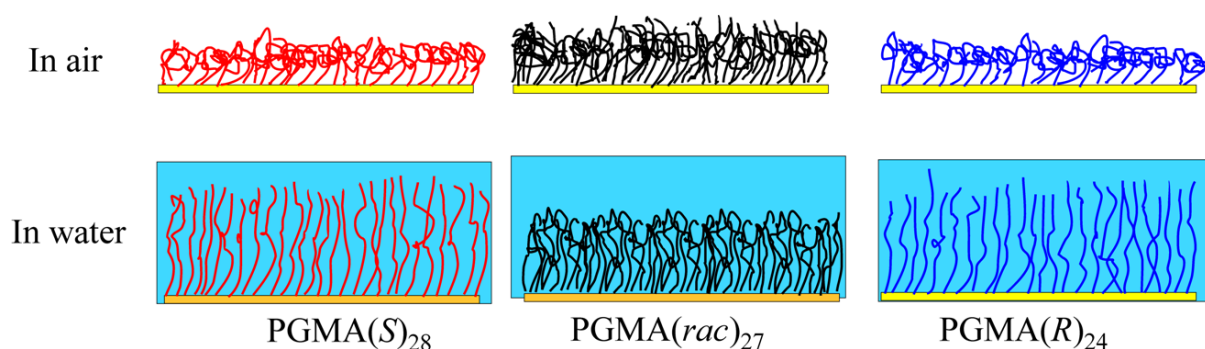
grafting density of  $\sim 0.48$  chains  $\text{nm}^{-2}$  than PGMA(*S*)<sub>28</sub> of  $\sim 0.31$  chains  $\text{nm}^{-2}$  and PGMA(*R*)<sub>24</sub> of  $\sim 0.34$  chains  $\text{nm}^{-2}$ , which is in good agreement with the SERS results discussed above.

The hydrated thicknesses of the PGMA SAMs were determined by ellipsometry equipped with a liquid cell and the data are also listed in Table 4.3. It can be seen that the hydrated thicknesses of the polymer SAMs are higher than the dehydrated thickness, showing the swelling of the polymer films in water. However, the enantiopure PGMA give a higher hydrated thickness compared to the racemic PGMA film, which is the opposite as measured for the dehydrated SAM thickness. In addition, PGMA(*R*)<sub>24</sub> and PGMA(*S*)<sub>28</sub> surfaces show a similar hydrated SAM thickness. Since the enantiopure PGMA surfaces bear the lower grafting density compared to the racemic PGMA surface, the higher hydrated SAM thickness of enantiopure polymer films represents more extended chains than the racemic SAMs in water. The high grafting density in PGMA(*rac*)<sub>27</sub> SAM can enhance the intermolecular hydrogen bonding effect among the OH groups on the polymer side chains due to the closer spatial distance. This leads to the fact that the polymer chains showing the higher affinity to each other than to water and results the less stretched polymer chains. A schematical drawing of the polymer film in dehydrated and hydrated state is shown in scheme 4.3.

**Table 4.3.** Characteristic data of PGMA SAMs obtained from ellipsometry measurements.

Polymer	WCA (°)*	Dehydrated thickness (nm)	Chain density (chains $\text{nm}^{-2}$ )	Hydrated thickness (nm)
PGMA( <i>rac</i> ) <sub>27</sub>	27±2	3.4	0.48	4.5
PGMA( <i>S</i> ) <sub>28</sub>	28±3	2.2	0.31	5.7
PGMA( <i>R</i> ) <sub>24</sub>	25±2	2.2	0.34	5.6

\*WCAs obtained from water contact angle measurements.



Scheme 4.3. Schematical drawing of polymer film on gold surfaces in air and in water.

#### 4.3.5 BSA adsorption to PGMA SAMs measured by SPR

The adsorption of BSA on the racemic and enantiopure PGMA SAMs was studied by using SPR at 25 °C. SPR spectroscopy is an ideal analytical technique for the detection of the interfacial binding process. It allows for real time and label free detection of protein adsorption with high sensitivity.<sup>60</sup> Figure 4.11a shows the SPR sensorgrams for the BSA adsorption on PGMA(*rac*)<sub>27</sub>, PGMA(*S*)<sub>28</sub>, PGMA(*R*)<sub>24</sub> SAMs and bare gold. According to the literature, a change of the SPR peak angle of 122 m° corresponds to ~ 100 ng cm<sup>-2</sup> adsorbed protein on the surface.<sup>60</sup> The adsorbed BSA amounts (*A*) on the polymer surfaces and bare gold, which are determined by subtracting the values after the last PBS washing and before the exposure to the protein solution, are summarized in Figure 4.11b. The relative protein adsorption compared to the bare gold sensor (%RA) was calculated by the equation %RA = (*A*<sub>PGMA</sub>/*A*<sub>Au</sub>)×100%.

Compared to the bare gold surface, the PGMA grafted surfaces show a dramatic decrease of BSA adsorption. The PGMA(*S*)<sub>28</sub> and PGMA(*R*)<sub>24</sub> surfaces display extremely low BSA adsorption of ~ 1.24 and ~ 0.80 ng cm<sup>-2</sup>, respectively, which are less than 1%RA. It appears that the *R* and *S* PGMA surfaces show the similar behavior on the BSA resistance. However, a significant larger amount of BSA is adsorbed on the PGMA(*rac*)<sub>27</sub> surface with a value of ~ 25.5 ng cm<sup>-2</sup>, i.e. ~ 21%RA. It has been reported by Sofia et al.<sup>8</sup> that proteins have the possibility to penetrate into the open spaces between the PEO chains in the case of low grafting density of the polymer film. This cannot be responsible for the higher BSA adsorption on the PGMA(*rac*)<sub>27</sub> surface since it has a higher grafting density than PGMA(*R*)<sub>24</sub> and PGMA(*S*)<sub>28</sub> surfaces.

The influence of the grafting density on the protein repellent ability of polymer surfaces is the subject of much discussion. Generally, higher grafting density polymer films impart greater

resistance to protein adsorption.<sup>8</sup> However, Unsworth et al.<sup>9</sup> found that there is a certain grafting density of tethered PEO chains on the gold surface to achieve the lowest protein adsorption amount, above which the protein adsorption begins to increase again due to the dehydration of the PEO chains. Using molecular simulations to investigate the protein interactions with SAM surfaces in the presence of explicit water molecules, Jiang and co-workers<sup>22,23</sup> found that the main contribution for the protein resistance comes from the water molecules which are hydrated with SAM surfaces, not from the original SAM surfaces. The formation of a highly hydrated layer is critical for the protein resistance since this layer can provide both a physical and an energy barrier for proteins. Thus, the different protein adsorption behavior of the enantiopure and racemic PGMA surfaces can be explained by the strength of polymer hydration at the surface since it is well known that the PGMA chains have high affinity to themselves due to the formation of hydrogen bonds. The high grafting density of PGMA enhances the interchain interactions and reduces the interactions of the polymer chains with water molecules. This leads to the fact that the PGMA(*rac*)<sub>27</sub> surface become less hydrated than PGMA(*R*)<sub>24</sub> and PGMA(*S*)<sub>28</sub>, which was observed in ellipsometry measurements, resulting in the increased protein adsorption. The increase of protein adsorption due to the intermolecular hydrogen bonding has also been observed in PHPMA<sup>12</sup> and polyglycerol<sup>61</sup> surface.

To interpret this hydrogen bonding effect, HS-PGMA(*rac*)<sub>27-92%</sub>, which contains 25 GMA units and 2 SMA units per chain, was prepared by partial hydrolysis of HS-PSMA(*rac*)<sub>27</sub> and grafted onto the gold surface to measure the BSA adsorption behavior. The SPR result observed in Figure 4.11a shows that the PGMA(*rac*)<sub>27-92%</sub> surface exhibits a much better BSA resistance ability than the PGMA(*rac*)<sub>27</sub> surface. The BSA adsorption on the PGMA(*rac*)<sub>27-92%</sub> surface sharply reduces to  $\sim 10 \text{ ng cm}^{-2}$ , only half of the value of the PGMA(*rac*)<sub>27</sub> surface. Generally, SMAs are considered to adsorb proteins through hydrophobic interactions. However, the introduction of a few SMA units to the PGMA chain can efficiently weaken the intermolecular hydrogen bonding effect and improve the polymer hydration in water because the SMA lacks the ability for the hydrogen bond formation. Similar phenomenon is also observed in poly(vinyl alcohol) (PVA), e.g., the conversion of parts of vinyl alcohol units to vinyl acetate in PVA lead to the higher solubility.<sup>62</sup>

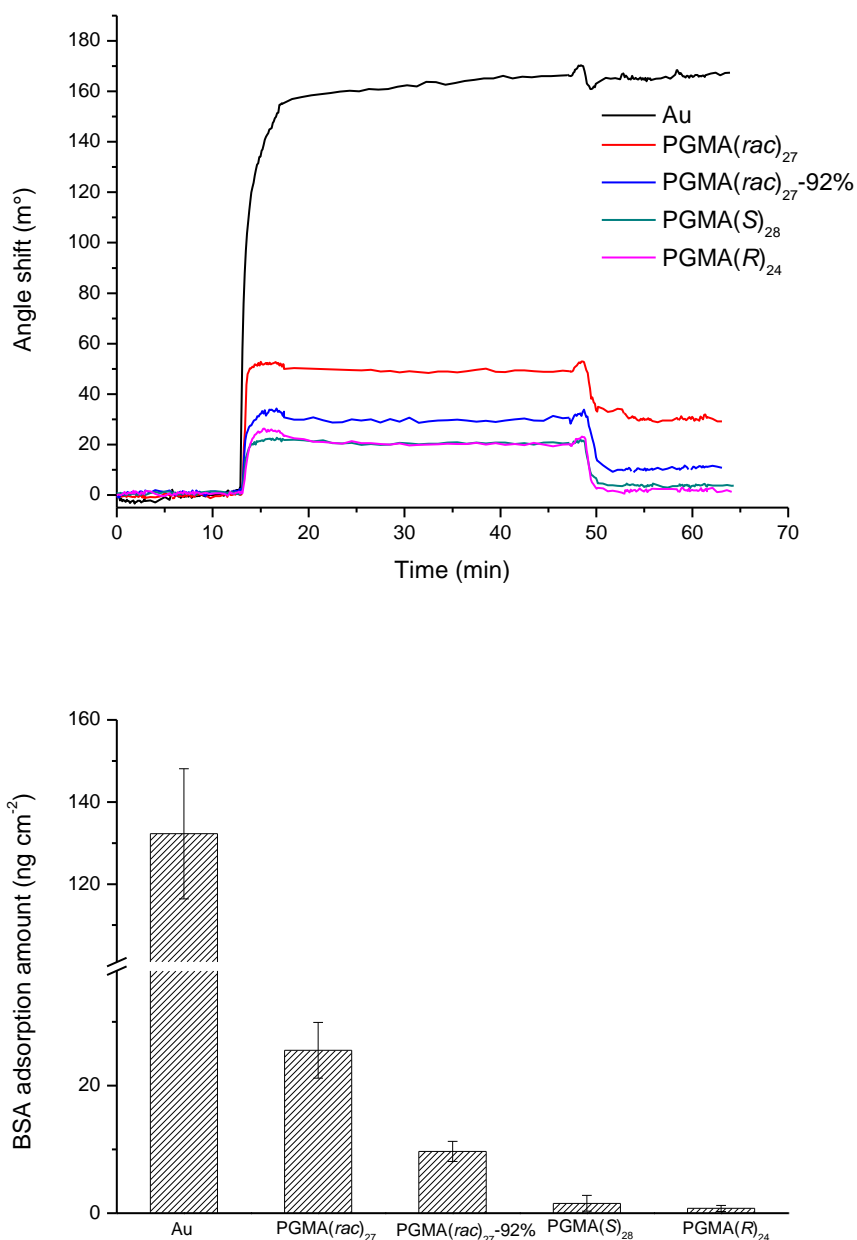


**Figure 4.11.** (a) SPR sensorgrams of 1 mg mL<sup>-1</sup> BSA in PBS buffer solution on PGMA(*rac*)<sub>27</sub>, PGMA(*rac*)<sub>27</sub>-92%, PGMA(*S*)<sub>28</sub>, PGMA(*R*)<sub>24</sub>, and bare gold surfaces measured at 25 °C. (b) The BSA adsorption amount on the PGMA(*rac*)<sub>27</sub>, PGMA(*rac*)<sub>27</sub>-92%, PGMA(*S*)<sub>28</sub>, PGMA(*R*)<sub>24</sub>, and bare gold surfaces calculated from (a).



#### 4.4 Conclusion

Well controlled racemic and enantiopure PGMA, i.e. PGMA(*rac*)<sub>27</sub>, PGMA(*R*)<sub>24</sub> and PGMA(*S*)<sub>28</sub>, with similar chain lengths have been prepared by ATRP and grafted onto gold surfaces via thiol groups to form the SAM surfaces. Their protein resistant properties have been evaluated using BSA as model protein. The PGMA modified surfaces can greatly reduce the BSA adsorption compared to the bare gold. Specifically, the enantiopure PGMA surfaces show an extremely low BSA adsorption. Although the influence of the stereostructure of the monolayer on the protein resistance ability is still in debate,<sup>30,31</sup> the PGMA(*R*)<sub>24</sub> and PGMA(*S*)<sub>28</sub> surfaces show an identical BSA adsorption in this system. Compared to PGMA(*R*)<sub>24</sub> and PGMA(*S*)<sub>28</sub> surfaces, the PGMA(*rac*)<sub>27</sub> surface is a less efficient in BSA repelling. The less protein resistant properties of the PGMA(*rac*)<sub>27</sub> surface is assumed as the result of a higher grafting density on the surface, which has been measured by ellipsometry measurements. The high packing density of the PGMA(*rac*)<sub>27</sub> chains on the surface enhances the intermolecular hydrogen bonding effect between the polymer chains and leads to less hydrated films. This is further confirmed by the fact that the introducing 2 SMA units in PGMA(*rac*)<sub>27</sub> can greatly improve the protein repelling ability. The CD measurements show that certain ordered conformations are adopted in enantiopure polymers but not in racemic polymer aqueous solutions since the enantiopure PSMA do not show the circular dichroism. The DLS results also indicate different physical properties of enantiopure and racemic polymers in water. This presumably causes the different grafting density since the polymer surfaces were prepared by the “grafting to” method in which the polymer properties in solution play an important role.

## 4.5 References

- (1) Chuang, H. Y. K. In *Blood Compatibility*; Williams, D. F., Ed.; CRC Press: Boca Raton, FL, 1987; Vol. 1, pp 87-102.
- (2) Kane, R. S.; Deschatelets, P.; Whitesides, G. M. *Langmuir* **2003**, *19*, 2388-2391.
- (3) Stickler, D. J.; McLean, R. J. C. *Cell Mater.* **1995**, *5*, 167-182.
- (4) Castner, D. G.; Ratner, B. D. *Surf. Sci.* **2002**, *500*, 28-60.
- (5) Senaratne, W.; Andruzzi, L.; Ober, C. K. *Biomacromolecules* **2005**, *6*, 2427-2448.
- (6) Langer, R.; Tirrell, D. A. *Nature* **2004**, *428*, 487-492.
- (7) Prime, K. L.; Whitesides, G. M. *J. Am. Chem. Soc.* **1993**, *115*, 10714-10721.
- (8) Sofia, S. J.; Premnath, V.; Merrill, E. W. *Macromolecules* **1998**, *31*, 5059-5070.
- (9) Unsworth, L. D.; Sheardown, H.; Brash, J. L. *Biomaterials* **2005**, *26*, 5927-5933.
- (10) Wyszogrodzka, M.; Haag, R. *Biomacromolecules* **2009**, *10*, 1043-1054.
- (11) Wyszogrodzka, M.; Haag, R. *Langmuir* **2009**, *25*, 5703-5712.
- (12) Zhao, C.; Li, L. Y.; Zheng, J. *Langmuir* **2010**, *26*, 17375-17382.
- (13) Bhat, R. B.; Chaney, B. N.; Rowley, J.; Liebmann-Vinson, A.; Genzer, J. *Adv. Mater.* **2005**, *17*, 2802-2807.
- (14) Xue, C. Y.; Yonet-Tanyeri, N.; Brouette, N.; Sferrazza, M.; Braun, P. V.; Leckband, D. E. *Langmuir*, **2011**, *27*, 8810-8818.
- (15) Zhang, Z.; Chen, S.; Chang, Y.; Jiang, S. Y. *J. Phys. Chem. B* **2006**, *110*, 10799-10804.
- (16) Zhang, Z.; Zhang, M.; Chen, S. F.; Horbetta, T. A.; Ratner, B. D.; Jiang, S. Y. *Biomacromolecules* **2006**, *8*, 122-127.
- (17) Cheng, G.; Zhang, Z.; Chen, S. F.; Bryers, J. D.; Jiang, S. Y. *Biomaterials* **2007**, *28*, 4192-4199.
- (18) Herrwerth, S.; Eck, W.; Reinhardt, S.; Grunze, M. *J. Am. Chem. Soc.* **2003**, *125*, 9359-9366.
- (19) Unsworth, L. D.; Sheardown, H.; Brash, J. L. *Langmuir* **2008**, *24*, 1924-1929.
- (20) Unsworth, L. D.; Sheardown, H.; Brash, J. L. *Langmuir* **2005**, *21*, 1036-1041.
- (21) Kingshott, P.; Tissen, H.; Griesser, H. J. *Biomaterials* **2002**, *23*, 2043-2056.
- (22) Hower, J. C.; He, Y.; Jiang, S. Y. *J. Chem. Phys.* **2008**, *129*, 215101-215107.
- (23) He, Y.; Chang, Y.; Hower, C. H.; Zheng, J.; Chen, S. F.; Jiang, S. Y. *Phys. Chem. Chem. Phys.* **2008**, *10*, 5539-5544.
- (24) Hazen, R. M.; Scholl, D. S. *Nat. Mater.* **2003**, *2*, 367-374.
- (25) Wang, X.; Gan, H.; Sun, T. L.; Su, B. L.; Fuchs, H.; Vestweber, D.; Butz, S. *Soft Matter* **2010**, *6*, 3851-3855.

- (26) Hanein, D.; Geiger, B.; Addadi, L. *Science* **1994**, *263*, 1413-1416.
- (27) (a) Tang, K. J.; Gan, H.; Li, Y.; Chi, L. F.; Sun, T. L.; Fuchs, H. *J. Am. Chem. Soc.* **2008**, *130*, 11284-11285. (b) Gan, H.; Tang, K. J.; Sun, T. L.; Hirtz, M.; Li, Y.; Chi, L. F.; Butz, S.; Fuchs, H. *Angew. Chem. Int. Ed.* **2009**, *48*, 5282-5286.
- (28) (a) Wang, X.; Gan, H.; Sun, T. L. *Adv. Funct. Mater.* **2011**, *21*, 3276-3281. (b) Wang, X.; Gan, H.; Zhang, M. X.; Sun, T. L. *Langmuir* **2012**, dx.doi.org/10.1021/la204143g.
- (29) (a) Ostuni, E.; Chapman, R. G.; Liang, M. N.; Meluleni, G.; Pier, G.; Ingber, D. E.; Whitesides, G. M., *Langmuir* **2001**, *17*, 6336-6343. (b) Hower, J. C.; He, Y.; Bernards, M. T.; Jiang, S. Y. *J. Chem. Phys.* **2006**, *125*, 214704-214711.
- (30) Metzke, M.; Guan, Z. B. *Biomacromolecules* **2008**, *10*, 208-215.
- (31) Bandyopadhyay, D.; Orashar, D.; Luk, Y-Y. *Chem. Commun.* **2011**, *47*, 6165-6167.
- (32) Barbey, R.; Lavanant, L.; Paripovic, D.; Schüwer, N.; Sugnaux, C.; Tugulu, S.; Klok, H. *Chem. Rev.* **2009**, *109*, 5437-5527.
- (33) Zdyrko, B.; Luzinov, I. *Macromol. Rapid. Commun.* **2011**, *32*, 859-869.
- (34) Fristrup, C. J.; Jankova, K.; Hvilsted, S. *Soft Matter* **2009**, *5*, 4623-4634.
- (35) Gates, G.; Harmon, J. P.; Ors, J.; Benz, P. *Polymer* **2003**, *44*, 207-214.
- (36) Amado, E.; Augsten, C.; Mäder, K.; Blume, A.; Kressler, J. *Macromolecules* **2006**, *39*, 9486-9496.
- (37) Carrot, G.; Hilborn, J. G.; Trollsås, M.; Hedrick, J. L.; *Macromolecules* **1999**, *32*, 5264-5269.
- (38) Zhang, D.; Oritz, C. *Macromolecules* **2004**, *37*, 4271-4282.
- (39) Kyeremateng, S. O.; Amado, E.; Kressler, J. *Eur. Polym. J.* **2007**, *43*, 3380.
- (40) Van Krevelen, D. W. *Properties of Polymers*; Elsevier: Amsterdam 1997; p 82.
- (41) Zdyrko, B.; Varshney, S. K.; Luzinov, I. *Langmuir* **2004**, *20*, 6727-6735.
- (42) Henn, G.; Bucknall, D. G.; Stamm, M.; Vanhoorne, P.; Jerome, R. *Macromolecules* **1996**, *29*, 4305-4313.
- (43) Thompson, K. L.; Armes, S. P.; York, D. W.; Burdis, J. A. *Macromolecules* **2010**, *43*, 2169-2177.
- (44) Kyeremateng, S. O.; Henze, T.; Busse, K.; Kressler, J. *Macromolecules* **2010**, *43*, 2502-2511.
- (45) Beers, K. L.; Boo, S.; Gaynor, S. G.; Matyjaszewski, K. *Macromolecules* **1999**, *32*, 5772-5776.
- (46) Matyjaszewski, K.; Wang, J.; Grimaud, T.; Shipp, D. *Macromolecules* **1998**, *31*, 1527-1534.

- (47) (a) Sperling, L. H. *Introduction to Physical Polymer Science*; John Wiley & Sons: New York, 2001. (b) Dünweg, B.; Reith, D.; Steinhauser, M.; Kremer, K. *J. Chem. Phys.* **2002**, *117*, 914-924.
- (48) Sperling, L. H. *Polymeric Multicomponent Materials*; John Wiley & Sons: New York, 1997.
- (49) Roig, B.; Chalmin, E.; Touraud, E.; Thomas, O. *Talanta* **2002**, *56*, 585-590.
- (50) Bloksma, M. M.; Hoepfener, S.; D'Haese, C.; Kempe, K.; Mansfeld, U.; Paulus, R. M.; Gohy, J. F.; Schubert, U. S.; Hoogenboom, R. *Soft Matter* **2012**, *8*, 165-172.
- (51) Armand, P.; Kirschenbaum, K.; Falicov, A.; Dunbrack, R. L., Jr.; Dill, K. A., Zuckermann, R. N.; Cohen, F. E. *Fold. Des.* **1997**, *2*, 369-375.
- (52) Lee, B. C.; Zuckermann, R.; Dill, K. A. *J Am. Chem. Soc.* **2005**, *127*, 10999-11009.
- (53) Bloksma, M. M., Rogers, S.; Schubert, U. S.; Hoogenboom, R. *Soft Matter* **2010**, *6*, 994-1003.
- (54) Watson, J. D.; Crick, F. H. C.; *Nature (London)* **1953**, *171*, 737-738.
- (55) (a) Natura, R.; Tabei, J. Masuda, T. *Macromolecules* **2002**, *35*, 2955-2961. (b) Tabei, J.; Shiotsuki, M.; Sanda, F.; Masuda, T. *Macromolecules* **2005**, *38*, 5860-5867.
- (56) Munch, M. R.; Gast, A. P. *Macromolecules* **1988**, *21*, 1366-1372.
- (57) Bijsterbosch, H. D.; Cohen Stuart, M. A.; Fleer, G. J. *Macromolecules* **1998**, *31*, 9281-9294.
- (58) Kanayama, N.; Kitano, H. *Langmuir* **2000**, *16*, 577-583.
- (59) Yeh, P. Y. J.; Kainthan, R. K. Zou, Y. Q.; Chiao, M.; Kizhakkedathu, J. N. K. *Langmuir* **2008**, *24*, 4907-4916.
- (60) Schasfoort, R. B. M.; Tudos, A. J. *Handbook of Surface Plasmon Resonance*; RSC: Cambridge, 2008.
- (61) Siegers, C.; Biesalski, M.; Haag, R. *Chem. Eur. J.* **2004**, *10*, 2831-2838.
- (62) Egret, H.; Dimonie, V. L.; Sudol, E. D.; Klein, A.; El-Aasser, M. S., *J. Appl. Polym. Sci.* **2001**, *82*, 1739-1747.

## Chapter 5

### *Detection of Chirality of Poly(glycerol methacrylate)s After Derivatization by $^1\text{H}$ NMR Spectroscopy*

#### 5.1 Introduction

Boronic acid reacts with diols instantaneously to give cyclic boronate esters in basic aqueous media or non-aqueous solution.<sup>1-3</sup> Considerable interest has been given to the understanding of the binding between materials carrying boronic acid and diols. This is considered as an important step for the development of biomedical materials, e.g. able for smart detection of saccharides.<sup>4-9</sup> Thus, some boronic acid containing materials, in particular derivatives of phenylboronic acid, have been developed as biosensors to detect different sugars which exhibit a different binding constant in the order of: fructose  $\gg$  mannose  $>$  galactose  $>$  glucose.<sup>10</sup>

Recently, the use of chiral derivatizing agents (CDAs) to determine the absolute configuration of chiral diols by NMR spectroscopy has received much attention.<sup>11-19</sup> Using NMR spectroscopy, the enantiomers cannot be distinguished in achiral solvents since the resonances of enantiotopic nuclei are isochronous.<sup>20</sup> However, the chirality of enantiomers can be determined by their derivatization with enantiopure CDAs to obtain the corresponding diastereoisomers, in which the resonances of certain diastereotopic nuclei are anisochronous. Extended studies by Bull and James<sup>21-23</sup> have confirmed that the chirality of a series of small molar mass chiral diols can be determined by NMR spectroscopy using boronic acid derivatives and additionally enantiopure CDAs. This approach has the advantage of the absence of a kinetic resolution, i.e. the chemical reaction of the (*R*)- and (*S*)-species occurs with the same rate during the derivatization reactions. Therefore, it is possible to calculate the enantiomeric purity of diols.<sup>22</sup> While this approach has been successfully applied for the determination of the chirality of low molar mass diols, we apply this method for the detection of the chirality of poly(glycerol methacrylate)s (PGMAs) having a diol functionality in the side chain of their repeat unit. To the best of our knowledge, this is the first report on the determination of the absolute configuration of synthetic polymers containing chiral diol moieties. This seems to be especially important since this class of water soluble polymers has several potential applications in the field of biomedical materials.<sup>24,25</sup>

## 5.2 Experimental Section

### 5.2.1 Materials

All the chemicals were purchased from Sigma-Aldrich unless otherwise stated. 2-Formylphenylboronic acid (FPBA) ( $\geq 95.0\%$ ), (*S*)-(-)- $\alpha$ -methylbenzylamine ((*S*)-MBA) ( $\geq 99.0\%$ ), (*R*)-(+)- $\alpha$ -methylbenzylamine ((*R*)-MBA) ( $\geq 99.0\%$ ) and dimethylsulfoxide- $d_6$  (DMSO- $d_6$ ) (99.96 atom% D). The HS-PGMA(*rac*)<sub>27</sub>, HS-PGMA(*R*)<sub>24</sub> and HS-PGMA(*S*)<sub>28</sub> were synthesized by ATRP as already discussed in Chapter 4.

**Table 5.1.** Characteristic data of the different polymers employed.

Polymers	$M_w/M_n^a$	$DP^b$	$M_n$ (g mol <sup>-1</sup> ) <sup>b</sup>
PGMA( <i>S</i> ) <sub>28</sub>	1.17	28	4900
PGMA( <i>R</i> ) <sub>24</sub>	1.21	24	4300
PGMA( <i>rac</i> ) <sub>27</sub>	1.27	27	4800

<sup>a</sup>SEC measurements of PSMA with THF as eluent and PMMA as standard.

<sup>b</sup>Calculated from <sup>1</sup>H NMR measurements of the 2,4-dinitrophenyl terminal PSMA in DMSO- $d_6$  at 25 °C.

### 5.2.2 NMR spectroscopy

The samples for NMR spectroscopy were prepared in 1 mL DMSO- $d_6$  by mixing FPBA (1 equiv), *S* or *R*-MBA (1 equiv) and PGMA polymers (1 equiv GMA repeat unit) and then the mixtures were stirred at room temperature for 20 min. Small amounts of molecular sieve was added to reduce the amount of water in DMSO- $d_6$ . The <sup>1</sup>H, <sup>13</sup>C DEPT-135 and 2D <sup>13</sup>C -<sup>1</sup>H HSQC NMR spectra (Figures 5.2-5.4) were recorded on a BRUKER Avance III spectrometer operating at 800 MHz for <sup>1</sup>H (32 acquisitions) and 200 MHz for <sup>13</sup>C (6000 acquisitions) in DMSO- $d_6$  at 50 °C with a polymer concentration of  $\sim 6 \times 10^{-3}$  M. The other <sup>1</sup>H NMR spectra were measured on a Varian Gemini 2000 spectrometer operating at 400 MHz (64 acquisitions) by using  $\sim 2 \times 10^{-3}$  M polymer solution in DMSO- $d_6$  at 25 or 50 °C. Chemical shifts are given in ppm relative to TMS, and the residual peak of DMSO is used as internal standard.

### 5.3 Results and Discussion

Figure 5.1 depicts the  $^1\text{H}$  NMR spectra of PGMA(*rac*)<sub>27</sub>, PGMA(*S*)<sub>28</sub> and PGMA(*R*)<sub>24</sub> in DMSO-*d*<sub>6</sub> at 25 °C and the signal assignment. These three polymers show identical resonance signals for the specific protons since they are composed of enantiomeric GMA repeat units in which the protons located at the same position in the polymers are enantiotopic in external comparison. In order to distinguish these three polymers, racemic and chiral PGMA are derivatized with enantiopure CDAs to obtain the diastereoisomeric repeat units, in which the resonances of certain diastereotopic nuclei appear at different chemical shift.

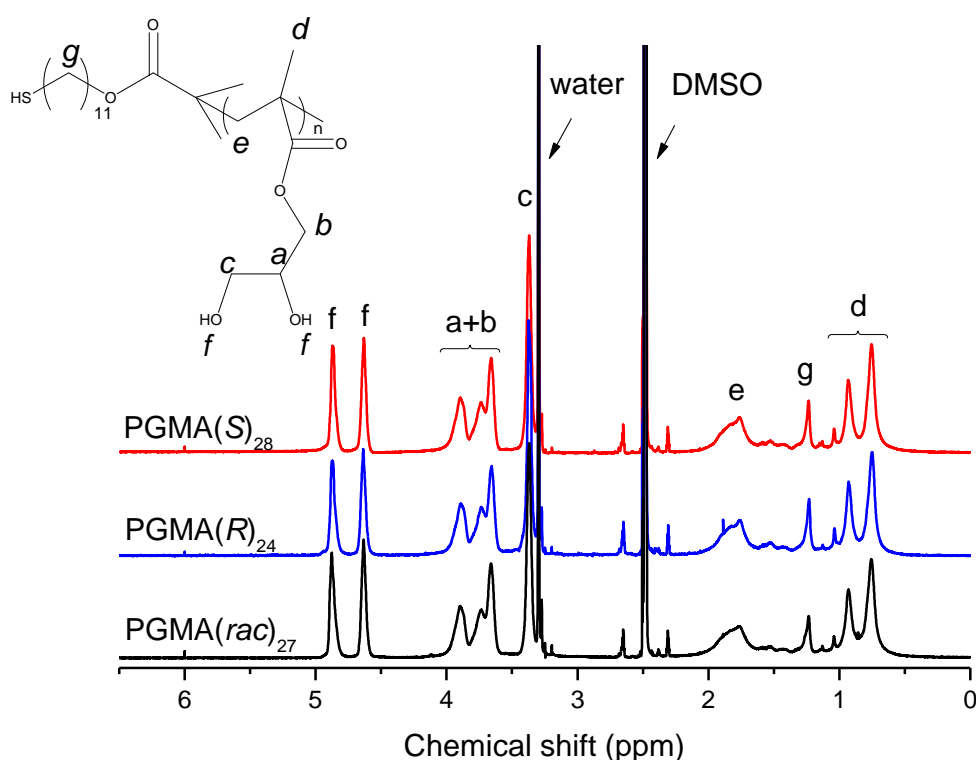
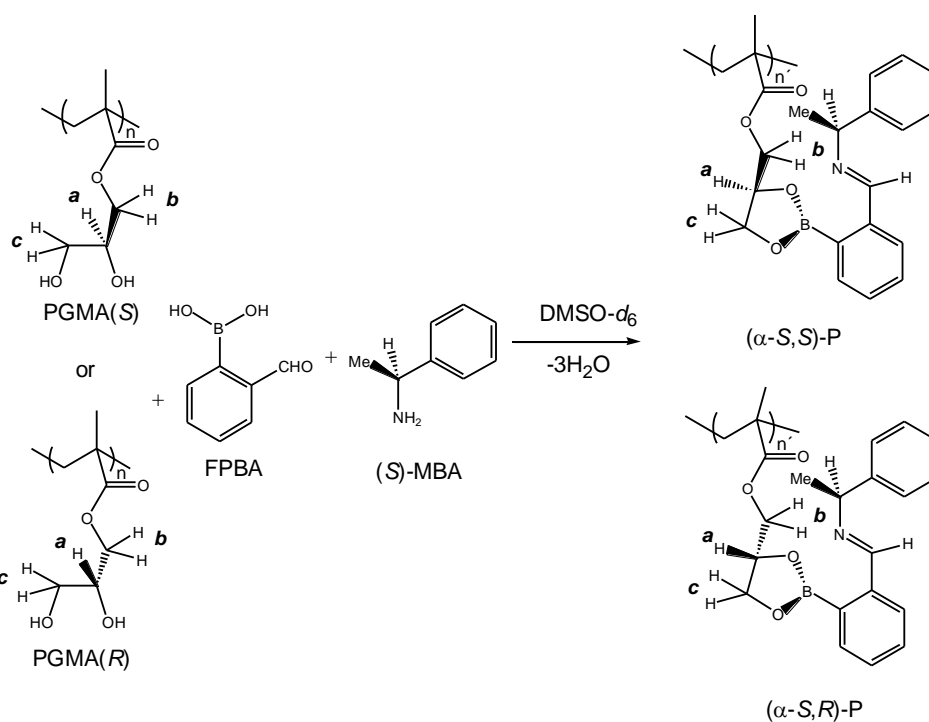


**Figure 5.1.**  $^1\text{H}$  NMR spectra of PGMA(*S*)<sub>28</sub>, PGMA(*R*)<sub>24</sub> and PGMA(*rac*)<sub>27</sub> in DMSO-*d*<sub>6</sub>, 400 MHz at 25 °C.

Based on the experiments of Bull and James<sup>22</sup>, a simple mixing and shaking procedure is applied to prepare the samples for NMR spectroscopy. Typically, 1 equiv 2-formylphenylboronic acid (FPBA), 1 equiv (*S*)-(-)- $\alpha$ -methylbenzylamine ((*S*)-MBA) and 1/27 equiv PGMA(*rac*)<sub>27</sub> are mixed and dissolved in DMSO-*d*<sub>6</sub> and stirred for 20 min at room temperature. These three compounds react readily in DMSO to give the imino-boronate ester containing polymers and water by a nucleophilic addition-condensation reaction between the

amine group in (*S*)-MBA and the formyl group in FPBA and an esterification reaction between the boronic acid group in FPBA with the diol in glycerol methacrylate (GMA) (Scheme 5.1). The water, which has a high miscibility with DMSO-*d*<sub>6</sub>, cannot be removed completely by the molecular sieve. It promotes the backward reaction and leads to an equilibrium situation. At the same time, the steric effect of the pendent groups of polymers can also decrease the polymer reactivity.<sup>26</sup> Thus, not all the diol groups of the GMA repeat units are converted to imino-boronate esters (approximately 80%, see Figure A8 of the Appendix). This has also been observed for the immobilization of boronic acid with poly(vinyl alcohol)<sup>27</sup> and hyperbranched polyglycerol<sup>28</sup>. The resonance signals of the protons from the unreacted FPBA and MBA, as well as water are observed in the <sup>1</sup>H NMR spectra in addition to the derivatized polymer (The detailed assignment is shown in Figure A8). The derivatization process is repeated using 1/28 equiv PGMA(*S*)<sub>28</sub> and 1/24 equiv PGMA(*R*)<sub>24</sub> to obtain the derivatized polymers.



**Scheme 5.1.** The reaction of PGMA(*S*), PGMA(*R*), FPBA and (*S*)-MBA to form diastereomeric boronate ester containing derivatized polymers. The <sup>1</sup>H NMR signals of the protons *a*, *b* and *c* are discussed in the text.

In this study, (α-*S,S*)-P<sub>28</sub>, (α-*S,R*)-P<sub>24</sub> and (α-*S,rac*)-P<sub>27</sub> are used to indicate the derivatized polymers formed by FPBA and (*S*)-MBA with polymers PGMA(*S*)<sub>28</sub>, PGMA(*R*)<sub>24</sub> and PGMA(*rac*)<sub>27</sub>, respectively. The completely assigned <sup>1</sup>H NMR spectrum of (α-*S,S*)-P<sub>28</sub>



measured at 50 °C and 800 MHz, is shown in Figure 5.2. The DEPT technique (Distortionless Enhancement by Polarization Transfer) is used to recognize primary, secondary and tertiary carbon atoms in the polymers. Figure 5.3 shows the  $^{13}\text{C}$  DEPT-135 spectrum of ( $\alpha$ -*S,S*)-P<sub>28</sub>, in which the signals from CH and CH<sub>3</sub> groups are shown as positive peaks and the signals from CH<sub>2</sub> appear as negative peaks. The proton resonance signals of *a*H (bound to the chiral carbon atom), *b*H (the methylene group between the chiral carbon atom and the ester group) and *c*H (the methylene group between the OH-functionalities) on the imino-boronate esters and their counterparts *a'*, *b'* and *c'*H of the unreacted GMA units are partially overlapped and cannot be assigned from the  $^1\text{H}$  NMR spectra alone. However, it can be assigned with the help of one-one correlation between carbon and proton signals in HSQC (Heteronuclear Single Quantum Correlation) spectrum. Figure 5.4 shows the 2D multiplicity edited  $^{13}\text{C}$ - $^1\text{H}$  HSQC NMR spectrum of ( $\alpha$ -*S,S*)-P<sub>28</sub> in DMSO-*d*<sub>6</sub> with the assignment of the defined cross-peaks, in which positive cross-peaks shown in red are assigned to the CH or CH<sub>3</sub> groups and negative cross-peaks shown in blue are assigned to the CH<sub>2</sub> groups. The analysis of this 2D  $^{13}\text{C}$ - $^1\text{H}$  HSQC spectrum reveals that the asymmetric broad proton resonance peak at ~ 3.72 – 4.02 ppm comprises the resonances from both *b* and *b'*H, in which the *b*H resonance contributes to the main peak and *b'*H resonance contributes to the shoulder. Furthermore, the proton resonance signal of *a'*H is overlapped with the resonances of *b* and *c*H. This leads to the decrease of the baseline resolution between the *b* and *c*H resonances in the  $^1\text{H}$  NMR spectrum. In the following, the proton resonances attributed to the *a'*, *b'* and *c'*H will not be mentioned because they are enantiotopic nuclei in (*R*) and (*S*)-GMA in external comparison and exhibit the same chemical shift as their corresponding counterparts.

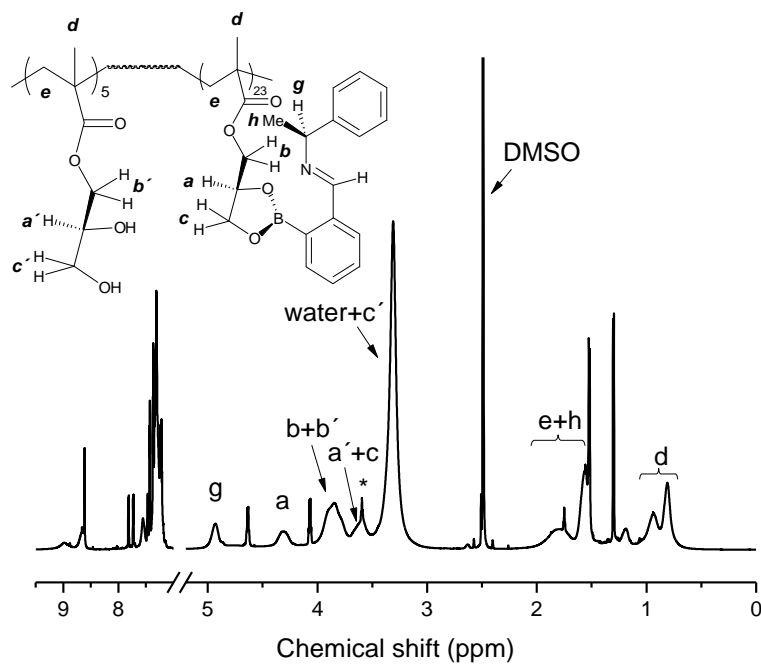


**Figure 5.2.**  $^1\text{H}$  NMR spectrum of  $(\alpha\text{-}S,S)\text{-P}_{28}$  in  $\text{DMSO-}d_6$  at  $50\text{ }^\circ\text{C}$  and 800 MHz. \* (impurity). This sample contains 5 unreacted repeat units. The peaks not assigned belong to some reactants not converted.

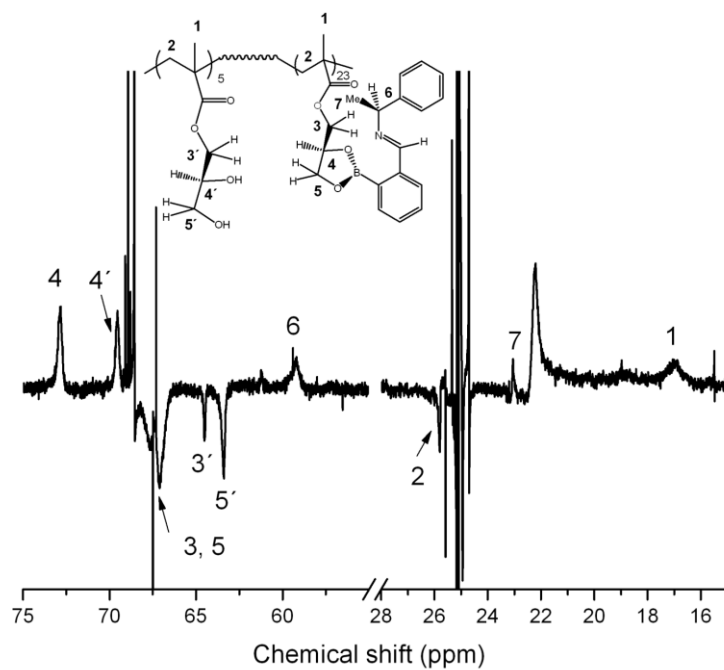


**Figure 5.3.**  $^{13}\text{C}$  DEPT-135 NMR spectrum of  $(\alpha\text{-}S,S)\text{-P}_{28}$  in  $\text{DMSO-}d_6$  at  $50\text{ }^\circ\text{C}$  and 200MHz.

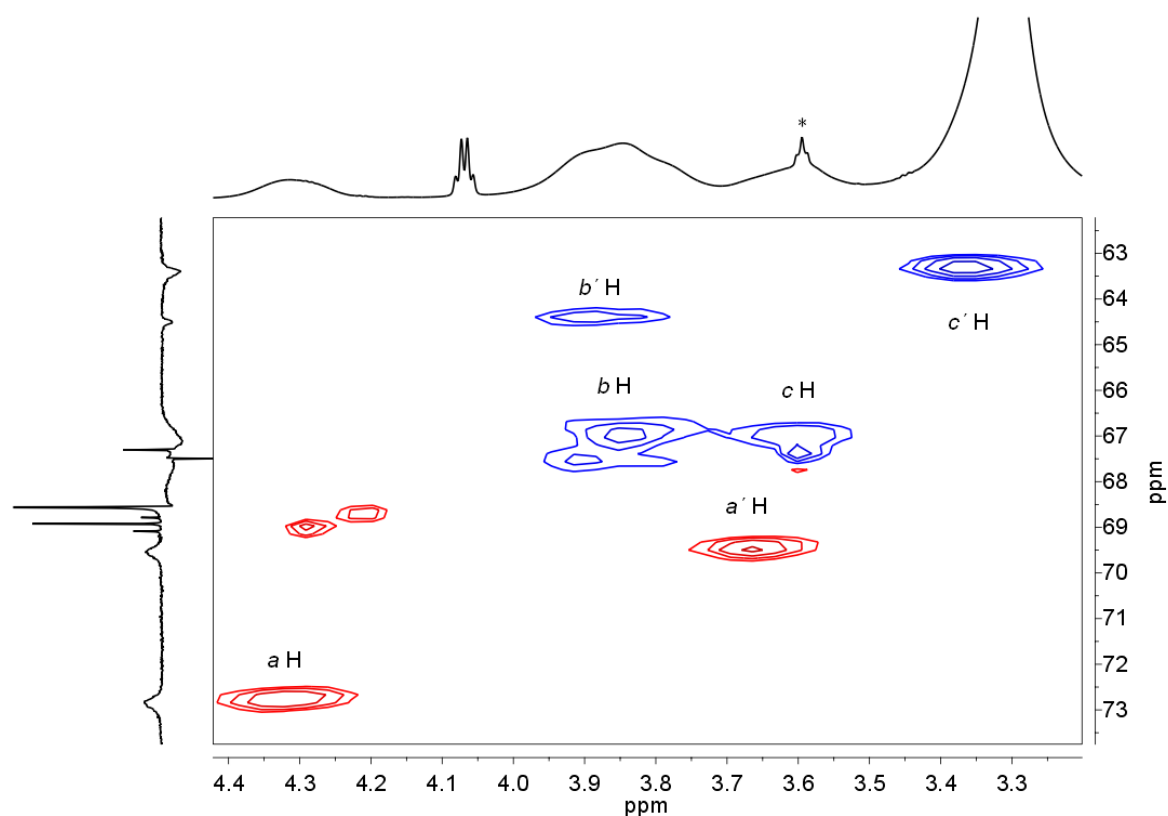
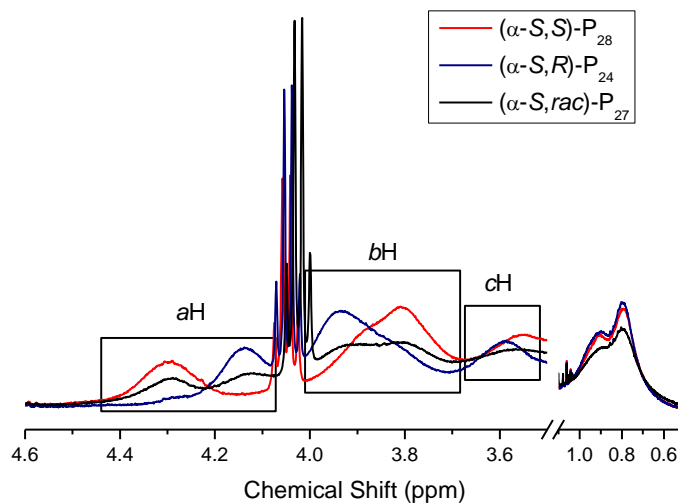


Figure 5.4. 2D multiplicity edited  $^{13}\text{C}$ - $^1\text{H}$  HSQC NMR spectrum in the interval from 3.1-4.4 ppm of ( $\alpha$ -*S,S*)-P<sub>28</sub> in DMSO-*d*<sub>6</sub> at 50 °C. The *a'*, *b'* and *c'*H and *a*, *b* and *c*H are the protons on the GMA and imino-boronate esters of the derivatized polymer, respectively. \*(impurity) The assignment of the  $^{13}\text{C}$  spectrum is given in Figure 5.3.

Figure 5.5 shows the  $^1\text{H}$  NMR spectra of ( $\alpha$ -*S,S*)-P<sub>28</sub>, ( $\alpha$ -*S,R*)-P<sub>24</sub> and ( $\alpha$ -*S,rac*)-P<sub>27</sub> in DMSO-*d*<sub>6</sub> at 25 °C. The complete spectra are shown in Figure 5.2. In the (*R*)- and (*S*)-PGMA derivatives, the resonance signals of the specific side group protons appear at different chemical shifts since the new formed imino-boronate esters in these two derivatives are diastereoisotopic in external comparison due to the addition of the chiral CDAs. The resonance signals at the chemical shift of ~ 0.5-1.1 ppm of the methyl group located at the polymer backbone of the derivatized polymers are more attenuated and slightly broader than their counterparts in PGMA (Figure 5.1) because the large side groups decrease the mobility of the polymers in solution.



**Figure 5.5.**  $^1\text{H}$  NMR spectra of  $(\alpha\text{-}S,S)\text{-P}_{28}$ ,  $(\alpha\text{-}S,R)\text{-P}_{24}$  and  $(\alpha\text{-}S,rac)\text{-P}_{27}$  in  $\text{DMSO-}d_6$ , 400MHz. The resonance signals of  $a\text{H}$ ,  $b\text{H}$  and  $c\text{H}$  are indicated according to the assignment given in Figure 5.2.

The analysis of the  $^1\text{H}$  NMR spectra of  $(\alpha\text{-}S,S)\text{-P}_{28}$  and  $(\alpha\text{-}S,R)\text{-P}_{24}$  reveals that the resonances of the protons located in the vicinity or directly bound to the chiral carbon atom of the PGMA side group appear at different chemical shifts. For example, the resonance of the proton  $a\text{H}$  in  $(\alpha\text{-}S,S)\text{-P}_{28}$  shifts more downfield than the  $a\text{H}$  in  $(\alpha\text{-}S,R)\text{-P}_{24}$ . On the opposite, the resonance of protons  $b\text{H}$  in  $(\alpha\text{-}S,S)\text{-P}_{28}$  shifts upfield compared to  $b\text{H}$  in  $(\alpha\text{-}S,R)\text{-P}_{24}$ . The resonance signals of the protons  $c\text{H}$  in the derivatized polymers partially overlap with the water resonance peak at 25 °C. However, it is clear that the resonance peak of the  $c\text{H}$  in  $(\alpha\text{-}S,S)\text{-P}_{28}$  shifts slightly upfield compared to the corresponding peak in  $(\alpha\text{-}S,R)\text{-P}_{24}$ . This chemical shift difference of the  $c\text{H}$  is more evident in the  $^1\text{H}$  NMR spectra recorded at 50 °C where the water resonance shifts upfield as shown in Figure 5.6. Furthermore, in the  $^1\text{H}$  NMR spectrum of  $(\alpha\text{-}S,rac)\text{-P}_{27}$ , which contains a 50:50 mixture of the diastereoisomeric  $(\alpha\text{-}S,S)$  and  $(\alpha\text{-}S,R)$  imino-boronate ester pendant groups, two distinct resonances are observed for  $a\text{H}$  and their chemical shifts are identical with the resonances of  $a\text{H}$  protons in  $(\alpha\text{-}S,S)\text{-P}_{28}$  and  $(\alpha\text{-}S,R)\text{-P}_{24}$ . Similarly, the  $b\text{H}$  protons of  $(\alpha\text{-}S,rac)\text{-P}_{27}$  show a broad resonance signal with the tendency to split into two peaks. This broad resonance peak can be considered as the result of the overlapping of the resonance peaks corresponding to the  $b\text{H}$  in the  $(\alpha\text{-}S,S)\text{-P}_{28}$  and  $(\alpha\text{-}S,R)\text{-P}_{24}$ . It can be seen that the resonance difference of the  $b\text{H}$  in  $(\alpha\text{-}S,S)$  and  $(\alpha\text{-}S,R)$  pendant groups is not large enough

to achieve the good baseline resolution as for *aH*. This is caused by the fact that the two diastereoisotopic protons in *bH* together with the low mobility of the polymers result in a broad and attenuated resonance signal.

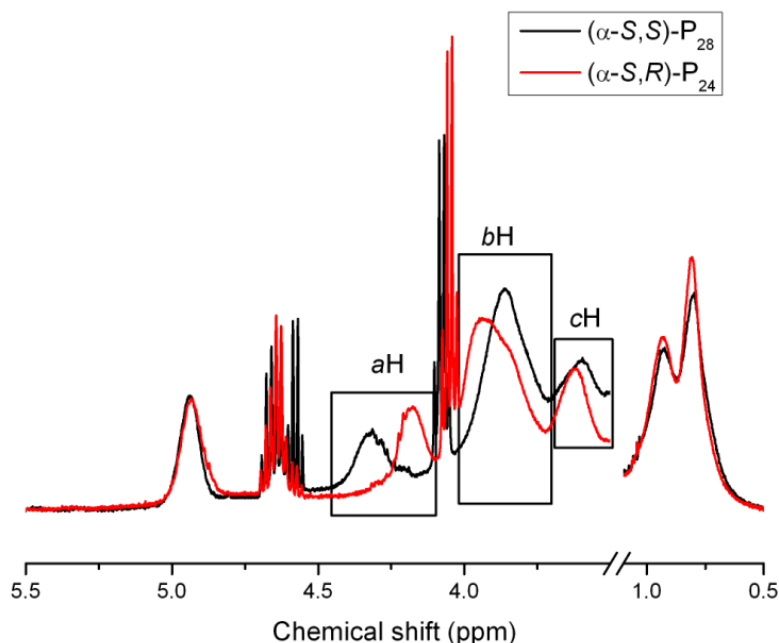


**Figure 5.6.**  $^1\text{H}$  NMR spectra of  $(\alpha\text{-}S,S)\text{-P}_{28}$ , and  $(\alpha\text{-}S,R)\text{-P}_{24}$  in  $\text{DMSO-}d_6$ , 400 MHz at 50 °C. The resonance signals of *aH*, *bH* and *cH* are indicated.

The chirality of the PGMA s can be determined on the basis of the anisotropic shielding /deshielding effect of the phenyl group in (*R*)- or (*S*)-MBA, i.e. the upfield shift of the protons above or below the aromatic ring due to the shielding effect and the downfield shift of the protons on the side of the aromatic ring due to the deshielding effect.<sup>29</sup> The sign of the chemical shift difference ( $\Delta\delta^{RS}$ ) of the specific resonance (*aH* or *bH*) of the derivatives from (*R*)- and (*S*)-MBA is employed, which contains the information necessary for the determination of the configuration. The chiral derivatization procedures for  $\text{PGMA}(S)_{28}$  and  $\text{PGMA}(R)_{24}$  are repeated using the (*R*)-MBA, the opposite enantiomer of (*S*)-MBA. As shown in Figure 5.7 a, four imino-boronate esters are obtained in the reactions of FPBA, (*R*)- or (*S*)-MBA and (*S*)- or (*R*)-GMA. The  $(\alpha\text{-}R,R)$  and  $(\alpha\text{-}S,S)$  derivatives are enantiomers and thus identical  $^1\text{H}$  NMR spectra are obtained as for  $(\alpha\text{-}S,R)$  and  $(\alpha\text{-}R,S)$  derivatives. Figures 5.7 b) and c) depict the  $^1\text{H}$  NMR spectra recorded at 25 °C of (*R*)- and (*S*)- $\text{PGMA}(S)_{28}$  derivatives,  $(\alpha\text{-}R,S)\text{-P}_{28}$  and  $(\alpha\text{-}S,S)\text{-P}_{28}$ , and (*R*)- and (*S*)- $\text{PGMA}(R)_{24}$  derivatives,  $(\alpha\text{-}R,R)\text{-P}_{24}$  and  $(\alpha\text{-}S,R)\text{-P}_{24}$ , respectively. Comparing the  $^1\text{H}$  NMR spectra of the  $(\alpha\text{-}R,S)\text{-P}_{28}$  and  $(\alpha\text{-}S,S)\text{-P}_{28}$  shows

that the  $\Delta\delta^{RS}$  value of *a*H is negative, suggesting that the *a*H proton of the (*R*)-MBA derivative is more shielded compared to the (*S*)-MBA derivative. The *b*H protons are more shielded in the (*S*)-MBA derivative than in the (*R*)-MBA derivative. Therefore, the  $\Delta\delta^{RS}$  value is positive. Similarly, the examination of the  $^1\text{H}$  NMR spectra of ( $\alpha$ -*R,R*)- and ( $\alpha$ -*S,R*)-P<sub>24</sub> reveals that the  $\Delta\delta^{RS}$  values of *a*H and *b*H show the opposite signs as their counterparts in ( $\alpha$ -*R,S*)- and ( $\alpha$ -*S,S*)-P<sub>28</sub>. The PGMA(*R*)<sub>24</sub> and PGMA(*S*)<sub>28</sub> derivatives have a similar resolution of  $\Delta\delta = \sim 0.16$  ppm for *a*H and  $\sim 0.14$  ppm for *b*H at 25 °C. To investigate the limitation of this approach, (*R*)-, (*S*)- and (*rac*)- PGMA with different chain lengths ( $DP = \sim 10$  and  $\sim 60$ ) are examined using the same procedure and similar results are obtained.

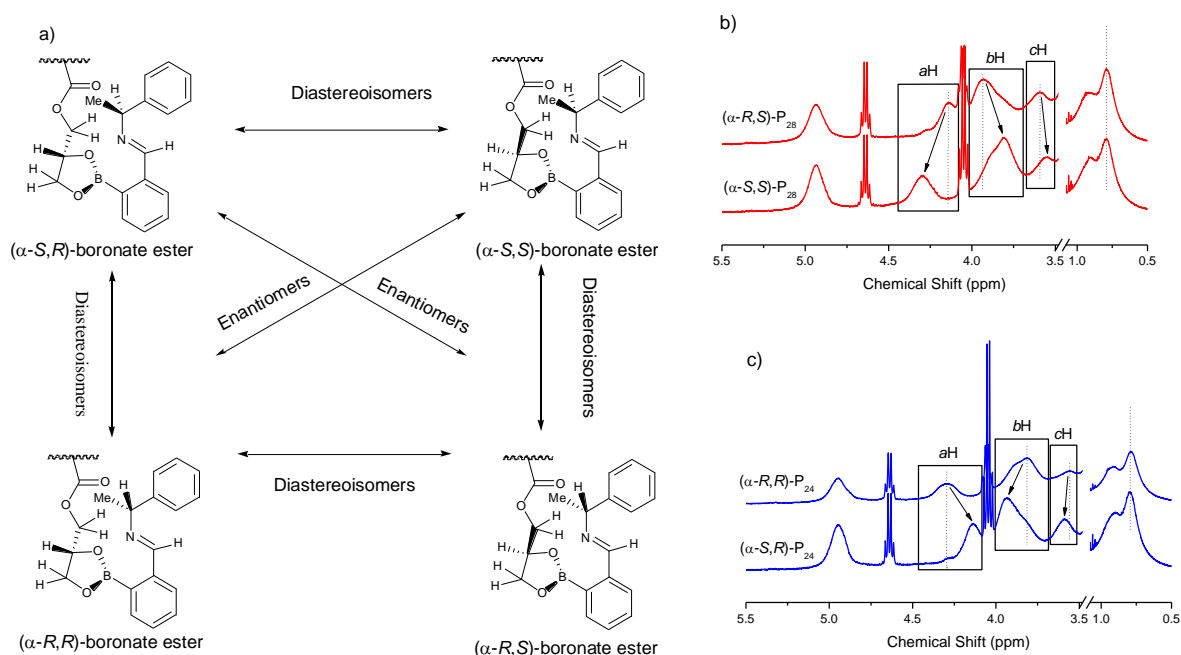


**Figure 5.7.** (a) Boronate esters obtained by the reactions of FPBA, (*R*)- or (*S*)-MBA and PGMA(*R*)<sub>28</sub> or PGMA(*S*)<sub>24</sub>.  $^1\text{H}$  NMR spectra of (*R*)- and (*S*)-MBA boronate esters of (b) PGMA(*S*)<sub>28</sub> and (c) PGMA(*R*)<sub>24</sub>. The spectra are taken in DMSO-*d*<sub>6</sub> at 400 MHz.

## 5.4 Conclusions

The reaction between the diol group of PGMA and FPBA together with the enantiopure MBA allows to distinguish between PGMA(*rac*)<sub>27</sub>, PGMA(*S*)<sub>28</sub> and PGMA(*R*)<sub>24</sub> by <sup>1</sup>H NMR spectroscopy. This so-called three-component chiral derivatization approach<sup>21-23</sup> is here for the first time successfully applied to polymers. In combination with the frequent use of PGMA and its analogues in the biomedical field, this procedure shows a promising methodology in biomaterials development where stereochemistry plays an important role. Since PGMA has been frequently used for the synthesis of amphiphilic<sup>30</sup> and triphilic<sup>31</sup> block copolymers, it will be an interesting problem to look to the physical properties of micelles formed when chiral PGMA are employed. Additionally, it is interesting to study the influence of chirality on protein adsorption after grafting the respective polymers with HS-end groups to gold surfaces.

## 5.5 References

- (1) Nishiyabu, R.; Kubo, Y.; James, T. D.; Fossey, J. S. *Chem. Commun.* **2011**, *47*, 1106-1123.
- (2) Nishiyabu, R.; Kubo, Y.; James, T. D.; Fossey, J. S. *Chem. Commun.* **2011**, *47*, 1124-1150.
- (3) Ferrier, R. J. *Adv. Carbohydr. Chem. Biochem.* **1978**, *35*, 31-80.
- (4) Yan, J.; Springsteen, G.; Deeter, S.; Wang, B. H. *Tetrahedron* **2004**, *60*, 11205-11209.
- (5) Zhang, D.; Thompson, K. L.; Pelton, R.; Armes, S. P. *Langmuir* **2010**, *26*, 17237-17241.
- (6) Takeuchi, M.; Mizuno, T.; Shinkai, S.; Shirakami, A.; Itoh, T. *Tetrahedron: Asymmetry* **2000**, *11*, 3311-3322.
- (7) Iwasawa, N.; Takahagi, H. *J. Am. Chem. Soc.* **2007**, *129*, 7754-7755.
- (8) Kanekiyo, Y.; Sato, H.; Tao, H. *Macromol. Rapid. Commun.* **2005**, *26*, 1542-1546.
- (9) Kitano, H.; Anraku, Y.; Shinohara, H. *Biomacromolecules* **2006**, *7*, 1065-1071.
- (10) Kanayama, N.; Kitano, H. *Langmuir* **2000**, *16*, 577-583.
- (11) Seco, J. M.; Quiñoá, E.; Riguera, R. *Chem. Rev.* **2004**, *104*, 17-117.
- (12) Leiro, V.; Freire, F.; Quiñoá, E.; Riguera, R. *Chem. Commun.* **2005**, *44*, 5554-5556.
- (13) Freire, F.; Seco, J. M.; Quiñoá, E.; Riguera, R. *J. Org. Chem.* **2005**, *70*, 3778-3790.
- (14) Seco, J. M.; Martino, M.; Quiñoá, E.; Riguera, R. *Org. Lett.* **2000**, *2*, 3261-3264.
- (15) Seco, J. M.; Quiñoá, E.; Riguera, R. *J. Org. Chem.* **1999**, *64*, 4669-4675.
- (16) López, B.; Quiñoá, E.; Riguera, R. *J. Am. Chem. Soc.* **1999**, *121*, 9724-9725.
- (17) Freire, F.; Seco, J. M.; Quiñoá, E.; Riguera, R. *Chem. Eur. J.* **2005**, *11*, 5509-5522.
- (18) Dufrasne, F.; Gelbcke, M.; Néve, J. *Spectrochimica Acta Part A* **2003**, *59*, 1239-1245.
- (19) Williamson, R. T.; Barrios Sosa, A. C.; Mitra, A.; Seaton, P. J.; Weibel, D. S.; Schroeder, F. C.; Meinwald, J.; Koehn, F. E. *Org. Lett.* **2003**, *5*, 1745-1748.
- (20) Parker, D. *Chem. Rev.* **1991**, *91*, 1441-1457.
- (21) Yeste, S. L.; Powell, M. E.; Bull, S. D.; James, T. D. *J. Org. Chem.* **2009**, *74*, 427-430.
- (22) Kelly, A. M.; Pérez-Fuertes, Y.; Arimori, S.; Bull, S. D.; James, T. D. *Org. Lett.* **2006**, *8*, 1971-1974.
- (23) Kelly, A. M.; Pérez-Fuertes, Y.; Fossey, J. S.; Yeste, S. L.; Bull, S. D.; James, T. D. *Nature Protoc.* **2008**, *3*, 215-219.
- (24) Gates, G.; Harmon, J. P.; Ors, J.; Benz, P. *Polymer* **2003**, *44*, 215-222.
- (25) Leung, B. K.; Robinson, G. B. *J. Appl. Polym. Sci.* **1993**, *47*, 1207-1214.
- (26) Odian, G. *Principles of polymerization*, 4<sup>th</sup> ed. New York: John Wiley & Sons, 2004.



- (27) Nishimura, H.; Donkai, N.; Miyamoto, T. *J. Polym. Sci. A: Polym. Chem.* **1998**, *36*, 3045-3050.
- (28) Hebel, A.; Haag, R. *J. Org. Chem.* **2002**, *67*, 9452-9455.
- (29) Günther, H. *NMR spectroscopy, basic principles, concepts, and applications in chemistry*, Chichester: John Wiley&Sons, 1994.
- (30) Amado, E.; Augsten, C.; Mäder, K.; Blume, A.; Kressler, J. *Macromolecules* **2006**, *39*, 9486-9496.
- (31) Kyeremateng, S. O.; Amado, E.; Blume, A.; Kressler, J. *Macromol Rapid Commun* **2008**, *29*, 1140-1146.

## Chapter 6

### Summary

Two hydrophobically modified poly(*N*-isopropylacrylamide) (PNIPAM) semitelechelics ( $P_xF_9$ ) were prepared by ‘clicking’ PNIPAM having an azide endgroup ( $P_xN_3$ ) with nonadecafluoro-1-decyl hex-5-ynoate ( $F_9$ ) using copper(I)-catalyzed alkyne-azide cycloaddition (CuAAC) reaction. The azide functional  $P_xN_3$  was obtained by polymerization of NIPAM using functionalized azido-initiators. The lower critical solution temperatures (LCST) of  $P_{28}N_3$  and  $P_{137}N_3$  show higher LCST values than PNIPAM homopolymers with the corresponding similar molar mass because of the hydrophilic azide end group. This effect is especially significant in  $P_{28}N_3$  due to the low molar mass. The  $F_9$  segments shifted the LCST to lower LCST when comparing  $P_xN_3$  with  $P_xF_9$ . Spherical micelles of  $P_xF_9$  in water with a core of  $F_9$ -segments and a PNIPAM corona were detected at the concentrations above the critical micellization concentrations (cmc) by dynamic light scattering (DLS) and by  $^1H$  and  $^{19}F$  NMR spectroscopy below the LCST. Just below the LCST the PNIPAM chains start to collapse onto the  $F_9$ -core followed by aggregation of several collapsed micelles to large particles in the range of  $\sim 110$  nm. The thermodynamics of the LCST of the  $P_xN_3$  and  $P_xF_9$  in water were investigated by differential scanning calorimetry (DSC). The collapse of  $P_xN_3$  at the LCST is much more cooperative than that of  $P_xF_9$ . Moreover, the existence of micelles in  $P_xF_9$  solutions also improved the reversibility of the LCST behavior. The  $P_{28}F_9$  shows a smaller heat of phase separation  $\Delta H$  and the related change in specific heat capacity  $\Delta C_p$  compared to  $P_{137}F_9$ . This suggests that the  $P_{28}F_9$  is more hydrophobic (partially dehydrated NIPAM segments) compared to  $P_{137}F_9$  below the LCST, which is mainly the result of dehydration of PNIPAM.

Unlike PNIPAM, poly(glycerol methacrylate) (PGMA) is a hydrophilic polymer which has the advantage of being water soluble at all temperatures and as such it is a suitable candidate for applications where high temperatures may be prerequisite. The  $F_9$  end capped amphiphilic semitelechelics  $PGMA_xF_9$  have been successfully synthesized by using atom transfer radical polymerization (ATRP) and CuAAC. ATRP is the method of choice due to the simple synthetic procedure and commercial availability of all necessary reagents. The molar mass values of the polymers were obtained from  $^1H$  and  $^{19}F$  NMR spectroscopy measurements. Size exclusion chromatography (SEC) analysis confirmed unimodal molar mass distributions

with generally low polydispersities ( $M_w/M_n < 1.35$ ). The PGMA<sub>x</sub>F<sub>9</sub> self-assemble in water to form spherical micelles bearing PGMA corona and fluorine moiety cores, which was detected from <sup>19</sup>F NMR, DLS, AFM and SEM measurements. The DLS measurements revealed that the micellar clusters are coexisting with polymeric micelles. These clusters are considered stabilized to be by intermolecular hydrogen bonding.

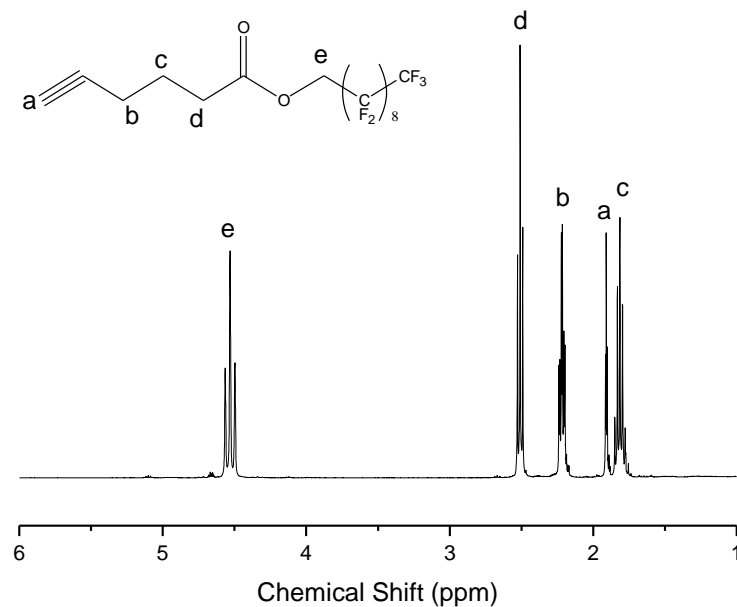
The thermodynamics of self-assembly of the PGMA<sub>x</sub>F<sub>9</sub> semitelechelics into micelles in water was studied and compared to the well studied PEOF<sub>9</sub>. This was done to assess the comparative influence of the hydrophilic PGMA block on the micellization behavior. Although the spherical micelles are formed in both PGMAF<sub>9</sub> and PEOF<sub>9</sub>, it was found that replacing the hydrophilic PEO with PGMA influences the micellization process very significantly. Temperature dependent surface tension measurements showed that the cmc values of PGMAF<sub>9</sub> in aqueous solution increase with temperature, which is opposite than for PEOF<sub>9</sub> and most amphiphilic polymers in water. The replacement of PEO with PGMA leads to a negative standard enthalpy,  $\Delta H^0_{mic}$ , and a much smaller standard entropy,  $\Delta S^0_{mic}$ , of the micellization process, which are estimated from cmc values at various temperatures. This indicates that the micellization of PGMAF<sub>9</sub> in water is driven by both the increase in entropy and the loss in enthalpy. While the self-assembly of PEOF<sub>9</sub> into micelles is driven only by gain of entropy and is enthalpically unfavourable. The opposite  $\Delta H^0_{mic}$  values between the PEOF<sub>9</sub> and PGMAF<sub>9</sub> are further confirmed from the isothermal titration calorimetry (ITC) measurements. These significant differences stem from the partial self-association through hydrogen bonding in the PGMA blocks, which is confirmed by the dynamic light scattering (DLS) and temperature dependent <sup>1</sup>H and <sup>19</sup>F NMR spectroscopy. The self-association effect leads to lesser interaction with water molecules giving PGMA a less hydrophilic character than PEO at low temperatures. Consequently, this hydrogen bonding is responsible for the negative  $\Delta H^0_{mic}$ , comparatively lower  $\Delta S^0_{mic}$  for the micellization of the PGMAF<sub>9</sub> semitelechelics in water.

PGMA is a typical chiral polymer because of the asymmetric carbon atom on each repeat unit. Many biomolecules in organisms show a high chiral preference. Recognizing the chiral effect is very important for the design of biomaterials for the treatment of surfaces or interfaces since it may further influence the biological processes. The protein adsorption on the racemic (*rac*), *R* and *S* PGMA surfaces were studied by using bovine serum albumin (BSA) as a model protein. The preparation of well-defined thiol end capped PGMA(*rac*)<sub>27</sub>, PGMA(*R*)<sub>24</sub> and PGMA(*S*)<sub>28</sub> bearing a similar chain lengths involves the polymerization of SMA monomers to

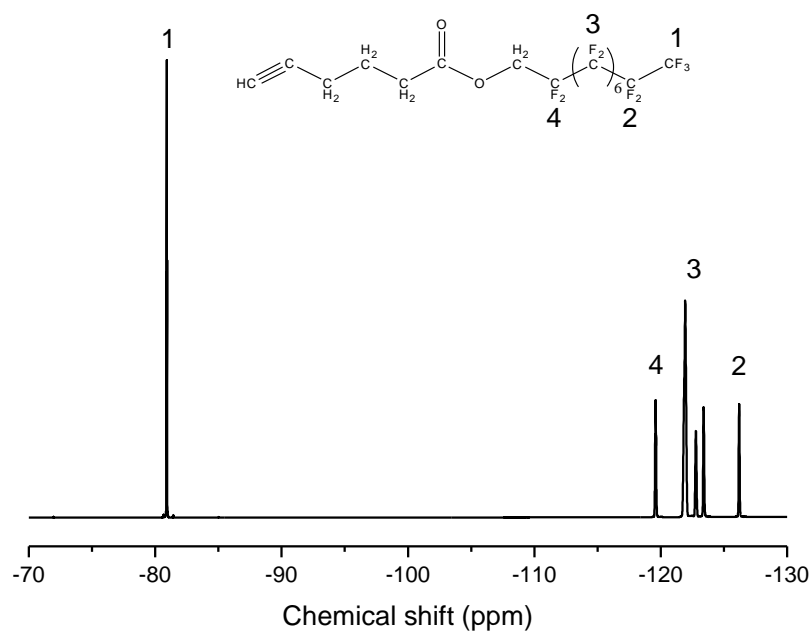
obtain the 2,4-dinitrophenyl functional PSMA by ATRP, conversion of the 2,4-dinitrophenyl group to the thiol group through an aromatic nucleophilic displacement reaction and hydrolysis of the PSMA to cleave the ketal groups to give HS-PGMA. The self-assembled monolayers (SAM) of polymers were prepared by immersing the gold surfaces in polymer solutions since thiol groups have a high affinity to gold by forming stable chemical bonds. The surface plasmon resonance (SPR) measurements revealed that the PGMA greatly reduce the protein adsorption compared to the bare gold surface. Interestingly, the enantiopure PGMA surfaces show a much stronger repelling ability against the BSA adsorption than racemic PGMA surface. This less effective protein resistance ability of the racemic PGMA surface compared to enantiopure surfaces was assumed to be due to the higher polymer grafting density, which was calculated from the dehydrated thickness of the polymer SAMs measured by ellipsometry. A less hydrated polymer film was formed for PGMA(*rac*)<sub>27</sub> surfaces compared to PGMA(*R*)<sub>24</sub> and PGMA(*S*)<sub>28</sub> surfaces due to the stronger intermolecular hydrogen bonding effect, which is in proportional to the grafting density. This less hydrated surface film results in higher protein adsorption. This is further confirmed by the fact that introducing 2 SMA units in PGMA(*rac*)<sub>27</sub> can greatly improve the protein repelling ability. The CD spectra of PGMA aqueous solutions indicate that certain ordered structures stabilized by intramolecular hydrogen bonding are adopted in enantiopure PGMA, while the racemic PGMA does not show this effect. This is presumably the factor which causes the different grafting density between the enantiopure and racemic PGMA surfaces.

The chirality of HS-PGMA(*rac*)<sub>27</sub>, HS-PGMA(*R*)<sub>24</sub> and HS-PGMA(*S*)<sub>28</sub> is determined via <sup>1</sup>H NMR spectroscopy employing a three-component chiral derivatizing process, involving the treatment of enantiopure polymers with 2-formylphenylboronic acid and enantiopure  $\alpha$ -methylbenzylamine, which yields cyclic boronate diastereoisomers on the pendent groups. The defined protons on the diastereoisomers show different chemical shifts in the <sup>1</sup>H NMR spectra due to the different relative positions with respect to the aromatic ring. The main advantage of this method is its simplicity as it only involves the mixing of all the components without any further purification steps.

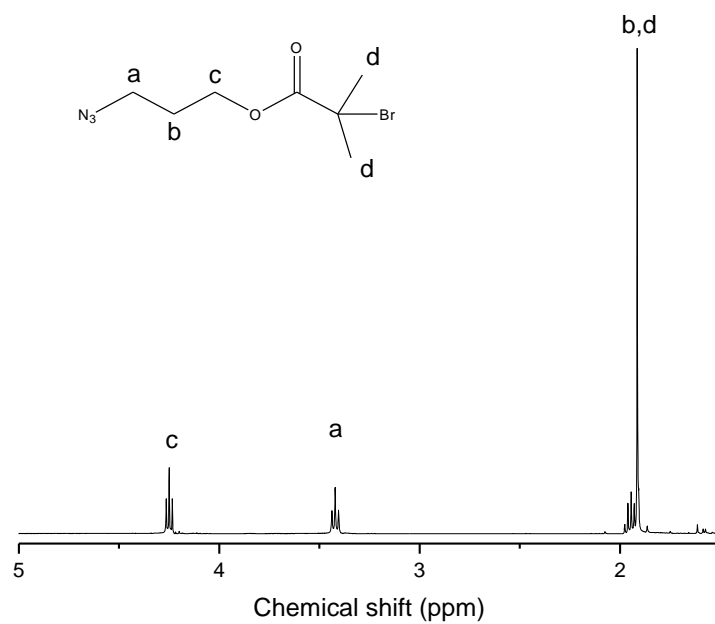
## Appendix



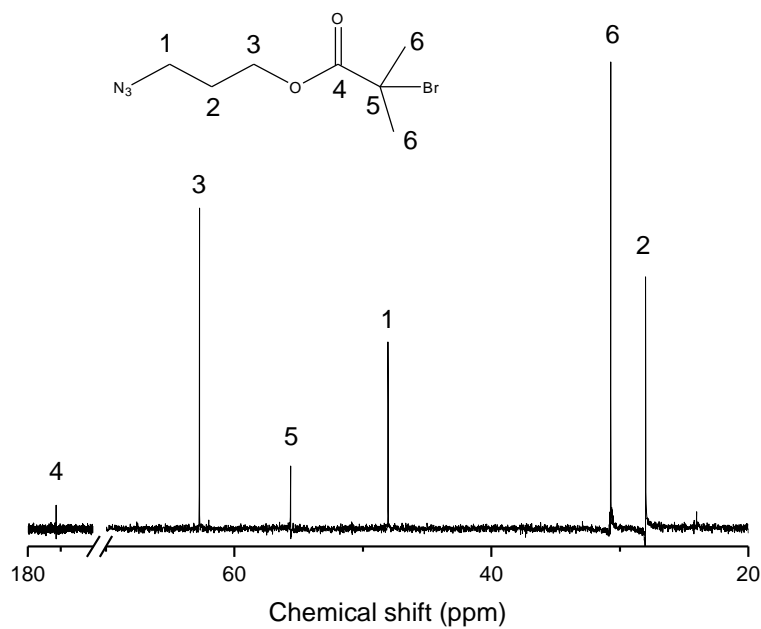
**Figure A1.**  $^1\text{H}$  NMR spectrum of nonadecafluoro-1-decyl hex-5-ynoate ( $\text{F}_9\text{C}\equiv\text{H}$ ) in  $\text{CDCl}_3$  (400 MHz).



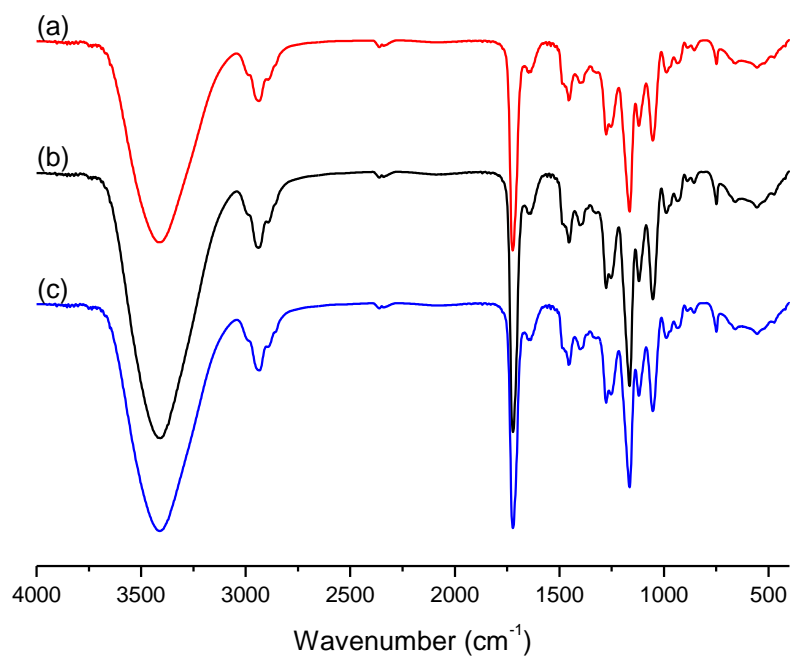
**Figure A2.**  $^1\text{H}$  NMR spectrum of nonadecafluoro-1-decyl hex-5-ynoate ( $\text{F}_9\text{C}\equiv\text{H}$ ) in  $\text{CDCl}_3$  (200 MHz).



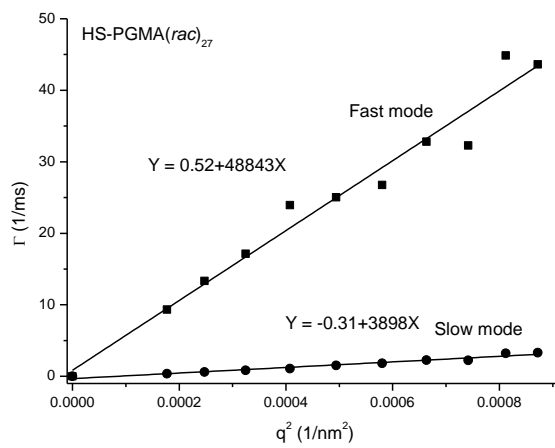
**Figure A3.** <sup>1</sup>H NMR spectrum of 3-azidopropyl-2-bromoisobutyrate (APBIB) in DMSO-*d*<sub>6</sub> (200 MHz).



**Figure A4.** <sup>13</sup>C NMR spectrum of 3-azidopropyl-2-bromoisobutyrate (APBIB) in DMSO-*d*<sub>6</sub> (400 MHz).



**Figure A5.** FT-IR spectra of (a), HS-PGMA(*S*)<sub>28</sub> (b), HS-PGMA(*rac*)<sub>27</sub> and (c) HS-PGMA(*R*)<sub>24</sub>.



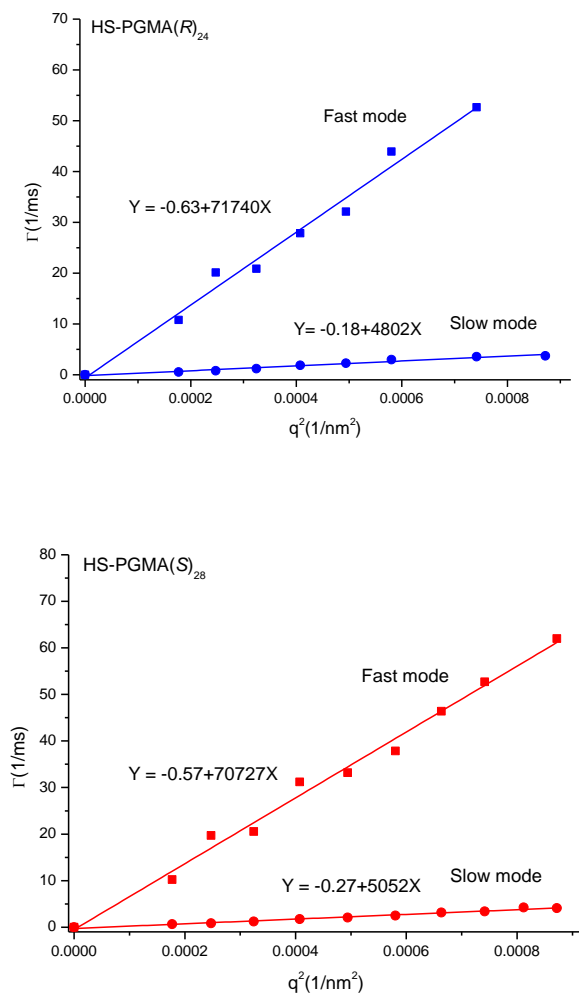


**Figure A6.** Relaxation rate ( $\Gamma$ ) as a function of the square of the magnitude of the scattering vector ( $q^2$ ) at 25 °C for 4 mg mL<sup>-1</sup> HS-PGMA(*rac*)<sub>27</sub> (black), HS-PGMA(*R*)<sub>24</sub> (blue) and HS-PGMA(*S*)<sub>28</sub> (red) aqueous solution.



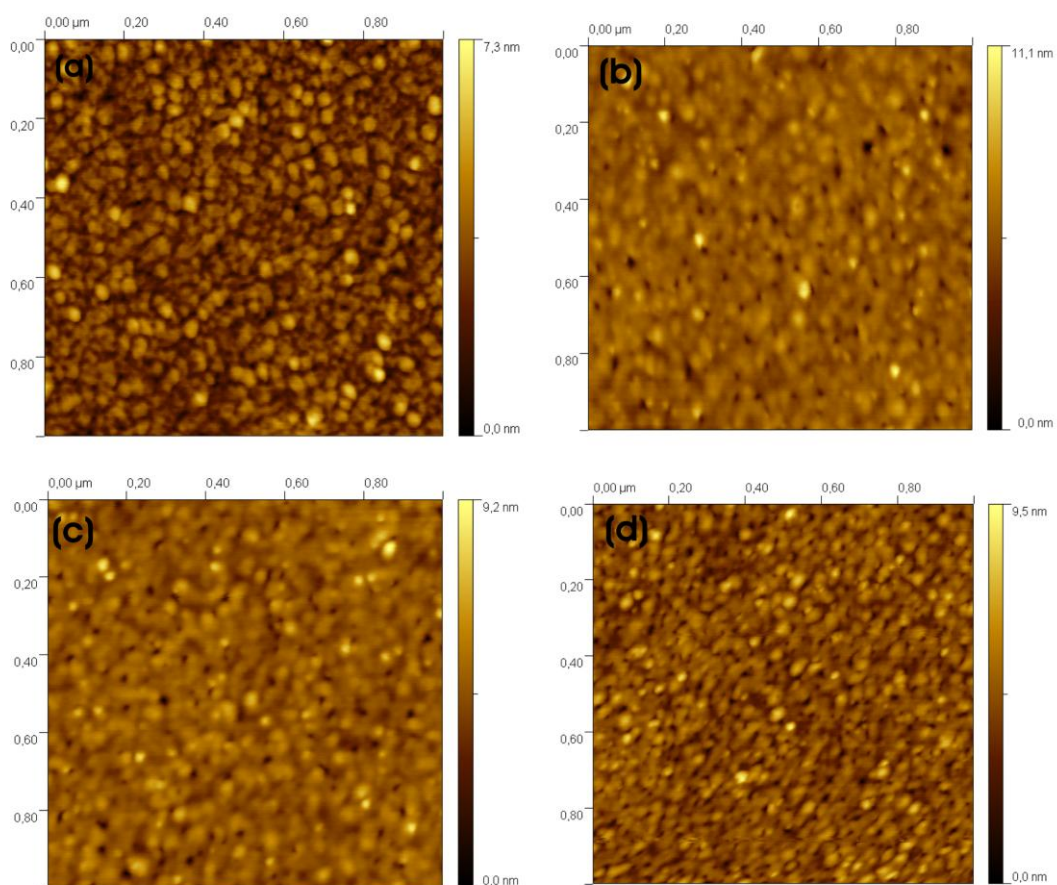


**Figure A7.** The AFM height image of bare gold (a) PGMA(*rac*)<sub>27</sub> SAM, (b) PGMA(*R*)<sub>28</sub> SAM, (c) and (d) PGMA(*S*)<sub>24</sub> SAM.

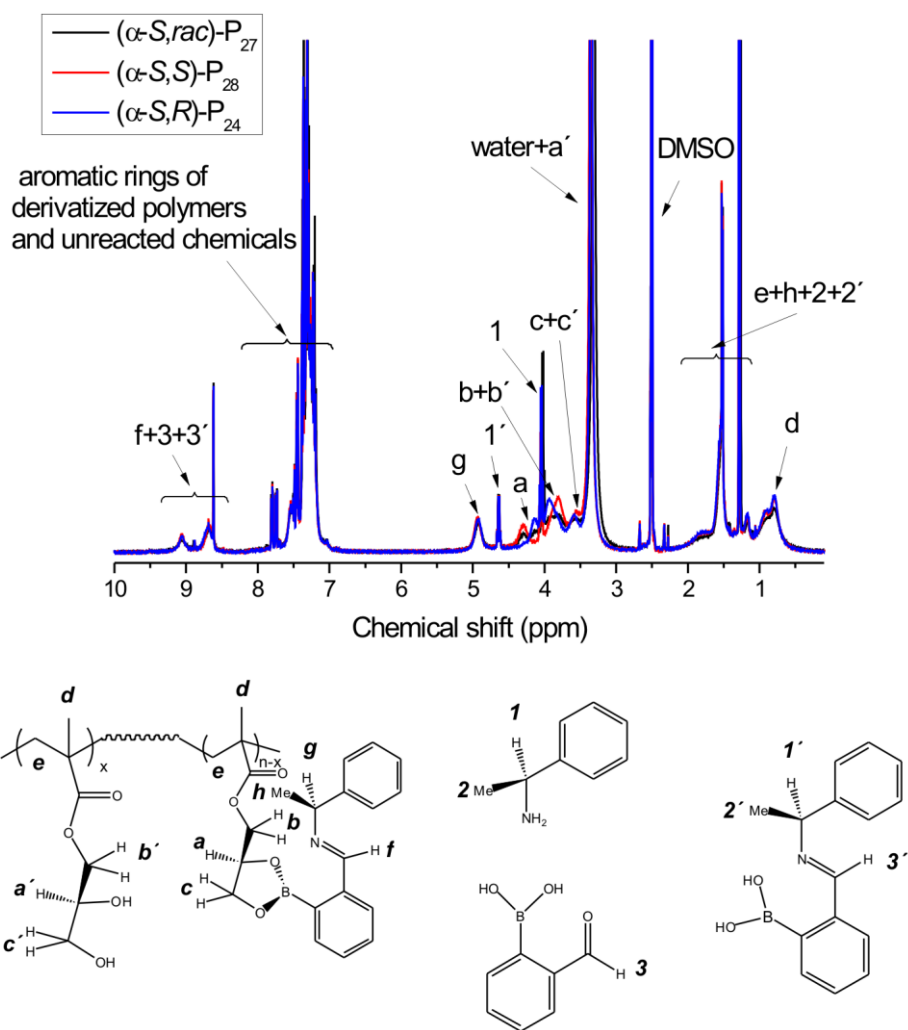


**Figure A8.**  $^1\text{H}$  NMR spectra of  $(\alpha\text{-}S,S)\text{-P}_{28}$ ,  $(\alpha\text{-}S,R)\text{-P}_{24}$  and  $(\alpha\text{-}S,\text{rac})\text{-P}_{27}$  in  $\text{DMSO-}d_6$ , 400 MHz at 25 °C. (The assignment of the protons is confirmed by the 2D  $^{13}\text{C}\text{-}^1\text{H}$  HSQC spectrum.) The conversion of GMA to imino-boronate ester is determined by the ratio of 3 times integral of resonance peak *a* to integral of resonance peak *d*. ~ 80% diols in GMA repeat units are converted to imino-boronate esters in the derivatized polymers.

## ACKNOWLEDGEMENTS

I am especially indebted to Prof. Jörg Kressler, my supervisor throughout my ph.D research period. His constructive comments and suggestions have brought me this far as a polymer scientist. Many thanks to all current and previous members of Prof. Jörg Kressler's group especially Dr. Kasten Busse, Dr. Henning Kausche, Dr. Zofia Funke, Dr. Regina Scöps, Dr. Elkin Amadon, Dr. Christian Albrecht, Dr. Christian Schwierger, Dr. Samuel O. Kyeremateng, Dr. Sacha Reuter, Dr. Dirk Pfefferkorn, Toufik Naolou, Frau Claudia Hochbach and Frau Elvira Stark.

I want to thank SKW Piesteritz and the Aninstitut – Agrochemisches Institut Piesteritz e. V. for providing the financial support of this work. I want to thank Prof. Dr. Niclas, Dr. Radics and Dr. Reihardt for their valuable suggestions and discussion.

I would also like to thank Prof. Thomas Groth of the Pharmacy Institute, Martin-Luther Unverstät, for his invaluable advice for the protein adsorption measurement and Alexander Köwitsch for the help in SPR performance. Many thanks to Dr. Bodo Furhmann in IZM, MLU, for the help in ellisometry measurement and gold substrates preparation, Dr. Annette Meister for the TEM measurements, Mr. Xiaopeng Li for the SEM measurement and Frau Otten in Physics Department, MLU for the IR and Raman spectroscopy.

Finally, I would like to thank my family especially my parents, Guorong Li and Qimei Wu, for their love and understanding during my study.

## Publications

**1.** Aggregation behaviour of poly(N-isopropylacrylamide) semitelechelics with a perfluoroalkyl segment in water

(Basis for Chapter 2)

Li, Z.; Kyeremateng, S. O.; Fuchise, K.; Kakuchi, R.; Sakai, R.; Kakuchi, T.; Kressler, J., *Macromol. Chem. Phys.* **2009**, *210*, 2138-2147.

**2.** Comparison of the monolayer formation of fluorinated and nonfluorinated amphiphilic block copolymers at the air–water interface

Li, Z.; Schön, V.; Huber, P.; Kressler, J.; Busse, K., *J. Phys. Chem. B.*, **2009**, *113*, 11841-11847.

**3.** Detection of chirality of poly(glycerol methacrylate)s after derivatization by <sup>1</sup>H NMR spectroscopy

Li, Z.; Chen, C.; Gröger, S.; Kressler, J., *Polymer* **2012**, *53*, 2613-2618.

(Basis for Chapter 5)

## Curriculum Vitae

### Personal Details:

Name: Zheng Li

Date of Birth: Juli 10<sup>th</sup> 1984

Place of Birth: Guangdong, China

Material Status: Single

### Education Details:

- |                 |  |
|-----------------|--|
| 11/2008-06/2012 | Ph. D student at the Institute of Chemistry, Martin-Luther-Universität Halle-Wittenberg, Halle(Saale), in the group of Prof. Jörg Kressler.  |
| 10/2006-10/2008 | Master of Science (M.Sc.) in Applied Polymer Science<br>(Grade 1.5- "excellent")<br>Martin-Luther-Universität Halle-Wittenberg, Halle(Saale) |
| 09/2002-06/2006 | Bachelor of Science (B. Sc.) in Chemistry<br>Zhejiang University of Technology<br>Hangzhou, China  |

## DECLARATION

I hereby declare that I have written and submitted this thesis independently without any help. I have not used any other sources or devices than indicated in this thesis. All quotations from literatures used, to the best of my knowledge, have been duly acknowledged. This thesis has neither been submitted to any other institution nor has been npreviously used to apply for a doctorate degree.

.....

Zheng Li

Halle(Saale), Juni 2012.